CHAPTER I

INTRODUCTION

"Evidence thus far…[toward]… unraveling the path from gene to behavior is encouraging. In any case, it is fun."

-Seymour Benzer

THE STUDY OF THE GENETICS OF BEHAVIOR

Mutagenesis screens to discover genes involved in behaviors

The ability of animals to respond to their environments with motor behaviors is a defining feature of the kingdom of Animalia. Rather than relearning motor behaviors each generation, animals inherit codes on how to perform basic motor tasks from their parents, allowing each animal to function as an individual being from an early age. Thus, understanding how animal offspring are able to move like their parents represents a fundamental step in our understanding of biology, but the topic has long mystified scientists. How can such complex behaviors as swimming, jumping, seeing, or even communicating be passed from a parent to an offspring with the parent only present to provide the material for the egg or sperm? Charles Darwin provided the first step in

understanding the nature of the inheritance of behaviors in *The Origin of Species*, where he noted that animal behavioral instincts appear to be inherited through natural selection (Darwin, 1859). Through the combination of Darwin's observations, and the advent of Mendelian genetics in the 20th century, which postulates that components of behavioral traits are embedded in an animal's genetic code, the field of behavioral genetics emerged.

Early contributors to the field of behavioral genetics aimed to find a single gene encoding a single behavior, which could allow subsequent elimination of problematic alleles such as those contributing to disease, disharmony, and even crime through the use of eugenics (reviewed in Greenspan, 2008). Nevertheless, the humbling complexity of how genes contribute to behaviors proved many of the field pioneers' goals both unrealistic and dangerous in their naivety. In reality, inheritance of single gene mutations that alter behavior in humans can occasionally be tracked over generations, but it is far more common for behaviors to result from a combination of many genes and alleles. Yet experimentally dissecting the genetic components of human behavior poses ethical and experimental problems. For these reasons, the use of genetic model organisms such as mice (*Mus musclus),* flies (*Drosophila melanogaster),* and worms (*Caenorhabditis elegans)* were developed, allowing scientists to model behaviors and dissect the genetics behind them experimentally.

A fundamental breakthrough in behavioral genetics occurred in the mid 1960s with Seymor Benzer's use of behavioral screens to separate mutagenized flies based on their preference for two behavioral alternatives (Benzer, 1967). There are two major advances in this technique that revolutionized that way behavioral genetics can be studied. 1) Interpreting whether a behavior originates from its genetics, often referred to

as the animal's "nature", or from the animal's interaction with its surroundings, referred to as the animal's "nurture", is difficult to separate. If a mutant fly strain displays a certain behavior over successive generations, it clearly differentiates a genetic component for the behavior from environmental components. 2) With thousands of genes in the *Drosophila* genome, selecting which genes might be worth studying in a behavioral pathway is difficult. A mutagenesis screen for a particular behavior provides an unbiased way to select for a set of mutants with defects in genes that contribute to that behavior. A gene responsible for a mutation can then be continually studied in a propagated mutant line, and catalogs of similar mutations can be used to paint a picture of the genes that make up a particular behavior. While these two primary advantages paved the way for countless studies of mutant flies, the foundation provided by these mutagenesis studies also allowed the next generation of genetic studies to blossom. The advent of genetic sequencing revealed abundant redundancy of genomes and pathways, and hypotheses about homologous genes and pathways could be inferred from mutagenesis screen mutations. Those genes could then be targeted for manipulation in order to test for new behavioral phenotypes, a method referred to as "reverse genetics". Suddenly, the connections between genetics and behaviors could be tested experimentally, and achieving the once impossible goal of understanding the genetics of behavior seemed possible.

While the use of mutagenesis screens of flies opened up the field of the genetics of behavior and gave a blueprint for the dissection of the genetics behind behaviors, many of the more complex behaviors dissected in detail such as courtship and sexual function have no obvious similarity to human behaviors. Mice, the most commonly used

genetic model organism, are closer evolutionarily to humans and have more genes and genetic pathways in common, but conducting large-scale mutagenesis screens for behaviors on a scale of those successfully conducted in *Drosophila*, is impractical and expensive. Furthermore, as embryogenesis in the mouse occurs in the mother's uterus, developmental studies of behavior are far more difficult. As an alternative, in the 1980's George Streisinger began to develop the use of the zebrafish *Danio rerio* as a complementary genetic model. Zebrafish have relatively short generation times and produce large clutches of embryos (100-200 per mating). Because they are externally fertilized, study at all developmental stages is possible. They are also optically transparent allowing a host of optical imaging experiments (Detrich et al., 1999). Streisinger and colleagues, recognizing these advantageous characteristics, rapidly developed the zebrafish as a genetic model, and soon began to conduct mutagenesis experiments with zebrafish (Walker and Streisinger, 1983). The field quickly developed from Streisinger's initial efforts, and the first large scale mutagenesis screens with saturation levels comparable to those in *Drosophila* screens were published in 1996. (Driever et al., 1996; Haffter et al., 1996). Mutagenesis screens for motility behaviors, were also performed, representing the emergence of the zebrafish as a model organism in the field of behavioral genetics (Granato et al., 1996). Mutants from these initial screens continue to be studied and have led to countless new research directions. With completion of the zebrafish genome only recently (Howe et al., 2013), the use of zebrafish as a genetic model organism is still not as developed as the fly or the mouse, but as the following sections demonstrate, the power of the zebrafish as a model organism is undeniable.

Zebrafish mutagenesis screens have revealed the swimming circuit

As a way to dissect the genes involved in simple motility behaviors in vertebrates, our lab conducted a mutagenesis screen for disrupted motility behaviors in zebrafish embryos. Normally at 17 hours post fertilization (hpf), zebrafish embryos exhibit spontaneous slow coiling of the body, at 22 hpf, touch-evoked escape contractions are seen, and touch-evoked swimming occurs by 28 hpf (Saint-Amant and Drapeau, 1998). Mutants containing defects in any of these behaviors were isolated and the genetics and defective behavioral circuits of mutants were then analyzed. Through the success of the mutagenesis screen approach, a scaffold of the components of the zebrafish escape circuit can be outlined, and thus the basic behavioral circuit for touch-evoked swimming in zebrafish can be illustrated by examples of mutants in the pathway. To illustrate this pathway, a sketch of the basic components of the zebrafish touch-evoked escape circuit is outlined below (Fig. 1-1).

The first step in activating the touch evoked escape response is activation of sensory neurons in the tail of the zebrafish embryo. Touching the tail activates sensory Rohon Beard (RB) neurons that innervate the skin and synapse onto Mauthner neurons and other reticulospinal neurons in the hindbrain to provide the initial stimulus for the touch induced neuronal escape circuit. The *mi310* mutant has a mutation in *pigu*, a subunit of glycosylphosphatidylinositol (GPI) transamidase, which is expressed in RB neurons, and is essential for surface expression of voltage gated sodium channels (Na_vs) (Nakano et al., 2010). With *pigu* disrupted, Na_vs are not expressed on the cell surface, and RB neurons are not able to fire, rendering the *mi310* mutant embryos touch-insensitive (Nakano et al., 2010). Similarly affecting RB neurons, the *touchdown* mutant

has a mutation in the cation channel TRPM7 that is not required for transduction of mechanosensory stimuli but may be required for neurotransmitter release by RB neurons (Low et al., 2011). Thus *touchdown* mutants are able to sense touch but do not respond with a swimming behavior.

Next, Mauthner and other reticulospinal neurons process input from sensory neurons and modulatory neurons in the brain, and send signals into the spinal cord via their caudally projecting axons. These hindbrain neurons synapse onto motor neurons and interneurons of the spinal cord to initiate the alternating contractions of trunk muscles that make up the escape response. The escape response requires coordinated activation of neurons on the two sides of the spinal cord by the hindbrain neurons, and a mutation in the *robo3* gene, which disrupts the axon guidance of Mauthner neurons and results in axons that do not project normally into the spinal cord, causes embryos to repeatedly turn to the same side in response to touch rather than an alternating contractions required for normal escape (Burgess et al., 2009). Mutations in the spinal interneurons also disrupt the coordinated escape responses. Two mutations that affect spinal interneurons, *bandoneon* and *shocked,* disrupt a glycine transporter (GlyT1) and glycine receptor (GlyR) respectively, resulting in abnormal escape responses and swimming (Cui et al., 2005; Hirata et al., 2005).

Interneuron output converges on motor neurons, which then synapse onto muscle at the neuronmuscular junction (NMJ), driving depolarization of the muscle through the binding of acetylcholine (ACh) to the acetylcholine receptor (AChR). The *ennui* mutation has a defect in AChR clustering at the NMJ, and thus contains reduced activation of the muscle which results in weak escape responses and swimming (Saint-Amant et al., 2008).

Finally, if the muscles are not functioning correctly, the zebrafish will not swim. Muscle depolarization is linked to Ca^{2+} release by the sarcoplasmic reticulum (SR) via excitation-contraction (EC) coupling. EC coupling involves two principal membrane proteins, the voltage-sensing dihydropyridine receptor (DHPR) located in the transverse tubules, and the ryanodine receptor (RyR) located in the SR. EC coupling is disrupted in the *relaxed* mutant in which the gene encoding the DHPRβ subunit ($Ca_v\beta1$) is defective, rendering mutant embryos immotile (Schredelseker et al., 2005; Zhou et al., 2006). Similarly, the *relatively relaxed* mutant has a nonsense mutation in the *ryr1b* gene which results in loss of the fast twitch muscle-specific RyR1b protein, and causes slow swimming embryos. With depolarization and contraction of the muscle, the wildtype embryo is able to complete the touch-evoked circuit and propel its body into a swimming motion.

A mutant embryo isolated from a mutagenesis screen, therefore, can have a defect in one or many of these points, and the first step towards characterizing a new mutation is to determine which parts of the behavioral circuit are functioning normally and which are not. Conveniently, zebrafish embryos are amenable to *in vivo* patch clamp electrophysiological recordings (Drapeau et al., 1999), which allow a researcher to record the activity of neurons or muscle at each step in the circuit in order to determine the locus of the synaptic or electrogenic defect within the neural circuit. In this way, a defect in a specific cell type can be identified, and the function of the mutated gene in that cell type can be further isolated.

Successful characterizations of mutations from these screens, while indispensible, are really only a starting point for research into the genetics involved in these behaviors. The stringency in zebrafish mutagenesis screens has thus far been fairly relaxed, focusing

on the most basic motility defects. Thus, only the most indispensible components of the behavioral circuit have been selected for. Furthermore, some genes have different functions or importance in different cellular subtypes, making the specific contributions of genes in neuron or muscle subtypes towards a phenotype difficult to unravel. Many of these gene pathways and circuits can be further studied using reverse genetics techniques such as targeted knockdowns with antisense Morpholino Oligonucleotides (MO) (Nasevicius and Ekker, 2000), or targeted mutagenesis strategies such as Zinc Finger Nucleases (Foley et al., 2009), Transcription Activator-like Effector Nucleases (TALENS) (Sander et al., 2011), and Clustered Regularly Interspaced Short Palindromic Repeats (CRISPR)-Cas (Hwang et al., 2013). Yet determining targets for gene disruption remains a challenge, and through the combination of forward genetics to provide initial targets for investigation, and reverse genetics to subsequently finely dissect the details of the genetic components, the next steps in the study of the contributions of genes towards behaviors can be taken.

HISTORY AND BACKGROUND OF THE EC COMPLEX

All motor behaviors require muscle activation. Motor neurons provide the stimulus for muscle activation at the NMJ, which quickly triggers muscle contraction. Amazingly, skeletal muscle can initiate a contraction within the center of a fiber within a millisecond or two of an action potential. This surprising fact puzzled muscle physiologists of the 1950's because diffusion of a secondary messenger or activating factor from the surface to the interior of the fiber would take hundreds of milliseconds.

Huxley and Taylor, provided the first clue to how this phenomenon occurs by showing that depolarization with a microelectrode at certain sensitive spots on the sarcolemma relative to the muscle striation pattern resulted in contraction even when external Na^+ solution was removed, while other spots on the sarcolemma did not induce contraction (Huxley and Taylor, 1958). From this observation, the authors hypothesized that a network of membranous tubules, which had been previously described with electron microscopy (Porter and Palade, 1957), might carry depolarization as a signal into the interior of the muscle fiber and subsequently activate contraction (Huxley and Taylor, 1958). These observations proved prescient, as the sensitive regions were later found to be the entrances to the transverse (t)-tubule network, which radiate from the surface of the muscle fiber into the interior of the cell, causing the surface of the fiber to be electrically continuous with the interior (Dulhunty and Gage, 1973).

By the time of Huxley and Taylor's study, Ca^{2+} release had been shown to immediately precede muscle contraction and a cytosolic increase in Ca^{2+} had been firmly established as the activator of the muscle contraction machinery (Bozler, 1952). Electron microscopy further showed that cisternae sacs of sarcoplasmic reticulum (SR), highly enriched with Ca^{2+}, were tightly associated on either side of the t-tubules at regular intervals, creating junctional triplet formations named triads (Fig. 1-4a) (Franzini-Armstrong, 1970). The junctions of the t-tubules and SR at triads, thus provided anatomical loci for the depolarization induced release of Ca^{2+} that was required for contraction (Ebashi et al., 1969). What remained to be determined was how the depolarization of the plasma membrane and t-tubule system network coordinated to cause release of SR Ca^{2+} stores, a process that became referred to as EC coupling.

The dihydropyridine receptor is the voltage sensor

An important clue to the mechanism of voltage transduction in skeletal muscle came from the discovery of small electrical signals preceding the voltage-dependent Na^+ currents underlying action potentials in squid giant axons. The activation and inactivation characteristics of these small currents suggested they represented movement of charge within the membrane that gated the flow of Na^+ ions across the membrane (Armstrong and Bezanilla, 1973, 1974). When attempts at detecting a charge movement in the t-tubules that could play a role in triggering the Ca^{2+} release from the SR were made, they were found to be a hundred times slower than Na_v charge movement in squid axons, suggesting that the observed charge movements in muscle were unlikely to be from Na_vs (Chandler et al., 1976; Schneider and Chandler, 1973). Nevertheless, the charge movement preceded Ca^{2+} release from the SR and its voltage dependence was compatible with EC coupling, suggesting it may be the trigger for intracellular Ca^{2+} release (Chandler et al., 1976).

Fortuitously, a group of organic compounds, the 1,4dihydropyridines (DHP), were found to modulate a subset of voltage-gated Ca^{2+} channels (Ca_v), the L-type Ca_vs, and EC coupling, but not other types of Ca_vs (Cauvin et al., 1983; Schramm et al., 1983). Furthermore, DHP compounds bound with high affinity to t-tubule membranes (Fosset et al., 1983; Galizzi et al., 1984), leading to the inference that the DHP sensitive Ca^{2+} channel acted as the voltage sensor in the t-tubules for EC coupling. Because of its high affinity interaction, DHP-Receptor (DHPR) complex could be purified from solubilized t-tubules using affinity purification with the DHP compound (Curtis and Catterall, 1984).

SDS-PAGE analysis showed five bands could be resolved at 1:1:1:1:1 stoichiometry, which were named the α1 (~175kDa,) α2 (~150kDa), β (~54kDa), δ (17-25kDa), and γ (~32kDa) subunits of the DHPR (Curtis and Catterall, 1984; Tanabe et al., 1987). Hydropathy analysis revealed each protein except the cytosolic β subunit contained trans-membrane regions. Cloning and sequencing of the cDNA of the α1 subunit of this complex (now referred to as $Ca_v1.1$), combined with hydropathy analysis revealed the encoded protein contained 24 trans-membrane domains that were homologous to Na_vs, indicating the $Ca_v1.1$ protein contains the necessary components to function as a voltage detector and pore for the DHPR complex (Tanabe et al., 1987). Confirmation that the DHPR acted as the voltage sensor finally came with discovery of a naturally occurring $Ca_v1.1$ mutant (*dysgenic)* mouse that dies at birth (Beam et al., 1986; Klaus et al., 1983). Cell lines and myotubes were taken from *dysgenic* mice, and the cells were found to be deficient in both charge movement and EC coupling, but expression of cDNA encoding $Ca_v1.1$ was found to restore both properties (Adams et al., 1990; Tanabe et al., 1988), indicating the $Ca_v1.1$ acts as the voltage sensor for EC coupling.

As skeletal muscle was used for the first purification experiments, the skeletal muscle specific $Ca_v1.1$ became the first voltage-gated Ca^{2+} channel to be cloned. A total of ten cDNAs encoding α1 subunit cDNAs have since been cloned and are divided into three classes, Ca_v1, Ca_v2, and Ca_v3 based on their electrophysiological properties (Catterall et al., 2005). Ca_v proteins, like Na_v channels, are organized in four repeated domains (TM I-IV), each containing six transmembrane segments (Tanabe et al., 1987). The N and C-termini of Ca_v are cytoplasmic, as are the loops connecting the TMI and TMII (L1-2), TMII and TMIII (L2-3), and TMIII and TMIV (L3-4) (Fig. 1-4). There are

four Ca_v1 members, $Ca_v1.1$, $Ca_v1.2$, $Ca_v1.3$ and $Ca_v1.4$ which are all sensitive to DHPR agonists and antagonists, and exhibit long lasting activation leading currents and thus were named "L-type" Ca^{2+} current (Catterall et al., 2005). Most Ca_vs have wide ranging and overlapping expression profiles except $Ca_v1.1$, which is exclusively expressed by skeletal muscle (Catterall et al., 2005). $Ca_v1.2$ is expressed in cardiac tissue and the brain, and is required for cardiac EC coupling (Fabiato, 1983), while all other Ca_vs are expressed in neurons (Catterall, 2011).

The ryanodine receptor is the Ca^{2+} release channel

The second key to defining the molecular players in skeletal muscle EC coupling was the identification of the Ca^{2+} release channels in the SR. Ca^{2+} release was found to be sensitive to a plant alkaloid with toxic effects on muscle called ryanodine (Meissner, 1986). Ryanodine was subsequently used to purify the protein from solubilized SR (Inui et al., 1987). The purified protein, named the ryanodine receptor (RyR), had a large molecular weight (~560kDa) and formed tetramers, nicely fitting with electron microscopic observations that large foot-like molecules extended from the SR cisternae to the t-tubules at triads (Franzini-Armstrong, 1970; Inui et al., 1987). Three ryanodine receptor isoforms have been identified: RyR1 serves as the primary Ca^{2+} release channel in skeletal muscle, although RyR3 is also present in skeletal muscle and is thought to be activated solely by Ca^{2+} induced Ca^{2+} release (Hamilton, 2005). RyR2 is expressed in cardiac tissue (Hamilton, 2005), and all three RyR isoforms are found in neurons (Sorrentino and Volpe, 1993). The purified RyR1 channels were reconstituted in planar bi-lipid membranes to allow functional studies *in vitro,* and were shown to have the same

conductance and pharmacological properties as the Ca^{2+} release channel in vivo, confirming previous data that the ryanodine sensitive channel is the Ca^{2+} release channel (Lai et al., 1988). Further confirmation of the identity of the RyR1 as the Ca^{2+} release channel came with the development of a RyR1 knockout mouse (*dyspedic)* which lacked EC coupling (Takeshima et al., 1994), and the subsequent restoration of EC coupling with the expression of cDNA encoding the RyR1 protein (Nakai et al., 1996).

The DHPR-RyR1 EC coupling complex was further characterized at an ultra-structural level by a series of elegant freeze fracture electron microscopy studies, which confirmed a close arrangement of DHPRs and the RyR1s consistent with direct interactions of the two Ca^{2+} channels within the triad (Block et al., 1988). RyR1, identified by their junction spanning feet, are found to form orderly arrays with a tetragonal arrangement along the SR sides of the triad (Fig. 1-2b) (Franzini-Armstrong and Jorgensen, 1994). On the t-tubule side of the junction, DHPR complexes can be seen as particles in their own patterned array, clustered in groups of four called tetrads that appear as small bumps in the membrane (Fig. 1-2). Notably, a tetrad of DHPRs aligns with every other RyR foot, an arrangement that leaves some RyR1 receptors without a corresponding DHPR tetrad (Block et al., 1988). Electron microscopy of skeletal muscle after application of high concentrations of ryanodine shows that ryanodine treatment affects the distance between DHPR particles in tetrads (Paolini et al., 2004), which corresponds with increases of L-type Ca^{2+} release (Bannister and Beam, 2009), indicating the two complexes are directly interacting.

Cardiac versus skeletal muscle EC coupling

Although both cardiac and skeletal muscle have been found to undergo EC coupling, the differences in EC coupling between the tissue types are notable and informative. In contrast to cardiac muscle, skeletal muscle will still twitch when bathed in Ca^{2+} deficient media and the calcium chelator EGTA (Armstrong et al., 1972). Thus, EC coupling in cardiac muscle primarily differs from cardiac EC coupling in the requirement of an influx of extracellular Ca^{2+}. In cardiac cells, extracellular Ca^{2+} entry occurs via $Ca_v1.2$ and this Ca^{2+} influx triggers activation of the cardiac RyR2 by Ca^{2+} induced Ca^{2+} release (Fabiato, 1983). The differences at the level of cellular anatomy partly account for these different requirements of extracellular Ca^{2+} in the two muscle types. In skeletal muscle, $Ca_v1.1$ channels in t-tubules align in tetrads across from the RyR1 in the SR at triads where they can directly interact (Block et al., 1988). In cardiac muscle, however, $Ca_v1.2$ channels align across from RyR2 but the Cav1.2 in t-tubules of cardiac muscle do not form tetrads and are clearly separated from the RyR2 in the SR preventing direct interactions (Franzini-Armstrong et al., 1998). Differences in EC coupling in cardiac versus skeletal muscles can also be attributed to differences in the properties of the DHPRs and RyRs expressed. EC coupling in *dysgenic* skeletal myotubes cannot be rescued by $Ca_v1.2$ expression, though $Ca_v1.2$ will still pass L-type Ca^{2+} current (Tanabe et al., 1990). Likewise, the cardiac and neuronal RyR2 is able to perform Ca^{2+} induced Ca^{2+} release when expressed in *dyspedic* myotubes, but is not able to rescue the reciprocal signaling characteristic of skeletal EC-coupling (Nakai et al., 1997).

A consequence of the direct interaction between $Ca_v1.1$ and RyR in skeletal muscle is that L-type current from the $Ca_v1.1$ is not required for EC coupling, explaining

the observation that skeletal muscle contraction does not require extracellular Ca^{2+} (Armstrong et al., 1972; Gonzalez-Serratos et al., 1982). Further support for the disposable nature of the L-type current in skeletal muscle comes in the finding that $Ca_v1.1$ in bony fish such as zebrafish have residue substitutions in their pore helix that block Ca^{2+} permeation, eliminating L-type current in skeletal muscle (Schredelseker et al., 2010). Nevertheless, $Ca_v1.1$ still shows charge sensing gating movement and function in their conserved role in triggering EC coupling (Schredelseker et al., 2010). Thus, the physiological importance of L-type current in skeletal muscle is still under debate, and its presence is indicative of $Ca_v1.1$ function in most vertebrates, but it is not required for skeletal muscle EC coupling.

HOTSPOTS IN EC COUPLING

While EC coupling has been heavily studied since the 1950's, and the basic apparatus has been defined, fundamental questions on EC coupling remain due to the complexity of the process (Beam and Bannister, 2010). While it is clear that the DHPR acts as the voltage sensor in EC coupling and induces Ca^{2+} release through the RyR1 by a direct mechanism, the details of this mechanism and of how this interaction occurs is still strikingly unclear.

Since the skeletal muscle EC coupling complex has not been successfully reconstituted heterologously (Suda et al., 1997; Takekura et al., 1995b) and knockout mice of some EC coupling proteins are perinatal lethal (Gregg et al., 1996; Klaus et al., 1983; Takeshima et al., 1994), most of the physiological data on skeletal muscle EC

coupling have been obtained through the use of myotubes harvested from knockout mice or zebrafish knockout mutants. Generally, a pattern of systematically deleting, manipulating, or substituting in and out components of the DHPR complex and looking at the resulting effect on EC coupling has emerged. Critically, these studies have established several parts of the EC coupling complex that are not required: The amino-terminus of the $Ca_v1.1$ was found to be dispensable for EC coupling, as deletion of the bulk of the region resulted in no effect on either L-type currents or Ca^{2+} transients (Bannister and Beam, 2005). Similarly, skeletal muscle specific γ1 subunit knockout mice showed slower inactivation of L-type current, but the mice have no abnormal phenotype, and therefore the γ1 subunit is considered dispensable for EC coupling (Freise et al., 2000). Likewise, α2δ1 subunit knockout mice have a cardiac defect, but their skeletal muscle architecture and function are grossly normal (Fuller-Bicer et al., 2009), and siRNA knockdown studies have shown limited influence on EC coupling in skeletal myotubes (Gach et al., 2008). In contrast to these straightforward examples, an extensive literature has developed covering several loci that are critical to EC coupling, which will be reviewed below.

L2-3 region is required for normal EC coupling

Early studies of the molecular interactions between the DHPR and RyR1 took advantage of *dysgenic* myotubes to unravel necessary components of the EC-coupling interaction. While *dysgenic* mice are perinatal lethal, myotubes can be harvested from homozygous mutants and can be rescued by increasing intracellular free Ca^{2+}(Klaus et al., 1983), or by expression of cDNA encoding wild type $Ca_v1.1$ (Tanabe et al., 1988).

The contrast between cardiac and skeletal muscle E-C coupling means the expression of $Ca_v1.1/Ca_v1.2$ hybrids in the *dysgenic* myotube background could be used to identify the critical regions in the $Ca_v1.1$ that were necessary for restoring EC coupling. These studies initially isolated a region in the intracellular L2-3 of the $Ca_v1.1$ that appears necessary for skeletal muscle type EC coupling (Tanabe et al., 1990). Further studies narrowed the critical region in L2-3 loop to a 46-amino acid stretch (residues 720-765) and found that it mediated a reciprocal interaction between the RyR1 and the DHPR (Grabner et al., 1999; Nakai et al., 1996). This region of the L2-3 loop was subsequently dubbed the "critical region" of L2-3. Concurrent biochemical studies reported that a purified peptide of the L2-3 region interacted with RyR1 in planar lipid bilayers and enhanced $[H^3]$ryanodine binding in isolated skeletal SR vesicles (Lu et al., 1994), suggesting the critical region may act as the point of direct interactions between the DHPR and the RyR1.

The contrast in secondary structure between $Ca_v1.1$ and $Ca_v1.2$ is thought to be informative in how the L2-3-RyR1 interaction may occur. The secondary structure of the critical domain of L2-3 from $Ca_v1.1$ is predicted to form a random-coil motif that allows it to interact with the RyR1. In contrast, the secondary structure of the homologous region of $Ca_v1.2$ forms an α-helix, which apparently does not support skeletal muscle EC coupling (Kugler et al., 2004b). Mutagenesis studies on the L2-3 region of the $Ca_v1.1$ identified four residues (A739, F741, P742, and D744) that when mutated to allow the formation of an α-helix, disrupted EC coupling without affecting $Ca_v1.1$ expression levels, indicating the random-coil secondary structure of the $Ca_v1.1$ L2-3 region is necessary for EC coupling (Kugler et al., 2004b). Subsequently, a later study indicated

that the region C-terminal to the critical region of L2-3 that is predicted to form an α-helix is sensitive to insertions of YFP, suggesting that the C-terminal region of the L2-3 region as also important for the function of the L2-3 domain (Bannister et al., 2009).

The use of freeze-fracture electron microscopy of skeletal muscle triads confirmed the use of $Ca_v1.1$ chimeras as a method to dissect the regions important in EC coupling. Using the same L2-3 chimeras previously used to demonstrate its importance for EC coupling (Kugler et al., 2004b), Takekura et al. (2004) found that tetrads were formed in *dysgenic* myotubes by all constructs that reconstituted EC coupling. By contrast, expression of $Ca_v1.2$, or the L2-3 region of $Ca_v1.2$ in the $Ca_v1.1$ backbone were not able to restore tetrads, just as they had not restored EC-coupling (Kugler et al., 2004b). However, through studies of the ancestral housefly $Ca_v1.1$ ($Ca_v1.1M$) a deeper relationship between tetrad formation and EC coupling was identified. A chimera of the L2-3 region from $Ca_v1.1M$ inserted into the rabbit $Ca_v1.1$ backbone restored some tetrad formation, but provided only a small amount of EC coupling (Kugler et al., 2004b; Takekura et al., 2004). While DHPR particles were present in the orthogonal array of the $Ca_v1.1M/Ca_v1.2$ chimera, completeness of the tetrads (the percentage of tetrad sites that contained four DHPR particles), was dramatically reduced compared to constructs that fully restored EC coupling, indicating the completeness of tetrads may be important for EC coupling (Kugler et al., 2004b).

While these chimera analysis studies raised hopes that the interaction between the DHPR and RyR1 suggested by electron microscopy studies was on a molecular level the interaction between the L2-3 region of the $Ca_v1.1$ and the RyR1, direct evidence of their interactions has still not been conclusively demonstrated. For example, regions within the

critical region of L2-3 have been reported to bind and activate RyR in vitro (Lu et al., 1994), but deletions of those same regions have shown no effect on EC coupling properties (Ahern et al., 2001a; Ahern et al., 2001b). Furthermore, while deletion of the critical region of L2-3 abolished EC coupling, co-deletion of the critical region with a more N-terminal region of the L2-3 restored some EC coupling, indicating that EC coupling can operate without the critical region, and more complicated interactions requiring secondary structure may be involved in the ability of the L2-3 critical region to interact with RyR1 (Ahern et al., 2001b). Thus, the general consensus has emerged that the molecular mechanisms underlying EC coupling are more sophisticated than a simple protein-protein interaction between the L2-3 region and the RyR1.

While clearly informative, one obvious problem with $Ca_v1.1/Ca_v1.2$ chimera analyses is that they are inadequate for generating sufficiency arguments because they fail to take into account the participation of other parts of the DHPR complex which may be conserved between the $Ca_v1.1$ and $Ca_v1.2$. For instance, quantitative analyses of Ca^{2+} release and charge movement using L2-3 $Ca_v1.1/Ca_v1.2$ chimeras expressed in *dysgenic* myotubes, showed that the restoration of EC coupling is in fact incomplete, indicating other loops of the $Ca_v1.1$ are also instrumental in normal EC-coupling (Carbonneau et al., 2005). Chimera analyses also fail to account for auxiliary proteins present in the *dysgenic* muscle that may be involved in supporting EC coupling, but interact with cardiac sequences in different ways. Thus, although chimera analyses have been helpful in identifying regions the L2-3 region of $Ca_v1.1$ as important for EC coupling, they do not present a complete picture of EC coupling interactions.

The L1-2 region and the $Ca_v\beta$1a are required for EC coupling

The most direct evidence of the influence of regions other than L2-3 on EC coupling comes from studies of the DHPR β subunit ($Ca_v\beta$) knockout mutants. Four families of $Ca_v\beta$ subunits ($Ca_v\beta$1-4) have been identified, each having splice variants with different expression patterns (Buraei and Yang, 2010). The splice variant $Ca_v\beta$1a, which contains a uniquely spliced exon, is exclusively expressed by skeletal muscle (Buraei and Yang, 2010; Zhou et al., 2008; Zhou et al., 2006). In the $Ca_v\beta$1 null mouse mutant *cchb1,* myotubes show complete loss of EC coupling, resulting in paralysis and perinatal lethality in the mouse (Beurg et al., 1997; Gregg et al., 1996). Importantly, although the *cchb1* mutants show decreased expression and assembly of the EC coupling complex in triads (Beurg et al., 1999; Gregg et al., 1996; Strube et al., 1998), heterologous expression of $Ca_v\beta$1a has shown it to be a potent regulator of the open probability of L-type Ca^{2+} channels, indicating it plays dual roles as a regulator of the properties of Ca^{2+} channels and thus EC coupling and as a chaperone for Ca_v1.1 during protein trafficking (Gerster et al., 1999).

The zebrafish $Ca_v\beta$1 subunit mutant, *relaxed,* shows a similar paralytic phenotype to mouse knockout mutants (Schredelseker et al., 2005; Zhou et al., 2006), and since zebrafish myotubes show a higher degree of differentiation in culture than mouse myotubes, studies on *relaxed* mutants have been integral in teasing apart the chaperone and EC coupling regulator functions of the $Ca_v\beta$1a in differentiated muscle (Schredelseker et al., 2009; Schredelseker et al., 2005). *Relaxed* myotubes show a dramatic reduction in charge movement (voltage sensing of the Ca_v1.1), and completely lack Ca^{2+} release, but still retain some expression of Ca_v1.1 at triads that is unable to

organize into tetrads (Schredelseker et al., 2005). As the reduction in levels of $Ca_v1.1$ at the triad alone is not enough to account for the complete loss of EC coupling, the necessity of $Ca_v\beta1a$ for function of the EC coupling complex thus appears to be more than its role in trafficking of $Ca_v1.1$ to the triad. Rescues of *relaxed* muscles with cardiac $Ca_v\beta2a$ and the ancestral $Ca_v\beta$ from the housefly, $Ca_v\beta1_M$, restored normal charge movement and full triad expression of the $Ca_v1.1$ in skeletal muscle, but failed to fully rescue EC coupling and normal tetrad formation (Schredelseker et al., 2009). Thus, more than the trafficking and support of voltage sensing functions that $Ca_v\beta$ provides, EC coupling requires an additional factor provided by $Ca_v\beta1a$ that correlates with normal tetrad formation for proper communication between the DHPR and RyR1.

Concurrent with studies of knockout phenotypes, biochemical studies have established that $Ca_v\beta$ directly interacts with Ca_v subunits. An epitope library of $Ca_v1.1$ fragments were screened for binding to the $Ca_v\beta1$ subunit, and an 18 residue sequence in the cytoplasmic region of the small cytoplasmic loop between the first and second 6-TM regions (L1-2) of the $Ca_v1.1$, coined the Alpha Interaction Domain (AID) was identified (Pragnell et al., 1994). The AID is conserved in all Ca_v1 and Ca_v2 and it interacts with all four $Ca_v\beta$ isoforms (De Waard et al., 1995). Mutations within the AID motif were subsequently shown to weaken or abolish the Ca_v-$Ca_v\beta1$ interaction and reduce or abolish Ca^{2+} current in heterologous systems, solidifying the evidence that the AID is the main point of interaction between the Ca_v and $Ca_v\beta1$ (De Waard et al., 1996).

The solution to the crystal structure of the complex between the cardiac $Ca_v\beta2a$ and the AID revealed that the $Ca_v\beta$ binds the AID at a deep groove pocket formed by several α helices distal to the SH3 domain of $Ca_v\beta2a$ which was named the α binding

pocket (ABP) (Van Petegem et al., 2004). Interestingly, the AID region falls only 24 amino acids away from the IS6 region in the $Ca_v1.1$ (Pragnell et al., 1994), which has been shown to be critical for Ca_v inactivation (Zhang et al., 1994). Furthermore, the interaction between $Ca_v\beta2a$ ABP and AID promotes an α-helical conformation of the AID, which is predicted to propagate through the proximal linker to the IS6 region, potentially allowing mechanical transduction or conformational support of gating states by $Ca_v\beta$ (Opatowsky et al., 2004). Supporting this hypothesis, variations in α-helical lengths among different Ca_v isoforms in the L1-2 region have been shown to correlate with different functional properties of the channels (Almagor et al., 2012). Nevertheless, despite several crystal structures of $Ca_v\beta$ isoforms in complex with Ca_vs, a mechanism for how the $Ca_v\beta1a$ functions in EC coupling is still unclear, and would be significantly helped by a crystal structure of the $Ca_v\beta1a$-$Ca_v1.1$ complex.

One problem with the crystal structures of the $Ca_v\beta$ thus far is they fail to account for the importance of the SH3 domain of $Ca_v\beta$, which is distal to the AID, yet clearly plays an integral role in EC coupling. The highly conserved $Ca_v\beta1$ SH3 domain is linked by a variable hook region to a guanylate kinase (GK) domain, which contains the ABD that binds to the AID of $Ca_v1.1$ (Chen et al., 2004; Hanlon et al., 1999). Using chimeras of the $Ca_v\beta1a$ and the neuronal $Ca_v\beta3$, which only marginally restores charge movement of the $Ca_v1.1$, Dayal *et al*., showed that both the SH3 domain of $Ca_v\beta1a$ and a putative SH3 binding domain in the C-terminus of the $Ca_v\beta1a$ are required for complete restoration of $Ca_v1.1$ charge movement in the $Ca_v\beta3$ backbone. Furthermore, a single proline (P) to alanine (A) missense mutation in the putative SH3 binding domain abrogated the rescue, suggesting potential cooperation between the $Ca_v\beta1a$ SH3 domain

and the putative SH3 binding domain is integral to voltage sensing by the DHPR (Dayal et al., 2013). However, no biochemical interaction between the two domains of the $Ca_v\beta1a$ subunit has been demonstrated, and the $Ca_v\beta1a$ subunit is unlikely to bind the canonical P residues in its own C-terminus as the SH3 binding domain in the C-terminus is blocked by an α-helix domain and regions of the Hook domain (Chen et al., 2004), suggesting another protein or factor may be involved in the cooperation of the two domains of the $Ca_v\beta1a$ subunit. The SH3 domain of $Ca_v\beta1a$ can conceivably still bind the SH3 binding domain of $Ca_v\beta1a$, but this would require the movement of the two domains blocking its binding interface, and such potential for a conformational change or changed state has not yet been seen in the crystal structures of either the $Ca_v\beta2a$ alone or in complex with the AID (Chen et al., 2004; Opatowsky et al., 2004; Van Petegem et al., 2004). The hook region is variable in sequence and length among different $Ca_v\beta$ subunits, and its crystal structure has not been resolved due to poor electron density which indicates a high degree of flexibility (Buraei and Yang, 2010). Thus, although the interactions mediated by the $Ca_v\beta1a$ SH3 domain and the SH3 binding domain in the C-terminus are required for EC coupling, our understanding of a mechanism in which they are used is incomplete.

Whether the $Ca_v1.1$ L1-2 plays a role in EC coupling is complicated due to its role in binding $Ca_v\beta1a$. At a minimum, its presence is required because $Ca_v\beta1a$ is required for EC coupling. Expression of a hemi-channel containing the I-II domains of $Ca_v1.1$ (and not containing the L2-3 critical domain) in dysgenic $Ca_v1.1$ null myotubes, while not capable of rescuing EC coupling, was found to restore some charge movement (Ahern et al., 2001a). Furthermore, immobilized $Ca_v\beta1a$ has been reported to bind a fragment of

RyR1 (Cheng et al., 2005), and a 35-amino acid peptide corresponding to the C-terminal region of the $Ca_v\beta1a$ increased [H^3]-ryanodine binding and RyR1 channel activity (Rebbeck et al., 2011). Nevertheless, the $Ca_v\beta1a$ fails to co-localize with RyR in *dysgenic* myotubes (Neuhuber et al., 1998), consistent with the notion that interactions between $Ca_v\beta1a$ and RyR are contingent on the presence of the $Ca_v1.1$ L1-2 AID.

While evidence that the $Ca_v\beta1a$ interacts with the $Ca_v1.1$ at the AID is conclusive, other points of contact between the $Ca_v1.1$ and $Ca_v\beta1a$ have also been postulated. Notably, a M245A mutation in $Ca_v\beta2a$ ABD, which reduces its affinity for $Ca_v2.1$ 65-fold, has no discernable effect on $Ca_v2.1$ Ca^{2+} currents, suggesting the presence of other points of contact between the $Ca_v\beta2a$ and $Ca_v2.1$ that are important for modulating gating of the channel (Maltez et al., 2005). Another example is the SH3 domain of $Ca_v\beta1a$, which is essential for function of $Ca_v1.1$, but is found distant from the interaction with the AID in the crystal structure (Dayal et al.; Opatowsky et al., 2004). As the $Ca_v\beta1a$ and the L2-3 region of $Ca_v1.1$ appear to act in similar ways to support EC coupling and the formation of tetrads, it is reasonable to predict a coordination between the $Ca_v\beta1a$ and the L2-3 region, and domain prediction software predicts the presence of four SH3 binding domains in the L2-3 loop of $Ca_v1.1$. However, whether any of these predicted SH3 binding domains has any relevance for EC coupling remains to be seen, and no interaction between the $Ca_v1.1$ L2-3 and the $Ca_v\beta1a$ has been reported. Thus to this point, the $Ca_v\beta1a$ and the AID, are the only known links between $Ca_v1.1$ and $Ca_v\beta1a$ required for EC-coupling.

The L3-4 and C-terminus of $Ca_v1.1$ may participate in EC coupling

In addition to the L2-3 and $Ca_v\beta1a$ subunit, the small cytoplasmic loop between the TMIII and TMIV (L3-4) has been postulated as a site involved in EC coupling as it is the locus in mutations of the DHPR linked with malignant hyperthermia (MH) (Carpenter et al., 2009; Monnier et al., 1997). Associated primarily with mutations in the RyR1, MH is a potentially lethal pharmacogenic disorder of skeletal muscle characterized by uncontrolled increase in muscle activity and heat production after exposure to volatile anaesthetics and depolarizing muscle relaxants (Bandschapp and Girard, 2012). These mutations in RyR1 are thought to decrease the sensitivity of RyR1 to inhibition and increase its resistance to inactivation, resulting in excess Ca^{2+} release (Yang et al., 2003). As mutations in the L3-4 region of $Ca_v1.1$ are implicated as a cause of MH, an interaction between the L3-4 region and the RyR1 in EC coupling has thus been inferred (Pirone et al., 2010). Biochemical studies have indicated that a peptide of the L3-4 region binds to the RyR1 at a site either adjacent or overlapping the region of the RyR1 that directly interacts with the L2-3 region, strengthening an argument for the involvement of the L3-4 in EC-coupling (Leong and MacLennan, 1998). Functional analysis of a R1086H mutation in the L3-4 region expressed in dysgenic myotubes indicated the mutation caused a hyperpolarizing shift in the activation of Ca^{2+} transients (Pirone et al., 2010). Nevertheless, chimera analysis using the highly divergent neuronal $Ca_v2.1$ L3-4 region in the $Ca_v1.1$ backbone showed the chimera trafficked less well to the membrane, and displayed more sensitivity to the L-type Ca^{2+} channel agonist Bay K 864, but retained its E-C coupling efficiency. Thus, the L3-4 region is not directly important to EC coupling

but rather is believed to be involved in supporting gating transitions during EC coupling (Bannister et al., 2008b).

Evidence for the influence of the C-terminus of the $Ca_v1.1$ on EC coupling has been conflicting. The C-terminus has been reported to directly interact with RyR1 at residue (AA1393-1527) (Sencer et al., 2001), and interrupt the binding of [H^3] ryanodine to RyR1 (Slavik et al., 1997), suggesting a possible role in EC coupling. However, it should be noted that in our hands, the C-terminus of $Ca_v1.1$ shows auto-activation activity in yeast 2-hybrid assays and immunoprecipitates with negative controls, suggesting that the domain may simply bind promiscuously (Linsley 2011, data not shown). Nevertheless, studies using FRET probes fused to the C-terminus and L2-3 of $Ca_v1.1$ produced significantly reduced resonance transfer efficiency when expressed in *dysgenic* myotubes missing DHPR than in *dyspedic* myotubes missing RyR1 (Polster et al., 2012). Thus the C-terminus has an influence on conformational structure of the $Ca_v1.1$-RyR1 complex, an observation in accord with the finding that C-terminal domains tagged with biotin were inaccessible to streptavidin in *dyspedic* myotubes, but not dysgenic myotubes (Lorenzon et al., 2004). Yet how this influence on conformational structure relates and whether it has a direct effect on EC coupling remains to be determined.

The ryanodine receptor sends retrograde signals in EC-coupling

Though the RyR1 clearly participates in orthograde EC coupling as the Ca^{2+} release channel, evidence has also accumulated that the RyR1 can affect EC-coupling by retrograde signaling back to the DHPR. This phenomenon was first discovered when the

L-type Ca^{2+} currents in *dyspedic* myotubes that were missing RyR1 were found to be substantially smaller than those in wild type siblings (Nakai et al., 1996). The retrograde effect was further observed in the presence of a Ca^{2+} chelator, and was found to require the L2-3 region of the $Ca_v1.1$, suggesting it is the result of direct protein-protein interactions between $Ca_v1.1$ and RyR1 (Grabner et al., 1999; Nakai et al., 1998). Further support for retrograde coupling came from the finding that exposure to high concentrations of ryanodine, which lock RyR1 in a permanently inactivated state, result in a 2 nm decrease in distance between adjacent DHPR particles in a tetrad (Paolini et al., 2004). The mechanism of retrograde coupling remains poorly understood, but appears to be integral in EC coupling as mutations that result in MH susceptibility, are found to alter the retrograde signal from RyR1 to DHPR, delaying the inactivation of the DHPR (Esteve et al., 2010).

In summary, while it is clear from ablation, substitution and mutagenesis experiments that some regions of the DHPR are more critical to EC coupling than others, it is important to acknowledge the complexity involved in this process. Evidence so far on the mechanism of EC coupling support the view of multiple "hot spots" in the complex that appear necessary for EC coupling, but expose the necessity of a more nuanced understanding of EC coupling than simply the necessity of region A of DHPR interacting with region B of the RyR1.

MECHANISMS FOR TRAFFICKING DHPR

Another way that the function of the DHPR in EC coupling can be affected is by controlling the expression level and targeting of the DHPR complex to the triad. A plethora of studies have focused on the trafficking of Ca_vs to the membrane in tissue or *in vitro* and have revealed a multitude of mechanisms at work, but fewer have focused specifically on $Ca_v1.1$ in skeletal muscle. While parts of or all of these mechanisms may be involved in the trafficking of the $Ca_v1.1$ to the triad, it is important to note that differentiated skeletal muscle is an unique cell type with unique trafficking requirements for membrane bound proteins. As such, the following will first review our knowledge of the process by which EC-coupling proteins are trafficked, and then focus on how trafficking and targeting of the DHPR to triads can regulate the function of the $Ca_v1.1$.

The unique cellular biology of skeletal muscle

Myofibers are some of the largest cells in organisms and contain myofilaments responsible for contraction distributed evenly throughout the muscle cell. Since neuronal activation of myofibers typically results in contractions within hundreds of milliseconds and a dramatic rise in cytosolic Ca^{2+} is required for initiation of myofilament sliding, there is a need for myofibers to have mechanisms for quick and simultaneous increase in Ca^{2+} throughout the cell. This is achieved by tubular infoldings of the plasmamembrane into the interior of myofibers called transverse tubules (t-tubules) intersecting with cisternae of SR that contain high levels of Ca^{2+} at junctions called triads. Thus, action potentials initiated at the neuromuscular junctions quickly invade the t-tubules to initiate

release of Ca^{2+} from the SR via the interaction of the DHPR in the t-tubule and RyR1 in the SR at triads. Myofibers, however, start out as spherical mononucleated myoblasts that lack t-tubules and triads. During myofiber differentiation, the Golgi apparatus disperses through the cell into Golgi elements both perinuclear and distributed throughout the cell (Tassin et al., 1985). At the same time the SR and the t-tubules begin to form (Flucher et al., 1993; Franzini-Armstrong, 1991). The SR is a complex network of smooth membrane cisternae and tubules that completely surrounds the myofilaments and is presumably contiguous with the ER. RyR1 resides in SR cisternae at triads and the cisternae at adjacent triads are connected by longitudinal SR that run parallel to the myofilaments, (Fig. 1-2). The SR contains unique protein signatures, and even subdomains of proteins (Rossi et al., 2008), yet how proteins are targeted to different regions of the SR is not clear.

Given the specialized architecture of the myofiber as well as the dramatic reorganization of the secretory machinery during differentiation of myotubes, how membrane proteins are targeted has been an ongoing and unresolved topic of research. The expression of viral envelope glycoproteins containing temperature sensitive mutations that allow arrest at various points in the secretory pathway has helped establish a trafficking pathway for membrane bound proteins through the myofiber. These studies demonstrated that under unpermissive temperatures, viral proteins could be found arrested in both the ER and the SR (Rahkila et al., 1996; Rahkila et al., 1998; Ralston et al., 1999). Surprisingly, when temperatures were shifted to permissive conditions while ER budding was blocked pharmacologically, viral proteins were still found to be able to move throughout the SR, indicating that the ER and SR membranes are continuous

(Rahkila et al., 1996). When viral proteins were allowed to traverse the entire muscle fiber under permissive conditions they were found to accumulate in the t-tubules, suggesting the viral particles followed a trafficking route from the ER/SR to the t-tubules (Rahkila et al., 1996). This ER/SR trafficking pathway has become the accepted route for trafficking of SR resident proteins such as SERCA (McFarland et al., 2010), which does not appear to receive Golgi processing (Karin and Settle, 1992). However, the presence of Golgi throughout the myofiber (Ralston et al., 1999) and the existence of proteins involved in glycosylation, folding, and export to the Golgi found throughout the SR, indicates a trafficking pathway for t-tubule resident proteins through the ER/SR and local Golgi may be used by t-tubule resident proteins (Kaisto and Metsikko, 2003; Rahkila et al., 1996; Volpe et al., 1992). Intriguingly, while multiple studies (Protasi et al., 1998; Schredelseker et al., 2009; Schredelseker et al., 2005) have recognized the importance of expression and targeting of the DHPR to triads, the path by which the DHPR finds its way to the triad has not been described, and represents another way the cell might regulate EC coupling.

The C-terminus of $Ca_v1.1$ contributes to trafficking of the DHPR complex

Similar to its ability to directly regulate EC coupling, how the C-terminus of $Ca_v1.1$ functions in targeting the $Ca_v1.1$ to the membrane is ambiguous. The C-terminus of $Ca_v1.1$ is proteolytically cleaved midway through the cytoplasmic tail, though the cleavage does not seem to affect EC coupling (Beam et al., 1992; De Jongh et al., 1989). Further deletions proximal to the proteolytic site, however, progressively reduce $Ca_v1.1$ – GFP expression in dysgenic myotubes (Proenza et al., 2000). A kinase-anchoring protein

(AKAP15) has been found to directly interact with the C-terminus of $Ca_v1.1$, and is thought to anchor $Ca_v1.1$ in the membrane (Hulme et al., 2002). Yet the interaction site in the C-terminus of $Ca_v1.1$ is distal to the proteolysis site, indicating for an anchoring mechanism to occur, the distal C-terminus would need to reattach to the $Ca_v1.1$ after proteolysis (Hulme et al., 2005). The C-terminus of $Ca_v1.1$ contains multiple other protein interaction motifs allowing interactions with the Ca^{2+} sensor calmodulin (CaM) (Pate et al., 2000), Homer (Feng et al., 2002), and JP-45 (Anderson et al., 2006), but whether such interactions regulate trafficking of the $Ca_v1.1$ remains unknown. Additionally, there is biochemical evidence that the C-terminus may direct interact with the RyR1 (Sencer et al., 2001; Slavik et al., 1997), but the physiological significance of these interactions or whether they mediate anchoring between the $Ca_v1.1$ and RyR1 has not been determined.

Further evidence of the importance of the C-terminus in promoting expression levels of the $Ca_v1.1$ in triads came from chimera studies. Using chimeras of regions of the triad targeting-deficient $Ca_v2.1$ in the $Ca_v1.1$ backbone, the C-terminus of $Ca_v1.1$ was found to be critical for trafficking of the chimera to triads (Flucher et al., 2000b). Nevertheless, while these experiments demonstrate the necessity of the C-terminus in trafficking of the $Ca_v1.1$ to triads, the C-terminus alone does not appear to be sufficient for trafficking to triads. A chimera of the highly divergent from $Ca_v3.2$ with both the L2-3 and the C-terminal trafficking domain from $Ca_v1.1$ failed to restore EC coupling in dysgenic myotubes (Wilkens and Beam, 2003). Furthermore, adding the C-terminus to a I-II domain hemichannel did not increase its membrane expression or triad targeting properties, but co-expression of the I-II and III-IV (containing the C-terminus)

hemichannels restored both triad expression and EC coupling (Flucher et al., 2002). Thus the C-terminus is clearly important in facilitating expression of the $Ca_v1.1$, but the C-terminus alone is not sufficient to target a protein to triads.

$Ca_v\beta1a$ is required for normal trafficking of the DHPR complex

$Ca_v\beta$ has been shown to be critically important for expression of the Ca_v in the membrane (reviewed in Buraei and Yang, 2010 and Dolphin, 2012). Heterologous expression studies with multiple $Ca_v\beta$ isoforms have shown that these subunits promote expression of the Ca_v at the membrane and potentially help fold the Ca_v in the process, suggesting that $Ca_v\beta$ subunits act as chaperones for $Ca_v1.1$ (Almagor et al., 2012; Buraei and Yang, 2010; Dolphin, 2012). In skeletal muscle, $Ca_v\beta1a$ knockout mutants show reduced membrane expression of $Ca_v1.1$ in skeletal muscle of both mice (Gregg et al., 1996) and zebrafish (Schredelseker et al., 2005). Yet the $Ca_v\beta1a$ subunit does not localize to triads in *dysgenic* myotubes, and requires the presence of $Ca_v1.1$ for proper trafficking (Flucher et al., 1991; Neuhuber et al., 1998). Apparently other $Ca_v\beta$ subunits are also capable of directing $Ca_v1.1$ to triads since expression of $Ca_v\beta2a$, the ancestral housefly $Ca_v\beta_M$ or Ca_v β3 in *relaxed* myotubes that are nulls for fully $Ca_v\beta1a$ restored expression of $Ca_v1.1$ in triads, (Schredelseker et al., 2009). Thus, the $Ca_v\beta1a$ cannot intrinsically promote triad targeting of the $Ca_v1.1$, yet is required for normal $Ca_v1.1$ trafficking.

There are several hypotheses that can account for how $Ca_v\beta$ increases membrane expression of Ca_v. One hypothesis is that the Ca_vs contain an ER retention signal in the L1-2 region that is blocked upon binding of the $Ca_v\beta$ at the AID. Consistent with this hypothesis, tagging of the *Shaker* K^+ channel with the L1-2 region from $Ca_v1.2$ or $Ca_v2.1$

severely decreases its expression at the membrane, while the co-expression of $Ca_v\beta3$ prevents this effect (Bichet et al., 2000). Moreover, deletion of the L1-2 region from $Ca_v1.2$ increases its expression at the membrane (Bichet et al., 2000). Nevertheless, tagging of membrane proteins such as CD8 (Cornet et al., 2002) or CD4 (Altier et al., 2010) to the $Ca_v1.2$ L1-2 region does not restrict its expression to the ER. Furthermore, a precise ER retention signal has not been identified to date.

A more recent study put forth evidence towards the hypothesis that the $Ca_v\beta1$ increases membrane expression of $Ca_v1.2$ by preventing the entry of the channel into the endoplasmic reticulum-associated degradation pathway complex (ERAD) (Altier et al., 2010). Accordingly, in mammalian culture cells without the $Ca_v\beta1$, $Ca_v1.2$ underwent ubiquitination and targeting to the ERAD complex, yet expression of $Ca_v\beta1$ or treatment with the proteasome inhibitor MG132 prevented this degradation and rescued membrane expression (Altier et al., 2010). It remains to be seen whether this mechanism is conserved with $Ca_v1.1$ in skeletal muscle.

PROTEINS REQUIRED FOR FORMATION OF TETRADS OF DHPRs

Once properly trafficked to the triadic region of the t-tubules, DHPRs are organized into tetrads with each tetrad in apposition to every other RyR1 tetramer in the triadic region of the SR (Nakai et al., 1997), however a mechanistic understanding of tetrad formation is lacking. Despite years of research on EC coupling and the proteins that affect EC coupling, the only non-$Ca_v1.1$ proteins that have been shown to affect tetrad formation are the $Ca_v\beta1a$ and the RyR1. Freeze fracture EM of *relaxed* mutants has shown that although $Ca_v1.1$ is trafficked to the triads, it does not align in orthogonal

arrays opposite the RyR1 feet in tetrads (Schredelseker et al., 2005). Expression of $Ca_v\beta 2a$ or the ancestral housefly $Ca_v\beta_M$ in *relaxed* myotubes fully restored expression of $Ca_v1.1$ in triads and charge movement of the DHPR, but only partially restored tetrad formation and EC coupling (Schredelseker et al., 2009). Furthermore, in a more recent report, expression of the neuronal $Ca_v\beta 3$ in *relaxed* myotubes was found to restore formation of tetrads, but only marginally restored the ability of the $Ca_v\beta 3$ to support normal charge sensing of the DHPR, indicating the charge sensing and tetrad formation properties of $Ca_v\beta$ can be separated (Dayal et al., 2013). Thus, it appears there are sequences in $Ca_v\beta 1a$ that are specifically required for normal tetrad formation and EC coupling that are distinct from those that support normal charge sensing (Schredelseker et al., 2009). Sequences in the L2-3 of $Ca_v1.1$ have also been found that are required for tetrad formation and EC coupling (Beam and Bannister, 2010; Takekura et al., 2004), however how these two distinct regions of the DHPR interact to facilitate tetrad formation remains unknown.

The other known component required for tetrad formation is the RyR1, which must be present to give EC coupling. Mouse *dyspedic* myotubes that are missing RyR1 display trafficking of DHPRs to triads (Takekura et al., 1995a), but the DHPRs are unable to form tetrads (Protasi et al., 1998). Thus the presence of the RyR1 may act as a template and anchor for $Ca_v1.1$ for tetrad formation. Direct interactions between $Ca_v\beta 1a$ (Rebbeck et al., 2011) and/or L2-3 of $Ca_v1.1$ (Proenza et al., 2002) and/or the C-terminus of $Ca_v1.1$ (Sencer et al., 2001) and RyR1 are likely to mediate the interaction with the DHPR to facilitate tetrad formation, but direct evidence of the contributions of each interaction has not yet been assayed.

ACCESSORY PROTEINS INVOLVED IN MODULATING EC COUPLING

The EC coupling complex contains many other accessory proteins that modulate function and expression of the complex. Some proteins that have been linked to the EC coupling complex, such as CaM, have not been found to show a clear physiological affect on DHPR and may work in more subtle ways (Tang et al., 2002). Thus, for the sake of brevity, I review here only the proteins that have a clear physiological effect on EC coupling.

Effects of accessory proteins Gβ1γ2, Rem, and JP-45 on EC coupling

The EC coupling complex is susceptible to modulation by signaling proteins that precisely control and fine-tune Ca^{2+} release by complex feedback mechanisms of the muscle cell. These involve G proteins and G protein coupled receptors. The RGK (Rem, Rad, Gem/Kir) family of monomeric GTP-binding proteins inhibit Ca_vs through their interaction with $Ca_v\beta$ subunits (Buraei and Yang, 2010), and have been found to bind the GK domain in the $Ca_v\beta$ subunit, distinct from the site where $Ca_v\beta$ binds Ca_v1 (Beguin et al., 2007). The interaction of RGK with the GK domain of the $Ca_v\beta$ facilitates modulation of either the expression levels of the Ca_v in the membrane (Beguin et al., 2006; Beguin et al., 2001) or the gating of the Ca_v (Yang et al., 2007). These dual modes of action are reminiscent of the dual function of the $Ca_v\beta$, and inhibition of the Ca_v by RGKs requires co-expression of $Ca_v\beta$ (Beguin et al., 2001). RGKs also directly interact with members of the adaptor protein family 14-3-3 and CaM (Beguin et al., 2005a; Beguin et al., 2005b).

Abolishing these interactions leads to nuclear accumulation of RGK proteins, suggesting 14-3-3 and CaM modulate RGKs, and by extension Ca_vs, by regulating the localization of the RGKs (Beguin et al., 2006; Beguin et al., 2007; Mahalakshmi et al., 2007).

Rem, an RGK expressed in skeletal muscle, has been reported to inhibit Ca^{2+} release by the SR in C2C12 myoblasts in response to depolarization (Finlin et al., 2003). Furthermore, expression of Rem in myotubes reduced the frequency of electrically evoked contractions, reduced voltage dependent Ca^{2+} release from the SR, and the expression of $Ca_v1.1$ in triads. However, Rem did not affect the voltage dependence of charge movement, indicating that Rem modulates expression of the DHPR in the membrane (Bannister et al., 2008a). The mechanism of how Rem modulates the surface expression of the $Ca_v1.1$ in skeletal muscle remains to be determined, but experiments in which Rem and the $Ca_v1.2$ are heterologously expressed in HEK293 demonstrate that the surface expression of the $Ca_v1.2$ is reduced by enhancement of dynamin-dependent endocytosis (Yang et al., 2010b).

Another signaling protein reported to have effects on EC coupling is Gβ1δ2. G protein coupled receptors (GPCRs) are a family of plasma membrane receptors involved in transduction of extracellular signals into cellular responses. Activation of GPCRs by extracellular agonist results in activation of two intracellular signaling molecules, Gα-GTP and a dimer of Gβδ. Ca_vs have been widely reported to be sensitive to modulation by the many isoforms of Gβδ, in a variety of ways (Buraei and Yang, 2010; McCudden et al., 2005). Expression of Gβ1δ2, but not Gβ2δ2, Gβ3δ2, or Gβ4δ2, in mouse skeletal muscle was reported to show a drastic reduction of L-type current, but no reduction in intramembrane charge movement, indicating the effect was independent of expression

levels of DHPR in the triad and consistent with regulation of the channel properties of calcium channels (Weiss et al., 2010). Nonetheless, the mechanism by which the Gβδ modulates Ca_vs is still unknown. Furthermore, the context in which either Gβ1δ2 or Rem might be up or downregulated in order to modulate the EC coupling remains unknown.

In contrast to the cytosolic signaling proteins Rem and Gβ1δ2, feedback mechanisms mediated by membrane bound anchoring proteins that can control of EC coupling have also been reported. The SR membrane protein JP-45 appears to act as an anchoring protein for the DHPR, and up or down-expression of JP-45 affects the functional expression of the DHPR in the EC coupling complex (Anderson et al., 2006). JP-45 binds Ca_vβ1a and the L1-2 and C-terminus of Ca_v1.1, and knockdown of JP-45 reduces charge movement by decreasing trafficking of Ca_v1.1 to the membrane. More recently, an investigation of the effects of JP-45 polymorphisms on MH populations found that two variants of JP-45 affected the functional properties of the Ca_v1.1, potentially explaining the variable phenotypes observed in MH susceptibility patients across different genetic background with the same RyR1 mutation (Yasuda et al., 2013). Yet, as with Gβ1δ2 and Rem, the functional context in which JP-45 modulates DHPRs remains unknown.

The endocytotic proteins Dynamin2 and Caveolin and EC Coupling

Once at the triadic t-tubule membrane of skeletal muscles, the amount of DHPR can be modulated by rates of turnover of the protein in the membrane and routing them into lysosomal or endosomal pathways. This process is mediated by the endocytic proteins dynamin and caveolin (Kumari et al., 2010). Caveolin-3 (Cav-3) is the muscle

specific caveolin isoform that localizes to small, uncoated plasma membrane pits called caveola, which mediate the sequestration of membrane-bound proteins to the endocytic pathway (Dowling et al., 2008; Nixon et al., 2005). Although Cav-3 mutations are implicated in human muscle diseases, referred to as caveolinopathies (Dowling et al., 2008), the process of caveolin mediated endocytosis is poorly characterized (Kumari et al., 2010). Nevertheless, Cav-3 has been reported to interact directly with L1-2 of $Ca_v1.1$, and dominant negative expression of Cav-3^{P104L} or expression of Cav-3 specific siRNA leads to significant reductions in L-type Ca^{2+} current by an as yet uncharacterized mechanism (Couchoux et al., 2011).

Dynamin is a GTPase that, upon stimulation by factors such as self assembly (Warnock et al., 1996) or SH3 domains (Gout et al., 1993), triggers fission, or "pinching off" of a budded vesicle from the parent membrane in both caveolin and caveolin–independent processes (Kumari et al., 2010; Marks et al., 2001; Sweitzer and Hinshaw, 1998). Mutations in Dynamin2, which is ubiquitously expressed, result in several muscle myopathies, though the mechanisms of Dynamin2 in muscle have not been characterized (Nance et al., 2012). Dynamin has been reported to interact with $Ca_v\beta$ to coordinate the endosomal pathway by an interaction mediated by the SH3 domain of $Ca_v\beta$ (Gonzalez-Gutierrez et al., 2007; Miranda-Laferte et al.). Isolated SH3 domain from $Ca_v\beta$ down-regulated membrane expression of $Ca_v1.2$, but this down-regulation was inhibited by co-expression of a dominant negative form of Dynamin in *Xenopus* oocytes (Gonzalez-Gutierrez et al., 2007). Additionally, the homodimerization of $Ca_v\beta$ driven by its SH3 domain, was found to be necessary for interaction with Dynamin2 and endocytosis of the $Ca_v1.2$, while the interaction of $Ca_v1.2$ with $Ca_v\beta$ reduced the oligomerization of the $Ca_v\beta$

(Miranda-Laferte et al.). Though a Dynamin-$Ca_v\beta$ interaction has thus far only been reported between the cardiac $Ca_v\beta$2a and Dynamin, interactions in skeletal muscle between Dynamin2 and $Ca_v\beta$1a are likely to also regulate endocytosis, as myopathies due to mutations in Dynamin2 result in defects in triad architecture and T-tubule organization (Cowling et al., 2011; Durieux et al., 2010).

The requirement of $Ca_v\beta$ in targeting (Schredelseker et al., 2005), function (Dayal et al., 2013), and endocytosis (Gonzalez-Gutierrez et al., 2007) of the Ca_v1 seems at first counterintuitive, but is likely to reflect the both importance of the $Ca_v\beta$ and its ability to act as a switchable effector for each of these disparate functions. Nevertheless, how these separate functions of the $Ca_v\beta$ are activated is still unknown. The crystal structure of the $Ca_v1.2$ AID domain in complex with the $Ca_v\beta$ indicates that the binding interface of the SH3 domain is obstructed, and would make a suitable candidate for a switch in $Ca_v\beta$ conformational states allowing Dynamin to bind and activate endocytosis (Chen et al., 2004; Opatowsky et al., 2004; Van Petegem et al., 2004). As removal of DHPR from triads by endocytosis is a delicate process that must balance the need to remove old and non-functional channels with the necessity of maintaining a pool of functional DHPRs at the triad, resolving the mechanisms of dynamin and Cav-3 mediated endocytosis is critical to our understanding of the EC coupling complex.

CONCLUSION

In contrast to the expansive wiring and complexity that underlie the vast array of neuronal circuits that generate and modulate vertebrate behaviors, the final step of excitation and contraction of muscle is relatively similar across all vertebrate behaviors.

This evolutionarily fine-tuned machine has been adapted to allow vertebrates of all kinds the ability to perform the most amazing motility behaviors. These include the muscles of a cheetah that allow it to run from 0 to 60 mile per hour in three seconds, the muscles of a salmon that propel it upstream from the ocean to its spawning site, and the muscles of a baseball slugger swing a bat to hit a 100 mph fastball into the seats. Without a direct interaction between the voltage sensing $Ca_v1.1$ and the RyR1 and the unique arrangement of these proteins in skeletal muscles that allows for an almost instantaneous increase in cytosolic Ca^{2+} in the interior of a muscle fiber, these amazing feats of movement would not be possible. While research in the past fifty years has made tremendous strides towards understanding EC coupling, our lack of a fundamental understanding of how the DHPR and RyR1 coordinate to allow Ca^{2+} release still needs to be elucidated. Furthermore, when nature does something well, it tends to repeat itself, and utilize similar mechanisms in other situations. Exciting new reports have indicated a DHPR-RyR interaction similar to skeletal muscle EC coupling, might also be present in neurons (Berrout and Isokawa, 2009; De Crescenzo et al., 2012; Lefkowitz et al., 2009), and may represent the next frontier in EC coupling research. Thus, through the continued research of the EC coupling complex, we can hope to not only understand critical unresolved mechanisms in basic biology of muscles and their diseases, but also explore similar processes in the CNS.

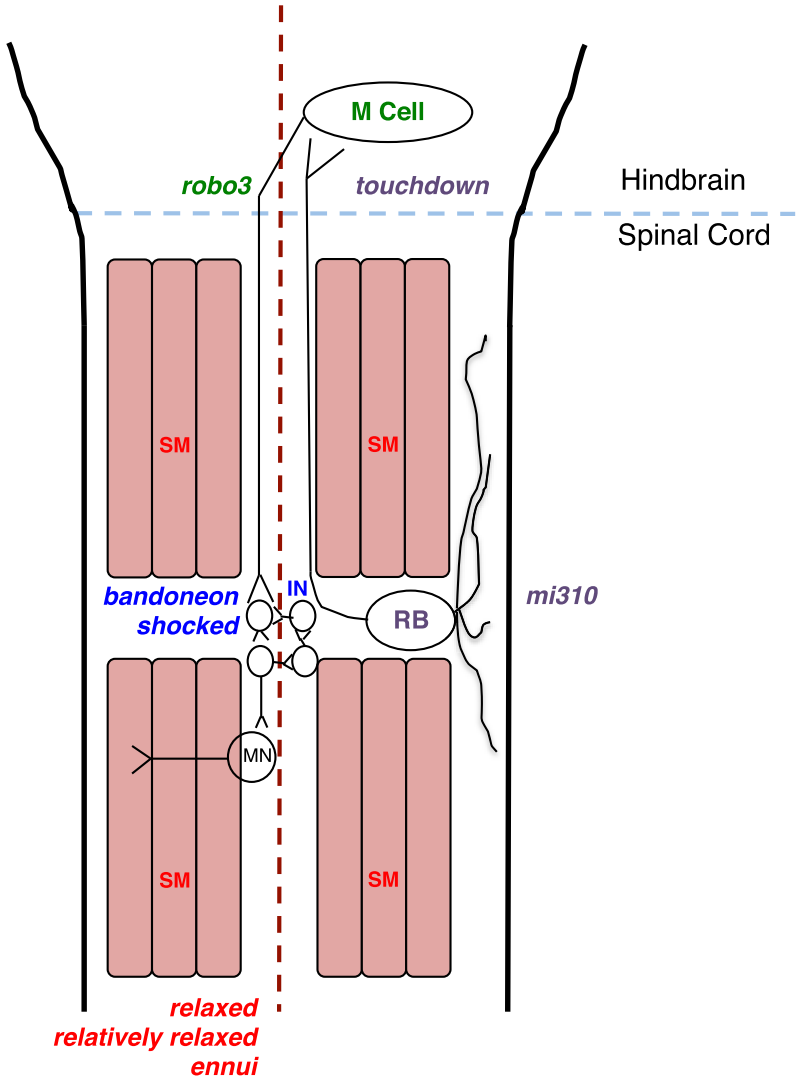

Figure 1-1. The basic swim circuit of a zebrafish embryo revealed by mutagenesis screen mutants. Schematic of a touch-evoked swimming circuit. Examples of zebrafish mutagenesis screen mutants that disrupt components of the circuit are labeled in respective colors. RB = Rohon-Beard sensory neurons (purple), M cell = Mauthner neurons (green), IN = interneurons (blue), MN = Motor Neurons (black), SM = Skeletal Muscle (red). See text for specific references. Dashed line indicates the dorsal midline, anterior is on top.

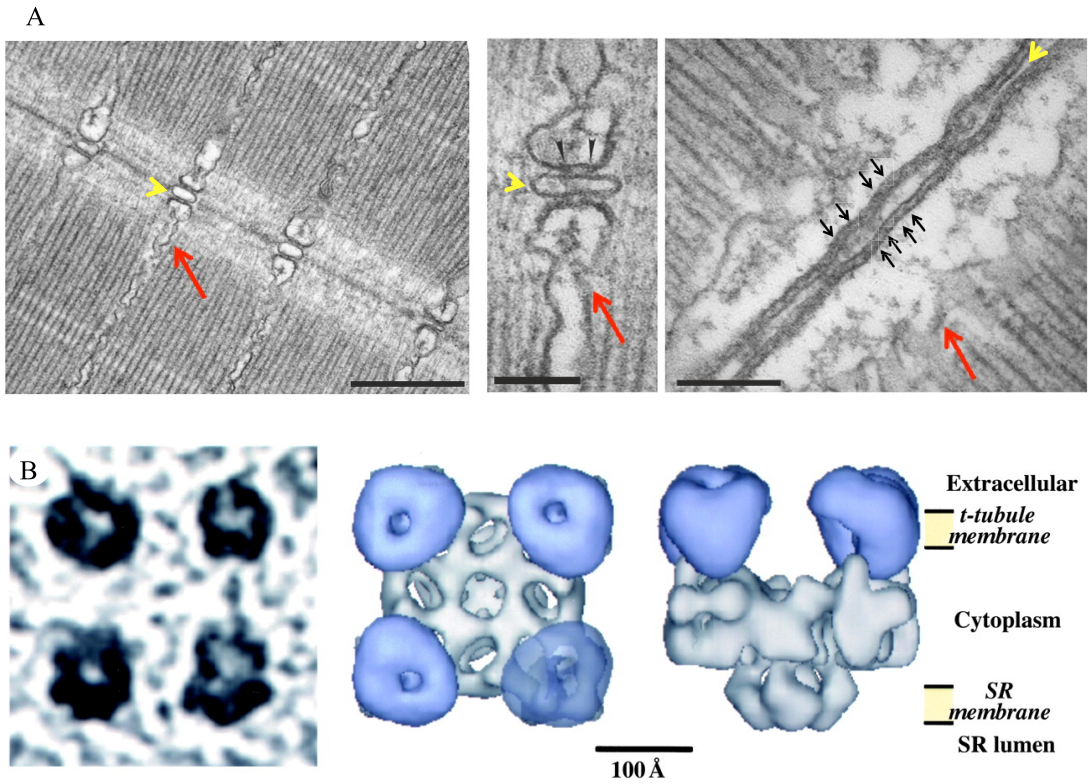

Figure 1-2. The EC coupling complex is located in the triadic junction between the t-tubules and the SR membrane. (A) Electron micrograph of the A-I junction of a zebrafish myofiber (Left, scale bar represents 500nm). In middle, a blown up micrograph of a single tetrad with RyR1 junctional feet marked with arrowheads (scale bar represents 250nm). On right, a cross section of the t-tubule with junctional feet along sides marked by black arrows (scale bar represents 250nm). The yellow arrowheads marks t-tubules and the red arrows mark the SR. Originally published in Horstick et al., 2013. (B) The structure of the DHPR-RyR1 EC coupling complex by freeze fracture electron microscopy (left). An end on (in middle) reconstruction of the EC coupling complex showing the extracellular face of the tetrad (in blue) coupled with the cytosolic domain of RyR1 in grey. On right, a side view of the fourfold axis of RyR1 in the image plane. Originally published in Serysheva et al., 2002.

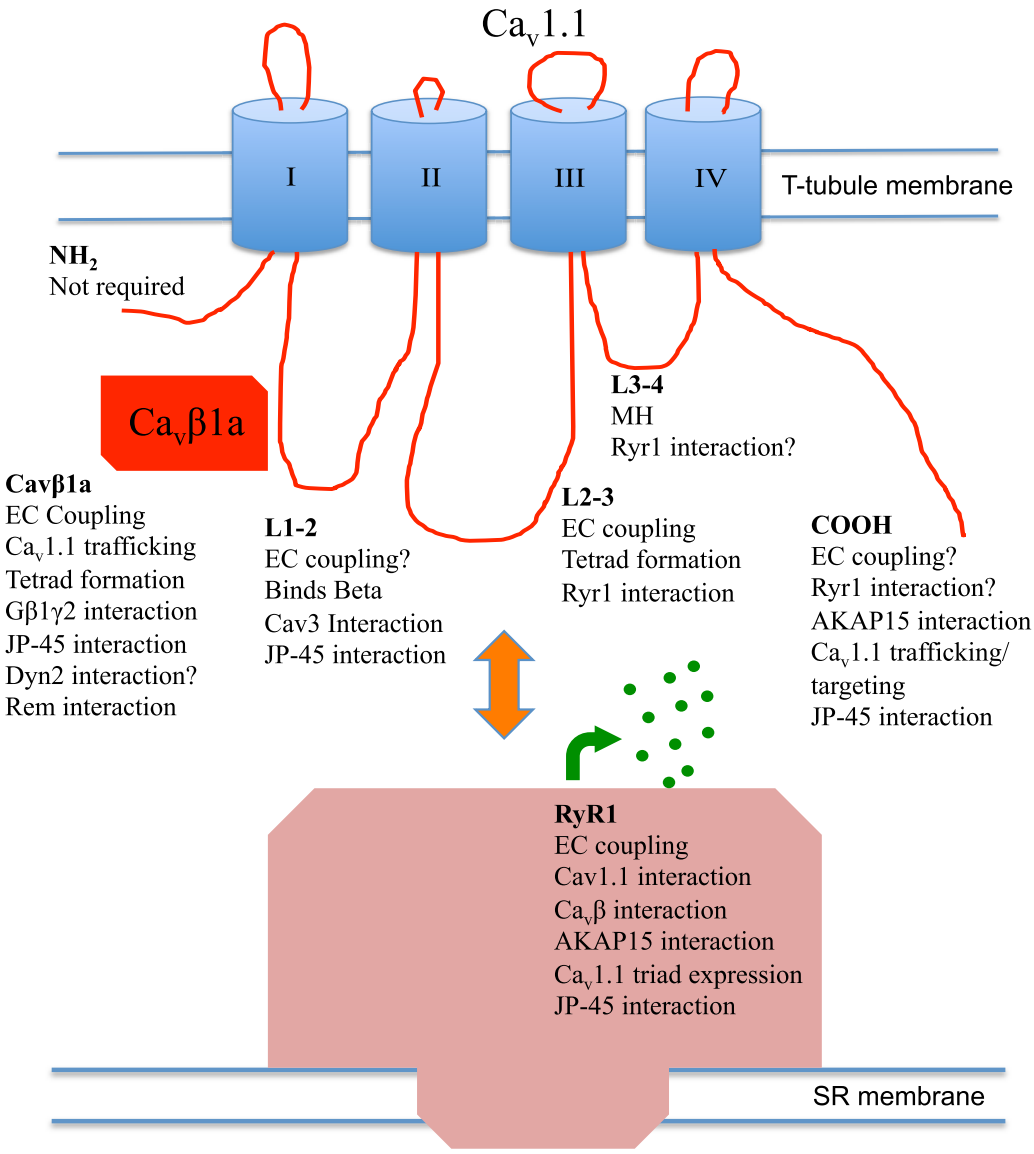

Figure 1-3. Schematic representation of the EC coupling complex with identified physiological roles of regions of the complex. The $Ca_v1.1$ (four blue cylinders connected by red loops) is localized to the t-tubule/sarcolema membrane where it directly interacts with the $Ca_v\beta1a$ (red polygon) and the RyR1 (pink polygon) which sits in the sarcoplasmic reticulum (SR) membrane to trigger Ca^{2+} release (green circles). See text for specific references.

CHAPTER II.

STAC3 IS A COMPONENT OF THE EXCITATION-CONTRACTION COUPLING MACHINERY AND MUTATED IN NATIVE AMERICAN MYOPATHY

Published as **Horstick, E.J., Linsley, J.W., Dowling, J.J.,** Hauser, M.A., McDonald, K.K., Ashley-Koch, A., Saint-Amant, L., Satish, A., Cui, W.W., Zhou, W, Sprague SM, Stamm D.S. Powell C.M. Speer M.C. Franzini-Armstrong C., Hirata H., Kuwada J.Y. (2013). *Nature communications 4*, 1952. Authors in bold contributed equally to this work.

Abstract

Excitation-contraction (EC) coupling, the process that regulates contractions by skeletal muscles, transduces changes in membrane voltage by activating release of Ca^{2+} from internal stores to initiate contraction. Defects in EC coupling are associated with muscle diseases. Here we identify Stac3 as a novel component of the EC coupling machinery. Using a zebrafish genetic screen, we generate a locomotor mutation that is mapped to *stac3*. We provide electrophysiological, Ca^{2+} imaging, immunocytochemical and biochemical evidence that Stac3 participates in EC coupling in muscles. Furthermore, we reveal that a mutation in human *STAC3* as the genetic basis of the

debilitating Native American myopathy (NAM). Analysis of NAM *stac3* in zebrafish shows that the NAM mutation decreases EC coupling. These findings enhance our understanding of both EC coupling and the pathology of myopathies.

Introduction

Muscle contractions are initiated by depolarization of the voltage across the plasma membrane resulting from synaptic release at the neuromuscular junction (NMJ). EC coupling is responsible for transducing the shift in the membrane voltage to increase cytosolic levels of Ca^{2+} that leads to contraction. Genetic defects in EC coupling components are associated with numerous congenital myopathies (Sewry et al., 2008) that appear in infancy and are characterized by a variety of symptoms that include muscle weakness, difficulty with breathing and feeding, slower development, muscle cramps, stiffness, and spasm and in some cases susceptibility to malignant hyperthermia, which is an adverse reaction to general anesthesia that can be fatal. Despite the debilitating nature of congenital myopathies, their pathology is for the most part poorly understood. Congenital myopathies are highly heterogeneous, and the genetic basis of many disorders is unknown.

In skeletal muscles EC coupling occurs at triads. Triads are junctions of the transverse tubules that are infoldings of the sarcomembrane and the sarcoplasmic reticulum (SR), an internal Ca^{2+} store. Changes in the membrane voltage of the transverse tubules are detected by the dihydropyridine receptor (DHPR), an L-type Ca^{2+} channel located in the transverse tubule membrane at triads (Adams et al., 1990; Rios and Brum, 1987; Tanabe et al., 1987). DHPR is composed of the principal α1s subunit also called $Ca_V1.1$ that contains the pore and several accessory subunits. Activated DHPR, in turn, is thought to directly activate ryanodine receptor 1 (RyR1) Ca^{2+} release channels in the SR membrane side of the triadic junctions (Bannister, 2007; Block et al., 1988; Paolini et al.,

2004; Takeshima et al., 1989). In mammalian skeletal muscles the DHPR also conducts extracellular Ca^{2+} to the cytosol but this is not required for EC coupling (Gonzalez-Serratos et al., 1982). Interestingly in teleost skeletal muscles EC coupling is similarly independent of Ca^{2+} influx from the exterior and the DHPR appears to have evolved so that it no longer conducts Ca^{2+} (Schredelseker et al., 2010). Activation of RyR1 leads to release of Ca^{2+} from the SR to the cytosol and subsequently to contraction mediated by the contractile machinery.

EC coupling involves a complex of proteins localized to triads that include DHPR and RyR1. Although DHPR and RyR1 are well studied, the identity and roles of other components of the complex, how EC coupling is regulated, and how the triadic molecular complex is established are poorly understood. Some of the other components of the triadic complex include FKBP12, triadin, junctin and calsequestrin. Triadin, junctin and calsequestrin are SR proteins that regulate RyR1 from the luminal side of SR (Beard et al., 2004; Chopra et al., 2009; Knollmann et al., 2006). FKBP12 is an immunophilin, an immunosuppressive drug binding protein, that co-purifies and co-immunoprecipitates with RyR1 in striated muscles, and stabilize RyRs in their open state *in vitro* (Brillantes et al., 1994; Jayaraman et al., 1992). Two other cytosolic proteins that interact with EC components are SepN1 and calmodulin (CaM). SepN1 is a selenoprotein that co-immunoprecipitates with RyR1a and is associated with myopathy (Moghadaszadeh et al., 2001) and is required for formation of slow twitch muscles in zebrafish (Jurynec et al., 2008). CaM can bind RyR and DHPR and modify EC coupling (Halling et al., 2006). Despite the identification of these factors, the mechanisms for how they regulate EC coupling is poorly understood. These analyses illustrate the complexity of the EC

coupling complex and its regulation, and suggest that a forward genetic strategy might be useful for identification of novel components for EC coupling.

Zebrafish have been useful for the analysis of a myriad of biological processes both because they are amenable to forward genetic screens and *in vivo* manipulations (Driever et al., 1996; Haffter et al., 1996). Pertinent to a genetic analysis of EC coupling, zebrafish muscles can also be analyzed *in vivo* with electrophysiology and live imaging (Buss and Drapeau, 2000; Schredelseker et al., 2005). We took advantage of these features to identify a zebrafish mutation in which EC coupling was defective. The gene responsible for the mutant phenotype encoded for Stac3, a putative muscle specific adaptor protein. Finally we found that a missense mutation in human *STAC3* is responsible for the debilitating, congenital Native American myopathy (NAM) (Stamm et al., 2008a; Stamm et al., 2008b).

Materials and Methods

Animals and Behavioral Analysis

Zebrafish were bred and maintained according to approved guidelines of the University Committee on Use and Care of Animals at the University of Michigan. The *stac3*^{mi34} mutation was isolated from a mutagenesis screen using procedures previously reported. Embryonic behaviors were video-recorded mounted on a stereomicroscope and analyzed with ImageJ. In some cases the heads of embryos were embedded in low melting temp agar with the trunk and tail free to move. Where indicated data were analyzed by t-tests.

Electrophysiology

Previously published protocols were followed to electrophysiologically record from zebrafish embryonic muscles (Saint-Amant and Drapeau, 1998). For recordings embryos were partially curarized (6 μM d-tubocurarine). Recordings of muscle responses to touch were made with patch electrodes (3-10 MΩ) filled with solution containing 105 mM K gluconate, 16 mM KCl, 2 mM $MgCl_2$, 10 mM Hepes, 10 mM EGTA and 4 mM Na_3ATP at 273 mOsm and pH 7.2 and extracellular Evans solution (134 mM NaCl, 2.9 mM KCl, 2.1 mM $CaCl_2$, 1.2 mM $MgCl_2$, 10 mM glucose and 10 mM Hepes at 290 mOsm and pH 7.8) using an Axopatch 200B amplifier (Axon Instruments), low-pass filtered at 5 kHz and sampled at 1 kHz. Mechanosensory stimulation was delivered by ejecting bath solution from a pipette using a Picospritzer. Voltage dependence of contraction was performed in a similar fashion except embryos

were exposed to 50 μM d-tubocurarine, voltage steps delivered to muscle via voltage clamp and muscle contractions video-recorded at 60Hz. Muscle contractions to caffeine applied by a Picospritzer (10 psi, 1 sec) of dissected embryos were video-recorded and measured.

Ca^{2+} Imaging

One cell stage embryos were injected with a plasmid using α-actin promoter (Higashijima et al., 1997) (*α-actin:GCaMP3*) resulting in embryos that mosaically expressed *α-actin:GCaMP3* within skeletal muscle. 48 hpf embryos were genotyped by behavior. Prior to imaging, tricaine was removed and embryos allowed to recover in Evans for 10 minutes and treated with 200 μM N-benzyl-p-toluene sulphonamide to inhibit contraction for 5 minutes. 100 μM NMDA was added to initiate the swimming motor network (Cui et al., 2005). GCaMP3 expressing cells were frame scanned at 200Hz using the resonance scanner of a Leica SP5 confocal microscope. Confocal software was used to measure relative fluorescence intensity changes and kinetics of induced Ca^{2+} transients.

Immunolabeling

Wholemounted embryos were immunolabeled as described previously (Hirata et al., 2005). For labeling dissociated skeletal muscle fibers, 48 hpf embryos were incubated in collagenase type II (3.125 mg/ml in CO_2-independent medium) at 20°C for 1.5 h with the muscle fibers triturated every 30 min. Fibers were spun at 380*g* for 5 min, supernatant removed and fibers resuspended and allowed to settle on polyornithine coated coverslips.

Fibers were washed then fixed. Dissociated muscles were labeled using 0.25% detergent in the incubation solutions containing the following primary antibodies/toxin: 1/200 dilution of anti-RyR (34C IgG1, Sigma); 1/200 anti-$DHPR_{a1}$ (1A IgG1, Affinity BioReagents); 1/10 bungarotoxin-Alexa594 (Invitrogen); 1/500 anti-SV2; 1/200 anti-α actinin; and 1/200 anti-dystrophin (all from Iowa Hybridoma Bank). In some cases nuclei were labeled with 0.1% DAPI.

Positional Cloning of *stac3*

To identify the gene mutated in *stac3*^{mi34} mutants, the mutation was meotically mapped to PCR-scorable, polymorphic CA repeats as described previously (Shimoda et al., 1999) by scoring 2009 mutant embryos derived from appropriate mapping crosses. Flanking markers were identified located on linkage group 9; z1830 that was 0.21 cM north of *stac3*^{mi34} and z1663 that was 1.24 cM south. Analysis of the zebrafish genome database (http://www.sanger.ac.uk/Projects/Drerio/clones.shtml) revealed that z1830 was located in a small contig of assembled sequence (Scaffold 450) from the zV5 assembly of the sequenced genome that contained the *pcbp2* gene. A new marker (zh1) located in *pcbp2* mapped 0.11 cM north of *stac3*^{mi34}. A sequenced 156 kb BAC (CR848672) that contained *pcbp2* was identified and analyzed for potential genes with the gene prediction program, GENSCAN (http://genes.mit.edu/GENSCAN.html), and BLASTing predicted genes against the NCBI database (http://www.ncbi.nlm.nih.gov/BLAST). These were *pcbp2, kif5a, arp5* and a gene similar to *stac*. New markers, zh34 in *kif5a* (0.04 cM north), zh16 in *arp5* (0.04 cM south) and zh31 in the *stac*-like gene (no recombinants), were identified. The *stac*-like cDNA from wildtype and mutant embryos were isolated

and sequenced and the mutant cDNA contained an insertion that included an in frame stop codon. Analysis of genomic sequences determined that the *stac3*^{mi34} allele contained a missense mutation that transformed a splice donor site for the intron between exon 4 and exon 5 (GT to AT) that presumably lead to incorrect splicing and inclusion of the intron in the cDNA.

Mutant Rescue

Rescue of *stac3*^{mi34} behavior was performed by subcloning zebrafish *stac3*^{wt}, *stac3*^{mi34}, *stac3*^{NAM} or human *STAC3* into *phsp70-EGFP*. Zebrafish *stac3*^{NAM} construct was generated by site-directed mutagenesis. Constructs (10 ng/µl) were injected into one cell stage progeny of *stac3*^{mi34} carriers with a Nanoject II. At 48 hpf *stac3*^{mi34} mutant embryos were behaviorally identified and heat induced by switching them from water at 28.5^{0}C to 37^{0}C for 1 h. Following heat induction embryos were switched back to 28.5^{0}C and assayed 3 and 24 h later. Embryos with approximately 10% or more skeletal muscle fibers expressing EGFP were used for behavioral assays. Responses of embryos to touch were video-recorded and measured. For Ca^{2+} imaging of Stac3^{wt} or Stac^{NAM} expressing muscle fibers *phsp70:stac3*^{wt}*-mCherry* and *phsp70:stac3*^{NAM}*-mCherry* were generated along with *α-actin:GCaMP3*. Embryos were injected with a 1:1 mixture of a *stac3* construct and *α-actin:GCaMP3* each at 10ng/µl. Following heat induction embryos with skeletal muscle fibers expressing both constructs were selected for Ca^{2+} imaging.

Analysis of Maternal Transcripts by RT-PCR

The start of mid-blastula transition and earliest zygotic transcription is at 3 hpf in zebrafish (Kane and Kimmel, 1993). 50 embryos at 2 and 3 hpf each were placed in Trizol and RT-PCR was performed for *stac3* and *tuba1* (*tubulin α1*), a housekeeping gene that is maternally expressed (McCurley and Callard, 2008). Exon-overlapping primer pairs shown below were designed to amplify ~200bp fragments of cDNA from the 5' (representing exons 3-6) or 3' (exons 4-10) region of mature *stac3* message.

5' primer pair

forward: 5'-GGACGACAACACTGTGTATTTTGTGTATG-3'

reverse: 5'-GAACCCAGGAGGTATTTTGCCGAAGCATCT-3'

3' primer pair

forward: 5'-ACGGATGATTGTTCTCAATAATAAGTTTGC-3'

reverse: 5'-CGCAACAGATGACAAGAACAAGAAGCAG-3'

Antisense Morpholino Oligonucleotide Knockdowns

4.6 nL of 400 μM solutions of translation blocking antisense MO (GeneTools) or standard control MO were injected into recently fertilized embryos from crosses of *stac3*^{mi34} carriers using a Nanoject II. The sequence of the antisense stac3 MO was: 5'-TCATATTGAGC**CAT**CAGTCCAGC-3' with **CAT** corresponding the start ATG. For morphant rescue experiments 10 ng/μL of *α-actin:stac3-gfp* was coinjected along with the antisense MOs. Embryos were assayed for response to touch with forceps at 48hpf and subsequently fixed and assayed with anti-Stac3.

Polyclonal Antiserum Production and Purification

Full-length zebrafish Stac3 was expressed as a His-Sumo fusion protein in B21(DE3) cells (Invitrogen), and affinity-purified using Ni-NTA agarose. Protein was further purified by electrophoresis in a NuPAGE 4-12% SDS-PAGE Bis-Tris Gel and subsequent excision of appropriate Coomassie stained band. Rabbits were immunized with gel slices of purified fusion proteins. Antiserum was purified by passing through a Sulfolink column (Thermo) containing the immobilized fusion protein. Fragment of Stac3 that was bound by anti-Stac3 was identified as follows. Full-length *stac3* cDNA and the fragment that encodes amino acids 1- 63 were cloned in frame into pGADGT7 (Clontech), which contains an N-terminal HA tag and Gal4 activation domain. Each construct was transformed into Y2HGold Yeast using Yeastmaker Yeast Transformation system 2 (Clontech) and plated on appropriate auxotrophic media. Yeast was grown, harvested, and protein extracted with YPER yeast protein extraction reagent (Thermo). Protein samples were loaded for SDS-PAGE analysis, blotted onto nitrocellulose, and probed separately with anti-HA or anti-Stac3.

Western Analysis and Immunoprecipitation

50 *stac3*^{mi34} mutant and sibling embryos each were collected, lysed and the isolated protein loaded and separated by SDS/PAGE (Hirata et al., 2005). Anti-DHPR$_{a1}$ was used for immunoblotting at 1:500, anti-pan-RyR at 1:2000. Adult female fish were sacrificed using 0.1% tricaine, skeletal muscle dissected on dry ice, and total protein extracted. Protein lysate from an individual fish was immunoprecipitated using anti-

$DHPR_{a1}$ (1:100), or anti-pan-RyR (1:200) crosslinked with BS^3 (Thermo) to Protein G Dynabeads (Invitrogen).

Generation of Stable Transgenic Line

α-*actin:stac3-gfp* construct was injected at 20 ng/μl into the cytoplasm of embryos at the 1-cell stage. Fish were raised to adulthood and germline founders identified by screening F1 progeny for GFP fluorescence. GFP-positive offspring were raised to establish the transgenic line.

Mass Spectrometry and Data Analysis

Skeletal muscle lysates from 10 adult α-*actin:stac3-gfp* transgenic fish were pooled for immunoprecipitation with anti-GFP (Torrey Pines Biolabs Inc.) or Normal Mouse IgG. The pulldown fraction was separated using SDS-PAGE, and the fractions in the gel stained using Silver Stain Kit (Pierce). Thirteen bands appearing in the anti-GFP pulldown fraction lane but not in normal IgG pulldown lane were excised, washed with 25 mM ammonium bicarbonate followed by acetonitrile, reduced with 10 mM dithiothreitol at 60°C followed by alkylation with 50 mM iodoacetamide at RT, and digested with trypsin at 37°C for 4 hours. Mass spectrometry was performed by the University of Michigan Proteomics and Peptide Synthesis Core using a nano LC/MS/MS with a Waters NanoAcquity HPLC system interfaced to a ThermoFisher LTQ Orbitrap Velos. Peptides were loaded on a trapping column and eluted over a 75 μm analytical column at 350 nL/min; both columns were packed with Jupiter Proteo resin (Phenomenex). The mass spectrometer was operated in data-dependent mode, with MS

performed in the Orbitrap at 60,000 FWHM resolution and MS/MS performed in the LTQ. The fifteen most abundant ions were selected for MS/MS.

MS/MS samples were analyzed using Mascot (Matrix Science, London). Mascot was set up to search the ipi.DANRE.v3.75.decoy database (74790 entries). Mascot was searched with a fragment ion mass tolerance of 0.50 Da and a parent ion tolerance of 10.0 PPM. Carbamidomethyl of cysteine was specified in Mascot as a fixed modification.

Scaffold (version Scaffold_3.1.2, Proteome Software Inc., Portland, OR) was used to validate MS/MS based peptide and protein identifications. Peptides were identified at greater than 95% probability and proteins were identified if they contained at least two identified peptides with each peptide identified in the protein at greater than 95% probability. Peptide and protein probabilities were assigned by the Protein Prophet algorithm (Nesvizhskii et al., 2003). Proteins that contained similar peptides and could not be differentiated based on MS/MS analysis alone were grouped to satisfy the principles of parsimony.

Molecular Analysis of Native American Myopathy

The cohort of individuals with NAM was previously described (Stamm et al., 2008b). NAM subjects were of Lumbee Indian descent with congenital muscle weakness who demonstrate two of more of the following phenotypic characteristics: myopathic facies, susceptibility to malignant hyperthermia, kyphoscoliosis, and cleft palate. The probands were ascertained from the University of North Carolina at Chapel Hill Pediatric Genetics Clinic and from the Duke University Muscular Dystrophy Clinic. All data and samples were collected following informed consent of subjects; this study was approved

by the Duke University Medical Center and the University of North Carolina Institutional Review Boards. DNA was extracted from whole blood using the Puregene system (Gentra Systems, Minneapolis, MN) and stored in the laboratory of the Duke Center for Human Genetics.

Initially, each exon and the surrounding splicing regions of *STAC3* were screened in 3 NAM patients and 3 related individuals through PCR amplification and automated Sanger sequencing. After identification of the NAM mutation in exon 10 of *STAC3*, the entire cohort of available samples from NAM pedigrees was screened by exon amplification and sequencing for the mutation. In all, a total of 18 individuals from 5 Lumbee families were sequenced, as well as 3 unrelated unaffected Lumbee individuals. In addition, genomic DNA was screened from 2 neurologically normal control individuals (Coriell Institute NDPT006 and NDPT009) and from a collection of 111 adult subjects without evidence of neurological disease (Rainier et al., 2006).

Electron Microscopy

Transmission electron microscopy was performed as previously described (Block et al., 1988; Dowling et al., 2009). A minimum of 3 larvae per condition was examined.

RESULTS

The *mi34* zebrafish mutant is defective in EC coupling.

In order to identify new genes involved in the regulation of EC coupling, a forward genetic screen in the zebrafish was performed to isolate motor behavior mutants (Cui et al., 2005; Hirata et al., 2005; Hirata et al., 2004; Hirata et al., 2007; Zhou et al., 2006). One mutation, *mi34*, was autosomal recessive with mutants dying as larvae and exhibiting defective motor behaviors at early stages of development. Normally zebrafish embryos exhibited spontaneous slow coiling of the body starting at 17 hours post fertilization (hpf), touch-induced escape contractions of the body at 22 hpf and touch-induced swimming by 28 hpf (Saint-Amant and Drapeau, 1998). Mutants were defective in all three motor behaviors with reduced amplitude of spontaneous coiling, decreased touch induced escape contractions and ineffective swimming (Fig. 1a).

Aberrant behavior in mutants could be due to defects in the nervous system and/or skeletal muscles. If signaling within the nervous system were abnormal in mutants, then one would expect the output of motor neurons to muscles to be aberrant. To determine this, the synaptic response of muscles to tactile stimulation of the embryo was electrophysiologically recorded *in vivo*. Tactile stimulation initiated synaptic responses in both slow and fast twitch muscles in both wildtype sibling and mutant embryos. The evoked responses were comparable in amplitude, duration and frequency when measured with a low concentration of curare (see Methods) used to minimize muscle contraction (Fig. 1b; Fig, 2-2). In order to see if the mutant muscles would generate action potentials

in response to synaptic input, we examine muscle responses following sensory stimulation without curare, which was possible because contraction by mutant muscles is minimal. These recordings showed that mutant fast twitch muscles do respond with a burst of overshooting action potentials (Fig. 1c). Furthermore there were no obvious differences in the distribution of motor neuron terminals and muscle acetylcholine receptors (AChRs) between wildtype sibs and mutants when assayed with an antibody against SV2, a synaptic vesicle protein, and a-bungarotoxin that specifically binds AChRs (Fig 2-3). Thus the activity the nervous system and NMJ between wildtype and mutants are comparable and mutant muscles can initiate bursts of action potentials in response to synaptic input. Although we cannot rule of subtle changes, the severity of the behavioral phenotype is consistent with the mutation causing a defect in the muscle response to electrophysiological activation.

Activation of the NMJ leads to depolarization of the muscle membrane potential that in turn initiates muscle contraction. To examine how the mutation affects the relationship between muscle voltage and contraction, the membrane voltage of skeletal muscles was depolarized to various values and the amount muscles contracted was measured. Mutant muscles contracted much less than wildtype sib muscles at depolarized membrane potentials (Fig. 2-4). The decreased contraction to depolarizations could be due to a defect in EC coupling or a defect in the contractile machinery. However, the fact that mutant and wildtype sib muscles contracted similarly when exposed to caffeine, an agonist of RyRs, (Fig. 2-5) suggested that the contractile machinery was intact in mutants and that the store of Ca^{2+} in the SR was not grossly perturbed. Corroborating this finding, mutant muscles exhibited no obvious morphological defects early in development with

apparent normal distribution of contractile proteins and other muscle proteins (Fig 2-5). Furthermore myofibers appeared normal in electron micrographs of larval skeletal muscles in *mi34* mutants (Fig. 2-6 a). These findings pointed to a defect in EC coupling in mutant muscles.

The hallmark of EC coupling is the release of Ca^{2+} from the SR to the cytosol. EC coupling was directly examined *in vivo* by imaging Ca^{2+} transients in skeletal myofibers expressing the GCaMP3 Ca^{2+} indicator (Tian et al., 2009) during swimming. Swimming was evoked by application of NMDA, which activated the swimming network in the CNS (Cui et al., 2005). Ca^{2+} transients were greatly reduced in both mutant slow and fast twitch fibers (Fig. 2-6 b,c). Thus EC coupling in skeletal muscles was defective in the *mi34* mutants. Since EC coupling takes place at triads, reduced EC coupling in mutants could be due to abnormal formation of triads. However, longitudinal sections examined with TEM showed that there were triads at every intermyofibrillar junction with triads exhibiting comparable anatomy including two rows of feet in wildtype sibling and mutant muscles (Fig. 2-6 a). Although we cannot rule out a quantitative change in triadic anatomy, these data showed that the decrease in EC coupling in mutant muscles was not due to any obvious defect in triad anatomy.

The gene *stac3* is the basis for the *mi34* phenotype

A combination of meiotic mapping and analysis of zebrafish genome resources identified the gene responsible for the *mi34* phenotype as *stac3* (Fig. 2-7, for details see Methods), a gene similar to murine *stac* that encodes an adaptor-like protein of unknown function (Suzuki et al., 1996). *stac3* encodes for a putative 334 residue soluble protein

with an N-terminal cysteine rich domain (CRD) similar to the C1 domain found in Ca^{2+}-dependent protein kinase and two SH3 domains (Fig. 2-8 a). The mutant allele carried a point mutation that disrupted a splice donor site that led to the inclusion of intron 4 and a premature stop codon in the transcript. The mutation in *stac3* predicted a protein that was truncated within the N-terminal CRD suggesting that the *stac3*^{mi34} mutation was functionally null. Western blotting with an antibody generated against Stac3 that recognized a fragment of Stac3 consisting of the residues 1 to 63 (see Methods) revealed an approximately 49 kDa protein in wildtype embryos but no protein in mutants (Fig. 2-8b) suggesting that a truncated protein was not synthesized in mutants. *In situ* hybridization showed that skeletal muscles selectively expressed *stac3* during embryogenesis (Fig. 2-9). Labeling with anti-Stac3 confirmed that Stac3 was specifically expressed by skeletal muscles and revealed that Stac3 co-localized with the $DHPR_{\alpha 1}$ and presumably RyR1 at muscle triads in wildtype but was not expressed in mutant embryos (Fig. 2-8 c). These findings suggested that a mutation in *stac3* was responsible for defective EC coupling and that Stac3 was a component of the triadic molecular complex.

The molecular identity of the mutation was confirmed by mutant rescue experiments. Induced expression of *hsp70:stac3*^{wt}*-egfp* in mutant muscles rescued the behavioral phenotype and triadic localization of Stac3 whereas induced expression of *hsp70:stac3*^{mi34}*-egfp* did not (Fig. 2-10). Furthermore Ca^{2+} imaging of mutant muscles co-expressing *stac3*^{wt}*-mCherry* and *GCaMP3* showed that wildtype Stac3 could restore Ca^{2+} muscle transients in mutant embryos (Fig. 2-10 b,c). Given that Stac3 may be an adaptor protein and co-localizes with $DHPR_{\alpha 1}$ and RyR1, we examined whether Stac3 may be part of the triadic molecular complex. Indeed co-immunoprecipations with antibodies

against pan-RyR and $DHPR_{\alpha 1}$ both pulled down Stac3 from wildtype adult muscles (Fig. 2-11) indicating that Stac3 is part of the DHPR/RyR1 complex found at triads. This was confirmed by generating a transgenic line of zebrafish (*a-actin:stac3^{wt}-egfp*) that expressed Stac3-EGFP in skeletal muscles and using anti-GFP to immunoprecipitate Stac3-EGFP from lysates of skeletal muscle of adult transgenic zebrafish. Mass spectrometry-based protein identification found that $DHPR_{a1s}$, $DHPR_{a2d1}$, $DHPR_{b1}$, RyR1 and RyR3 immunoprecipitated with Stac3-EGFP (Table 1). Thus Stac3 is a component of the triadic complex that is required for EC coupling in skeletal muscles.

Although motor behaviors are greatly diminished in *stac3^{mi34}* mutants, they were not immotile. One possible reason for this might be the existence and action of Stac3 derived from maternally deposited *stac3* mRNA. In fact RT-PCR from 2hpf embryos (prior to zygotic expression (Kane and Kimmel, 1993)) found that *stac3* was maternally expressed (Fig. 2-12). To see if the residual activity of skeletal muscles in *stac3^{mi34}* mutants was due to Stac3 translated from maternal mRNA, we knocked down Stac3 by injecting a translation blocking antisense Morpholino oligonucleotide (MO) against *stac3* message into embryos from crosses between heterozygous carriers. Anti-Stac3 labeling showed that *stac3* antisense MO injected embryos did not express Stac3 in skeletal muscles (Fig. 2-12 b) confirming that the MO was effective. At 48 hpf wildtype embryos normally respond to tactile stimulation by swimming away. As expected from a cross between heterozygous carriers approximately 75% of the progeny injected with control MO responded to touch with swimming while 25% responded by slight muscle contractions (shivering) that failed to move the embryos effectively or were totally immotile (Fig. 2-12 c) indicative of the mutant phenotype. In antisense MO injected

embryos, however, there was a significant increase in embryos that were either immotile or shivered and decrease in embryos that swam compared with control progeny. Significantly the proportion of immotile embryos increased from approximately 5% of control MO injected progeny to almost 40% of antisense MO injected progeny. Furthermore, the morphant phenotype was rescued by coinjecting an expression plasmid for *stac3*^{wt} along with the antisense MO demonstrating that the increased defective motility observed was not due to an off-target effect of the antisense MO, but rather a specific knockdown of maternal *stac3*. This suggests that elimination of both maternal and zygotic Stac3 results in immotility.

A mutation in human *STAC3* causes a congenital myopathy.

The loss of Stac3 resulted in a progressive breakdown of myofibers during larval stages with apparent swollen SR observed by 7 dpf (Fig 2-13). Given the myopathic features of mutants we explored whether *stac3* mutations might cause congenital human myopathies. Human *STAC3* mapped to chromosome 12q13-14, and its specific location was within the previously defined genetic locus for the congenital Native American myopathy (NAM) (Stamm et al., 2008a; Stamm et al., 2008b). NAM is an autosomal recessive disorder found within the Lumbee Native American population of North Carolina that was characterized by a constellation of clinical features including congenital onset of muscle weakness, susceptibility to malignant hyperthermia (MH), multiple joint contractures and dysmorphic facial features including ptosis. Patient muscle biopsies revealed a non-specific myopathic pattern. Furthermore, 36% of afflicted individuals die by the age of 18. The genetic basis of NAM remained unsolved, though

the presence of susceptibility to MH as a clinical feature suggested a defect in a component of the EC coupling apparatus. To see if a mutation in *STAC3* was the basis for NAM, *STAC3* coding regions were sequenced in a cohort of 5 NAM families that included 5 affected and 13 unaffected individuals. As expected for an autosomal recessive disorder, all affected individuals were homozygous for a G>C missense mutation of base pair 1046 in exon 10 of the *STAC3* gene (Ensembl transcript ID ENST00000332782), while all obligate carriers were heterozygous. This mutation resulted in a tryptophan (W) to serine (S) substitution at amino acid 284 in the first SH3 domain (Fig. 2-14). The sequence change perfectly segregated with the NAM phenotype, and was not found in an additional three unaffected, unrelated Lumbee individuals (Fig 2-15), nor in 113 Caucasian control individuals. In addition, *STAC3* has been sequenced as part of the 1000 genome project, and this mutation has not been detected. This pattern of inheritance suggested that *STAC3* was the basis for the congenital myopathy.

Next the functional consequences of the W284S mutation was investigated in the zebrafish model system. The analogous W>S substitution was encoded in zebrafish *stac3* (*hsp70:stac3*^{NAM}*-egfp*) and expressed in *stac3*^{mi34} null mutant muscles to assay for phenotypic rescue. Unlike *stac3*^{wt}*-egfp*, expression of *stac3*^{NAM}*-egfp* failed to rescue touch induced swimming although some Stac3^{NAM} localized to triads (Fig. 2-16a). Furthermore, Ca^{2+} imaging of mutant fast but not slow twitch muscles expressing *stac3*^{NAM}*-mCherry* and *GCaMP3* exhibited Ca^{2+} transients that were decreased compared with mutant muscles expressing *stac3*^{wt}*-mCherry* and *GCaMP3* (Fig. 2-10b, Fig. 2-16 b,c). Presumably the mosaic expression of a partially effective allele was insufficient to result in behavioral rescue. Decreased Ca^{2+} transients in fast twitch but not slow twitch

muscles expressing *stac3*^{NAM} predicts defective swimming since by 48 hpf swimming is dependent on fast twitch muscle contractions and independent of slow twitch contractions (Naganawa and Hirata, 2011). Additionally, expression of wildtype human *STAC3* in mutant zebrafish muscles rescued the motor phenotype (Fig. 2-17). Thus the NAM mutation appeared to diminish EC coupling in fast twitch muscles and was causative for the congenital myopathy.

DISCUSSION

This study identified Stac3 as a novel component of EC coupling in skeletal muscles, and a mutation in STAC3 as the cause for Native American myopathy. A recent study suggested that MO mediated knockdown of *stac3* in zebrafish embryos resulted in defective myofibrillar formation in skeletal muscles (Bower et al., 2012), but we found that myofibrils in embryonic and larval zebrafish were comparable between *wt* sibs and *stac3* mutants. This discrepancy might be due to the maternal wt *stac3* transcript found in *stac3* nulls, which could have been sufficient for normal myofibrillar formation in mutants.

How does Stac3 regulate EC coupling?

In principle Stac3 could participate in EC coupling via a variety of mechanisms. One possibility is that Stac3 might modulate the channel properties of DHPR and/or RyR1. The triadic localization of Stac3 and biochemical demonstration that Stac3 is part of the DHPR/RyR1 complex is consistent with this possibility. Regulation of DHPR or RyR1 channel properties by other triadic components includes modulation of the

properties of DHPR by RyR1 and of RyR1 by FKBP12. In murine RyR1-deficient myotubes the complement of DHPR on the muscle membrane is normal, but the DHPRs pass much less Ca^{2+} than normal (Nakai et al., 1996). The immunophilin, FKBP12, copurifies with RyR and anti-FKBP12 can pull down RyR in striated muscles (Chopra et al., 2009). When RyR were examined with single channel recordings, FKBP12 was found to optimize channel function (Jayaraman et al., 1992). The β subunits of voltage-dependent Ca^{2+} channels are also known to regulate properties of a variety of Ca^{2+} channels (Dolphin, 2003). It is possible that Stac3 could interact with the β_{1a} subunit to regulate DHPR channel properties in skeletal muscles.

Another possibility is that Stac3 may regulate the precise organization of DHPRs and RyR1s at triadic junctions of the t-tubules and SR. At triads DHPRs and RyR1s are organized in a precise manner with DHPRs arranged in geometrically arranged groups of four called tetrads with each tetrad apposed to every other RyR1 homotetramer (Block et al., 1988). The β_{1a} subunit of DHPR also appears to be critical for this since β_{1a} is required for formation of DHPRs into tetrads (Schredelseker et al., 2005).

Stac3 might also regulate the amount of DHPR and/or RyR1 at triads perhaps by modulating protein trafficking and/or stability of DHPR and/or RyR1. An example of a factor that may be important for trafficking or stability of DHPRs is REM, a member of the RGK GTP-binding protein family. REM can bind β subunits of voltage-dependent Ca^{2+} channels when expressed heterologously and overexpression of REM inhibits L-type Ca^{2+} channels in C2C12 cells (Finlin et al., 2003) and in skeletal muscles due to a decrease of DHPR in the muscle membrane (Bannister et al., 2008a) via dynamin dependent endocytosis (Yang et al., 2010b). Although the loss-of-function phenotype for

REM is not known, these results suggest that REM inhibits localization of DHPRs in triads either by decreasing processing of the channels into triadic junctions or by increasing the removal of the channel from triads. Interestingly the $DHPR_{\beta 1}$ subunit regulates levels of plasmamembrane $DHPR_{\alpha 1c}$ ($Ca_V1.2$) that is expressed by cardiac muscle cells and neurons by inhibiting the degradation of these channels via endoplasmic reticulum-associated protein degradation (Altier et al., 2011). Examination of the amount of DHPR and RyR1 at triads in *stac3* mutants versus wildtype muscles should clarify whether Stac3 controls the levels of these key components in skeletal muscles. It should also be possible to investigate whether Stac3 regulates protein trafficking of key components of EC coupling using various transgenics combined with live-imaging strategies in zebrafish to directly examine fluorescently labeled EC components as they are trafficked from the ER to triads and as they are endocytotically removed from the triads. Furthermore, the availability of mutants deficient for DHPR (Schredelseker et al., 2005; Zhou et al., 2006) and RyR1 (Hirata et al., 2007) in addition to the *stac3*^{mi34} mutant should be invaluable for mechanistic analysis of Stac3 for EC coupling.

How does the missense mutation in *STAC3* lead to Native American myopathy?

Our finding that expression of $Stac3^{NAM}$ in Stac3 null zebrafish leads to decreased EC coupling suggests that interactions of the 1st SH3 domain in Stac3 is important for normal EC coupling. SH3 domains are found in many proteins and thought to mediate protein/protein interactions. The domains contain approximately 60 residues and share considerable sequence identity and a common structure made up of a five-stranded anti-parallel β-sheet assembled into two orthogonally packed sheets (Lim et al., 1994) (Fig. 1-

3a). Despite being a well-characterized protein interaction module, the diversity of function and specificity of SH3 domains defy a generalized characterization (Kaneko et al., 2008; Mayer, 2001). Since SH3 domains exhibit average selectivity, moderate affinity, and ubiquity throughout the cell, the nickname "molecular Velcro®" fits them well (Morton and Campbell, 1994). In one sense, having only moderate affinity in protein-protein interactions can be seen as an advantage for a domain that is continually involved in on and off interactions with different binding partners. How the cell reconciles the domain's promiscuity and weak interactions into important cellular functions remains somewhat perplexing. One general solution to controlling the specificity of the domain is by compartmentalization and spatial confinement. For example, if the SH3 domain is localized to the plasma membrane, the concentration of that particular SH3 domain and its ligand in that microenvironment of the cell may be high enough to precipitate a specific interaction.

SH3 ligands bind to a flat and hydrophobic surface in the SH3 domain consisting of three shallow pockets formed by conserved aromatic residues on the surface of the domain (Zafra-Ruano and Luque, 2012). One of these aromatics, W284, is converted to a serine (S) in NAM. This highly conserved W of the SH3 domain, determines the class and direction of the SH3 domain binding site depending on its conformation, and aids in the recognition of proline residues of the ligand (Fig. 2-18a) (Zafra-Ruano and Luque, 2012). Modeling of the Stac3 SH3 domain W284 residue using the solved Stac1 SH3 domain (PDB ID: 2DL4) (Qin, 2006), which contains high sequence identity (43% identical), reveals that W284 is found at the base of the β3 α-helix at the surface of the SH3 binding domain (Fig. 2-18 a). Mutation of the W to S results in a loss of the surface

exposed residue, and the modification of the binding pocket from one containing a hydrophobic surface to a hydrophilic one (Fig. 2-18b). Nevertheless, the W284S mutation in the SH3 domain of Stac3 appear to result in only a negligible effect on the secondary structure of the SH3 domain in comparison to the SH3 domain of $Stac3^{WT}$ (Fig. 2-18a). Thus, the NAM mutation appears to specifically disrupt the binding properties of the first SH3 domain of Stac3, implicating the importance of this domain and its interaction partner(s) in the function of Stac3. Interestingly, components of the EC coupling complex including $DHPR_{\alpha 1s}$, $DHPR_{\beta 1a}$ and RyR1 contain numerous SH3 binding sequences in their predicted cytoplasmic portions. Thus it would be interesting to see if Stac3 might interact with triadic components such as DHPR and/or RyR1 via the Stac3 SH3 domain and whether such an interaction is necessary for normal EC coupling.

The generation of transgenic lines of *stac3*^{NAM} mutant zebrafish will be useful to delineate the pathology of NAM and the function of the SH3 domains, as well as for identifying potential therapeutic agents. This is particularly relevant given the increasing recognition of mutations in genes associated with EC coupling in a growing range of human muscle diseases. In addition, *STAC3* is a candidate for the genetic basis of currently undefined congenital myopathies, particularly those associated with susceptibility to MH and/or those with phenotypes similar to those of patients with *RYR1* or *DHPR* mutations.

What might the CRD be for?

A CRD is a small structural unit of around 50 amino acids that was originally discovered as a lipid-binding subunit of PKCs (Colon-Gonzalez and Kazanietz, 2006). CRD domains have been commonly found to play a crucial role in targeting proteins from the cytosol to the membrane (Johnson et al., 2000) (Movilla and Bustelo, 1999; Zhou et al., 2002). Furthermore, crystallization studies have suggested mechanisms by which CRD domains can associate with membranes. Co-crystallization of the PKCδ C1 CRD domain with its ligand, phorbol 13-acetate revealed that the CRD domain is made up of two β-sheets, plus a small α-sheet at the C-terminus (Fig. 2 -18c) (Zhang et al., 1995). Comparison to the crystallized PKCδ C1 CRD domain without ligand, shows that upon ligand binding the β-sheets are pulled apart and a continuous hydrophobic surface is created that allows for the association of the CRD domain with membrane (Zhang et al., 1995).

Recently, the structure of the CRD domain of human Stac3 was solved, and directly deposited into the Protein Data Bank (Fig. 2-18c) (Abe, 2006). Comparison of the structure of the CRD domain of Stac3 with the solved structure of PKC C1 CRD in complex with phorbol ester reveals structural similarities as well as the location of the putative binding site of the Stac3 CRD (Fig. 2-18c). Unique among crystalized CRD domain structures, Stac3 contains two additional short anti-parallel β-sheets within the binding loop (Fig. 2-18c). A fifth solo β-sheet sits between the binding loop and the conserved antiparallel β-sheets (Fig. 2-18c). As the interaction with ligands combined with unzipping of β-sheets of CRD domains is thought to provide a hydrophobic surface

for membrane association, the presence of additional sheets may indicate the site of a complicated membrane interaction site. Furthermore, as the EC coupling complex is located at the triadic junction between SR and T-tubules, a role for Stac3 in targeting proteins to the membrane or assisting insertion of proteins into membranes is also an intriguing possibility.

Overall, these results reflect the first step in understanding the function of the Stac3 protein in skeletal muscle. As Stac3 is a critical component of the EC coupling complex that is required for normal Ca^{2+} release in skeletal muscle, understanding the mechanism by which Stac3 modulates Ca^{2+} release in the muscle will help gain new understanding of both basic muscle biology, as well as the mechanisms of EC coupling. Furthermore, as Stac3 is the genetic basis for NAM, which is characterized by MH susceptibility, new insights into the mechanisms of Stac3 may help generate treatments as well as new insights into the pathology of NAM, MH, and similar congenital myopathies.

Author Contributions

The zebrafish mutagenesis screen that isolated stac3^{mi34} was performed by Saint-Amant, L., Satish, A., Cui, W.W., Zhou, W, Sprague S.M. Hirata H., and Kuwada J.Y. The behavioral analysis of stac3^{mi34} was performed by H.H. and Horstick, E.J., The electrophysiological and Ca^{2+} imaging analysis of stac3mi34 was performed by Horstick, E.J., with some initial electrophysiological characterization by Saint-Amant, L. Mutant rescue and NAM allele expression experiments were performed by Horstick, E.J. Expression pattern of Stac3 was delineated by Horstick, E.J., and H.H. Generation of anti-Stac3, immunoblots, co-immunoprecipitations, demonstration of maternal *stac3*

transcript and Morpholino knockdown of Stac3 were performed by Linsley, J.W., Meiotic mapping and molecular identification of stac3^{mi34} was performed by Hirata H. Electron microscopy was performed by Franzini-Armstrong C., and Dowling, J.J., Human STAC3 was cloned by Satish, A., NAM clinical phenotyping, original pedigree analysis and biological sample collection were performed by Powell C.M., Stamm D.S and Speer M.C. Pedigree analysis of STAC3 and Native American Myopathy was performed by Dowling, J.J., Hauser, M.A., McDonald, K.K., Ashley-Koch, A., The research was designed and the paper written by Kuwada J.Y.

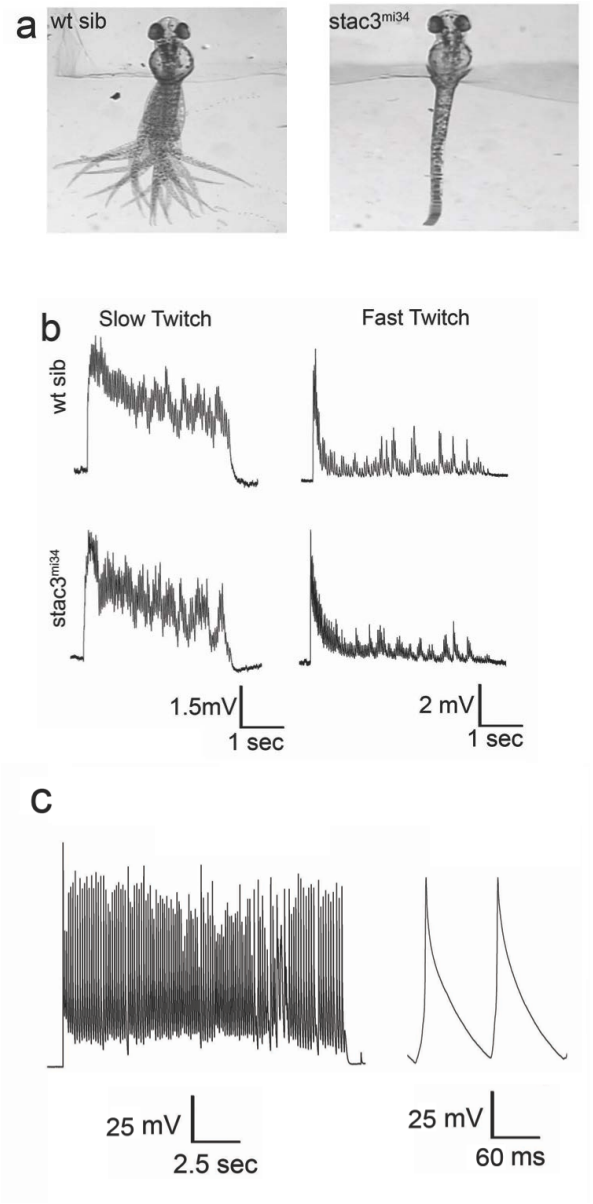

Fig. 2-1. *mi34* mutant zebrafish exhibit defective swimming but CNS output is normal
(a) Touch evoked swimming in wt but not *stac3*^{mi34} embryos (48 hpf). Panels show superimposed frames (30 Hz) of swimming motion from wt sibling and *stac3*^{mi34} embryos with heads embedded in agar. Contributed by Dr. Hiromi Hirata. (b) Voltage recordings with 6 mM curare showing that touch evoked synaptic responses of slow twitch (wt sib: n=5; mut: n=6) and fast twitch muscles (wt sib: n=6; mut: n=4) of wt sibling and *stac3*^{mi34} mutants (48 hpf) are comparable. Arrowhead denotes tactile stimulation. (c) Voltage recordings with no curare showing that mutant fast twitch muscles (48 hpf) respond to tactile stimulation with a burst of action potentials (n=8). (b) and (c) contributed by Dr. Louis Saint-Amant.

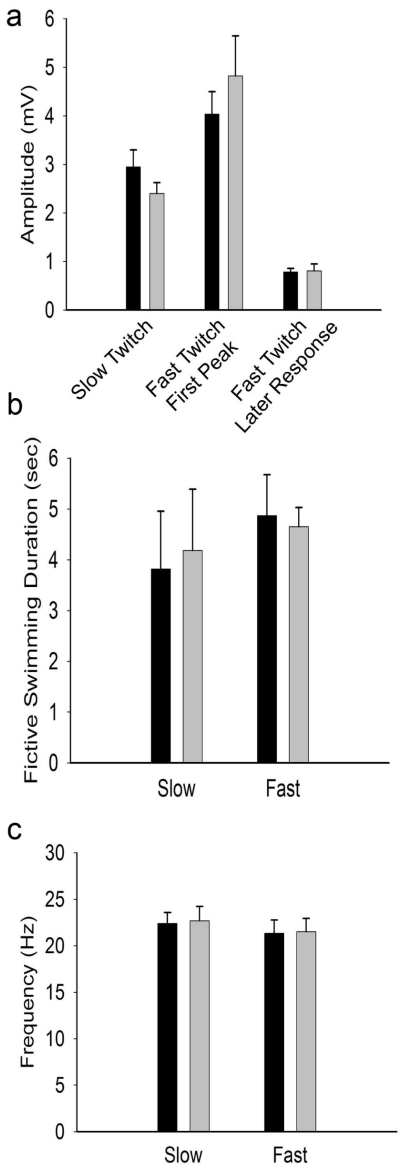

Fig 2-2. The synaptic responses of skeletal muscles initiated by tactile stimulation in 48 hpf embryos are comparable between wt sib and *stac3*^{mi34}. All recordings were made in 6 mM of curare to minimize muscle contractions (n=5 for slow twitch; n=6 for fast twitch) and *stac3*^{mi34} (n=6 for slow; n=4 for fast). Muscles responded to tactile stimulation with a burst of excitatory endplate potentials (epp; see Fig. 1b). (A) Histograms showing that the amplitude of epps in slow twitch muscles during a burst (left), peak amplitude of the 1st epp in a burst in fast twitch muscles (middle) and the peak amplitude of epps recorded for a duration of 1 sec starting 1 sec after the 1st epp (right) were comparable between wtsib and mutants. (B) Histograms showing that the duration of the synaptic bursts in slow and fast twitch muscles were comparable between wtsib and mutants. (C) Histograms showing that the frequencies of epps within bursts in slow and fast twitch muscles were comparable. Error bars represent standard error of the means. Contributed by Dr. Eric Horstick.

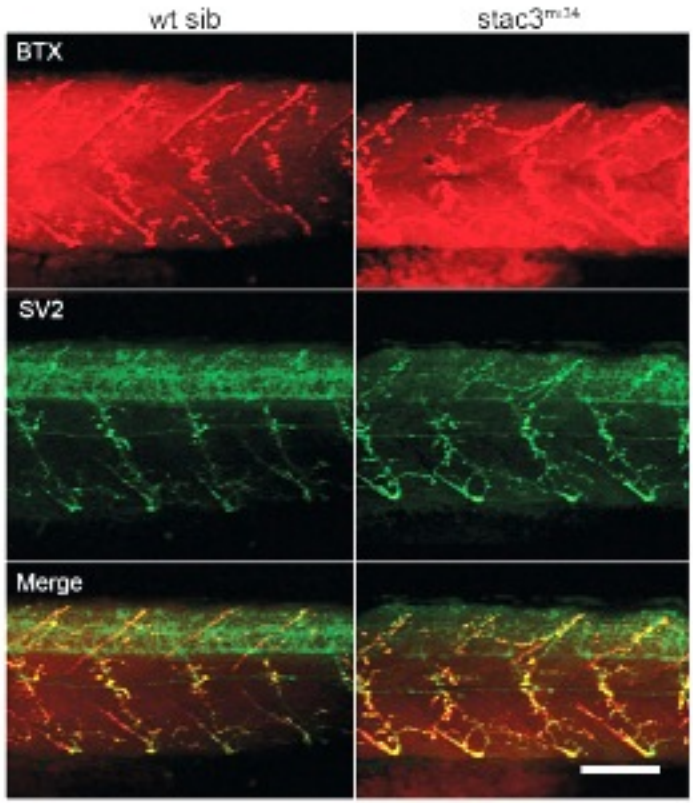

Fig 2-3. Distribution of the neuromuscular junction (NMJ) is unperturbed in *stac3*^{mi34} embryos. Side view of the trunk of a 48 hpf wt sib and *stac3*^{mi34} embryo showing bungarotoxin-Alexa594 (BTX) labeled distribution of AChRs (red) is normal (top) as is the anti-SV2 (green) labeled presynaptic terminals (middle). The BTX and anti-SV2 labeled panels are merged to show co-localization (bottom). Scale: 60 μm. Contributed by Dr. Eric Horstick.

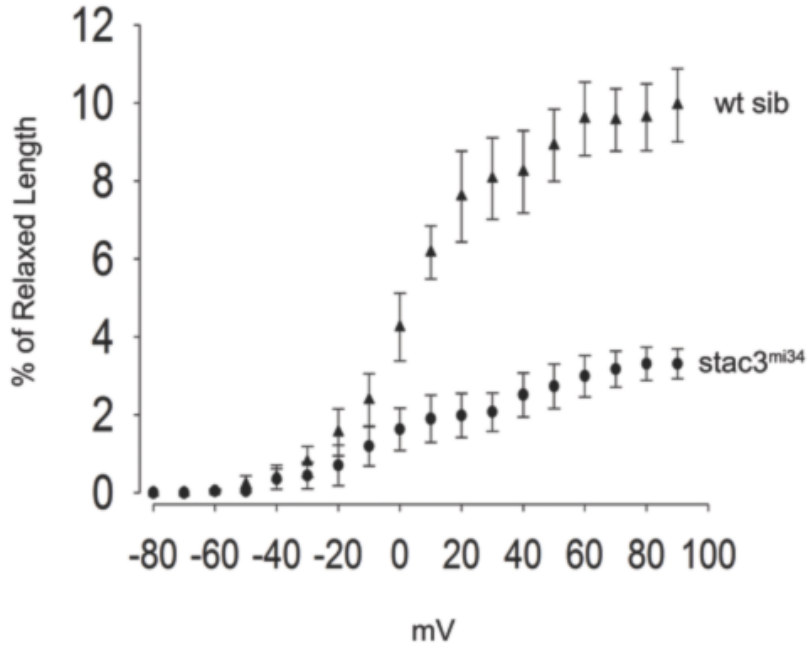

Fig. 2-4. Depolarization initiated muscle contraction is decreased in *stac3*^{mi34} embryos at 48 hpf. Muscle fibers were voltage clamped *in vivo* to different membrane potentials for 200 ms and imaged at 60 Hz to measure the amount of contraction as a % of the relaxed fiber length. Wt sib fibers (n=5) and *stac3*^{mi34} fibers (n=4) are denoted by triangles and circles, respectively. The difference in contraction was first significant ($p<0.01$) starting at 10 mV through to 90 mV. Error bars represent standard error of the means. Contributed by Dr. Eric Horstick.

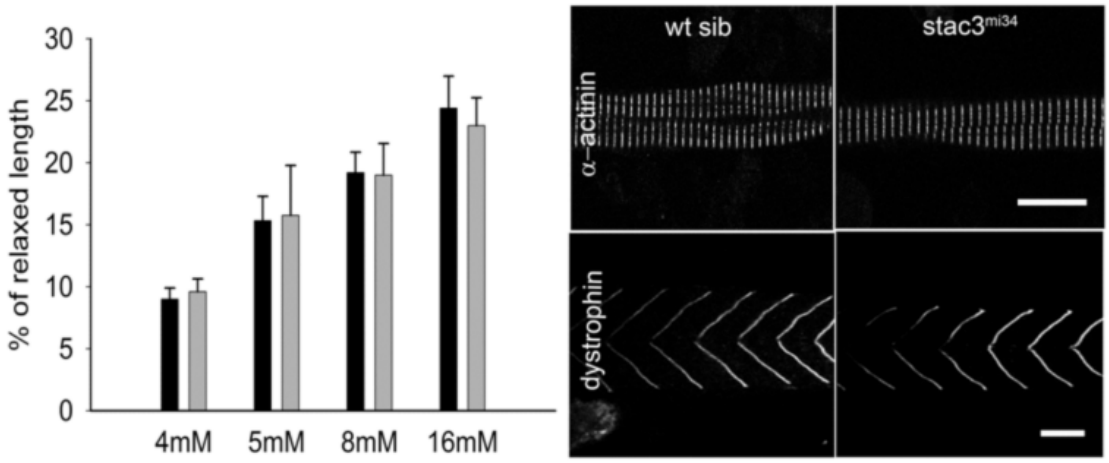

Fig. 2-5. Caffeine induces skeletal muscle contractions that were similar between wt sib and *stac3*^{mi34} embryos at 48 hpf. Left, histogram of contraction induced by caffeine in the presence of 50 mM curare (n=5 each for wtsib and mut for 4mM, 8mM and 16 mM caffeine; n=4 each for wtsib and mut for 5mM caffeine). Right, the distribution of a-actinin and dystrophin are comparable in *stac3*^{mi34} and wt sib embryos. Anti-a-actinin labeling is shown on dissociated muscle fibers (scale: 10 μm) while anti-dystrophin is on wholemounted embryos (scale: 60 μm). Error bars represent standard error of the means. Contributed by Dr. Eric Horstick.

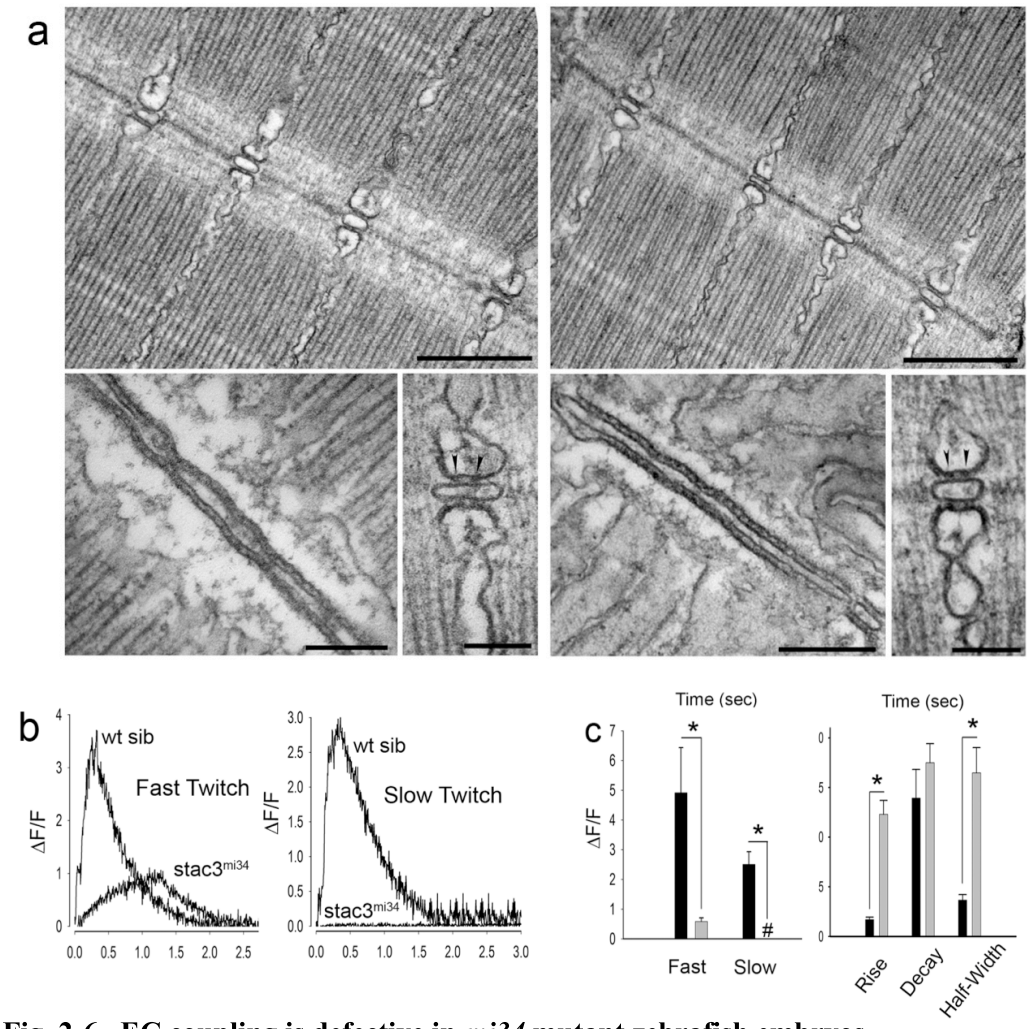

Fig. 2-6. EC coupling is defective in *mi34* mutant zebrafish embryos
Electron micrographs showing that the ultrastructure of myofibrils and triadic junctions are comparable between the muscles of 4 dpf wt sibling (a, left) and *mi34* mutants (a, right). Top: Longitudinal sections showing several myofibrils and triads sectioned at right angle to the T tubule long axis. Scale: 500 nm. Bottom: at left a section tangent to the triad, showing one of the two long rows of feet (RyR) that occupy the junctional gap. Scale: 250 nm. Bottom: at right a section transverse to the triad axis showing two feet (arrowheads) in the junctional gap of the triad. Scale: 100 nm. (b) Ca^{2+} transients recorded from GCaMP3 expressing fast and slow twitch fibers are significantly decreased and slower in 48 hpf *stac3*^{mi34} mutants. (c) Left: quantification of peak Ca^{2+} release with black and gray bars representing wt sib (fast, n=5; slow, n=5) and *stac3*^{mi34} (fast, n=9; slow, n=7) fibers, respectively. # denotes that peak Ca^{2+} was 0. Right: quantification of Ca^{2+} transient kinetics in fast fibers with black and gray bars representing wt sib and *stac3*^{mi34}, respectively. Half width denotes the duration the transient is greater than 50% of peak value. Error bars represent standard error of the means . Asterisks signifies $p<0.01$, t-test. EM contributed by Dr. Clara Franzini Armstrong, Ca^{2+} imaging contributed by Dr. Eric Horstick.

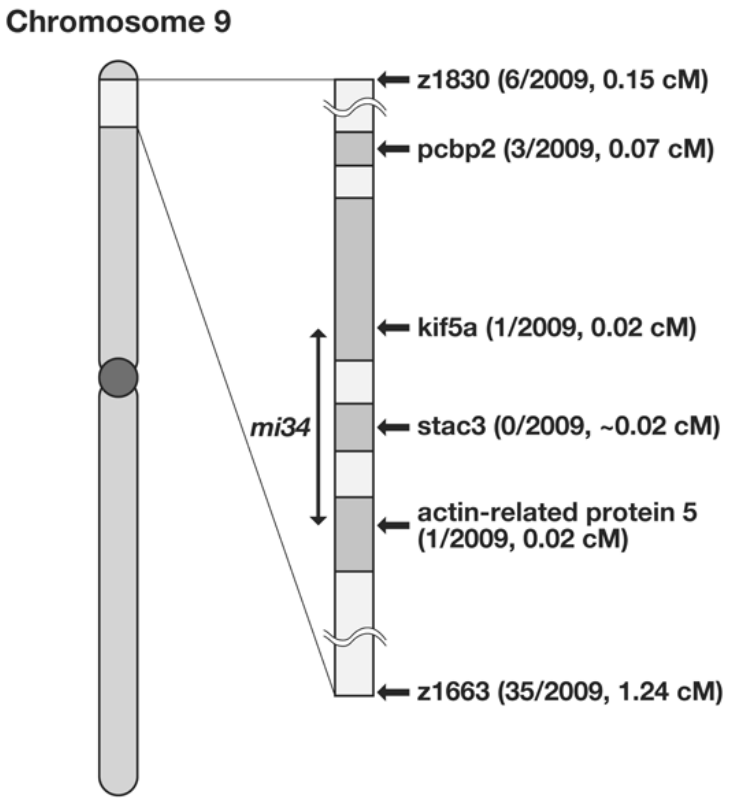

Fig. 2-7. Meiotic mapping of the *stac3*^{mi34} locus to the *stac3* gene. Initial meiotic mapping of *stac3*^{mi34} located it to chromsome 9 between markers z1830 and z1663. Numbers in parentheses denote x recombinants in y mutants. A sequenced 156 kb BAC (CR848672) was identified that contained z1830 and high resolution mapping identified new markers (zh1, zh34 and zh16) that flanked the mutation within the BAC. A 4th marker, zh31, located in the *stac3* gene showed no recombination with the mutation out of 2009 mutant embryos suggesting that the mutant locus was *stac3*. Contributed by Dr. Hiromi Hirata.

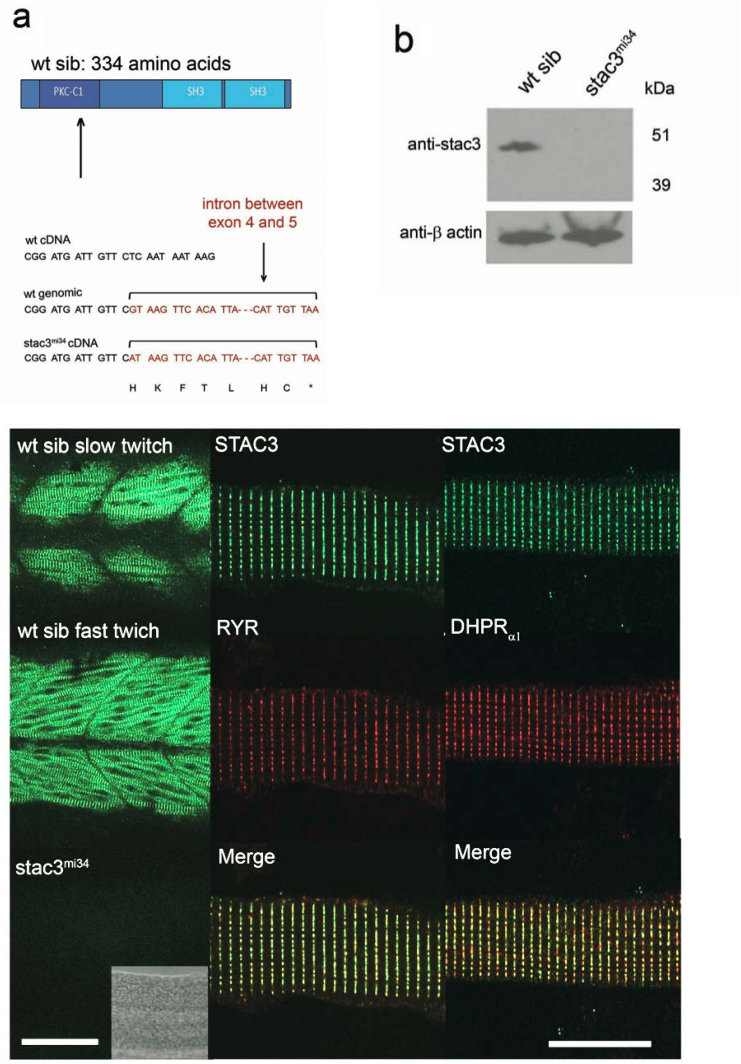

Fig. 2-8. The muscle-specific gene *stac3* underlies the *mi34* phenotype
(a) Diagram of the predicted wt Stac3 protein (top). Arrow denotes location of the stop codon. DNA sequence of corresponding regions of wt cDNA, wt genomic DNA, and *stac3*^{mi34} cDNA showing that a missense mutation in a splice donor site lead to the inclusion of the intron (bracket) and stop codon (asterisk) in the mutant cDNA. (b) Stac3 protein appears not to be synthesized in mutants. Western blot of showing that anti-Stac3 labels a band from wt but not mutant embryos at 48 hpf. b actin was the loading control. (c) Stac3 co-localizes with RyR and DHPR$_{a1}$ in skeletal muscles. Left, side view of the trunk of 48 hpf embryos labeled with anti-Stac3 showing that both fast twitch and slow twitch express Stac3 in wt but not mutant embryos. Scale: 60 mm. Inset shows the brightfield image of the trunk of the mutant. Right, dissociated 48 hpf wildtype muscle fibers labeled with anti-Stac3 and anti-RyR or anti-DHPR$_{a1}$ showing that Stac3 co-localizes with RyR and DHPR$_{\alpha 1}$. Scale: 10 mm. Partially contributed by Dr. Eric Horstick.

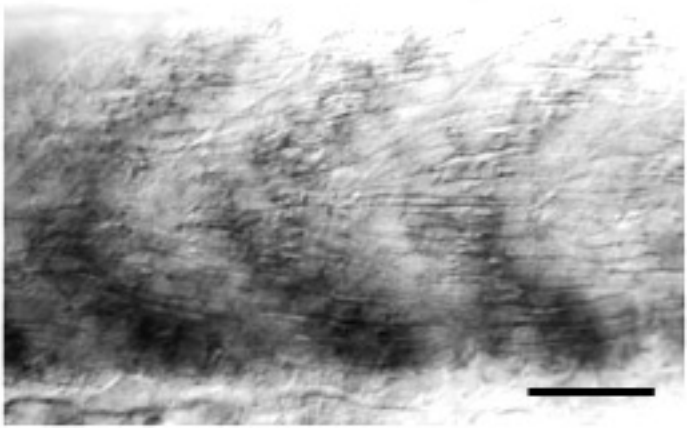

Fig. 2-9. *stac3* is expressed specifically by skeletal muscles in zebrafish embryos. Sideview of the trunk of a wildtype embryo (27 hpf) labeled with an antisense riboprobe against *stac3* mRNA showing several segments of *stac3*-positive skeletal muscles. *stac3* was not expressed in any other cells at this stage. The sense riboprobe did not label any cells (not shown). Scale: 60 μm. Contributed by Dr. Eric Horstick.

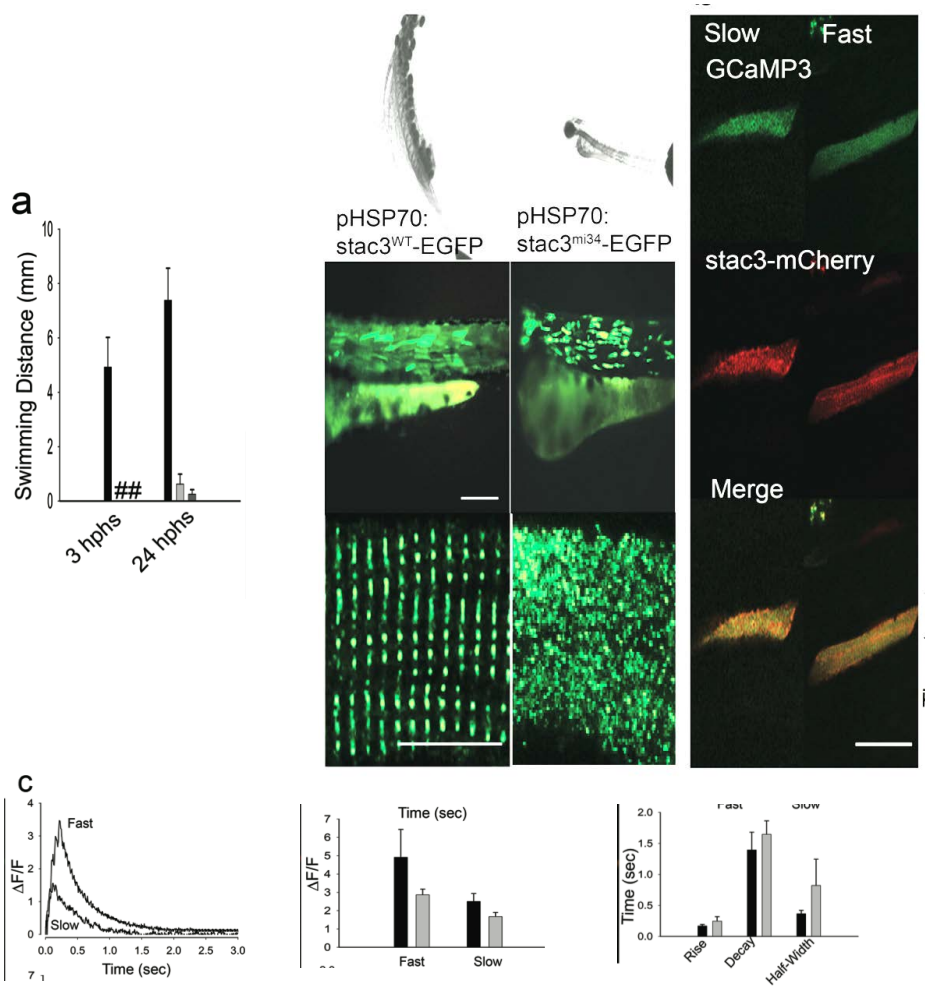

Fig. 2-10. Expression of wt Stac3 in muscles rescues the *stac3^{mi34}* phenotype
(a) Left, histogram showing that mutant embryos expressing heat inducible *stac3^{wt}-egfp* (black, n=32) but not *stac3^{mi34}-egfp* (light gray, n=4) nor uninjected mutant embryos (dark gray, n=10) exhibited touch evoked swimming at both 3 h post heat shock (hphs) and 24 hphs. # denotes no swimming. Right panels, superimposed frames (30 Hz, 1 sec) (top) show that mutant embryos expressing *stac3^{wt}* but not *stac3^{mi34}* swim in response to touch although both are similarly expressed by muscles (middle, scale: 180 mm). In dissociated mutant muscles Stac3^{wt}-EGFP localizes to the triads but not Stac3^{mi34}-EGFP (bottom, scale: 10 mm). (b) *In vivo* expression of Stac3^{wt}-mCherry by mutant muscle fibers rescues Ca^{2+} transients. Left panels, *stac3^{mi34}* mutant slow and fast twitch fibers co-expressing *a-actin* driven GCaMP3 and heat induced Stac3^{wt}-mCherry. The triadic localization of Stac3^{wt}-mCherry cannot be seen due to the low resolution of the resonance scans used to detect the fluorescent proteins. (c) Top, Ca^{2+} transients from mutant fast and slow fibers co-expressing Stac3^{wt}-mCherry and GCaMP3. Middle, histogram showing that peak Ca^{2+} release is comparable between wt (black) fast (n=5) and slow (n=5) fibers and rescued mutant (gray) fast (n=6) and slow (n=2) fibers. Bottom, histogram showing that the kinetics of Ca^{2+} transients from wt (black) and rescued mutant (gray) fast twitch fibers are comparable. Error bars represent standard error of the means. Contributed by Dr. Eric Horstick

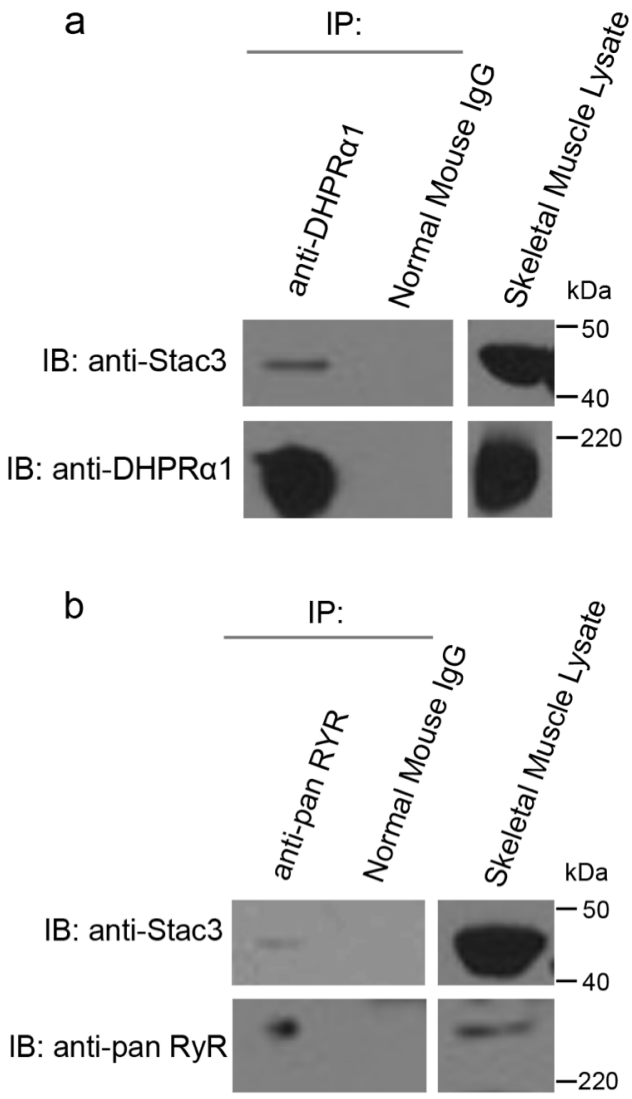

Fig. 2-11. Stac3 forms a Molecular Complex with DHPR and RyR
(a) Immunoblots (IB) showing that immunoprecipitation (IP) with anti-$DHPR_{a1}$ but not mouse IgG pulls down $DHPR_{a1}$ and Stac3 from adult skeletal muscle lysate (n=3). Skeletal muscle lysate lane is a immunoblot showing Stac3 and $DHPR_{a1}$ are expressed by muscles. (b) Immunoblots showing that immunoprecipitation with anti-pan RyR but not mouse IgG pulls down RyR and Stac3 from adult skeletal muscle lysate (n=3). Skeletal muscle lysate lane is an immunoblot showing Stac3 and RyR are expressed by muscles.

Table 2-1. Selected identified proteins by MS/MS

Selected Identified Proteins	Accession Number	Molecular Weight	# Peptides Matched
Stac3	IPI00493641	39 kDa	220
Green Fluorescent Protein	CON_GFP	27 kDa	206
RyR1b	IPI00771673	575 kDa	9
$DHPR_{a2d1}$	IPI00498816	121 kDa	5
$DHPR_{a1s}$	IPI00493269	209 kDa	4
RyR3	IPI00897644	551 kDa	3
$DHPR_{b1}$	IPI00627451	57 kDa	2

Selected zebrafish proteins identified from MS/MS analysis after co-immunoprecipitation with anti-GFP of skeletal muscle lysates from transgenic α-*actin:stac3-gfp* zebrafish. Protein identifications were accepted if they contained at least two identified peptides and could be established at greater than 95% probability. Probabilities of protein assignments were determined by the Protein Prophet algorithm (see Methods).

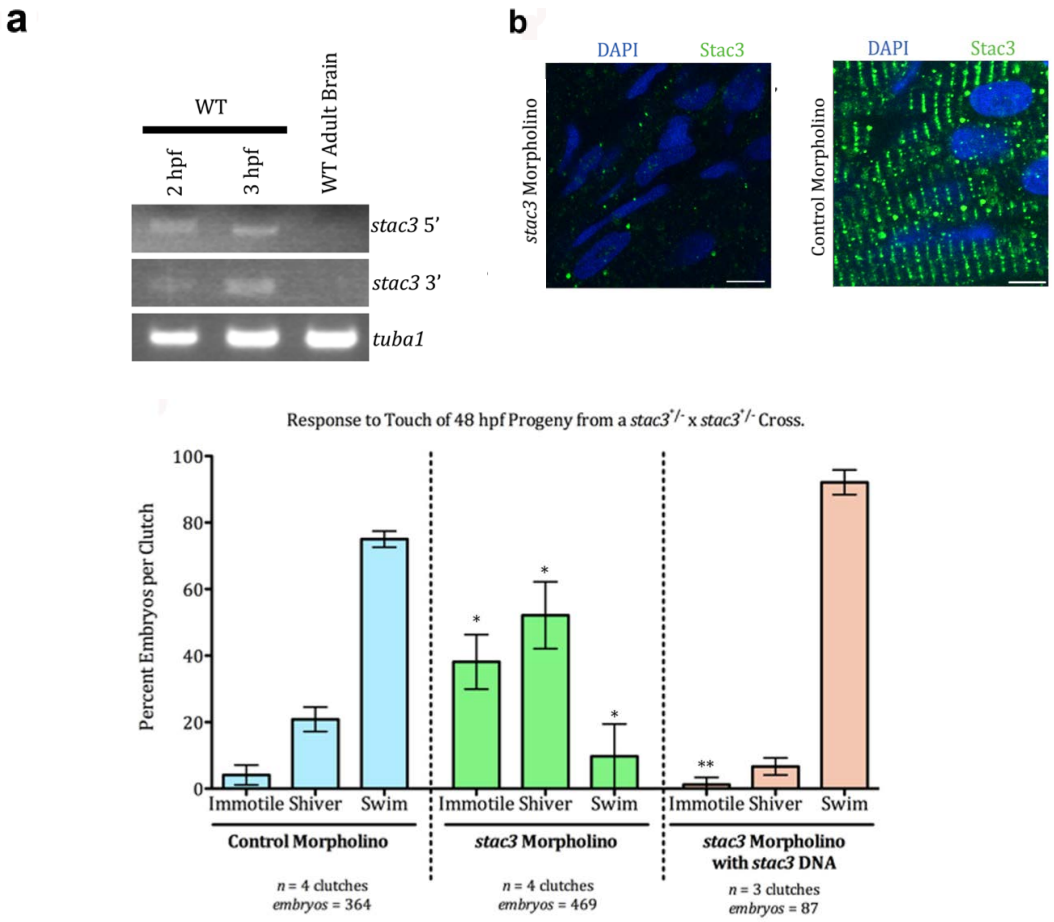

Fig. 2-12. *stac3* mRNA is maternally expressed

(a) RT-PCR from 2 and 3 hpf embryos showing that *stac3* mRNA is maternally expressed. Midblastula transition starts at 3 hpf. *stac3* mRNA is not expressed in adult brain. *tuba1,* a house-keeping gene that is maternally expressed serves as a positive control and *stac3* in adult brain as a negative control. *stac3* 5' and 3' refer to primers used for amplifying either 5' or 3' fragments of *stac3* from *stac3* cDNA (see Methods). (b) Micrographs showing anti-Stac3 labeled embryos (48 hpf) that had been injected with *stac3* antisense MO (top) but not control MO (bottom) exhibit little to no Stac3. Muscle nuclei are labeled with DAPI (blue). Scale: 5 mm. (c) Knocking down Stac3 in 48 hpf embryos significantly increases the proportion of progeny from a cross between *stac3*^{mi34} heterozygous carriers that are immotile or shiver and decreases those that swim in response to touch. * denotes that the percent *stac3* MO injected progeny that were immotile or shivered was greater than control MO injected progeny (respectively, $p < 0.001$ and $p < 0.01$; t test); percent *stac3* MO injected progeny that swam was less than control MO injected progeny ($p < 0.001$, t test). ** denotes that co-injection of an expression plasmid for *stac3*^{wt} with *stac3* antisense MO decreases immotility and restores swimming in a great majority of progeny. Percent *stac3* MO + expression plasmid for *stac3*^{wt} injected progeny that were immotile was much less than *stac3* MO alone progeny ($p < 0.001$, t test). Error bars represent standard error of the means.

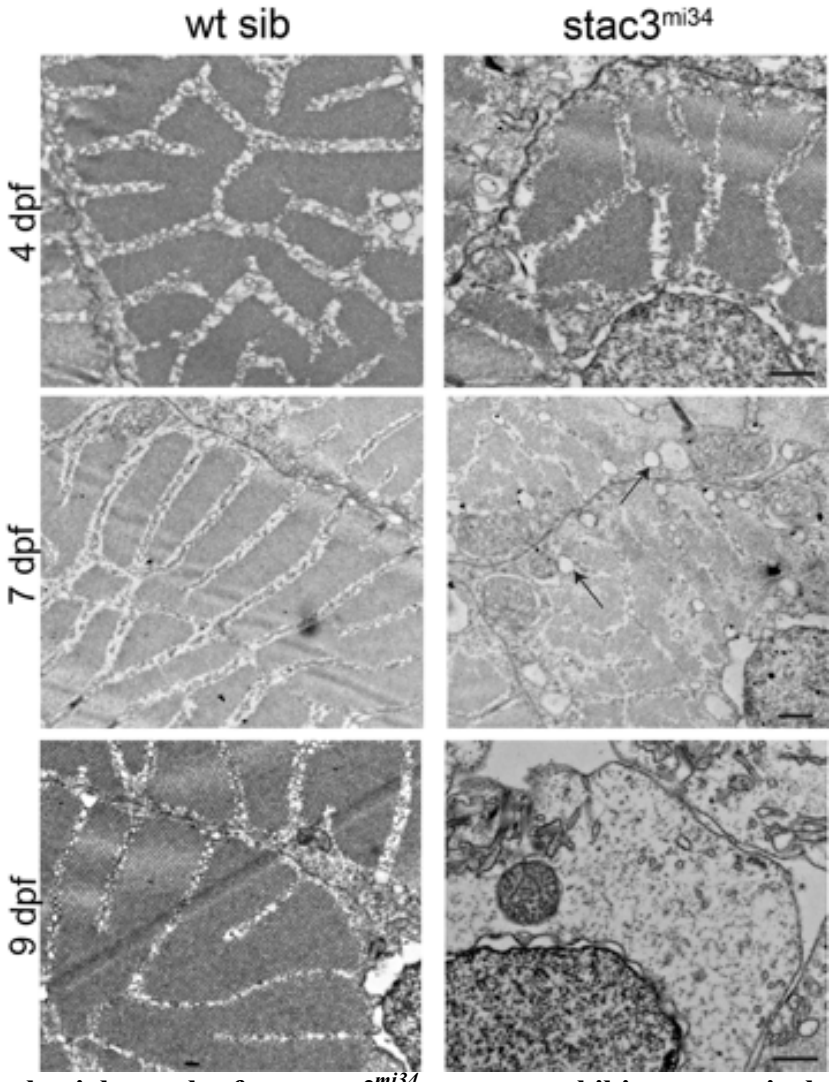

Fig. 2-13. Skeletal axial muscles from *stac3*^{mi34} mutants exhibit progressively defective SR. Electron micrographs of SR (arrayed circular profiles) from wtsib and mutant skeletal muscles showing that mutant muscles have relatively normal SR at 4 dpf and swollen ones (arrows) by 7 dpf. Mutant myofibers are breaking down at 9 dpf. Scale: 500 nm. Contributed by Dr. James Dowling.

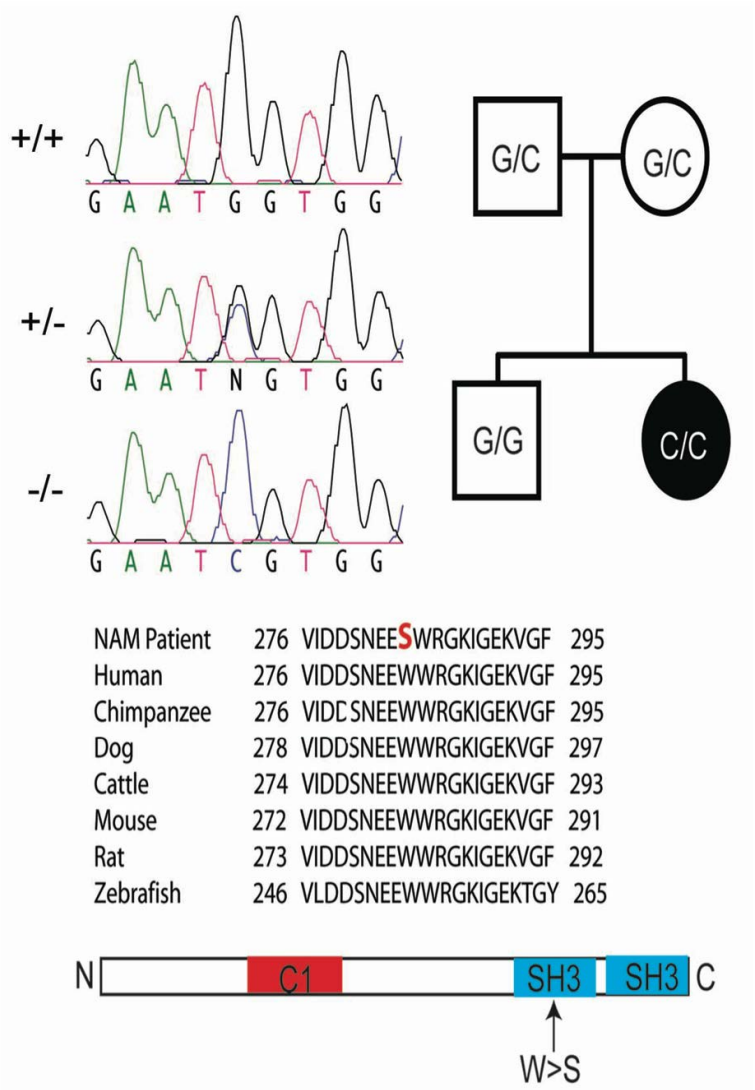

Fig. 2-14. Missense mutation in human *STAC3* causes Native American Myopathy (NAM)

Left top, sequence chromatographs of corresponding exonic region of the *STAC3* gene of individuals +/+, +/- and -/- for the NAM locus showing the G>C missense mutation in the *stac3* gene. N denotes the G/C heterozygous nucleotide. Right top, pedigree of an individual exhibiting NAM (black) and homozygous for the missense mutation (C/C). Unaffected parents were carriers for the mutation (G/C) and the unaffected sibling was homozygous for the wt nucleotide (G/G). Middle, alignment of the corresponding region of Stac3 containing NAM mutation showing that the missense mutation results in a W>S substitution in NAM individuals and that this W is completely conserved between various mammals and zebrafish. Bottom, diagram showing that the missense mutation in $Stac3^{NAM}$ is located in a SH3 domain. Contributed by Dr. James Dowling.

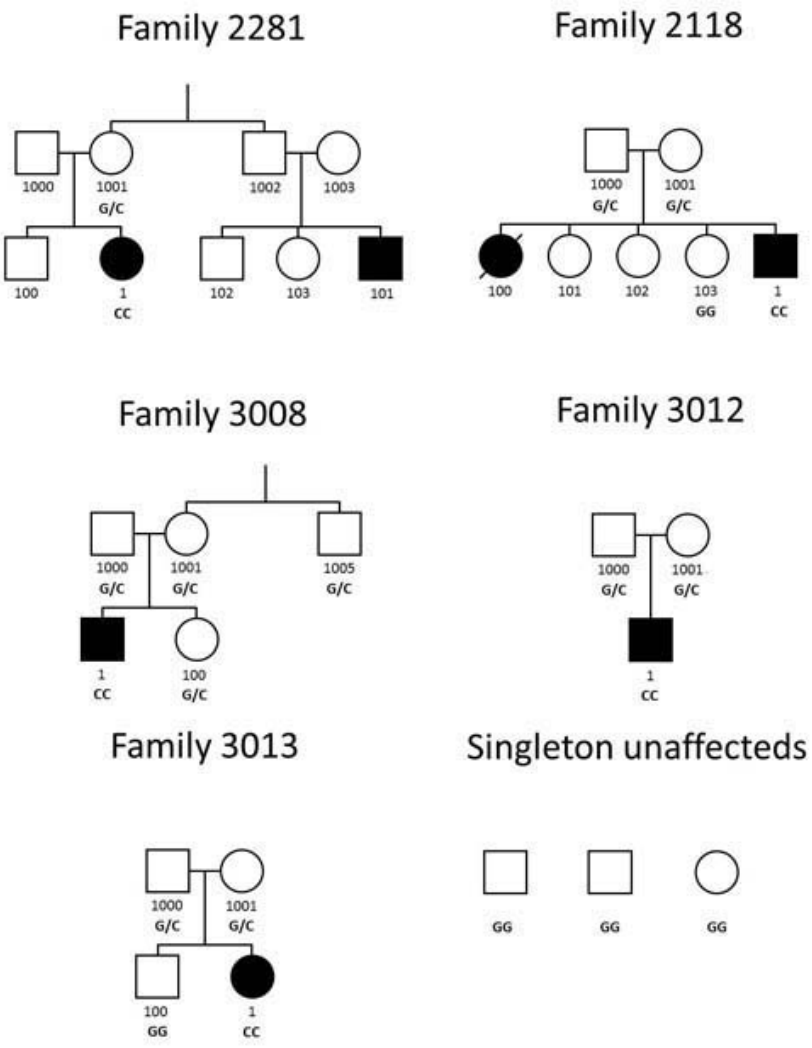

Fig. 2-15. Pedigrees of five families with individuals exhibiting Native American myopathy. Sequenced individuals and their genotype are denoted as G/C, GG & CC. Five of the 18 family members were affected (black) and 13 not. 3 unaffected singletons also pictured. Contributed by Dr. James Dowling.

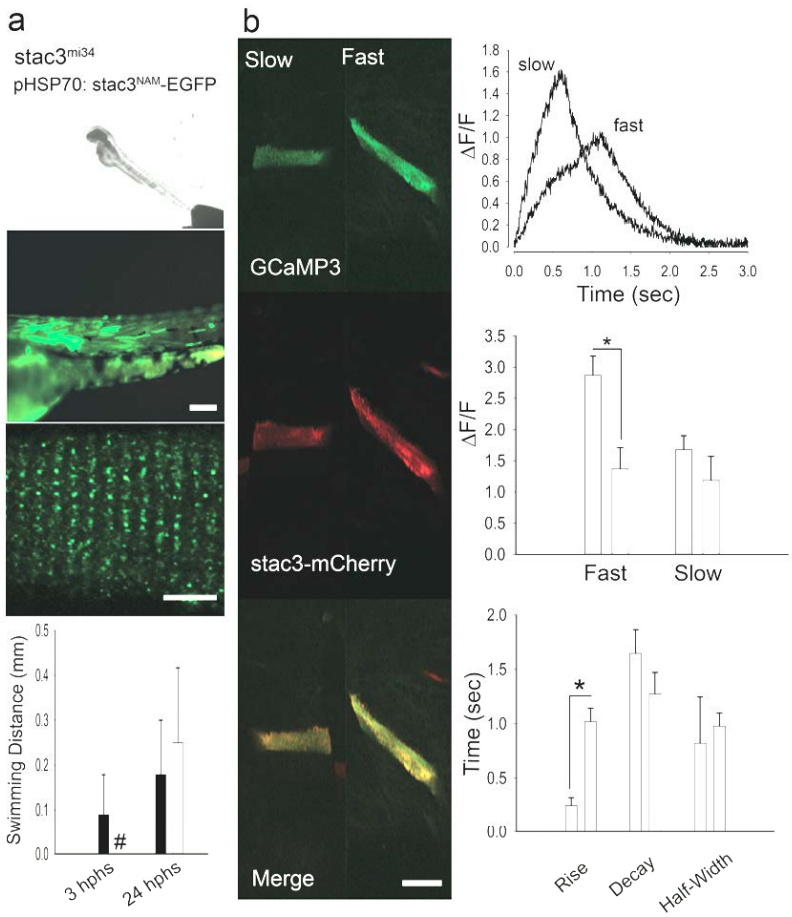

Fig. 2-16. The *stac3^{NAM}* allele decreases EC coupling
(a) Expression of Stac3^{NAM} by muscle fibers in *stac3^{mi34}* embryos does not rescue touch evoked swimming. Superimposed frames (30 Hz) showing that a heat induced mutant embryo previously injected with *pHSP70:stac^{NAM}-egfp* does not swim following tactile stimulation (top) despite expression of zebrafish Stac3^{NAM}-EGFP in myotomes and triadic localization of zebrafish Stac3^{NAM}-EGFP (middle, scale bars: 180 mm and 10 mm). Histograms (bottom) quantify the comparable lack of touch evoked swimming of *stac3^{mi34}* mutants expressing the NAM allele (black) and uninjected mutants (gray) both 3 and 24 hphs. Note the difference in scale of the y axis from that in Fig. 4a that shows swimming in mutant rescued embryos. # denotes zero movement. (b) Expression of Stac3^{NAM} by muscle fibers in *stac3^{mi34}* embryos partially rescues Ca^{2+} transients *in vivo*. Left panels, examples of *stac3^{mi34}* mutant slow and fast twitch fibers co-expressing *a-actin* driven GCaMP3 and *hsp70* regulated zebrafish Stac3^{NAM}-mCherry. The triadic localization of Stac3^{wt}-mCherry cannot be seen due to the low resolution of the resonance scans used to detect the fluorescent proteins. (c) top, Ca^{2+} transients from mutant fast and slow fibers co-expressing Stac3^{NAM}-mCherry and GCaMP3. Right middle, histogram showing that peak Ca^{2+} release is decreased between mutant fast fibers expressing *stac3^{wt}* (gray, n=6) and *stac3^{NAM}* (white, n=6). Peak Ca^{2+} was not different for mutant slow twitch fibers (wt, n=2; NAM allele, n=2). Bottom, histogram showing the kinetics of Ca^{2+} transients of mutant fast fibers expressing *stac3^{wt}* (gray, n=5) and *stac3^{NAM}* (white, n=9). Asterisk signifies $p<0.01$, t-test. Error bars represent standard error of the means. Contributed by Dr. Eric Horstick.

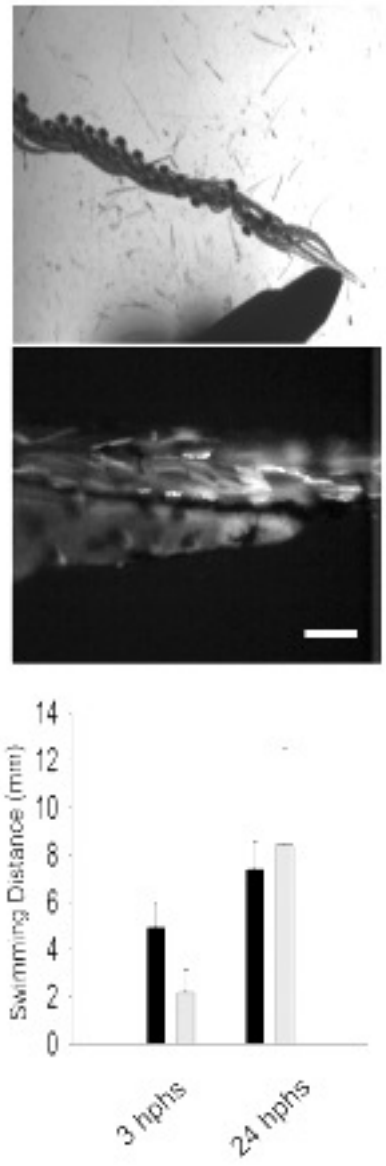

Fig. 2-17. Expression of human wt *stac3* by skeletal muscles of *stac3*^{mi34} embryos rescues the mutant behavior. Top, superimposed frames (30 Hz) showing swimming by a *stac3*^{mi34} mutant embryos injected with heat inducible constructs for human stac3 fused to EGFP following heat induction. Middle, sideview of the trunk of a *phsp70:hstac3*^{wt}*-egfp* injected *stac3*^{mi34} embryo showing expression of human Stac3-EGFP in myotomes in the embryo shown above (scale: 60 μm). Bottom, histogram showing that mutant embryos expressing human Stac3-EGFP (gray, n=4) swim as effectively as mutant embryos expressing zebrafish Stac3-EGFP (black, n=32). Error bars represent standard error of the means. Contributed by Dr. Eric Horstick.

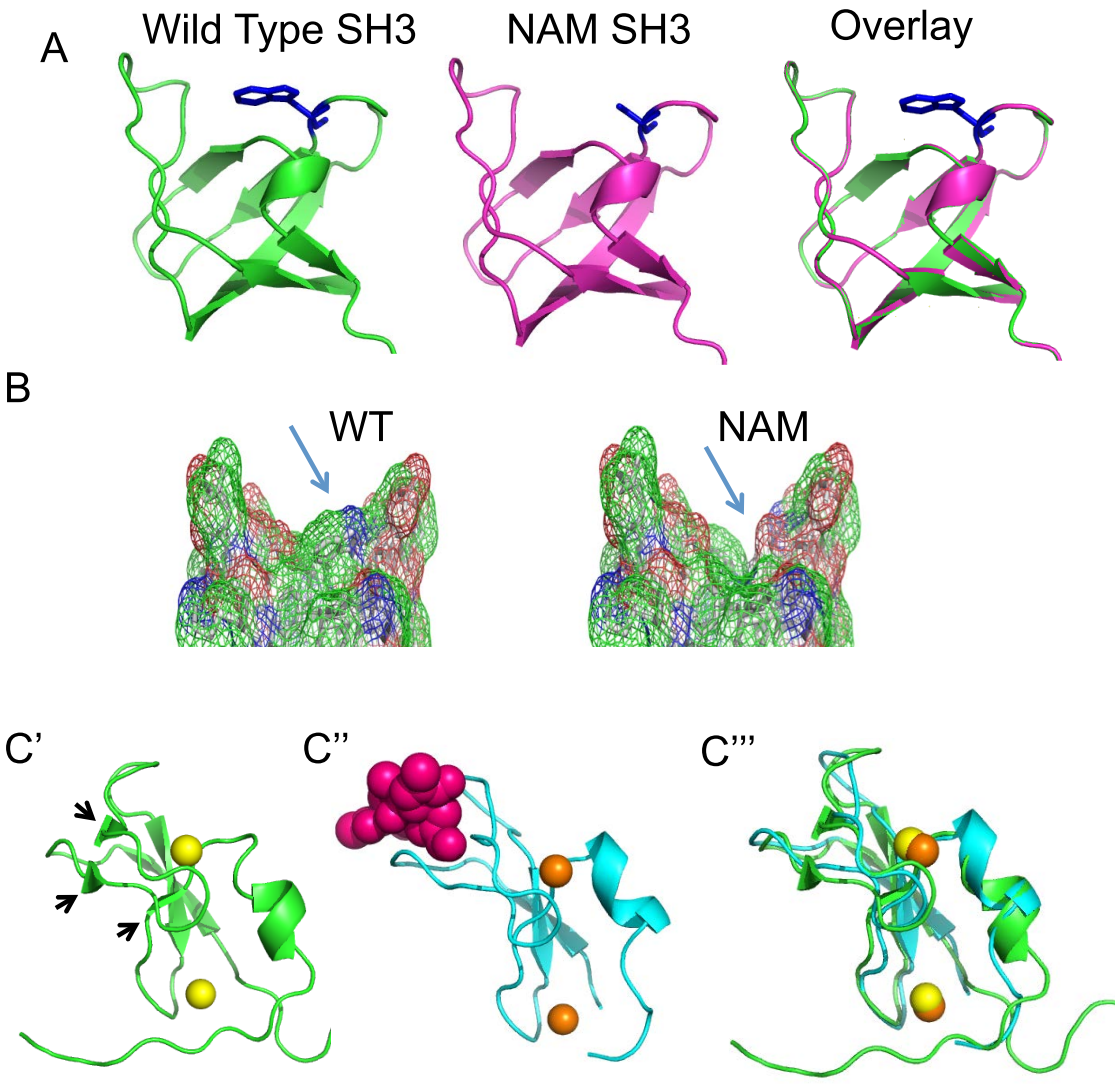

Figure 2-18. Models of Stac3 Domains. The solved first SH3 domain of Stac1 (PDB ID: 2DL4) was used as a template for modeling the first SH3 domain of Stac3. The ribbon cartoon of the SH3 domains with the WT W residue, (A, left, in gray), the NAM S residue, (A, middle, in gray), and the overlay of the two models (A, right, in red), showing the surface exposed residue. (B) Surface hydropathy model of the first Stac3 SH3 domain. The arrow points to the W284 (left), which contributes a positive charge (in blue) to the surface of the SH3 binding domain. The model of the NAM mutation shows a fissure in the SH3 binding surface, and the contribution of a negative charge (in red). Green is neutral. (C') Cartoon structure of the solved Stac3 CRD domain (PDB: 2D6B). Additional small β-sheets are marked with arrowheads. Structural Zn^{2+} ions are in yellow. (C'') The solved PKC C1 CRD domain in complex with phorbol ester (in pink) (PDB:1PTR) . Structural Zn^{2+} ions are in orange. (C''') Overlay of the two structures.

CHAPTER III

STAC3 IS REQUIRED FOR NORMAL TRAFFICKING OF THE DHPR AND FORMATION OF TETRADS IN THE EC COUPLING COMPLEX

[Manuscript in preparation to be published as Jeremy W. Linsley, Eric J. Horstick, Clara Franzini-Armstrong, Richard I. Hume, and John Y. Kuwada.]

Abstract

Excitation-contraction (EC) coupling is the mechanism by which the muscle translates depolarization of the sarcolemma into Ca^{2+} release from the sarcoplasmic reticulum (SR) required for muscle contraction. EC coupling is dependent on interactions between the dihydropyridine receptor complex (DHPR) α1-subunit ($Ca_v1.1$) in the transverse tubules (t-tubules) that serves as the voltage detector and the ryanodine receptor (RYR1) in the SR that is the Ca^{2+} release channel. The Stac3 protein is a component of the EC-coupling complex, and although its presence is required for normal release of Ca^{2+} in skeletal muscle, the mechanism by which Stac3 supports proper Ca^{2+} release has not been established. Electron micrographs of triads in *stac3* mutant zebrafish indicate a deficit in the ability to form DHPR particles into groups of four called tetrads, suggesting abnormal trafficking or stability of the DHPR. Using $Ca_v1.1$-GFP and the photoactivatable $Ca_v1.1$-mEos3.2 expressed in live, anaesthetized embryos, we find that

trafficking rate of $Ca_v1.1$ into and out of triads is significantly increased in *stac3* mutants versus wildtype embryos. Furthermore, the Stac3 protein is found to directly interact with both the DHPRβ subunit, and a region of the $Ca_v1.1$ protein, both previously implicated as required for normal EC coupling and tetrad formation. These results suggest that Stac3 affects EC coupling by regulating trafficking of Cav1.1 and formation of tetrads.

INTRODUCTION

Muscle contraction is triggered when electrical depolarization of the muscle membrane following synaptic release by motor neurons is translated into release of Ca^{2+} from the sarcoplasmic reticulum (SR) and subsequent activation of the contraction machinery, a process known as excitation-contraction (EC) coupling. In skeletal muscle, this process occurs through a direct interaction between the dihydropyridine receptor complex (DHPR), which acts as a voltage sensor on the plasmamembrane/transverse (t) -tubule membrane, and the ryanodine receptor 1 (RyR1) in the SR membrane, which acts as a Ca^{2+} release channel. The DHPR is an L-type voltage-gated Ca^{2+} channel, and is made up of a principle pore forming α1s subunit ($Ca_v1.1$) containing four repeated six-transmembrane (6-TM) regions, as well as auxiliary subunits $Ca_vβ1a$, $Ca_vα2δ1$, and $Ca_vγ1$ (Flucher et al., 2005). The DHPR subunits are thought to traffic together through skeletal muscle myofibers to their target at intracellular junctions of the SR and either the t-tubules or the plasma membrane, called triads and peripheral couplings respectively (Franzini-Armstrong et al., 1998). Trafficking in differentiated muscle is complicated by the presence of SR, an intricate network of tubules and cisternae winding through the cell, which appears to be contiguous with the ER, and contains components of the protein folding machinery (Volpe et al., 1992). As such, SR resident proteins appear to traffic through contiguous ER/SR to specified targets in the SR (McFarland et al., 2010), and expressed viral glycoproteins directly traffic through the SR to their terminal targets (Kaisto and Metsikko, 2003; Rahkila et al., 1998). Although multiple studies (Protasi et al., 1998; Schredelseker et al., 2009; Schredelseker et al., 2005) have recognized the

importance of expression and targeting of the DHPR to triads, the path by which the DHPR finds its way to the triad has not been described, and represents another way the cell might regulate the complex.

Freeze fracture electron microcopy of skeletal muscle has shown that DHPRs are arranged in groups of four called tetrads in orthogonal arrays in triads and peripheral couplings (Block et al., 1988). RyR1s are arranged in a corresponding orthogonal array of homotetramers in the SR membrane with each tetrad apposed to every other RyR1 presumably with each DHPR of a tetrad contacting a single RyR1 of the homotetramer. The formation of DHPRs into tetrads requires the presence of RyR1s (Protasi et al., 1998), which extend large, electron-dense feet across the intracellular junction between the SR and t-tubule/plasmamembrane to contact DHPRs (Franzini-Armstrong and Jorgensen, 1994). The presence of tetrads correlates with functional EC coupling in skeletal muscle, and EC coupling has not been found to be normal without a normal array of tetrads (Dayal et al., 2013; Schredelseker et al., 2009; Takekura et al., 2004). Chimeras between $Ca_v1.1$ and the cardiac $Ca_v1.2$, which does not support tetrad formation, has shown that the presence of the intracellular loop between the second and third 6-TM repeat (L2-3) of the $Ca_v1.1$ is required to both restore tetrad formation and EC coupling in the $Ca_v1.2$ backbone when expressed in *dysgenic* ($Ca_v1.1$ null) myotubes (Grabner et al., 1999; Takekura et al., 2004). Furthermore, the immotile zebrafish $Ca_v\beta1$ mutants *relaxed* that lack EC coupling, contain a reduced amount of DHPR particles in triads, and the particles are not arranged in tetrads (Schredelseker et al., 2005). Rescues of *relaxed* mutants with cardiac $Ca_v\beta2a$ and the ancestral $Ca_v\beta M$ isoform from housefly (*Musca domestica*) have shown that the amount of complete or near complete, *i.e.* three or four

DHPR particles in a tetrad, correlates with the amount of EC coupling (Schredelseker et al., 2009). Nevertheless, the presence of tetrads does not guarantee EC coupling, as rescue of *relaxed* mutants with neuronal $Ca_v\beta3$ restores some tetrad formation, but not the charge sensing capability of the DHPR required for EC-coupling, indicating EC coupling requires both tetrad formation and charge sensing for function, and the $Ca_v\beta1$ in addition to the $Ca_v1.1$ is required for both (Dayal et al., 2013).

Previously, we showed that Stac3 is a member of the EC coupling complex and is required for normal Ca^{2+} release in vertebrate skeletal muscles (Horstick et al., 2013). Furthermore, a mutation in *STAC3* was the basis for a congenital myopathy, Native American Myopathy (NAM), characterized by muscle weakness and susceptibility to malignant hyperthermia. Yet how Stac3 functions within the EC coupling complex to support normal Ca^{2+} release was not known, and represented a deficit in the understanding of how EC coupling functions. Towards this goal, we used qPCR, immunocytochemistry, live cell imaging, freeze fracture electron microscopy and biochemistry to look at the expression levels, trafficking, and arrangement of the DHPR in the triad. We found that *stac3* null mutants have normal levels of $Ca_v1.1$ and RyR1 transcripts but a mild reduction in levels of steady state DHPR but not RyR1 in the triad, as well as a substantial reduction in numbers of full tetrads of four DHPR particles in the triad. Furthermore, we find that Stac3 biochemically interacts with specific regions of the DHPR *in vitro*, and increased trafficking rate of DHPR to and from the triad. These results mark the first mechanistic evidence of the influence of Stac3 on the EC coupling complex.

MATERIALS AND METHODS

Animals and behavioral analysis.

Zebrafish were bred and maintained according to approved guidelines of the University Committee on Use and Care of Animals at the University of Michigan.

Antibody conjugation and immunolabeling

Anti-$Ca_v1.1$, MA3-920 (Thermo), and Anti-pan RyR 34c (DSHB) were each purified using a Nab Protein A/G Spin Kit (Thermo). Purified flow through was buffer exchanged with PBS pH7.0 and concentrated to 1mg/ml with Pierce Protein Concentrators PES, 10K MWCO. Antibodies were conjugated with Alexafluor 488 or 568 Protein labeling kits. Dye/IgG ratio was estimated by spectrophotometry with a Nanodrop (Invitrogen). Anti-Cav1.1-alexa488 was found to give ideal labeling at 2.1 dye/IgG, and Anti-panRyR-alexa568 at 5.5 dye/IgG. Anti-panRyR-alexa568 was used at 1:500, anti-$Ca_v1.1$ at 1:100 unless otherwise noted, anti-SERCA (Abcam) at 1:1000, anti-α-tubulin (Sigma) at 1:1000, anti-Stac3 at 1:100 (Horstick et al., 2013). Whole mount immunolabeling was performed after fixation with 4% PFA (anti-$Ca_v1.1$ and anti-SERCA), or Dent's fixative (Chen et al., 2010) (anti-α-tubulin and anti-SERCA) at 4°C overnight using previously described methods (Hirata et al., 2005).

Disassociation of Zebrafish Myotubes and Quantification of Triadic fluorescence

Progeny from *stac3*^{mi34} carriers were raised to 48hpf and *stac3*^{mi34} mutant embryos were behaviorally identified as previously described (Horstick et al., 2013).

Approximately 30 mutant or sibling embryos were incubated in collagenase type II (3.125 mg/ml in CO2-independent medium) at 20 °C for ~1.5 h with the muscle fibers triturated every 30 min. Fibers were spun at 380 g for 5 min, the supernatant was removed, and the pellet was re-suspended and allowed to settle on poly-lysine coated cover slips. Fibers were fixed in 4% PFA, and washed with PBS and 0.5% detergent and blocked with 100mg/ml BSA and heat inactivated goat serum (Invitrogen). Quantification of immunolabeled $Ca_v1.1$ or RyR triad expression was determined by measuring the average fluorescence intensity of Alexafluor 488 or 568 along a line across a row of triadic junctions. Five measurements were made from each myotube, over three separate cultures for each titration of antibody on wildtype siblings and *stac3* mutants.

Freeze Fracture Electron Microscopy

Four day old embryos were fixed with 6% glutaraldehyde in 0.1 M cacodylate buffer at neutral pH after removal of tail skin and processed as previously described (Arikkath and Campbell, 2003; Schredelseker et al., 2009).

Cloning of cacna1sa

Pooled mRNA from 50 wildtype 48 hpf embryos was extracted using TRIzol (Invitrogen) reagent, and SuperScriptII and Oligo dT (Invitrogen) were used for reverse transcription to create a cDNA library. cDNA was amplified by PCR and subcloned into pGemT-easy using Max Efficiency Stbl2 competent cells (Invitrogen). Kozak sequence containing EGFP and mEos3.2 were amplified using *SacII* tagged primers, digested with Fast Digest *SacII* (Thermo), and ligated in frame to the N-terminus of *cacna1sa* which

has been shown to produce a fully functional $Ca_v1.1$ protein (Grabner et al., 1998). $Ca_v1.1$ -GFP and $Ca_v1.1$-mEos3.2 were digested out of the pGemT-Easy backbone, Gel purified using a SNAP UV Free Gel purification kit (Invitrogen) and ligated into pα-*actin:SV40* backbone for skeletal muscle expression. Sanger sequencing using 17 primers spaced through the length of the *cacna1sa* confirmed 100% sequence identity with ZV9 amino acid prediction.

In vivo live cell imaging and quantification

Progeny from *stac3*^{mi34} carriers were injected at 1 cell stage with pα-*actin:* $Ca_v1.1$-GFP or $Ca_v1.1$-mEos3.2*,* raised to 24hpf at 28.5°C, enzymatically dechorionated using 2mg/ml Pronase (Protease, Type XIV, Sigma) for 20 minutes, and put into 200 μM 1-phenyl 2-thiourea (PTU) E2 medium at 28.5°C to inhibit melanogenesis (Karlsson et al., 2001; Nusslein-Volhard, 2002). At 48 hpf *stac3*^{mi34} mutant embryos were identified behaviorally and left at room temperature (20°C). All imaging experiments were conducted on embryos from 2-4 days post fertilization (dpf) at room temperature (20°C). GFP or mEos3.2 expressing embryos were identified using a fluorescent dissecting microscope, and anaesthetized in 0.02% Tricaine in 200 μM PTU (Sigma) for at least 2 hours. For mounting, embryos were embedded in 1% low melting point agarose on a plastic petri dish, covered with 0.02% Tricaine and 200 μM PTU, and imaged using a 40x objective on a Leica Sp5 upright confocal microscope using a 10x digital zoom. Photo-activation of mEos3.2 was performed with a 405 nm laser scanning a region of interest spanning several t-tubules (ROI) 30 times over the coarse of ~1 minute. In mEos3.2 imaging, PMT settings were set so that no bleed-through of pre-activated Green

fluorescence was seen in the Red channel (band-pass 575-730nm). Low laser intensities were used to minimize bleaching (8% 488nm and 10% 568nm excitation laser intensities). FRAP bleaching was achieved with 10 scans of 100% 488nm laser intensity over the course of 1 minute, and subsequent imaging with 8% 488nm excitation laser (band-pass 493-555 nM).

Quantification of fluorescence in live imaging was done by quantifying the average fluorescence intensity of a polygon drawn across a string of triadic junctions of $Ca_v1.1$-GFP or $Ca_v1.1$-mEos3.2 at each time point sampled. For $Ca_v1.1$-mEos3.2 imaging, red fluorescence was normalized as the percentage of intensity of the first image after photo-activation with the pre-photo-activation image subtracted as background. A minimum photo-activation cutoff of at least 10 (F_{post} activation – F_{pre} activation) was used as the amount of photo-activation of mEos3.2 was found to vary based on the depth the $Ca_v1.1$-mEos3.2 expressing cell within the animal and affected the signal to noise of the confocal imaging (data not shown).

Data for $Ca_v1.1$-mEos3.2 photo-activation assays are displayed in units of *normalized percentage of initial fluorescence* as calculated according to the equation $(F(x)-F_{pre})/(F_{post}-F_{pre})*100$ where F(x) = fluorescence at time x in minutes after activation, F_{post}= fluorescence immediately after photo-activation, F_{pre}= fluorescence before photo-activation. Data for $Ca_v1.1$-GFP FRAP assays are displayed in units of *normalized percentage of pre-bleach fluorescence* as calculated according to the equation $(F(x)-F_{post})/(F_{pre}-F_{post})*100$ where F(x)= fluorescence at time x in minutes after bleaching, where F_{post}= fluorescence immediately after bleaching, and F_{pre}= fluorescence before bleaching. Data was plotted and each time-lapse was fit to a non-linear regression for a

one phase decay ($Ca_v1.1$-mEos3.2) or plateau followed by one phase association ($Ca_v1.1$-GFP) using Prism6, and a best fit plateau value and rate constant (k) were derived. Nocodazole was dissolved at 1ug/ml in 1% DMSO, PTU/E2 medium, and 48 hpf embryos were incubated in the media or DMSO control for 24 hrs. After imaging, embryos were removed from agarose mount and used for whole mount immunolabeling.

Cell culture constructs, Transfections, Immunoprecipitation and Western Analysis

Zebrafish *stac3* was amplified with primers containing EcoRI and BamHI tags, digested with appropriate the enzyme, and inserted into pEGFPN-1 to create C terminally tagged zstac3-EGFP. $Ca_v\beta1a$, and the N-Terminus, L1-2, L2-3, L3-4, and C-Terminus cytoplasmic regions of $Ca_v1.1$, were amplified with EcoRI and BamHI tags digested with appropriate digestion enzymes and sub-cloned into pGBKT7 (Clontech) to create N-terminal fusions with a c-Myc epitope tag. Resulting fusions were again amplified with T7-*NheI* forward and DNABD-NotI R primers, and inserted into pCDNA3.1+ (Invitrogen). After sequencing to check correct configurations, all expression plasmids midipreped for transfection experiments (Qiagen).

Cos-7 cells were grown in 10 cM dishes in DMEM media with 10% FBS until ~90% confluence and then co-transfected with 14μg of each construct in each combination using Lipofectamine 2000 (Invitrogen). Cells were allowed to incubate overnight to allow protein expression to mature, and then were washed three times with ice cold PBS, and collected using cell scrapers. Protein purification and co-immunoprecipitation was conducted as previously described (Horstick et al., 2013) using anti-Myc (Clontech) 1:200, anti-GFP (Torrey Pine Biosciences) 1:200, rabbit pre-

immune serum 1:200, or mouse normal IgG 1:200 (Santa Cruz). Western analysis was conducted as previously described (Horstick et al., 2013).

Primer Sequences Involved

zcacna1sa F 5'-ATGGAGGGAAACGGCGAAGC-3'

zcacna1sa R 5'-TTAGACATGGCAGTGTGTAATGTCTGA-3'

rB1a ecori F aaagaattccATGGTCCAGAAGACCAGCATGT

rB1a bamhi R aaaggatccCTACATGGCGTGCTCCTGCT

meos3.2 F aaaccgcggCGCTACCGGTCGCCACCATGAG

meos3.2 R aaaccgcggttTCGTCTGGCATTGTCAGGCAATCC

zstac3 pegfp f aaagaattcATGGCTCAATATGACCAACTGGAGGATAA

zstac3 pegfp R aaagtcgacaaGAGCTCATGCAGCAGATCCGC

gfp sacii f aaaccgcggATGGTGAGCAAGGGCGAGGAG

gfp sacii r aaaccgcggttcttgtacagctcgtccatgcc

RESULTS

Expression of DHPR but not RyRs at triads is reduced in *stac3* mutant embryos

As EC coupling is dependent on the interactions of the DHPR and the RyR1, we hypothesized that Stac3 may affect the expression levels of one or both of the core components of the EC coupling complex. Using fluorophore-conjugated anti-$Ca_v1.1$ (anti-Ca_v488) labeling of disassociated muscle cells, we detected a small but significant decrease ($p< 0.05$) in the steady state expression of $Ca_v1.1$ at triads of disassociated *stac3* mutant myotubes over a range of antibody concentrations compared to those of wildtype siblings (Fig. 3-1 a,b,c). Using fluorophore-conjugated anti-RyR, no difference was found in expression of RyR at the triads (Fig. 3-1 d), consistent with our previous results in which we found the function and ultrastructure of RyR and the SR are normal in *stac3* mutants (Horstick et al., 2013). Thus Stac3 may be affecting EC coupling primarily by regulating DHPRs at triads.

Transcription of $Ca_v1.1$ and $Ca_v\beta$ are unperturbed in *stac3* mutants

Stac3 could potentially regulate transcription of $Ca_v1.1$ and thus result in a decrease in transcripts of $Ca_v1.1$ in *stac3* mutants (Horstick et al., 2113). To see if the decrease in $Ca_v1.1$ could be due to decreased synthesis, the message levels for $Ca_v1.1$ and RyR1 were assayed by qPCR (Fig. 3-2). In zebrafish, *dhpra1sa* and *dhpra1sb* are genes that encode $Ca_v1.1$ expressed by the slow and fast twitch muscles, respectively (Schredelseker et al., 2010). Transcript levels of both *dhpra1sa*, and *dhpra1sb* relative to the housekeeping *succinate dehydrogenase a* (*Sdha*) gene were comparable between

wildtype siblings and mutants. Message levels of *ryr1a* and *ryr1b* that are expressed by slow and fast twitch muscles, respectively, were also comparable between wildtype siblings and *stac3* mutants (data not shown) (Hirata et al., 2007).

Because *stac3* mutants exhibit fewer DHPRs at triads, we wondered if increasing expression levels of $Ca_v1.1$ would restore EC coupling in mutants. However, overexpression of $Ca_v1.1$-GFP, which has been reported to traffic to triads and rescue EC coupling in dysgenic muscles (Grabner et al., 1998), did not rescue swimming at 48hpf in *stac3* embryos (Table 3-1). So it appears that simply increasing the amount of triadic $Ca_v1.1$ is not sufficient to rescue the EC coupling defect in *stac3* mutants.

stac3 mutant embryos have fewer DHPR particles per tetrad and fewer particles per cluster

Since there is only a modest decrease in DHPRs at triads in *stac3* mutants, but a large decrement in EC coupling, we examined the molecular geometry of DHPRs at triads with freeze fracture electron microscopy of 4 dpf wildtype and *stac3* mutant larval skeletal muscles. In wildtype larvae, DHPR particles are arranged in diamond shaped, groups of four called tetrads (Fig. 3-3 a). The center of each tetrad is aligned opposite an underlying RyR1 homotetramer, which forms an orthogonal array in the membrane of the SR (Franzini-Armstrong and Jorgensen, 1994). Tetrad arrays are determined by the array of DHPR particles in the junctional t-tubules and since tetrads within arrays exhibit consistent spacing, the spatial location of tetrads can be inferred, even when tetrads contain fewer than 3 particles (Schredelseker et al., 2005; Takekura et al., 1995a; Takekura et al., 2004). Most (94%) of tetrads in wildtype embryos contain on average

between three (near complete tetrad) and four (complete tetrad) DHPR particles (mean = 3.4, se = 0.5) (Fig. 3-2a). In contrast, tetrads in *stac3* mutant embryos are less organized and have significantly fewer particles per tetrad (mean = 2.6, se = 0.6, $p < 0.0001$). Overall, tetrads in *stac3* mutants contain a 52% reduction in the amount of complete tetrads (Fig. 3-3 c,d,e). Furthermore, only 46% of the total DHPR particles are found within complete tetrads in *stac3* mutants, compared to 74% of total particles in wildtype fish that are a part of a complete tetrad. Consistent with the immunolabeling results of $Ca_v1.1$ in triads, *stac3* mutant embryos have a small (~25%) overall reduction in DHPR particles per cluster (compare Fig. 3-3e and Fig. 3-1c). These results suggest that the functional unit of DHPRs required for EC coupling are complete or nearly complete tetrads.

$Ca_v1.1$ is removed from triads of *stac3* mutant embryos at a faster rate

Another way Stac3 may affect the EC coupling complex is by regulating protein trafficking of DHPRs to triads and/or stability of DHPRs at triads. To test this hypothesis, we directly visualized $Ca_v1.1$ in live skeletal muscle fibers to determine the stability of $Ca_v1.1$ at triads in *stac3* mutants and wildtype siblings. $Ca_v1.1$ was tagged with the photoactivatable fluorophore mEos3.2 (Zhang et al., 2012), and the stability of photoactivated fusion protein was monitored by time lapse confocal microscopy in live, immobilized embryos over the course of an hour. $Ca_v1.1$-mEos3.2 localized to triads in both wildtype sibling and *stac3* embryos (Fig. 3-4a,b). The red fluorescence of activated $Ca_v1.1$- mEos3.2 at triads gradually decreased over the course of an hour in both wildtype sibling and *stac3* mutant embryos with relative fluorescence decreasing faster in mutant

muscles compared to wildtype sibling muscles (Fig. 3-4 a,b). The percentage of initial fluorescence of activated $Ca_v1.1$-mEos3.2 in the triads was quantified over the course of an hour and fit to a non-linear regression (Fig 3-4c). The mean of the derived best fit rate constants indicated that the fluorescence decay of $Ca_v1.1$-mEos3.2 in *stac3* mutant triads occurred at a significantly faster rate than in wildtype siblings (Fig. 3-4 c,d) (T-test, $p < 0.05$, comparison of fits $p < 0.0001$), but the plateau of decay was not significantly different (Comparison of fits, $p = 0.1$) (Fig. 3-4c, Table 3-2). These data suggest that the normal stability of triadic DHPRs requires Stac3.

Trafficking rate of $Ca_v1.1$ to triads is increased in *stac3* mutant muscle

A reduced stability of $Ca_v1.1$ in triads must be compensated for by an increased rate of trafficking of the protein to the triad, or else the steady state protein level would eventually decrease to zero. As a gradual reduction of DHPR levels in *stac3* mutants has not been observed (Figs. 3-1a and 3-3a,b), we reasoned that the trafficking rate of the DHPR in *stac3* mutants must be increased. To examine the trafficking rate of the DHPR to the triad, we expressed $Ca_v1.1$-GFP in muscles of live immobilized embryos, and performed fluorescence recovery after photobleaching (FRAP) to analyze the fluorescence recovery of $Ca_v1.1$-GFP to the triads. Within five minutes after bleaching, $Ca_v1.1$-GFP could be seen moving in straight, longitudinal lines perpendicular to the columns of triads through muscle fibers, eventually accumulating at triads in both *stac3* mutants and wildtype siblings (Fig. 3-5 a). Fluorescence recoveries at triads over time were quantified, standardized to fluorescence values before and immediately after bleaching, and fit to a non-linear regression to obtain best-fit values for plateaus and rate

of recovery to the plateau (Fig. 3-5b). Traces of mean of fluorescence from wildtype siblings and *stac3* mutants showed that the majority of fluorescence recovery occurred in the first 15 minutes after bleaching, before leveling off to a plateau (Fig. 3-5b). The plateaus of fluorescence recovery were not significantly different between *stac3* mutants and wildtype siblings (Table 3-2). However, the rate of recovery of $Ca_v1.1$-GFP fluorescence to the plateau at the triad was significantly higher ($p<0.001$) in triads of *stac3* mutant than in wildtype siblings (Fig. 3-5c, Table 3-2). Thus trafficking to the triads occurred faster in mutant versus wild type muscles.

Trafficking of $Ca_v1.1$-GFP proceeds along the longitudinal ER/SR

Expression of $Ca_v1.1$-GFP in myofibers revealed that in addition to triads, $Ca_v1.1$-GFP was found in longitudinal lines, intersecting the t-tubules of the myofiber, in both *stac3* mutants and wildtype siblings (Fig. 3-5a). After photobleaching in FRAP assays, fluorescence recovery appeared to proceed along the same longitudinal lines before accumulating in triads (Fig. 3-5a). Electron microscopy of vertebrate skeletal muscle showed membranous tubules representing the longitudinal SR connecting the cisternae of SR in triads along the longitudinal axis of the myofibers (Franzini-Armstrong, 1970; Horstick et al., 2013) that corresponded with longitudinal lines of $Ca_v1.1$-GFP. Thus we reasoned that the longitudinal lines of $Ca_v1.1$-GFP might represent $Ca_v1.1$-GFP being trafficked through the longitudinal SR. We tested this by immunolabeling myofibers expressing $Ca_v1.1$-GFP with anti-SERCA, a marker for longitudinal SR (Rossi et al., 2008). Indeed the longitudinal lines of $Ca_v1.1$-GFP coincided with anti-SERCA labeling and thus with the longitudinal SR (Fig. 3-6a). Since $Ca_v1.1$-GFP expression in zebrafish

myofibers may induce overexpression artifacts, we further examined fixed dissociated skeletal muscles immunolabeled with anti-$Ca_v1.1$-488 and found longitudinal lines of $Ca_v1.1$ similar to those seen in $Ca_v1.1$-GFP expressing myofibers (Fig. 3-6a,b). Thus it appears that trafficking of $Ca_v1.1$ involves trafficking through the longitudinal SR.

Previous studies have described trafficking of membrane proteins through the longitudinal SR/ER in skeletal muscle to ER exit sites (ERES) distributed throughout the myofiber (Kaisto and Metsikko, 2003). In fact immunolabeling with anti-Sec23B, a marker for ERES (Saito et al., 2009), revealed ERES in a pattern similar to triads and t-tubule striations in zebrafish muscle (Fig. 3-6c), consistent with results found in mammals (Kaisto and Metsikko, 2003).

$Ca_v1.1$-GFP traffics through skeletal muscle in a nocodazole resistant manner

An alternative explanation for the longitudinal movement of $Ca_v1.1$ through skeletal muscle is that it represents the microtubule-based vesicular trafficking of $Ca_v1.1$ from the Golgi complex to the t-tubule membrane at triads. While orthograde transport of vesicles through the ER to the Golgi complex occurs via a microtubule independent mechanism in mammalian cells (Rogalski et al., 1984; Salas et al., 1986; Tartakoff and Vassalli, 1977), retrograde trafficking and normal vesicular trafficking from the Golgi complex to the plasmamembrane is disrupted by perturbations of microtubules (Lippincott-Schwartz et al., 1990). Thus disruption of microtubules, would be predicted to inhibit Golgi to membrane vesicular trafficking of $Ca_v1.1$-GFP but have no effect on orthograde longitudinal ER/SR trafficking. To disrupt microtubules, we bathed $Ca_v1.1$-GFP expressing embryos in nocodazole, a well-characterized microtubule

depolymerizing agent (De Brabander et al., 1976), and monitored the effect on trafficking rate. Nocodazole clearly disrupted microtubule formation in zebrafish skeletal muscle as demonstrated by a reduction in anti-α-tubulin immunolabeling (Fig. 3-7a). Nevertheless, nocodazole exposure had no effect on the rate of $Ca_v1.1$-GFP trafficking to triads (Fig. 3-7b), indicating $Ca_v1.1$-GFP traffics through muscle in a nocodazole-resistant mechanism and supporting the hypothesis of striations of $Ca_v1.1$-GFP as moving through ER/SR.

$Ca_v1.1$ is trafficked in longitudinal lines to its target in the triad, independently of Stac3

We next investigated how Stac3 could limit the trafficking rate of $Ca_v1.1$ to the triads. One potential mechanism might include Stac3 playing the role of a chaperone of $Ca_v1.1$ through the ER/SR to the triads, similar to the role $Ca_v\beta$ is thought to play with Ca_v1 (Buraei and Yang, 2010). As $Ca_v1.1$ traffics in distinct lines of longitudinal SR through the cell (Fig. 3-6 a,b), Stac3 would then be predicted to do the same. Yet, while fluorescence of $Ca_v1.1$-GFP can be seen in longitudinal lines in FRAP assays both pre-bleach and post-bleach, Stac3-GFP appears at and recovers directly to the triads in both cases without forming noticeable longitudinal patterns (Fig. 3-8 a,b). Furthermore, co-immunolabeling with anti-Stac3 indicates that while $Ca_v1.1$-GFP is in the longitudinal SR in between triads, Stac3 is not, indicating that the two proteins colocalize only at the triads (Fig. 3-8c). Thus the trafficking pathway of $Ca_v1.1$ to the triads is independent of Stac3, and Stac3 must affect $Ca_v1.1$ solely at the triad.

Stac3 biochemically interacts with $Ca_v1.1$ L2-3 and $Ca_v\beta$ *in vitro*

As Stac3 has an effect on the triadic expression, tetrad arrangement, and trafficking of the DHPR, we next looked for evidence of biochemical interactions between Stac3 and components of the DHPR. The $Ca_v\beta$ subunit and the intracellular regions of the $Ca_v1.1$ were tagged with the Myc epitope, co-expressed with Stac3-GFP in Cos7 cells, and immunoprecipited from cell lysate. Stac3 was found to co-immunoprecipitate with the $Ca_v\beta$ 1 (Fig. 3-9a) and the L2-3 region of $Ca_v1.1$ (Fig. 3-9b), but not with other regions of the $Ca_v1.1$ (data not shown). These results suggest that Stac3 affects the DHPR through interactions with these components of the DHPR.

DISCUSSION

In the present study we established a mechanism by which Stac3 affects the trafficking and stability of the DHPR complex but not RyR in triads, and provided evidence of interactions between Stac3 and specific components of the DHPR complex that might mediate these effects. We showed through electron microscopy and direct fluorescent antibody immunolabeling that *stac3* mutants have a small but significant decrease in steady state levels of DHPR in triads, a reduction in numbers of DHPR particles per tetrad, and a dramatic decrease in the number of complete tetrads compared to wildtype siblings. We showed that this defect in DHPRs was not due to decreased synthesis of DHPRs and could not be rescued by overexpression of DHPR in *stac3* mutants. Additionally, through the use of live cell imaging, we observed an increased rate of $Ca_v1.1$ trafficking into and out of the triad, and that trafficking involved movement of

DHPRs through the longitudinal SR. These results contribute new insights on how the DHPR is trafficked and stabilized in the EC coupling complex, and provide a new understanding of the requirements for the stability and organization for the DHPR in the EC coupling complex. While previous studies have characterized paralog or homolog chimeras of the $Ca_v1.1$ or $Ca_v\beta1a$ that partially disrupt the formation of tetrads (Schredelseker et al., 2009; Schredelseker et al., 2005; Takekura et al., 2004), this study presents the first evidence that disrupted tetrad formation can occur as the result of a genetic mutation, and suggests that partial disruption of tetrad formation can lead to a defect in EC coupling. Furthermore, this study represents the first evidence of a protein other than the $Ca_v1.1$, $Ca_v\beta$, or RyR1 that specifically affects tetrad formation. Coupled with our previous finding that a *STAC3* mutation is the causative factor for a human congenital myopathy, NAM, these findings hold immediate relevance for both our understanding of the mechanism of EC coupling and human disease.

This study took advantage of several novel approaches that were instrumental in furthering our understanding of the mechanisms of Stac3. First, since DHPRs are normally arranged in tetrads in close proximity (~10nm apart) to one another (Serysheva et al., 2002), and the antibody epitope for anti-$Ca_v1.1$ (mAb1) is on the L2-3 of the $Ca_v1.1$ which is in close contact with the RyR1 at the triadic junction (Kugler et al., 2004a), we reasoned that the size of a primary IgG antibody (~10 x 7 x2 nm) (Houde et al., 2009) combined with the size of multiple dye-conjugated secondary IgG antibodies used in standard immunofluorescence measurements (another IgG plus 1.4nm radius per dye) (Masuda et al., 2005) and the close proximity of the L2-3 epitopes with each other could influence quantification. Hypothetically, as DHPR particles in *stac3* mutants are

less tightly packed in tetrads (Fig. 3-3b), steric hindrance for secondary antibody labeling in mutant triads would be reduced in comparison to wildtype triads potentially leading to an underestimation of the differences in DHPR concentrations at triads between wildtype and mutant myotubes. Similar arguments hold for quantification of RyR1s at triads. Therefore, instead of using indirect immunofluorescence measurements, we generated directly conjugated antibodies of anti-$Ca_v1.1$ (mAb1) and anti-RyR (34c) for quantification of protein expression at triads. Directly conjugated antibodies not only allowed more accurate quantification of relatively small differences in expression levels at triads, but because signal amplification from the secondary antibody was not present, minority fractions of endogenous $Ca_v1.1$ localized in longitudinal SR between triads were visualized for the first time (Fig. 3-6a).

Modest decreases in DHPR were found by freeze fracture electron microscopy and direct immunofluorescence measurements. Since these methods only give a static picture of DHPRs at triads, protein trafficking defects that could not be detected in fixed samples could potentially be important for the dramatic effects Stac3 loss for EC coupling (Horstick et al., 2013). Yet as heterologous expression of a functional EC-coupling complex has not yet been achieved, and muscle cell culture lines have dramatically different subcellular structure and trafficking properties (Lu et al., 2001; Percival and Froehner, 2007), assay of protein trafficking of EC components have not been previously achieved. To address whether trafficking of DHPRs is affected in *stac3* myofibers, we developed a method for live cell imaging of $Ca_v1.1$-GFP and $Ca_v1.1$-mEos3.2 in immobilized zebrafish embryos to allow us to monitor the dynamics of $Ca_v1.1$ trafficking. In particular the recently developed mEos3.2, which is substantially

brighter, more photo-stable, and possibly more monomeric than previous generations of genetically-encoded photo-activatable proteins such as Dendra2 (Zhang et al., 2012), allowed accurate time-lapse imaging of $Ca_v1.1$ in live skeletal muscles.

Both GFP and mEos3.2-tagged $Ca_v1.1$ expressed in wildtype and *stac3* mutants appeared to localize to triads, yet did not appear to rescue the *stac3* motility phenotype (Figs. 3-4a,c, 3-5a, data not shown), indicating that limited forward trafficking of $Ca_v1.1$ to triads did not appear to be a cause of the decreased levels of $Ca_v1.1$ in the triad, or the cause of the defect in EC coupling in *stac3* mutants. However, live cell imaging of photoactivated $Ca_v1.1$-mEos3.2 indicated that $Ca_v1.1$-mEos3.2 decayed from the triads at a significantly faster rate in *stac3* mutants than in wildtype siblings (Fig. 3-4c,d, Table 3-2), confirming that there is indeed a trafficking defect present in *stac3* mutants. Furthermore, with live cell imaging FRAP assays, we were able to visualize and determine the rate of trafficking of the $Ca_v1.1$ into the triad, which indicated that the trafficking of $Ca_v1.1$-GFP into the triads was actually significantly faster in *stac3* mutants than in wildtype siblings (Fig. 3-5, Table 3-2).

Although the trafficking rate of $Ca_v1.1$ in *stac3* mutants is accelerated, we were unable to detect a dramatic decrease in steady state expression levels using live cell imaging assays. The presence of plateaus of fluorescence recoveries and fluorescence decays indicate that a stable, immobile fraction (the % of fluorescence above the plateau in FRAP assays, and below the plateau in photoactivation assays) of $Ca_v1.1$s is present in both *stac3* mutants and wildtype siblings through the length of time we measured (Figs. 3-3d, 3-5b). Additional steps of decay of $Ca_v1.1$ beyond the first hour are likely also present, as eventually both photo-decay and FRAP recovery should reach 0% and 100%

respectively. Thus, whether there are differences in later steps of decay between *stac3* mutants and wildtype siblings cannot be ruled out. However, within the time frame monitored, $Ca_v1.1$ appears to be relatively stable in triads in both *stac3* mutants and wildtype siblings.

Comparisons of means of the plateaus of both decay and fluorescence recovery using $Ca_v1.1$-mEos3.2 and $Ca_v1.1$-GFP respectively, indicate that mean plateaus are not significantly different in *stac3* mutants and wildtype siblings (Table 3-2). Although the lack of difference of immobile expression levels of Cav1.1 between *stac3* mutants and wildtype siblings at triads in live imaging assays appears at odds with differences detected in steady state levels of $Ca_v1.1$ and the DHPR determined with immunolabeling techniques and electron microscopy respectively, the precision of live imaging assays for detecting small differences in steady state levels of Cav1.1 is compromised by overexpression. Overexpression assays may hide the stability defect by either compensating for losses with extraneous expression, or masking the presence of a difference due to the existence of the endogenous unlabeled Cav1.1. Furthermore, the plateau of fluorescence expression from $Ca_v1.1$-GFP FRAP assays is a particularly noisy measurement because trafficking of $Ca_v1.1$-GFP appears to proceed *en passant* of triads, meaning much of the steady state measurement of a particular triad at a time point is sampling both the trafficking lanes headed to another triad and the newly accumulated triad fraction (see Fig. 3-8a,b), which may mask the detection of true levels of immobile $Ca_v1.1$ in both *stac3* mutants and wildtype siblings. Measurements of endogenous steady state levels, in contrast, are likely to be better measures of differences in expression of DHPR at triads, and electron microscopy and direct immunofluorescence measurements

indicate a modest (25%), but significant decrease in levels of DHPR in triads. Taken together, these results indicate that Stac3 plays only a minimal role in fully stabilizing most of the $Ca_v1.1$ in the triad, but has a significant role in slowing trafficking through the triad.

Do the decreased expression levels of DHPR particles in triads, or the abnormal trafficking rates of DHPR particles to and from tetrads explain the motility phenotype?

Previously, we reported that *stac3* mutant zebrafish embryos have a severe motility defect characterized by an inability to swim in response to touch, and a corresponding 90% decrease in evoked Ca^{2+} release (Horstick et al., 2013). While this study provides the first mechanistic detail on how the Stac3 protein affects the EC coupling complex, it does not comprehensively explain the *stac3* mutant behavioral phenotype and the corresponding dramatic defect in Ca^{2+} release. EC coupling depends on the interaction between the DHPR and RyR1, and no defects in RyR expression levels (Fig. 3-1e), function or ultrastructure have yet been reported in *stac3* mutants (Horstick et al., 2013; Nelson et al., 2013), suggesting the defect in EC coupling is in some aspect of DHPR. At first glance, the 25% reduction in steady state DHPR levels (Figs. 3-1b, 3-3e) is hard to reconcile as a cause of the dramatic Ca^{2+} release defect in *stac3* mutants. However, expression of DHPR in the triad does not guarantee EC coupling. *relaxed* mutants, for example, contain a 60% reduction in DHPR particles in triads but a complete loss of EC coupling due to the complete inability of DHPR particles to organize in tetrads (Schredelseker et al., 2005). Furthermore, the level of complete or near complete tetrad formation of *relaxed* mutants rescued with expression of $Ca_v\beta2a$ or $Ca_v\beta M$ correlates

with the level of restoration of EC coupling, indicating complete tetrad formation is required for EC coupling (Schredelseker et al., 2009; Takekura et al., 2004). Thus although *stac3* mutants have only a 25% reduction in total DHPR particles, they have a more substantial 52% decrease in the proportion of full tetrads compared to wildtype which is more indicative of their EC coupling defect. If decreased tetrad formation in *stac3* mutants were due simply to the decrease in total DHPR particles, we would expect to see the percentage of total DHPR particles in tetrads are the same as in wildtype siblings despite the decrease. However, as only 46% of the total triadic DHPR particles are found in complete tetrads in *stac3* mutants, compared to 74% that are a part of a complete tetrad in wildtypes, these data suggest that decreased tetrad formation in *stac3* mutants is not simply due to decreased DHPR particles in the triad. Thus, Stac3 is necessary for the normal formation of full tetrads, and the lack of full tetrads in *stac3* mutants is consistent with the requirement of complete tetrads for normal EC coupling.

One complication is that not all tetrads from wildtype embryos are complete as seen with freeze fracture EM (Fig 3-3). The reason behind the presence of incomplete tetrads in wildtype animals is unknown but not unique to our results; clusters of fully complete tetrads have not been seen in any muscles of any age (Franzini-Armstrong, personal communication). One way to account for this phenomenon is that the number of complete tetrads required for normal EC coupling may be smaller than the number of tetrad sites so some may remain incomplete without consequence. This sort of overcompensation would be reminiscent of the fact that the amount of AChRs at the neuromuscular junction is much higher than needed for normal synaptic transmission (Wood and Slater, 2001). Furthermore, the amount of complete tetrads observed in our

data may be an underestimate due to experimental artifacts, as the freeze fracture process may cause the removal of some DHPR particles from tetrads.

A threshold of DHPRs per tetrad could also explain the lack of EC coupling in *stac3* mutants. For instance, a tetrad of four DHPR particles could provide maximum EC coupling, while 3 particles provides 10% EC coupling, and 2 particles are 1% functional. Such a model could account for the decrease in Ca^{2+} release in *stac3* mutants as due to the decreased functioning of tetrads rather than the lack of complete tetrads in *stac3* mutants. Unfortunately, the contributions of each DHPR particle in a tetrad to EC coupling has not yet been tested.

An alternative, and equally likely hypothesis to explain the dramatic Ca^{2+} release defect in *stac3* mutants, is that Stac3 directly modulates EC coupling by affecting the channel properties of DHPRs in addition to its function in promoting more complete tetrads. As $Ca_v\beta1$ and the L2-3 region of the $Ca_v1.1$ are known to regulate both tetrad formation and the channel properties of $Ca_v1.1$ (Kugler et al., 2004b; Schredelseker et al., 2009; Schredelseker et al., 2005; Takekura et al., 2004), our finding that Stac3 binds these two regions of the DHPR may be pertinent. A recently published study from the Grabner laboratory in which *relaxed* ($Ca_v\beta1$) mutants were rescued with the neuronal $Ca_v\beta3$ and chimeras of the $Ca_v\beta3$ in the $Ca_v\beta1a$ background showed that while $Ca_v\beta3$ is able to restore some tetrad formation (although the completeness and amount of tetrads was not reported), charge sensing as measured by gating movement of the DHPR is only minimally restored (Dayal et al., 2013). Thus tetrad formation and physiological regulation of DHPRs appear to be separable. Chimera analysis further revealed that the SH3 domain and a C-terminal putative SH3 binding site in $Ca_v\beta1a$ were required for

DHPR charge movement (Dayal et al., 2013). As Stac3 contains a SH3 domain that is critical for normal EC coupling (Horstick et al., 2013), the binding of Stac3 to $Ca_v\beta1$ via the SH3 domain may regulate DHPR channel properties. As SH3 domains in $Ca_v\beta1a$ (Dayal et al., 2013) and Stac3 (Horstick et al., 2013), and SH3 binding domains in the $Ca_v\beta1a$ (Dayal et al., 2013) and Cav1.1 L2-3 "critical region" (Grabner et al., 1999) are all required for EC coupling, it appears interactions mediated by SH3 domains are integral for EC coupling. Thus, biochemically dissecting the interactions mediated by SH3 domains, perhaps even with the use of chimeras of the neuronal Stac1 homolog, hold the promise of significantly increasing our understanding of EC coupling, especially if *stac3* acts in multiple functions in promoting EC coupling.

A previously unrecognized route for $Ca_v1.1$-GFP trafficking

This study represents the first description of the trafficking pathway for the $Ca_v1.1$ *in vivo* in differentiated skeletal muscle. Studies with primary dysgenic myotubes or derived cell culture lines have previously considered the role of $Ca_v1.1$ expression in ER/SR, but it was thought to be due to lack of differentiation of the muscle as the expression in the ER/SR which was reportedly reduced in more differentiated cells (Flucher et al., 2000a; Flucher et al., 2000b; Powell et al., 1996). However, muscle differentiation is heavily impacted when studied *in vitro* (Percival and Froehner, 2007), and studies using myotubes harvested from perinatal mice do not achieve a high degree of differentiation. Zebrafish larvae, in contrast, achieve a high level of differentiation early in larval development (Schredelseker et al., 2009; Schredelseker et al., 2005), and

differentiated zebrafish muscle fibers clearly show $Ca_v1.1$ expression in ER/SR (Figs. 3-5a, 3-6a,b).

Furthermore, taking advantage of the translucence of zebrafish larvae, we were able to observe *in vivo* time lapse imaging of trafficking of $Ca_v1.1$-GFP through the ER/SR. Our results indicate that $Ca_v1.1$-GFP, after synthesis in the rough ER, traffics in a microtubule independent fashion (Fig. 3-7) through the ER/SR to ERES nearby the triads (Fig. 3-6). This suggests that the RyR1 and the DHPR can be contiguous neighbors in the junctional SR membrane before the $Ca_v1.1$-GFP is subsequently trans-located from the SR to the t-tubule membrane and into a triad (Fig. 3-10). Whether the $Ca_v1.1$-GFP makes a stop at a Golgi outpost in its route to the triad remains an intriguing possibility as previous studies on mice indicate that Golgi outposts exist nearby triads (Ralston et al., 1999), but this was not resolved in the current study.

Curiously, the trafficking rate of $Ca_v1.1$ through the myofiber to triads is not affected by nocodazole exposure and persists despite disruption of microtubules (Fig. 3-7). On its face, the finding that such a widespread trafficking mechanism could operate independent of microtubules seems remarkable, yet dramatic rearrangements of Golgi, Nuclei, and ERES have been reported to occur in differentiating myofibers despite the presence of multiple microtubule-altering drugs, including nocodazole (Zaal et al., 2011). Furthermore, orthograde trafficking of membrane-bound proteins through the ER to the Golgi in cell culture is nocodazole resistant, operating through an apparently microtubule-independent mechanism (Rogalski et al., 1984; Salas et al., 1986; Tartakoff and Vassalli, 1977). Thus this data further indicates $Ca_v1.1$ trafficking through the SR/ER is analogous to previously described orthograde trafficking through the ER (Salas et al.,

1986). Transport of proteins through the ER has been reported to be sensitive to temperatures below 16°C (Saraste et al., 1986), to require ATP (Saraste et al., 1986), and to be sensitive to glycolytic inhibitors (Jamieson and Palade, 1968), and future studies of the trafficking rate of $Ca_v1.1$ under conditions known to block ER transport may help in characterizing this mechanism.

The function and localization of Stac3 in the trafficking of $Ca_v1.1$

While the current study does not provide the details of how the function of DHPR is disrupted by the disorganization of the tetrads of DHPR, it does suggest a mechanism by which the disorganization of DHPR particles can occur in *stac3* mutants. Although the trafficking rates into and out of the triad are increased in *stac3* mutants, the Stac3 protein does not co-localize with $Ca_v1.1$ during trafficking, instead navigating directly to the triads (Fig. 3-8). Thus, Stac3 must control the trafficking rate of $Ca_v1.1$ into and from the triad without leaving the triad. With this data, two alternative hypotheses can be proposed. One model for how this could occur is if Stac3 acts as a stabilizer of a conformational state of $Ca_v1.1$ in triads (Fig. 3-11). While providing only temporary pause that serves to simply slow the trafficking of the $Ca_v1.1$ through the triad (Figs. 3-4d, 3-5b, 3-11a), the pause provided by Stac3 could help stabilize an allosteric state of the $Ca_v1.1$ that allows it to form a complete tetrad. $Ca_v1.1$ in *stac3* mutants, on the other hand, would be unable to pause during trafficking through the triad, resulting in a faster trafficking rate into and out of the triad (Fig. 3-11b). Furthermore, the difference in endogenous expression levels of $Ca_v1.1$ and DHPR in triads could be simply due to the increase in the ability of wildtype siblings to form tetrads of four particles compared to

stac3 mutants, in which the majority of tetrads contain three or fewer DHPR particles (Figs. 3-1, 3-3). In this sense, Stac3 might function by a similar mechanism as molecular chaperone proteins in the ER, which hold membrane proteins in kinetic states that favor correct folding (Ellgaard et al., 1999; Morello et al., 2000). Without chaperone proteins to assist in the folding process, protein folding is reduced, resulting in less membrane expression as well as targeting for proteoloysis (Amaral, 2004; Kopito, 1999). Yet manipulating the cell by lowering the temperature, which slows kinetics, or adding chemicals that assist in folding have been found to rescue membrane expression (Denning et al., 1992; Morello et al., 2000). Thus, reduced trafficking rate of $Ca_v1.1$ by Stac3 may be essential in assisting the assembly of tetrads. Consistent with this hypothesis, the $Stac3^{NAM}$ allele has been found to show temperature-dependent motility rescue in the *stac3* mutant background (Horstick, 2012). As lower temperatures are thought to facilitate forward trafficking, lower temperatures may provide the extra boost that $Ca_v1.1$ needs with the hypomorphic $Stac3^{NAM}$ to increase tetrad formation to normal levels. Thus, permissive temperatures might be predicted to facilitate slower trafficking of the $Ca_v1.1$ in $Stac3^{NAM}$ expressing cells, but $Ca_v1.1$ in zebrafish myofibers at unpermissive temperatures would be predicted to traffic at the higher, *stac3* mutant-like rate.

Alternatively, Stac3 could act as a stabilizer of a four-DHPR particle tetrad. Without Stac3, DHPR particles mostly form two and three-particle tetrads (Fig. 3-3 c,d), which may leave a vacant, unstable spot in the tetrad. If the trafficking rate of DHPR particles through the triad is limited by the vacancy of tetrad positions, and *stac3* mutants are more likely to have an extra vacant spot, this would cause DHPR particles to cycle in

and out of the triad faster resulting in increased trafficking rates. Necessary for distinguishing between these two models is a detailed understanding of the logistics of how DHPR particles are inserted into triads and tetrads, which is unknown at this time. However, while in the second model trafficking rate is contingent on a bottleneck for insertion of DHPR particles into the triad that is determined by vacant tetrad positions, the first model is independent of a limit on tetrad positions, but rather posits that Stac3 limits the trafficking rate of DHPR particles once in the triad by actively slowing the trafficking rate through the triad. In support of the second model, freeze facture EM of wildtype zebrafish triads contain very few if any free DHPR particles that are not found at a tetrad site, suggesting insertion of DHPR particles into triads could be tightly regulated by vacant tetrad sites (Franzini-Armstrong, personal communication). However, in support of the first model, in the *relaxed* mutant, DHPR particles are found floating through the triad, and are not in positions opposite the RyR1 (Schredelseker et al., 2005), indicating DHPR particles can be inserted into the triad even if tetrads are not present, at least in a mutant state. To help resolve this issue, it may be useful to perform freeze fracture EM on wildtype zebrafish muscle that contains overexpressed $Ca_v1.1$-GFP. Thus if triads of overexpressed $Ca_v1.1$-GFP muscle contain free DHPR particles, it would suggest that DHPR particles are first trafficked into triads regardless of the presence of vacant tetrad positions. However, if triads contain a limited amount of DHPR particles that are all associated with tetrads, this would support the hypothesis that a bottle neck into the triads at the level of the tetrad is a way in which Stac3 could limit the trafficking rate of DHPR particles.

How does Stac3 fit into the EC coupling complex

While this study makes major contributions to our understanding of the mechanism of Stac3 function in the EC-coupling complex as well as providing an understanding of how the DHPR is trafficked through the myofiber, it represents only a small step towards understanding the complex interactions that are involved in EC coupling and how Stac3 fits into these complex interactions. Previous studies have identified the $Ca_v\beta1a$ and L2-3 of the $Ca_v1.1$ as critical regions of the DHPR for tetrad formation and EC coupling (Schredelseker et al., 2009; Schredelseker et al., 2005; Strube et al., 1998); (Grabner et al., 1999; Takekura et al., 2004; Tanabe et al., 1990), yet how these regions cooperate in coordinating the two processes remains unknown despite years of investigation (Beam and Bannister, 2010). This study establishes the first biochemical connection between these two "hot spots" for EC coupling. As Stac3 directly interacts with the $Ca_v\ \beta$ 1a and L2-3 of the $Ca_v1.1$ *in vitro* (Fig. 3-8) and co-immunoprecipitates with the *in vivo* EC coupling complex (Horstick et al., 2013), it is tempting to speculate that Stac3 is the link between $Ca_v\ \beta$ 1a and L2-3, thus far overlooked in EC coupling complex research. Further biochemical studies are clearly needed before drawing conclusions, but as evidenced by the severity of the *stac3* mutant phenotype, the Stac3 protein is clearly an integral factor in the functioning of EC coupling. Furthermore, as the NAM mutation in Stac3 is the only known locus producing malignant hyperthermia susceptibility other than mutations in the DHPR or RyR1, the mechanism of Stac3 holds particular relevance in human disease (Horstick et al., 2013). Thus, further research into the mechanisms of Stac3 function, furthered by this study, not only promise to uncover

the previously undiscovered basic biology of the EC coupling complex, but also mechanisms that contribute to human muscle myopathies.

Author Contributions

Freeze fracture electron microscopy was performed by Clara Franzini-Armstrong. All other experiments including antibody conjugation and immunocytochemistry, quantitative RT-PCR, live cell imaging, and co-immunoprecipitations were performed by Jeremy Linsley.

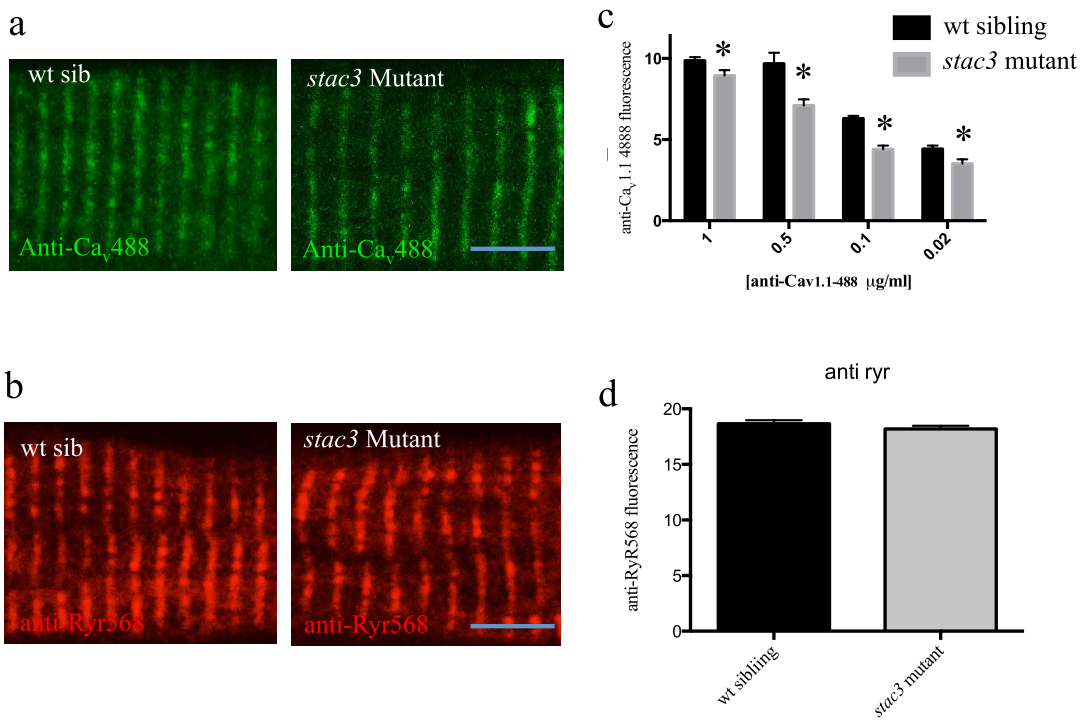

Figure 3-1. $Ca_v1.1$ expression is reduced in triads of *stac3* mutants. Representative images of disassociated myofibers from wildtype siblings (left) and *stac3* mutants (right), labeled with (a) anti-$Ca_v1.1$-488 and (b) anti-Ryr-568. Scale represents 2.5 µm. (c) Quantification of fluorescence across triads of wild type siblings (black) and *stac3* mutants (grey) across a range of concentrations of anti-$Ca_v1.1$-488 (n = 25 wt sib, n = 25 *stac3* mutant each titration). Bars represent mean fluorescence +/- SEM. * indicates significance $p < 0.05$ T-test with Holm –Sidak method. (e) Quantification of fluorescence across triads of wild type siblings (black) and *stac3* mutants (grey) of anti-Ryr-568 (n = 60 wt sib, n = 60 *stac3* mutant).

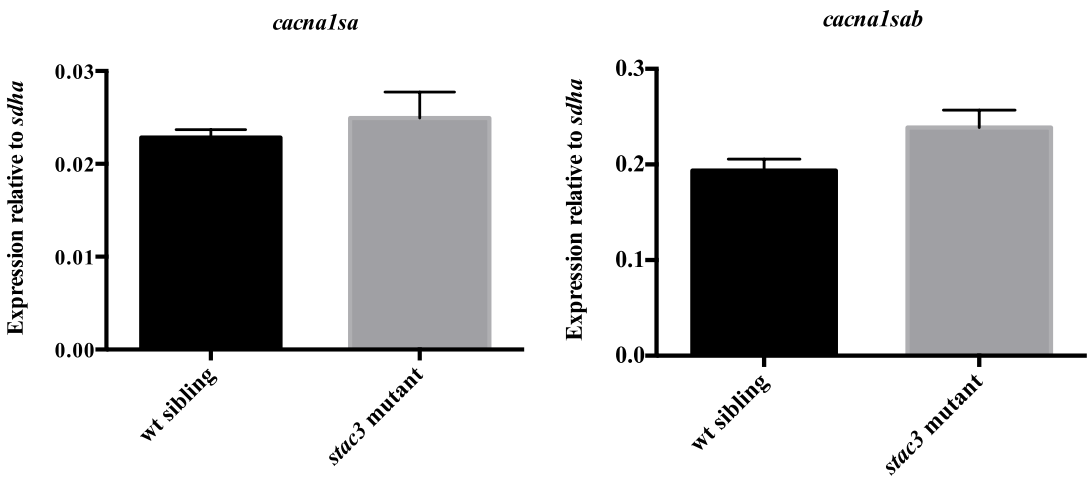

Figure 3-2. Transcript levels of *cacna1sa* and *cacna1sb* are comparable between wild type siblings and *stac3* mutants. Quantitative RT-PCR reveals the expression of the genes *cacna1sa* (left) and *cacna1sb* (right), which encode $Ca_v1.1$ in slow and fast twitch muscle fibers, respectively are comparable between wt siblings *n = 3* (black bar) and *stac3* mutants *n = 3* (grey bar).

Table 3-1. Phenotypes of progeny of *stac3*$^{+/-}$ *x stac3*$^{+/-}$ crosses

Expressed Protein	*stac3* mutant	*stac3* mutant %	wildtype Sibling	Total
None	252	24%	758	1039
$Ca_v1.1$-GFP	156	24%	494	650

Counts of embryo phenotypes found from crosses of *stac3*$^{+/-}$ *x stac3*$^{+/-}$ parents uninjected (top) or injected with DNA encoding $Ca_v1.1$-GFP. Embryos were individually phenotyped by touch evoked swim responses at 48hpf, and classified as either *stac3* mutant (shivering or no motility) or wildtype sibling (forward swim). Neither population differed from expected Mendelian ratio of 3:1 (binomial test $p = 0.6$ for both).

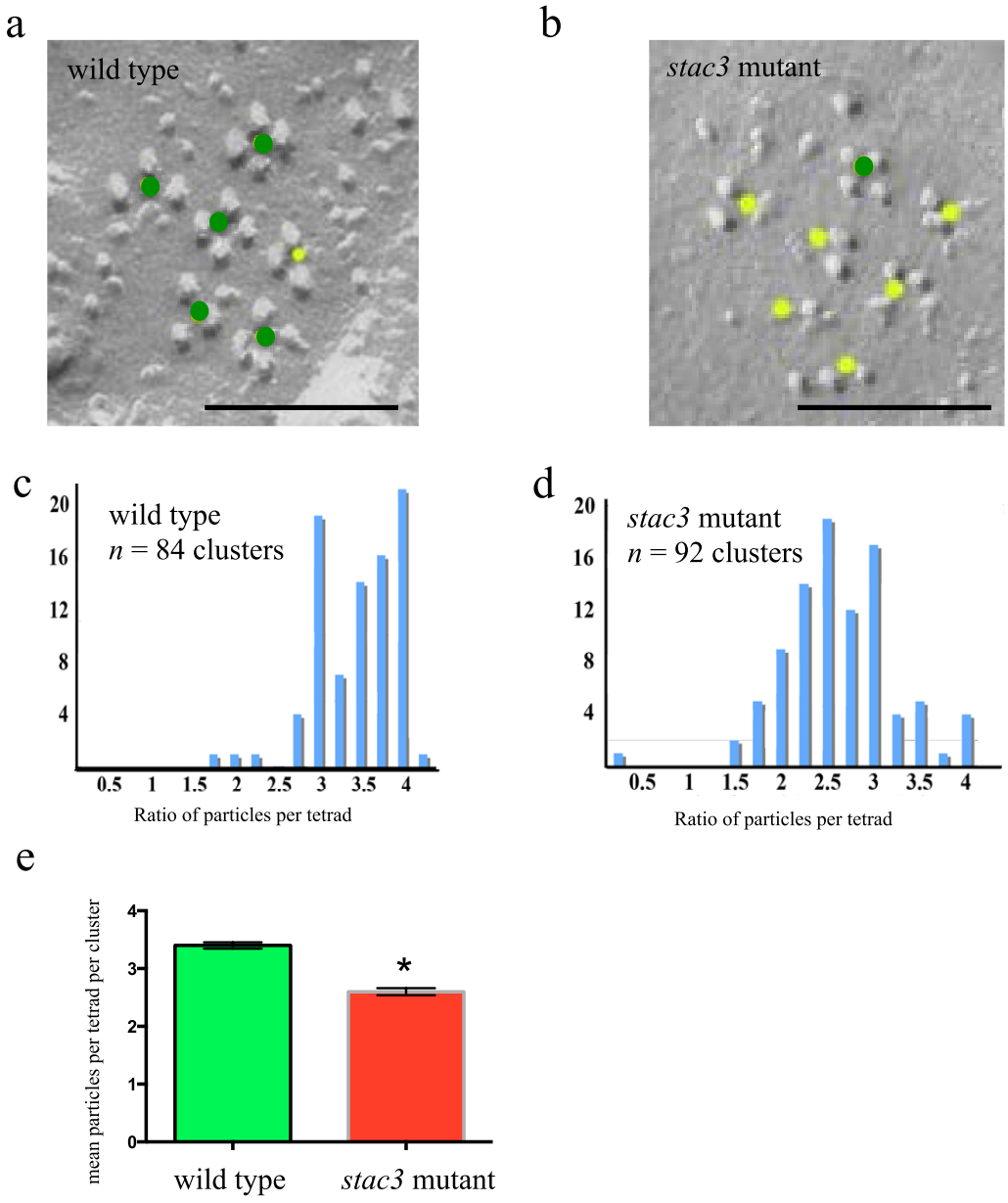

Figure 3-3. Triadic clusters of *stac3* embryos have fewer DHPR particles and fewer particles per tetrad. Representative freeze fracture electron micrographs of triadic junctions from 4 dpf wild type (a) and *stac3* mutants (b). Scale bars are 0.1 µm. Green dots mark tetrads with four DHPR molecules, yellow dots mark tetrads with less than four DHPR particles. (c) Histogram showing distribution of the ratio of particles per tetrad site per cluster in wild type and (d) in *stac3* mutant. (e) Comparison of the mean particles per tetrad site in a cluster of DHPR particles from wild type (3.4 +/- 0.05, n = 84) and *stac3* mutants (2.6 +/- 0.06, n = 92). Students T test $p < 0.0001$. Bars indicated mean +/- SEM. EM contributed by Dr. Clara Franzini-Armstrong.

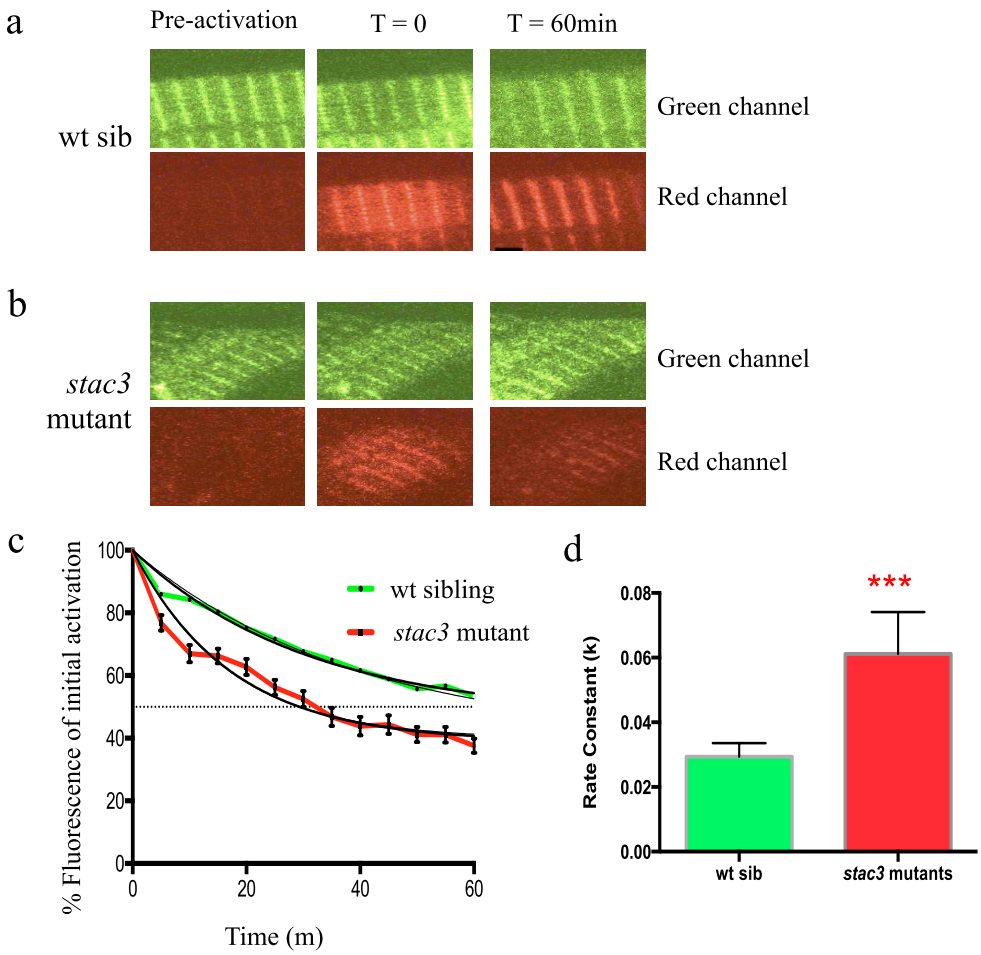

Figure 3-4. $Ca_v1.1$ disperses from triads of *stac3* mutant embryos at a faster rate. (a) Representative images of $Ca_v1.1$-mEos3.2 expression in wild type siblings and *stac3* mutants. Scale is 2.5 µm**.** (b) skeletal muscle localizes to t-tubule striations and remains present after photoactivation over the course of an hour. (c) Mean percentage of fluorescence decay of photoactivated $Ca_v1.1$-mEos3.2 protein in triads of *stac3* mutants (red, $n = 24$) and wild type siblings (green $n = 27$) over the course of an hour. Error bars are +/- SEM. Black lines indicate non-linear regression fit to data. Comparison of fits k, $p < 0.001$, plateaus, $p = 0.1$. Dotted line indicates 50% fluorescence.

Table 3-2. Dynamic Rates of Fluorescent Tagged Proteins at Triads

Expressed Protein	Assay	Embryo phenotype	Decay rate (k)	Recovery Rate	Plateau
$Ca_v1.1$-mEos3.2	Decay	wildtype, *n* = 27	0.06	NA	46.73 +/- 3.0
	Decay	*stac3* mutant *n* = 24	0.03*	NA	38.82 +/- 1.9
$Ca_v1.1$-GFP	FRAP	wildtype, *n* = 45	NA	0.18 +/- 0.01	29.02 +/- 1.7
	FRAP	*stac3* mutant *n* =43	NA	0.12 +/- 0.01*	29.25 +/- 1.8

All values are represented as mean +/- S.E.M. Values that were significantly different from wildtype by students T-test are marked *, indicating $p < 0.05$. Significance of plateau values were determined by best fit values from non-linear regressions, and were not significantly different form wildtype siblings ($p = 0.1$ in $Ca_v1.1$-mEos3.2 decay assay, $p = 0.7$ in $Ca_v1.1$-GFP FRAP assay).

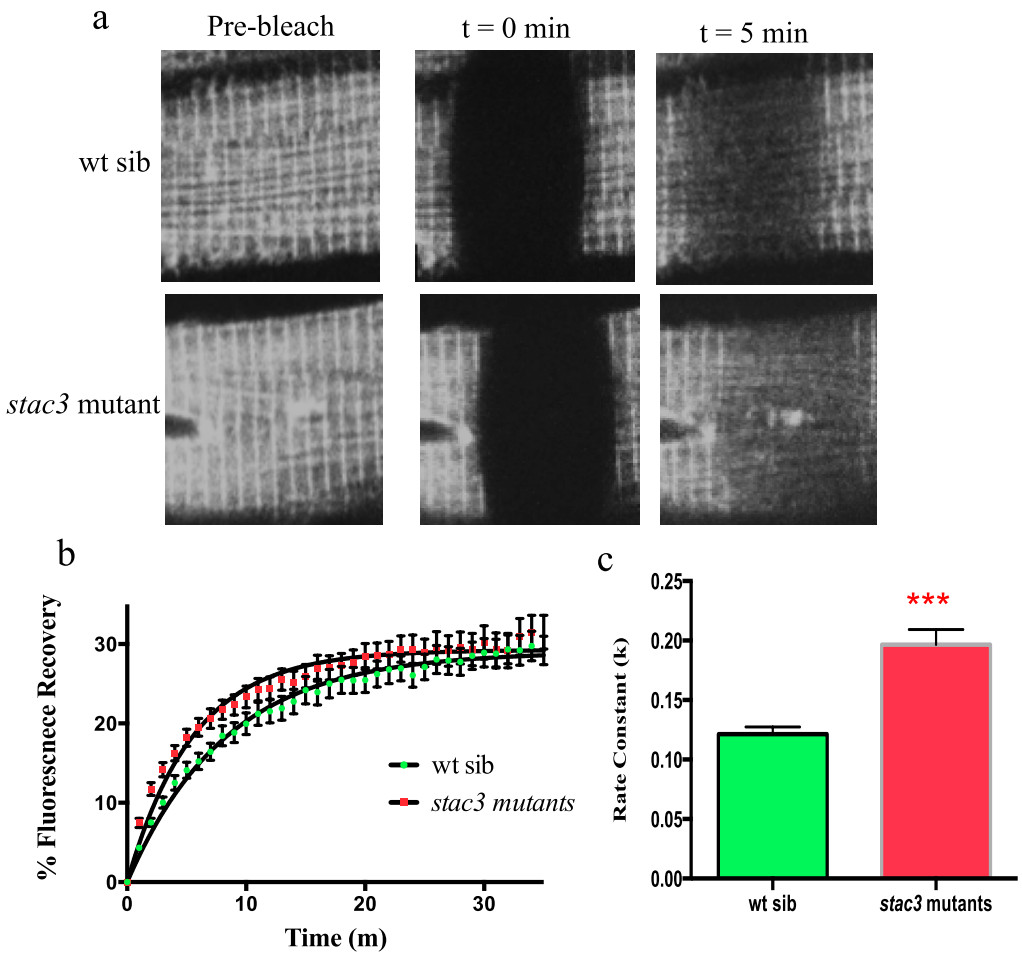

Figure 3-5. Trafficking rate of Cav1.1 is increased in *stac3* mutant muscle. (a) Representative images of recovery of fluorescence after bleaching of $Ca_v1.1$-GFP expressing muscle myofibers of wild type siblings (top), and *stac3* mutants (bottom). Left panels are pre bleach, middle panels are immediately post-bleach, and right panels are five minutes post-bleach. (b) Mean standardized fluorescence recovery after photo-bleaching as a percentage of plateau of wild type siblings (red $n = 43$) and *stac3* mutants (green $n = 45$). Black lines are non-linear regressions fit to data. Comparison of fits, k, $p < 0.0001$, plateaus, $p = 0.7$. (c) Distribution plot of the derived rate constants (k) of wild type siblings and *stac3* mutants. Bars indicate mean +/- SD.

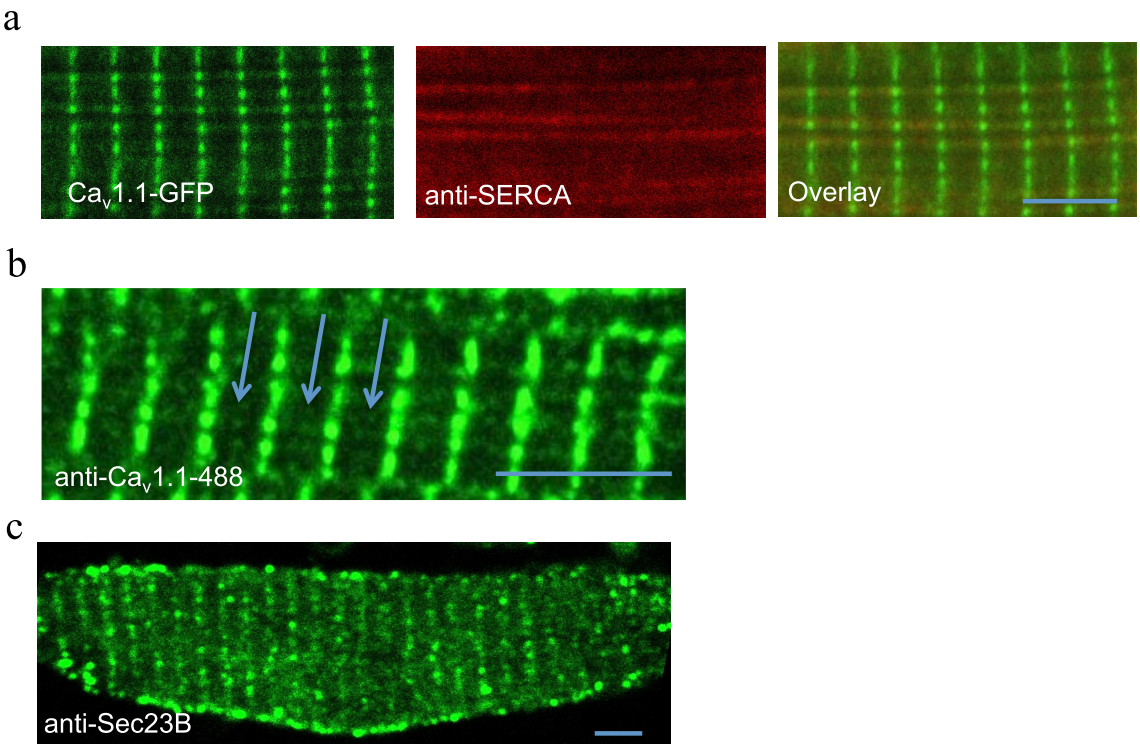

Figure 3-6. Trafficking of Cav1.1-GFP proceeds through the lumen of the longitudinal ER/SR. (a) Whole-mount immunofluorescence labeling with anti-Ca$_v$1.1-alexa488 of a 48 hpf wild type embryo muscle myofiber. Arrow indicates presence of anti-Ca$_v$1.1-alexa488 labeling between triads. (b) Whole-mount co-immunofluorescence labeling of a 6 dpf wild type Ca$_v$1.1-GFP expressing muscle myofiber with anti-SERCA. (c) Disassociated muscle fiber from wild type embryo labeled with anti-Sec23B. All scale bars represents 2.5 µm. Each image representative of at least three separate experiments.

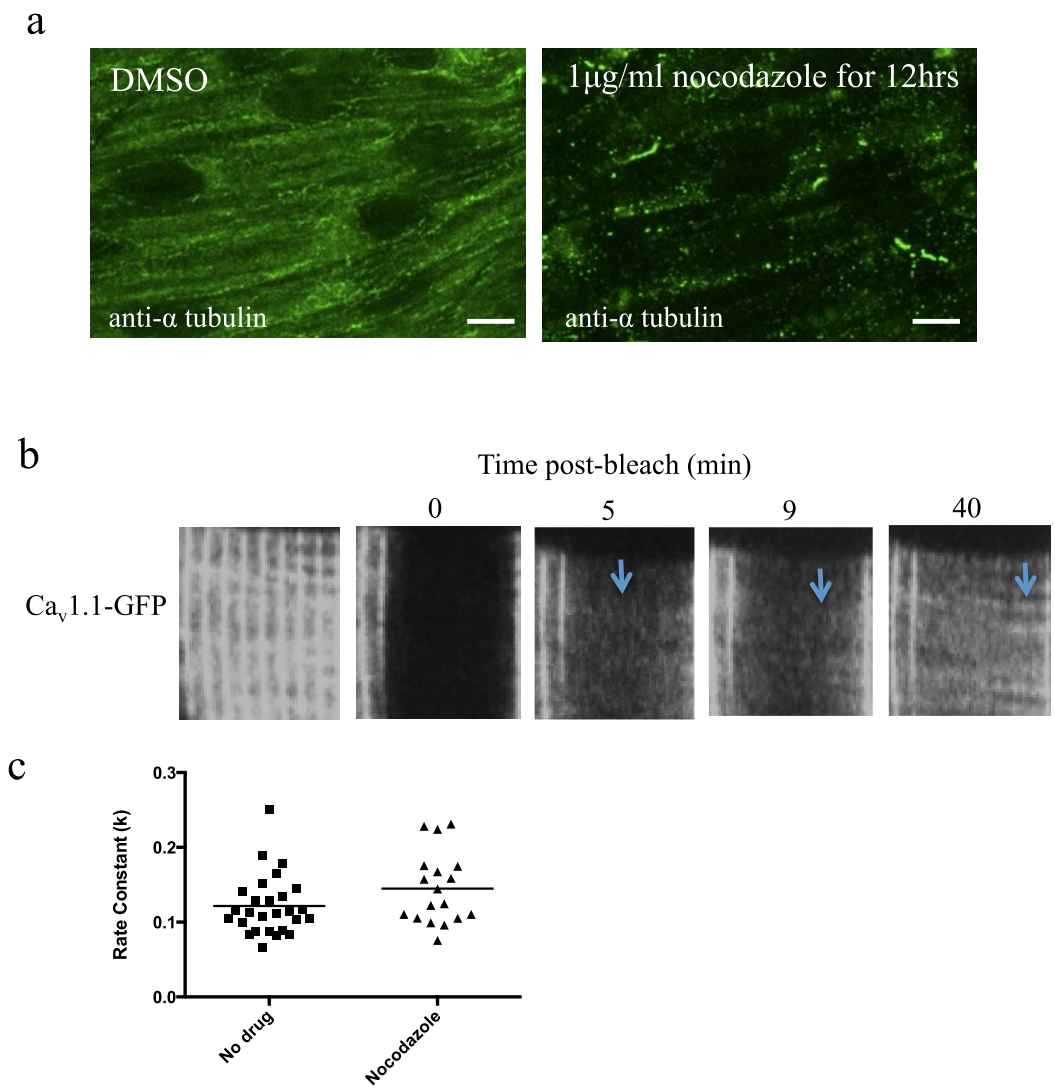

Figure 3-7. Cav1.1-GFP traffics longitudinally through skeletal muscle in a nocodazole resistant manner. (a) Representative images of whole mount immunolabeling of skeletal muscle of 72 hpf embryos labeled with anti-α tubulin incubated for 24 hours in DMSO (left) or 1µg/ml nocodazole (right) scale bar is 5 µm. Nocodazole exposure results in reduced, disorganized, and spotty labeling with anti-α tubulin (b) FRAP assay on 72 hpf $Ca_v1.1$-GFP expressing myofibers incubated in nocodazole for 24 hours. Arrows point to recovery of longitudinal expression of $Ca_v1.1$-GFP. (c) Rate constants from FRAP assays on 72 hpf wild type embryos (left $n = 27$) and embryos nocodazole incubated in nocodazole for 24 hrs (right, $n = 18$). Bar indicates mean, unpaired T test, $p = 0.08$.

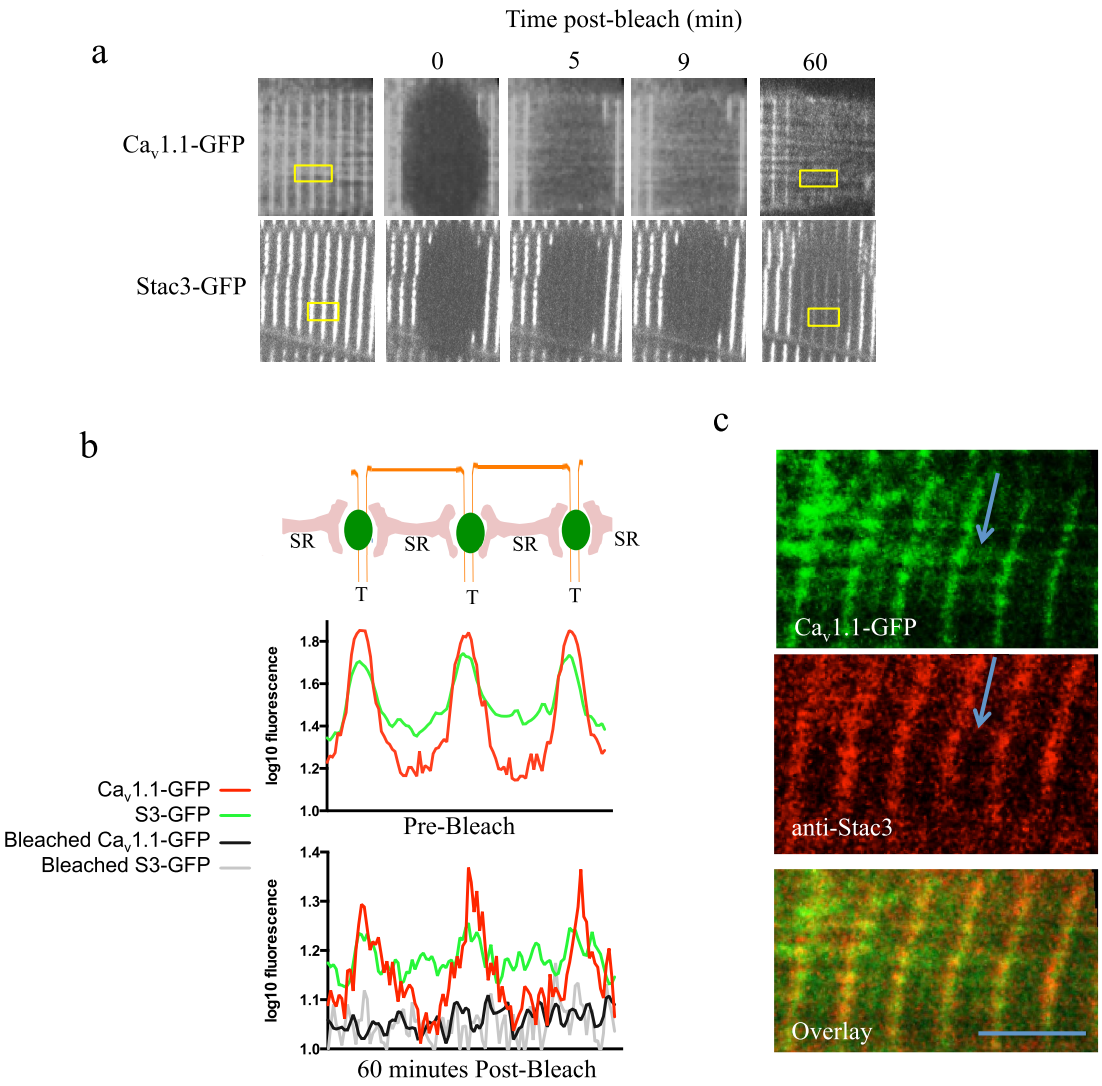

Figure 3-8. Cav1.1 is trafficked in longitudinal lines to its target in the triad, independently of Stac3. (a) Representative images comparing FRAP recoveries of muscle myotubes expressing $Ca_v1.1$-GFP (top) or Stac3-GFP (bottom) over 60 minutes. (b) Plot profile of yellow squares in (A) along schematic illustrated on top. SR = sarcoplasmic reticulum (in pink), T = t-tubule (in orange), and green circle indicates triadic junction. Below schematic are traces of pre-bleach (middle axes) and 60 minutes post-bleach (bottom axes) fluorescence for $Ca_v1.1$-GFP (green middle and bottom), Stac3-GFP (red middle and bottom), and bleached $Ca_v1.1$ (black bottom only) and Stac3-GFP (grey bottom only). (c) Whole mount immunolabeling of 48 hpf wild type muscle myofiber expressing $Ca_v1.1$-GFP (top), labeled with anti-Stac3 (middle). Arrows signify the location of intra-t-tubule $Ca_v1.1$ fraction. Bottom is overlay. Scale bar represents 2.5 μm. Each image representative of at least three separate experiments.

.

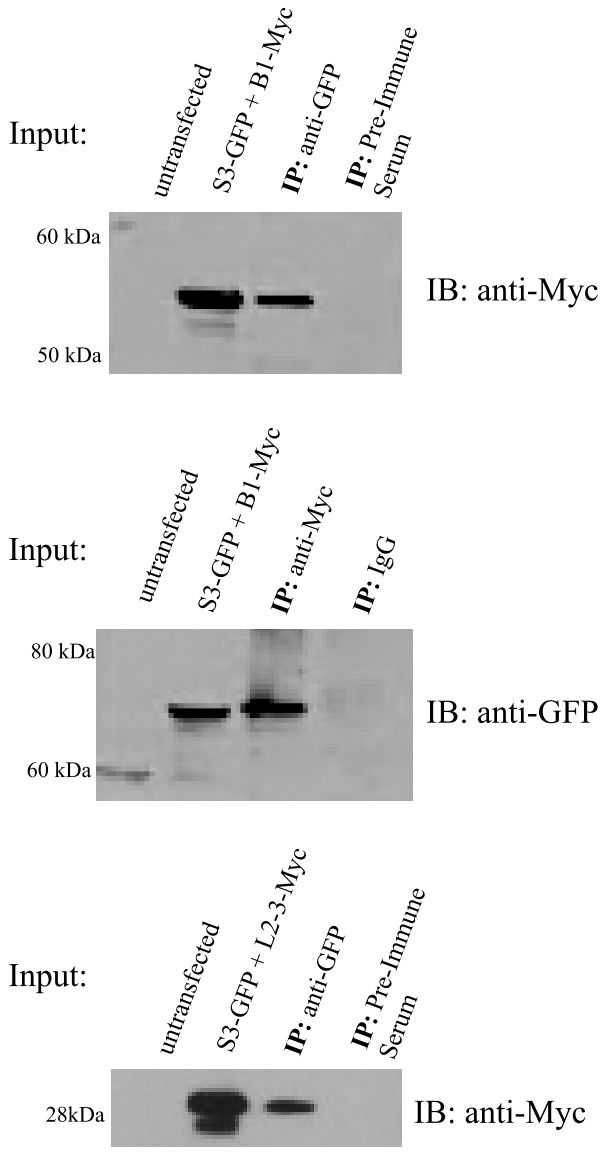

Figure 3-9. Stac3 biochemically interacts with $Ca_v\beta$ and $Ca_v1.1$ L2-3 *in vitro.* (a) Immunoblots (IB) showing that immunoprecipitation (IP) with anti-GFP from lysate of Cos cells co-transfected with Stac3-GFP and β1-Myc pulls down β1-Myc (top), and reciprocally, IP with anti-Myc pulls down Stac3-GFP (bottom). IP with rabbit pre-immune serum (top) does not pull down β1-Myc, and IP with mouse IgG (bottom) does not pull down Stac3-GFP. (b) Immunoblot showing that immunoprecipitation (IP) with anti-GFP from lysate of Cos cells co-transfected with Stac3-GFP and L2-3-Myc pulls down L2-3-Myc. IP with rabbit pre-immune serum does not pull down L2-3-Myc.

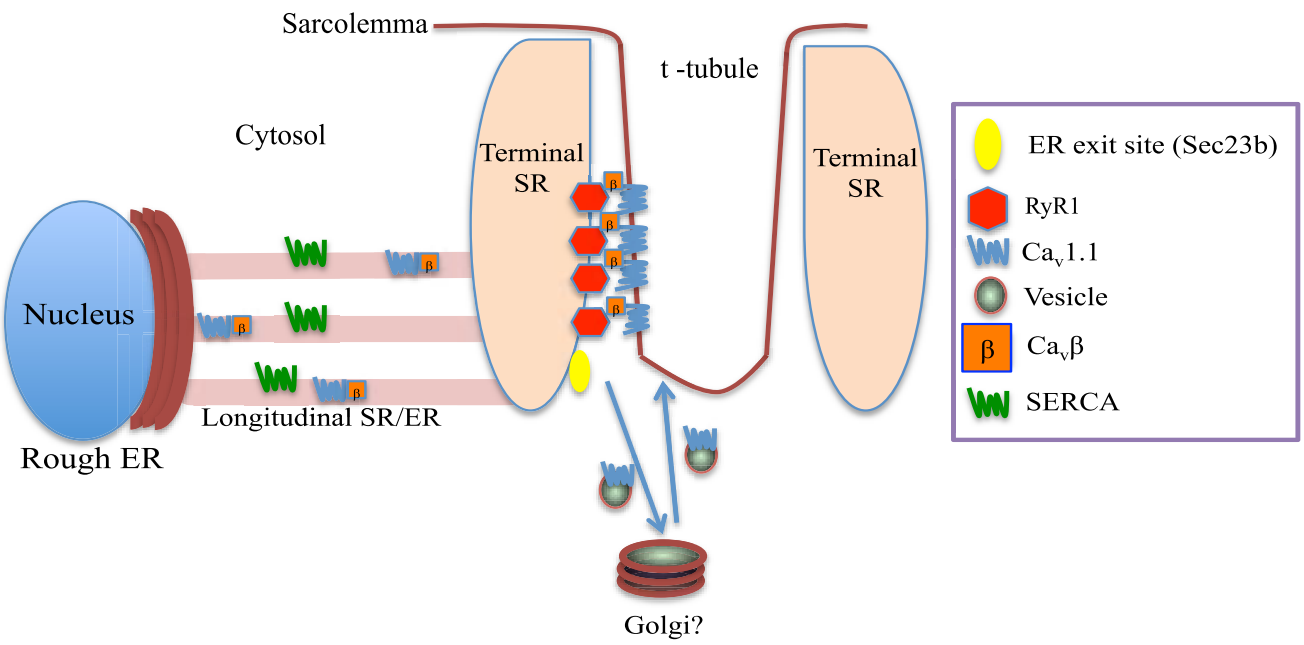

Figure 3-10. Models of trafficking of the DHPR. (a) $Ca_v1.1$ (blue springs) traffic through the longitudinal SR marked by SERCA (green springs) to ER exit sites (yellow oval) marked by Sec23b in the terminal SR (peach object) marked by RyR1 (red hexagon). By an unknown mechanism, the $Ca_v1.1$ translocates from the terminal SR into the triadic junction in the t-tubules (brown line) where they form into tetrads. When or if the $Ca_v1.1$ reaches the Golgi is unknown.

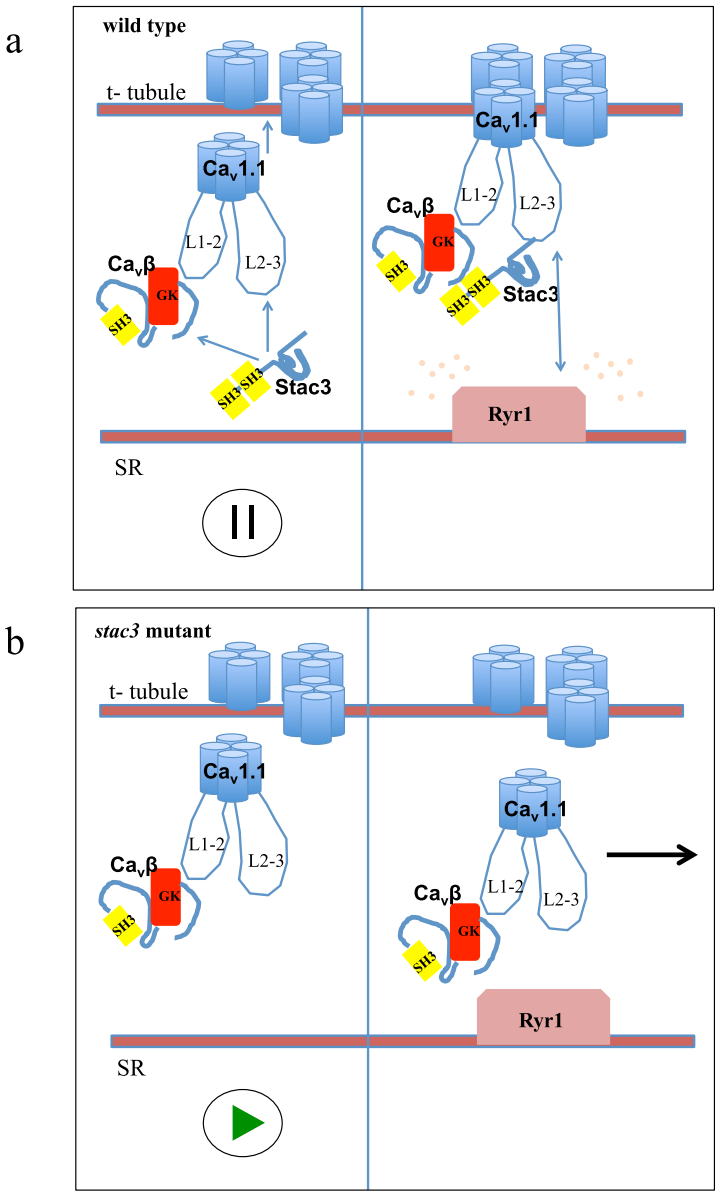

Figure 3-11. Model of trafficking of Ca$_v$1.1 trafficking and tetrad formation. (a) In wild type background, Ca$_v$1.1 (four blue cylinders with only loops L1-2 and L2-3 displayed) attached to Ca$_v$β passes through the triadic junction and is paused by a direct interaction with Stac3 (left). The pause provides the stabilization of a transition stage that allows Ca$_v$1.1 to form a complete tetrad of four DHPR particles (right), allowing functional EC coupling with the RyR1 and Ca^{2+} release. (c) In *stac3* mutant background, Ca$_v$1.1 is not paused when passing through the triadic junction (left), causing the Ca$_v$1.1 to continue out of the triad, and disrupting normal Ca^{2+} release (right).

CHAPTER IV

STAC1, A NOVEL NEURONAL PROTEIN IS EXPRESSED IN KA INTERNEURONS AND REQUIRED FOR NORMAL FUNCTION OF THE CENTRAL PATTERN GENERATOR

[Manuscript in preparation to be published as Jeremy W. Linsley, Eric J. Horstick, Kenichi Iwasaki, and John Y. Kuwada]

Abstract

The *stac1* gene encodes a member of a family of adaptor proteins that are highly conserved in vertebrates and are believed to be important for regulation of Ca^{2+} channels. *stac1* is extensively expressed by neurons in the nervous system of vertebrates, but its function remains unknown. In zebrafish embryos *stac1* is expressed specifically in the ventrally located GABAergic spinal neurons named Kolmer-Agdur (KA) interneurons. Activation of KAs drives swimming and thus, presumably, the swimming central pattern generator (CPG) in zebrafish larvae, and are believed to be required for swimming. Injection of translation blocking antisense morpholino oligonucleotides (MO) against *stac1* into wild type zebrafish embryos leads to a progressive loss of touch-induced swimming, suggesting that Stac1 in KAs may be required for the swimming response to tactile stimulation. We used a GAL4 enhancer trap line that expresses Gal4 in KA neurons to drive light sensitive channelrhodopsin (UAS:ChR2-mCherry) in KAs, and found that activation of the channel with blue light was able to drive swimming behavior in wild type zebrafish embryos, but not in *stac1* MO injected embryos. These results are consistent with the requirement of Stac1 for KA interneuron function downstream of

neuronal activation, and suggest Stac1 might be a required for activation of the swimming CPG.

INTRODUCTION

How the nervous system processes sensory input to generate appropriate responses including motor behaviors has been a central question in neurobiology. Although behaviors are sometimes extremely complex, the motor output of an animal can often be used as a simple, reliable readout of the integrated activities of the neuronal circuits that control motor function. Thus, the neuronal circuits that underlie relatively simple motor behaviors such as locomotion and breathing are some of the best understood circuits in the CNS and principles gleaned from these circuits could potentially be useful for analysis of circuits for more complex behaviors (Goulding, 2009; Marder and Bucher, 2001; Roberts et al., 1998). Using this strategy, at least as far back as the 18th century, neuroscientists noticed that simple coordinated behaviors in vertebrates appear to be generated by self-contained circuits in the spinal cord that are able to emit rhythmic movements in the absence of sensory or descending input (Brown, 1914). In the 1750's, for example, Whytt demonstrated that pinching the leg of a decapitated frog will still cause the frog to kick in a rhythmic motion, yet destruction of the spinal cord stopped all kicking (Buck, 1888). The presence of an intrinsic ability to generate rhythmic patterns of activity in the spinal cord was ultimately confirmed centuries later by showing that the isolated spinal cord could generate rhythmic neuronal activity (Delcomyn, 1980). The network of spinal cord neurons that are capable of generating rhythmic locomotor firing patterns was named the central pattern generator (CPG), which now applies to any circuit that can generate a patterned output.

The organization of the CPG is evolutionarily conserved among vertebrates. Analysis of the CPG in the lamprey (*Petromyzon marinus*) helped characterize many of

the details of CPG neurons, including their neurotransmitter subtypes, intrinsic membrane properties, and how they are connected, which have been found to be representative of the CPG of mammals as well (Goulding, 2009; Marder and Bucher, 2001). Despite the lamprey's advantages as a model organism for the analysis of CPGs, it has not yet become a viable model for genetic studies of the CPG. Zebrafish, in contrast, have been developed as a vertebrate model organism amenable to both forward (Golling et al., 2002; Granato et al., 1996) and reverse genetic manipulations (Foley et al., 2009; Hwang et al., 2013; Nasevicius and Ekker, 2000; Sander et al., 2011). Zebrafish embryos develop externally starting with fertilization, are optically clear, develop rhythmic motor behaviors early in development and can be analyzed using electrophysiological techniques making them a favorable model system to study neuronal circuits (Goulding, 2009; Saint-Amant and Drapeau, 2003; Wyart et al., 2009). These features of zebrafish have lead to the generation of mutations that affect particular loci in the neuronal circuits for touch induced escape contractions and swimming allowing for the genetic analysis of these neural circuits (Cui et al., 2005; Hirata et al., 2009; Hirata et al., 2005; Low et al., 2011; Low et al., 2010a; Low et al., 2010b; Nakano et al., 2010; Saint-Amant et al., 2008).

The CPG is thought to be made up of four functional classes of locomotor cell types: motor neurons that innervate the muscle, glycinergic commissural interneurons that project to the opposite side of the spinal cord, excitatory glutamatergic neurons, and glycinergic ipsilaterally-projecting inhibitor neurons of unknown function (Goulding, 2009). Yet other neuronal subtypes exist in the spinal cord (Drapeau et al., 2002), and the contribution of these neurons to the CPG has not been well studied. One type of

interneuron in the spinal cord that does not fit into known locomotor neuron types is the GABAergic Kolmer-Agdur (KA) interneuron. KA interneurons are a group of ventrally located neurons that extend cilia from their cell bodies that contact the central canal (Dale et al., 1987). They are formed early in embryogenesis and are found across many vertebrate classes. KAs are of mixed origin, with more dorsal KAs originating from *olig2* expressing motor neuron precursors, and the ventral KAs originating from the lateral floor plate (Park et al., 2004; Yang et al., 2010a). Both types of KAs send ipsilaterally ascending axonal projections in the zebrafish embryonic spinal cord that run in proximity of nearby motor neurons (Bernhardt et al., 1992).

Although long recognized as an early component in the development of the neuronal network of spinal cord neurons (Dale et al., 1987), the function of KAs remained obscure until recently, when it was reported that the optogenetic activation of KA interneurons triggers swimming in zebrafish (Wyart et al., 2009). Swimming was initiated by optogenetic activation of KAs even in decapitated zebrafish larvae, indicating that KAs activate the CPG. Moreover, genetically silencing a subset of KAs diminished the frequency of swimming, suggesting that KAs provide a positive drive to the CPG.

Genes expressed specifically in KA interneurons have not been identified. The *stac1* gene (originally named *stac)* was identified by restriction landmark genomic scanning using methylation-sensitive endonuclease displays of mouse brains (Suzuki et al., 1996). *stac1* mRNA is expressed in neurons of mouse brains, and its expression increases as mice develop (Suzuki et al., 1996). Cell fractionation was used to determine that the Stac1 protein is cytosolic, and at the time of its discovery, the Stac1 protein was the first example of a protein consisting of only a cysteine-rich domain (CRD) and Src

Homology 3 (SH3) domains with no apparent catalytic domain (Suzuki et al., 1996). The discovery of *stac2* expressed by neurons and *stac3* expressed by skeletal muscles, which share similar domain architecture possibly formed by gene duplication (Gerhard et al., 2004; Strausberg et al., 2002), along with *stac1* defined a small gene family. Lacking an obvious catalytic domain, the function of Stac1 likely derives from its SH3 and CRD domains in an adaptor-like fashion, but the function and significance of Stac1 and Stac2 for neurons is unknown (Hardy et al., 2005; Kawai et al., 1998; Satoh et al., 2006).

Studies of the Stac3 protein, the muscle-expressed homolog of Stac1, have led to the discovery of an important and unique function for Stac3 for the release of Ca^{2+} in skeletal muscle (Horstick et al., 2013; Nelson et al., 2013). Furthermore, the experiments described in Chapter III demonstrate that Stac3 affects EC coupling by regulating DHPR, the skeletal muscle voltage gated Ca^{2+} channel. Thus, we wondered if Stac1 might regulate voltage-gated Ca^{2+} channels in neurons similar to Stac3's regulation of DHPRs in skeletal muscle. We first investigated the expression pattern of *stac1* in zebrafish embryos and found that *stac1* is expressed specifically in KA interneurons starting from 22 hpf up to at least 48 hpf. We then used a reverse genetics approach to investigate the function of Stac1 in KA neurons by Morpholino Oligonucleotide (MO) mediated knockdown of Stac1. Our results indicate that Stac1 is required for normal function of the KA neurons and thus for activation of the swimming CPG in zebrafish embryos, providing the first evidence of a function for the *stac1* gene.

MATERIALS AND METHODS

Animals and behavioral analysis

Zebrafish were bred and maintained according to approved guidelines of the University Committee on Use and Care of Animals at the University of Michigan.

Cloning, 5' RACE, *in situ* hybridization and Immunolabeling

mRNA was extracted from 50 pooled WT embryos at 48 hours post fertilization (hpf) using TRIzol (Invitrogen) reagent, and SuperScriptII and Oligo dT (Invitrogen) were used for reverse transcription to create a cDNA library. Full length *stac1* was cloned using the forward primer: 5'-ATGATTCCGCCAGCAAACATGA-3', and the reverse primer 5'AAATTAGTTCTGAGAAAAGCTCTGGC-3', and was subsequently cloned into pGemT-Easy (Promega). 5'RACE (GIBCOBRL) was performed using an intermediate 3' primer 5'CCGAAGGCCCAGCTTAGCATTG3' and a nested 3' primer CAGCTTAGCATTGGTGCCTACAATCAT3'. Electrophoresis revealed a single band that was PCR purified, cloned using pGemT-easy (Promega), and sequenced to reveal 5' untranslated region in the transcript. Sequencing was performed at the University of Michigan DNA sequencing core. The cloned plasmid was linearized with NcoI, and used as a template for antisense probe synthesis using a DIG RNA labeling kit (Roche) and Sp6 polymerase (Promega). *In situ* hybridization was conducted as previously described (Zhou et al., 2008). Anti-DIG-AP Fab fragments (Roche) were used to carry out color reactions using NBT/BCIP as a substrate (Roche). For fluorescent double-labeling, Fast Red (Roche) was used as a substrate for in situ hybridization and immunolabeling was

carried out with primary antibodies anti-GABA (1:500, Sigma–Aldrich), anti-GFP (1:1000, Torrey Pines Biolabs), and secondary antibody alexa488-anti-mouse/rabbit IgG (1:500, Invitrogen, Life Technologies). The labeled embryos were mounted in Vectashield mounting medium (Vector Laboratories) and fluorescent images were acquired with a Leica SP5 laser scanning confocal microscope.

Polyclonal antiserum production, purification and Western Analysis

Full-length zebrafish Stac1 was expressed as a His–Sumo fusion protein in B21(DE3) cells (Invitrogen), affinity-purified, and used for rabbit immunization according to methods previously described (Horstick et al., 2013). Anti-serum was purified by passing through a N-link column (Thermo) containing the immobilized fusion protein. Fifty Stac1 MO injected and 50 standard MO injected embryos were lysed and the isolated protein loaded and separated by SDS–PAGE as previously described (Horstick et al., 2013). Purified Stac1 antiserum was diluted 1:100 and anti-β actin (Santa Cruz) was used at 1:1000.

Antisense MO knockdowns and Rescues

Full length cloned *stac1* construct was linearized with SalI, and mRNA was synthesized using mMessage mMachine T7 ultra kit (Invitrogen). Translation-blocking antisense MO to *stac1* contained the sequence 5' CTGGCGGAATCATGCCGATAACAGT 3' (GeneTools). IVT *stac1* mRNA or standard MO alone (GeneTools) were injected into one-cell stage embryos with a Nanoject II. Embryonic behaviors were video recorded with a CCD camera mounted on a

stereomicroscope and analyzed with ImageJ. Where indicated data were analyzed by T-tests.

Transgenic Zebrafish and Optogenetic behavioral assays

Tg:*hb9*-mGFP fish have been previously described (Flanagan-Steet et al., 2005). Previously published GAL4:1020t (Scott et al., 2007), and UAS:ChR2-mcherry (Schoonheim et al., 2010) were crossed to obtain a GAL4:1020t, UAS:ChR2-mcherry line. Progeny of GAL4:1020t, UAS:ChR2-mCherry x wildtype crosses were injected with Stac1 translation-blocking antisense MO or standard control MO at the one cell stage with a Nanoject II, raised to 48 hpf, dechorionated enzymatically, and then sorted for mCherry expression. Blue light activation was provided with a metal halide FLU03 lamp on a Leica FLUO3 upright microscope using an EGFP filter set (Leica) at fixed 2.5x zoom. Digital movies of light activated swimming were recorded and quantified importing into ImageJ by the length of a vector representing the forward distance of tail movement in pixels after 15 seconds of blue light illumination, though embryos that swam out of the field of vision swam further than were measured.

Transient expression of Stac1-GFP

The sequence that encodes the full-length *stac1* cDNA was cloned by RT-PCR from total RNA of 48hpf embryos, and inserted into pGemT-easy. The sequence was then subcloned by amplification of the full length *stac1* sequence with primers containing EcoRI and BamHI tags, and inserted in frame into the *hsp70:gfp* vector to create *hsp70:stac1-gfp* (Halloran et al., 2000). The *hsp70:stac1-gfp* or *hsp70:stac3-gfp* was

injected into 1-cell stage progeny from *stac3*^{mi34} carriers (Horstick et al., 2013). At 48 hpf, *stac3*^{mi34} mutant embryos were behaviorally identified and heat induced by switching them from water at 28.5 °C to 37 °C for 1 h. After heat induction, embryos were switched back to 28.5 °C and assayed 3 and 24 h later. Embryos with at least 10% or more skeletal muscle fibers expressing GFP were used for behavioral assays. Embryos were subsequently fixed in 4% PFA and mounted in Vectashield mounting medium (Vector Laboratories) and fluorescent images were acquired with a Leica SP5 laser scanning confocal microscope.

RESULTS

Zebrafish genome contains single copies of *stac1* and *stac3*

We cloned the *stac1* cDNA by RT-PCR from total RNA of 48 hpf zebrafish embryos and found that it encoded a protein that is 37% identical to the zebrafish Stac3 protein and 63% identical to the human Stac1 protein with particularly high conservation in the CRD and SH3 domains (Fig. 4-1). Furthermore, the protein is only 45% identical to the human Stac2 protein, which is consistent with the protein corresponding to the neuronal Stac1 rather than Stac2. To analyze the relationships among *stac* genes across species, phylogenetic analysis of the family of *stac* genes from vertebrate genomes was generated using ensemble (Vilella et al., 2009). The phylogenetic tree of genome-sequenced animals shows that *stac* genes are present throughout the vertebrate lineage (Fig. 4-2). A first duplication of the ancestral *stac* gene occurred ~535 million years ago (mya), at which point the muscle specific *stac3* diverged (Fig. 4-2). A second duplication (~420 mya) subdivided the neuronal version into *stac1* and *stac2* (Fig 4-2). A duplication of the *stac2* gene appears to have occurred ~200 mya, consistent with the hypothesis of a whole-genome duplication of the teleost lineage (Jaillon et al., 2004). Surprisingly, there is no evidence of a *stac2* gene in the essentially complete zebrafish sequenced genome (ZV9) (Howe et al., 2013), suggesting the possibility that zebrafish lost *stac2* after duplication of neuronal *stac* in the teleost lineage. Although a lost *stac2* gene would leave zebrafish as unique among all sequenced bony fishes (2 copies) and all sequenced tetrapods (1 copy), the lamprey also appears to have only a single *stac1* and no *stac2*, similar to zebrafish (Figure 4-2).

Misexpressed Stac1 in skeletal muscle appears to localize to triads, but fails to rescue *stac3* mutant swimming

As Stac1 shows high homology to the Stac3, we first decided to test the functionality of Stac1 by assaying whether expression of the Stac1 protein in skeletal muscles can rescue the motility defect of *stac3* mutant fish (Horstick et al., 2013). The cloned *stac1* cDNA was C-terminally tagged with *gfp*, inserted into a zebrafish heat shock promoter (*hsp70*) expression vector, and injected into the progeny of *stac3*$^{+/-}$ x *stac3*$^{+/-}$ crosses. Induced expression of *hsp70:stac3-gfp* rescued swimming in *stac3* mutants (Horstick et al., 2013), but induced expression of *hsp70:stac1-gfp* did not (Table 4-1). Labeling with anti-GFP in *stac3* mutants expressing Stac1-GFP, however, indicated Stac1-GFP is localized in a striation pattern similar to Stac3 in skeletal muscle myofibers suggesting that Stac1 can be trafficked to the triads (Fig. 4-3) (Horstick et al., 2013). In contrast, induced expression of GFP in skeletal muscle is found to be diffuse throughout the cell, and does not form striations (Fig 4-3b). Thus it appears that Stac1 contains sequences that direct trafficking to triads but do not restore EC coupling.

***stac1* is expressed in a discreet subset of interneurons in zebrafish embryos, and in the brain beginning at 72hpf**

To investigate the function of *stac1* we next determined the expression pattern of *stac1* in zebrafish embryos. By 22 hpf *stac1* is expressed specifically by a small subset of cells in the ventral spinal cord (Fig. 4-4 a). Expression by ventral spinal cells was maintained to 48 hpf time points with no expression elsewhere (Fig. 4-4 b,c,d, data not shown). By 72hpf expression of *stac1* extended to the hindbrain, forebrain, and retina

(Fig. 4-4 e2-4) in addition to the ventral spinal cord (Fig. 4-4 e1). Previous reports indicated *stac1* is expressed in various regions of the brain of adult mice such as the CA1 and CA2/3 neurons of the hippocampus, Purkinje cells of the cerebellum, and neurons in the inferior olive of medulla oblongata (Legha et al., 2010; Suzuki et al., 1996). Thus, if the function of the Stac1 protein is conserved across vertebrates, we expected *stac1* to also be expressed in the adult zebrafish brain. Indeed expression of *stac1* in the brain of mature 7 wk zebrafish was found in the habenular nucleus (Fig 4-5a), the optic tectum (Fig. 4-5b), and the dorsal cerebellum (Fig. 4-5c). Thus *stac1* appears to be selectively expressed by neurons in both zebrafish and mammals.

stac1 is expressed in KA interneurons in zebrafish embryos

The finding that *stac1* was expressed selectively by ventral spinal cells in zebrafish embryos at a time when they exhibit simple motor behaviors would allow for a straightforward analysis of the function of *stac1*. With this in mind we next sought to identity the *stac1* expressing cells in the ventral spinal cord. Since the embryonic ventral cord contains motor neurons (Westerfield et al., 1986), we examined whether they might express *stac1*. *In situ* hybridization with *stac1* riboprobe of *hb9:mgfp* transgenic embryos, which express membrane tagged GFP in primary and secondary motor neurons showed that motor neurons do not express *stac1* (Fig. 4-6). Another set of neurons found in the early ventral spinal cord are GABA-positive KAs (Bernhardt et al., 1992; Yang et al., 2010a). Co-labeling with *stac1* ribo-probe and anti-GABA showed that KAs were the stac1-positive neurons in the early spinal cord (Fig. 4-6 a,b). The majority of expression

of *stac1* at 36hpf occurs in the more dorsal KA' interneurons, though it also appears to be present in more ventral KA'' interneurons (Fig. 4-6 a).

Knockdown of Stac1 protein results in motility defects in zebrafish embryos

Since KAs play a role in swimming by zebrafish (Wyart et al., 2009), we next investigated the role of Stac1 for KA function and swimming. To test this a translation blocking antisense morpholino oligonucleotide (MO) against *stac1* was injected into recently fertilized zebrafish embryos. At 22 hpf, zebrafish embryos show stereotyped spontaneous coiling of the body and touch-evoked escape contractions (Saint-Amant and Drapeau, 1998). *stac1* MO injected embryos at 22 hpf showed no obvious morphological defects and no obvious defects in spontaneous coiling nor touch evoked escape contractions (data not shown). By 28 hpf, zebrafish embryos exhibit robust, stereotyped swimming in response to touch (Saint-Amant and Drapeau, 1998). At 48hpf, *stac1* MO injected embryos displayed reduced swimming in response to touch compared to standard control MO injected embryos ($p < 0.0001$, Fig. 4-8 a,b). *stac1* MO injected embryos continued to show motility defects up to 4-5 dpf (data not shown), the time point at which a previous study reported that optogenetically silencing KAs reduces swimming (Wyart et al., 2009). An antibody was generated to purified zebrafish Stac1 protein, and Western blotting with affinity purified anti-Stac1 showed reduced expression of Stac1 protein in 48 hpf *stac1* MO injected embryos compared to standard control MO injected embryos (Fig. 4-8 c) demonstrating that Stac1 was knocked down by *stac1* MO injections. Furthermore, co-injection of *stac1* MO with *stac1* mRNA, restored some swimming when compared to embryos injected with *stac1* MO alone ($p < 0.001$) (Fig. 4-8b).

Optogenetic activation of KA interneurons is capable of driving swimming in embryos, but not when Stac1 is knocked down.

Previously, optogenetic activation of KAs was achieved by expressing LiGluR, a light-gated glutamate receptor (Wyart et al., 2009). LiGluR requires the chemical agonist MAG1 for light activation (Volgraf et al., 2006), but MAG1 is unable to penetrate into zebrafish until day four, possibly due to the development of an open mouth at 4 dpf (Wyart, 2012). Furthermore, swimming starting at 3-4 dpf is characterized by short spurts of swimming separated by periods of gliding called beat and glide while swimming at 48 hpf consists of a single continuous swim (Drapeau et al., 2002). Thus the role of KAs for swimming in earlier embryos is unknown. To examine this we used progeny from crosses of transgenic zebrafish carrying a UAS regulated channelrhodpsin (*Tg:UAS:ChR2-mCherry*) (Scott et al., 2007) with transgenic zebrafish which express Gal4 in KAs and motor neurons (*Tg1020t:gal4*) (Wyart et al., 2009). *Tg:1020t:gal4; UAS:ChR2-mCherry* embryos could be identified by red fluorescence in the spinal cord, and were found to be respond to blue light by swimming at 48 hpf (Fig. 4-9a) and as early as 28 hpf (data not shown). One issue here is that *Tg:1020t:gal4; UAS:ChR2-mCherry* embryos express ChR2 in motor neurons as well as KAs. One might expect activation of many spinal motor neurons would initiate uncoordinated muscle contractions. However, it was previously reported that optogenetic activation of only motor neurons using a driver to express LiGluR only in motor neurons required at least ten-fold higher intensity of light than KAs and induced muscle contractions but not swimming (Wyart et al., 2009). These

results suggest that activation of KAs expressing ChR2 is sufficient to initiate continuous swimming exhibited by embryos prior to 3 dpf.

We next sought to isolate the defect in the touch induced swim circuit in *stac1* MO injected embryos by optogenetic activation of KAs in *stac1* morphants. At 48 hpf, all standard control MO injected *Tg:gal4:1020t; UAS:ChR2-mCherry* embryos were able to swim out of the field of vision ($n = 8$, Fig. 4-9). However, *stac1* MO injected embryos, swam significantly less distance and none were able to leave the field of view ($n = 7$, t test $p < 0.0001$, Fig. 4-9). Assuming that KAs were optogenetically activated in *stac1* morphants, these results suggest that a decrease in Stac1 in KAs blocks the initiation of swimming by KA activation.

DISCUSSION

The present study demonstrates for the first time a function for Stac1. We find that Stac1 is required for neuronal function in KA neurons of the spinal cord and swimming by zebrafish embryos. KAs have been previously shown to be capable of providing positive drive to the CPG for beat and glide swimming seen at 3-4 dpf (Wyart et al., 2009). Thus we presume that the KAs provide excitatory drive to the CPG for continuous swimming at earlier stages and that Stac1 in KAs is required for the excitatory input to the CPG. These results in conjunction with recent reports of the importance of Stac3 for Ca^{2+} release in skeletal muscle (Horstick et al., 2013; Nelson et al., 2013) demonstrate the importance of the *stac* gene family for normal cell physiology of electrically excitable cells.

Stac1 and Stac3 proteins share conserved domain motifs and appear to share some characteristics when expressed in skeletal muscle. When Stac1-GFP is expressed in skeletal muscle, it appears to localize to triads just as Stac3-GFP does (Figure 4-3). This suggests that the two Stac proteins share motifs that can direct trafficking in skeletal muscles. Nevertheless, Stac1-GFP is unable to rescue the motility defects of *stac3* mutants (Table 4-1), suggesting that Stac1 does not contain sequences required for EC coupling. As such, the region of Stac3 that directs triadic localization can be identified by mutagenesis studies of regions of Stac3 that are shared by Stac1. Furthermore, since Stac1 appears to be deficient in supporting EC-coupling in skeletal muscles, domain swapping experiments between Stac1 and Stac3 and assaying for rescue of EC coupling in *stac3* mutants, may be useful for identifying the domains of Stac3 important for EC coupling.

Our results indicate that *stac1* is expressed from 22-48 hpf specifically in KAs of the embryonic zebrafish spinal cord (Fig. 4-4). *stac1* was originally identified in mammals based on the increase in its expression levels by the CNS as development proceeded in mice (Suzuki et al., 1996), and we observed a similar increase in expression pattern of *stac1* during zebrafish development. By 72 hpf *stac1* expression extends beyond the KAs in the spinal cord to include presumptive neurons in the caudal hindbrain, the forebrain and retina, and by 7 weeks post fertilization into regions of the brain such as the habenular nucleus, the periventricular grey zone of the optic tectum, and the cerebellum (Figs. 4-4, 4-5). The expression of *stac1* in the retina coincides approximately with the onset (72hpf) of the first visually evoked behavioral responses (Glass and Dahm, 2004), indicating visually evoked behavioral responses may also

require *stac1*. However, this study took advantage of the highly restricted expression pattern of *stac1* to a single class of neurons from 22 to 48 hpf embryos in order to unambiguously examine the function of Stac1 in a specific neuron. Since *stac1* is expressed in many neurons at later stages, the requirement of Stac1 for neuronal function may be attributable to many other neurons.

Knockdown of Stac1 did not affect the two early embryos motility behaviors, spontaneous coiling and touch-evoked escape contractions (data not shown), but did reduce touch-evoked swimming (Fig. 4-8). One explanation for the requirement of Stac1 specifically for touch-evoked swimming is that KA interneurons are part of the swimming behavior circuit, but not in the circuit mediating spontaneous coiling and touch-evoked escape contractions. Since activation of KA interneurons is involved in beat and glide swimming at later stages (Wyart et al., 2009), it is likely that Stac1 is similarly important for the generation of beat and glide swimming.

In the spinal cord of zebrafish embryos, KAs are ventrally located and send ipsilaterally ascending axons in the ventral longitudinal fasciculus in close proximity to motor neurons (Bernhardt et al., 1990). The proximity of KAs to motor neurons in the spinal cord, and their apparent function in the motor circuit, begs the question of how synaptic connectivity between KAs, motor neurons, and other spinal interneurons is linked, but thus far the connectivity of KAs in the spinal cord is unknown. The traditional way to resolve these questions is by electrophysiologically stimulating one neuron while recording from another (Saint-Amant and Drapeau, 2003). Whether any potential connection is a monosynaptic or polysynaptic one can then be tested by increasing the concentration of Ca^{2+} and Mg^{2+} coordinately which will increase the voltage threshold for

action potentials but not the release of neurotransmitters (Frankenhaeuser and Hodgkin, 1957; Kimura et al., 2006). Since neurons in the embryonic spinal cord are small, two electrode experiments are technically difficult. Alternatively one might use genetically encoded factors to simultaneously activate and record from multiple neurons. Genetically encoded red shifted optogenetic proteins (C1V1) (Yizhar et al., 2011), Ca^{2+} indicators (GCaMP7a) (Muto et al., 2013), and voltage indicators (ArcLight) (Jin et al., 2012) have already been employed to examine connectivity in a variety of nervous systems (*e.g.*(Cao et al., 2013; Muto et al., 2013; Yizhar et al., 2011)). These can be applied to the embryonic zebrafish to clarify the circuits that KA neurons participate in. For example, neurons that are activated by KAs could be identified by imaging neurons in transgenics in which KAs express C1V1 and all spinal neurons express ArcLight or GCaMP7a.

This study found that optogenetic activation of KA neurons induced swimming but not when Stac1 is knocked down. This suggests that Stac1 is actually required for action potentials or is important for events downstream of action potentials. The former can be tested by recording from KA neurons either electrophysiologically or optically while optogenetically activating KA neurons. If action potentials are generated by optogenetic activation, then some event initiated by action potentials requires Stac1. Since Stac3 regulates a voltage-gated Ca^{2+} channel (Ca_v) in skeletal muscle it is tempting to hypothesize that Stac1 may regulate Ca_vs in neurons. One attractive idea would be that Stac1 regulates Ca_vs required for the increase in cytosolic Ca^{2+} that initiates the fusion of synaptic vesicles with the presynaptic membrane and release of neurotransmitters.

The hypothesis that Stac1 is required for increasing cytosolic Ca^{2+} in the presynaptic terminals can be directly tested with the use of genetically encoded (Tian et

al., 2009) or chemical Ca^{2+} indicators (Paredes et al., 2008) targeted to presynaptic elements such as the synaptic vesicles in KA neurons. Furthermore, Ca^{2+} levels in presynaptic terminals have been assayed by targeting a fusion of synaptophysin and GCaMP to synaptic vesicles in cultured mammalian neurons and zebrafish neurons *in vivo* (Dreosti et al., 2009).

How might Stac1 regulate presynaptic Ca^{2+} channels? Although the EC coupling complex has long been thought to be unique to skeletal muscle, evidence of the existence and functional coupling between Ca_v and the Ryanodine receptor (RyR) has been reported in neurons as well (Chavis et al., 1996; De Crescenzo et al., 2006; Murmu et al., 2010). Furthermore dihydropyridine sensitive voltage-gated Ca^{2+} increases have been demonstrated in presynaptic terminals of hypothalamic terminals (Lemos and Nowycky, 1989) and ryanodine dependent Ca^{2+} release from the ER may also play a role in synaptic release (Liu et al., 2005; Llano et al., 2000; Murmu et al., 2010). This suggests the intriguing possibility that Stac1 may be regulating Ca_v of a Ca_v/RyR complex that under some conditions is required for normal synaptic transmission in neurons.

Overall, while our results using Stac1 MO have been informative to probe the locus of Stac1 function and the importance of Stac1 to KAs and the CPG, further analysis of the mechanism by which Stac1 is required for KA function will be enhanced by the generation of a knockout mutant through targeted mutagenesis techniques (Foley et al., 2009; Hwang et al., 2013; Nasevicius and Ekker, 2000; Sander et al., 2011). *stac1* mutant zebrafish will facilitate optical and electrophysiological recordings of KA neurons, Ca^{2+} imaging from the presynaptic terminals of KA neurons, and examination of protein

trafficking of potential Ca_v targets, helping to further elucidate the molecular mechanism by which Stac1 regulates neuronal function.

Author Contributions

Characterization of *stac1* expression patterns in 72 hpf zebrafish embryos and in juvenile brain slices was performed by Kenichi Iwasaki. All other experiments including phylogenetic analysis, molecular biology, expression analysis, western blot analysis, behavioral analyses, and optogenetic experiments were performed by Jeremy Linsley.

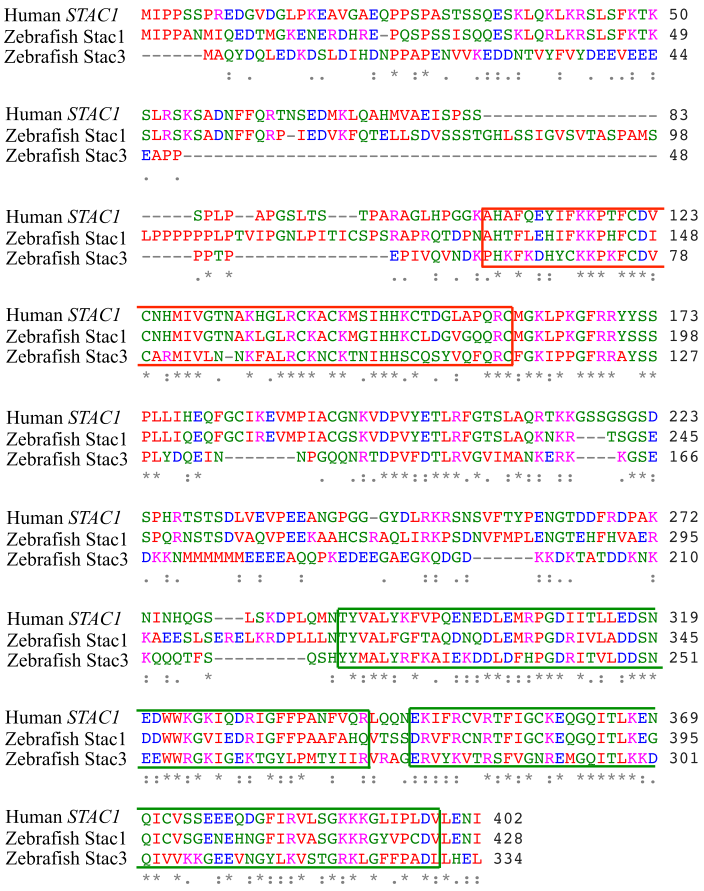

Figure 4-1. Zebrafish Stac1 is similar to human *STAC1* and zebrafish Stac3. Completely conserved residues are marked below with *, similar residues are marked with :. Red box indicates C1 domain, green boxes indicate SH3 domains. Red residues indicate small hydrophobic residues, blue indicates acidic residues, magenta indicates basic residues, and green indicates hydroxyl, sulfhydryl, amine, and H and G. Alignment generated with ClustalΩ.

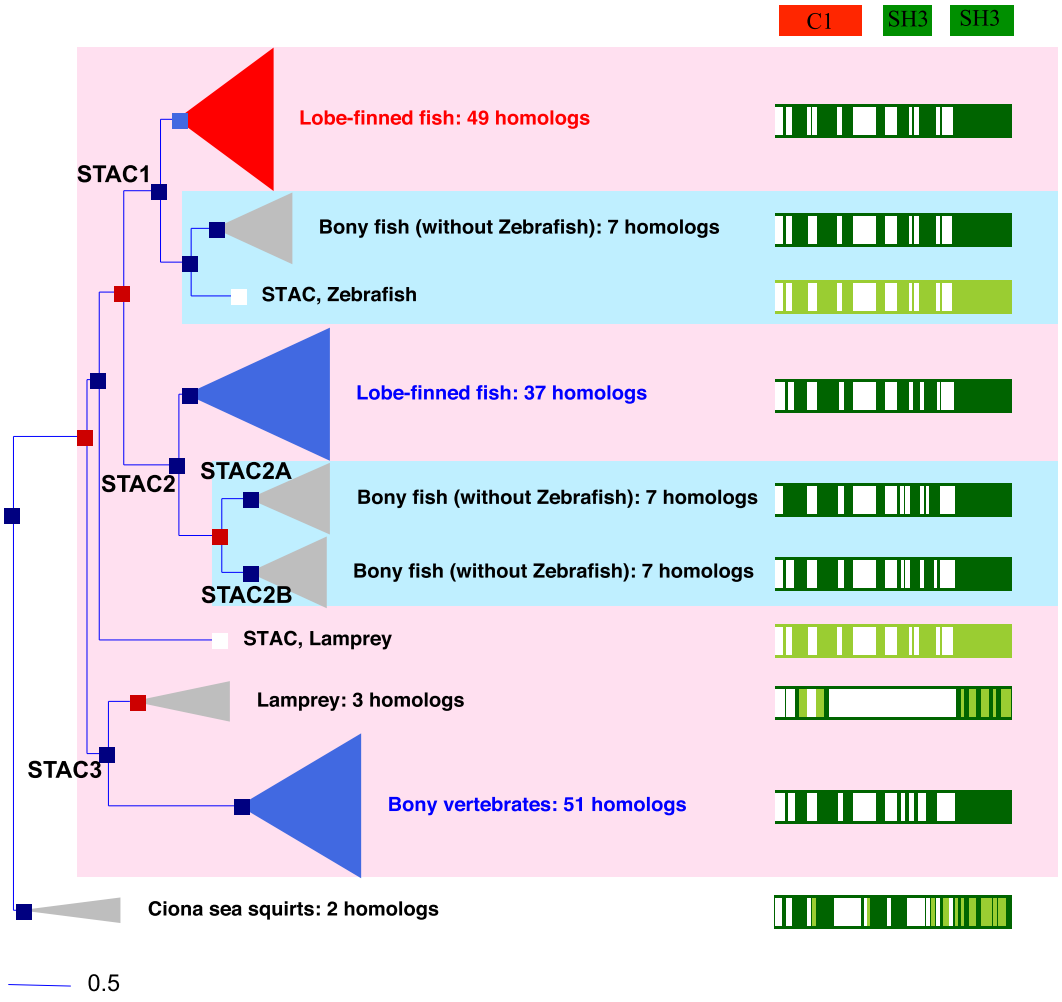

Figure 4-2. Phylogenetic tree of the Stac protein family. The *stac* genes are expressed in vertebrates (pink box). Gene duplication (marked by red squares) resulted in neuronal *stac* genes *stac1* and *stac2*, and the muscle specific *stac3*. All *stac* genes share conserved C1 and SH3 domains, shown in translated protein alignment in top right (red box is C1 domain, green boxes are SH3 domains). Dark green indicates 66-100% alignment, light green indicates 33-66% alignment. An additional gene duplication of *stac2* occurs in bony fish (bottom turquiose box). However, zebrafish appear to have no copies of *stac2*. Small blue squares indicate speciation. Small red squares indicate gene duplication. Scale represents 0.5 billion years. Tree compiled using Ensembl release 73, September 2013.

Table 4-1. Phenotypes of progeny of identified *stac3* mutants after induced expression of *hsp70-stac3-GFP* or *hsp70-stac1-GFP*

Induced Protein Expression	*stac3* mutants (immotile)	Forward movement	% Forward Movement
Stac3-GFP	15	5	30
Stac1-GFP	12	0	0

Counts of embryos showing forward swimming movement in response to three tail touches. Binomial test $p < 0.05$.

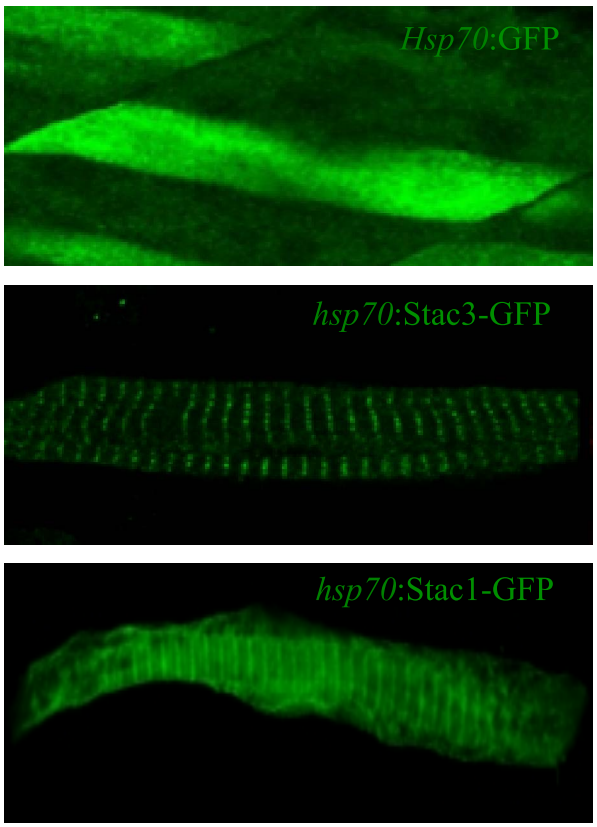

Figure 4-3. Stac1-GFP localizes in a striation pattern in skeletal muscle. Heat shock activated expression of GFP (Top), Stac3-GFP (middle), and Stac1-GFP expressed in *stac3* mutant muscle. GFP expression is diffuse throughout the cell, while Stac3-GFP and Stac1-GFP form striation patterns corresponding to t-tubules. Each image representative of three separate experiments.

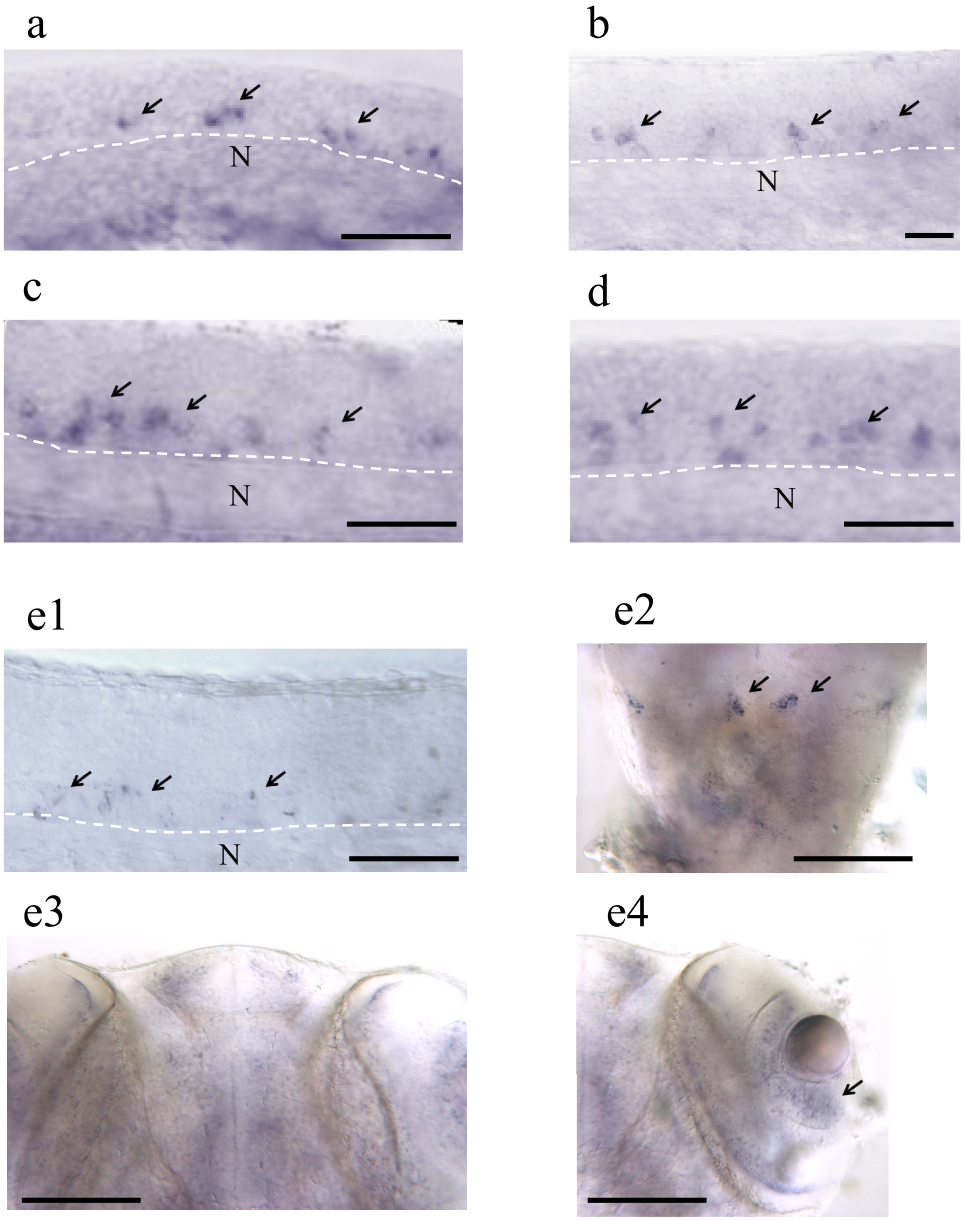

Figure 4-4. *stac1* is expressed in discrete Populations of Neurons in the Spinal Cord of 22- 72hpf embryos. Lateral views of *in situ* hybridization of embryos at a) 22hpf, b) 27hpf, c) 36hpf, and d) 48hpf showing ventrally located *stac1* expressing neurons in purple. White dashed line highlights the lateral floor plate, N denotes notocord. Arrows designate representative clusters of *stac1*+ neurons. At 72hpf expression of *stac1* is still restricted to a subset of spinal cord neurons marked by arrows (e1), but also expands to subsets of neurons in the hindbrain marked with arrows (e2), with trace expression in the the forebrain (e3), and retina marked by an arrow (e4). For e1, anterior is left, dorsal is up. e2-e4 are dorsal views and anterior is up. Scale bars are 25 µm for a-d and e1, 100 µm for e2-e4. 72 hpf labeling provided by Kenichi Iwasaki. Each image representative of at least three separate experiments.

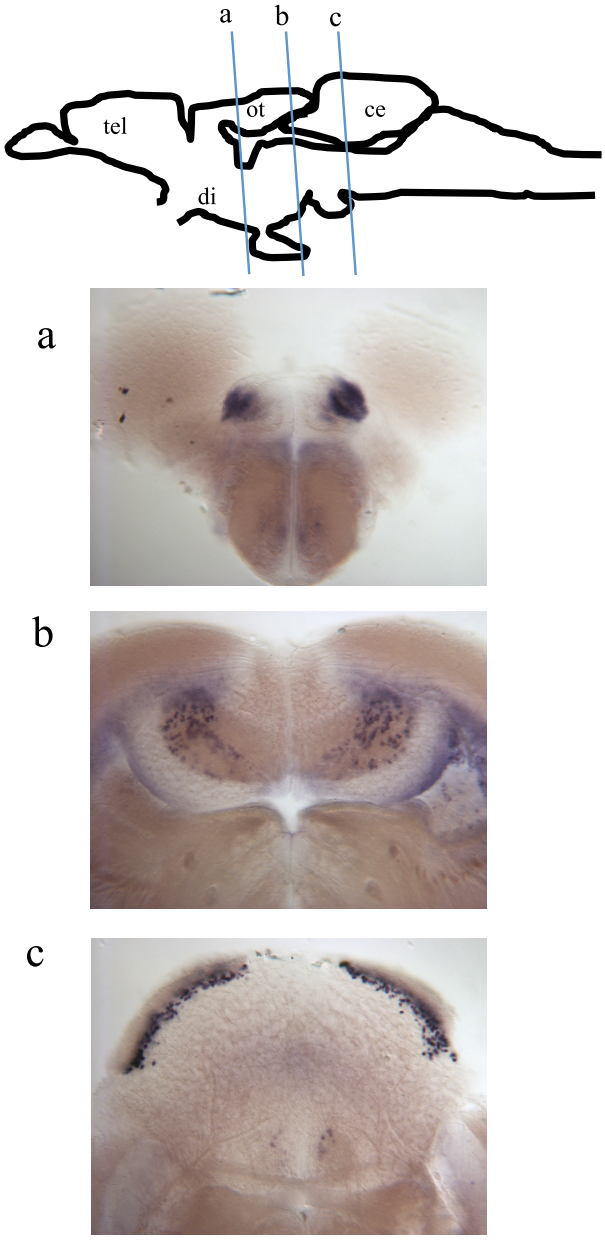

Figure 4-5. *stac1* is expressed in the brain of juvenile zebrafish. (Top) Sagittal section schematic of locations of coronal sections of adult zebrafish brain. Tel = telencephalon, di = diencephallon, ot = optic tectum, ce = cerebellum. (a) Coronal section showing expression in the habenular nucleus. (b) Coronal section showing expression in the periventricular grey zone of the optic tectum and the cerebellum. (c) Coronal section showing expression in the dorsal cerebellum. Images provided by Kenichi Iwasaki.

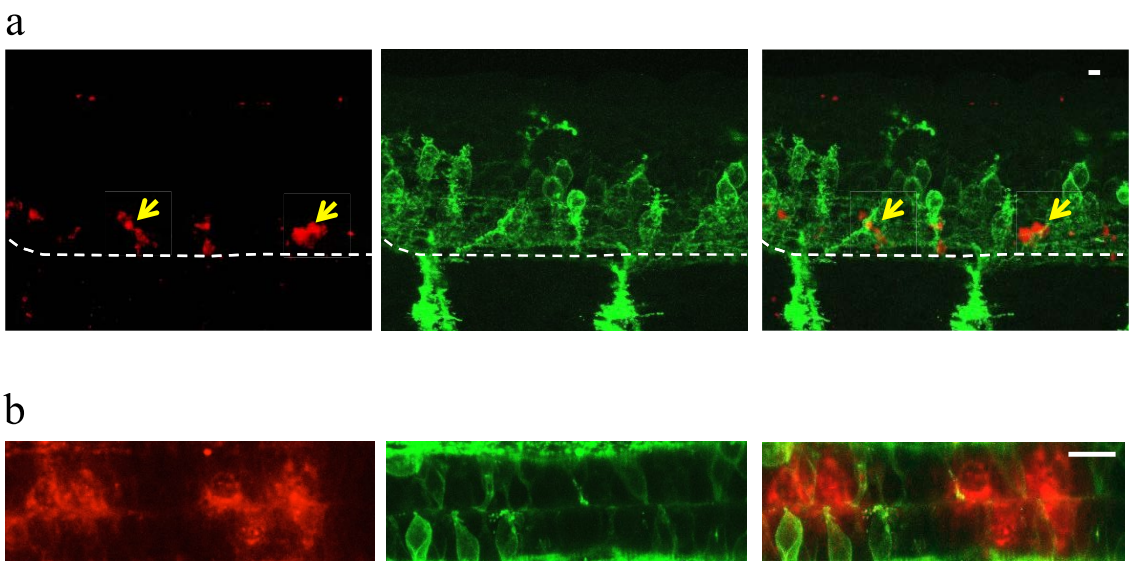

Figure 4-6. *stac1* is not expressed in motor neurons. (a) Lateral view of combined *in situ* hybridization of *stac1* (left, red), in *Tg:hb9*:mGFP embryos labeled with anti-GFP (middle, green), and combined overlay (right) showing lack of co-expression. Yellow arrows indicate clusters of *stac1*+ neurons. Anterior is right, dorsal is up. (b) A dorsal view of ventral spinal cord showing *stac1* (left, red) labeling of *Tg:hb9*:mGFP embryos labeled with anti-GFP (middle, green) , and combined overlay (right) showing lack of co-expression. Anterior is right. Scale bar is 10μm. Images representative of at least three separate experiments.

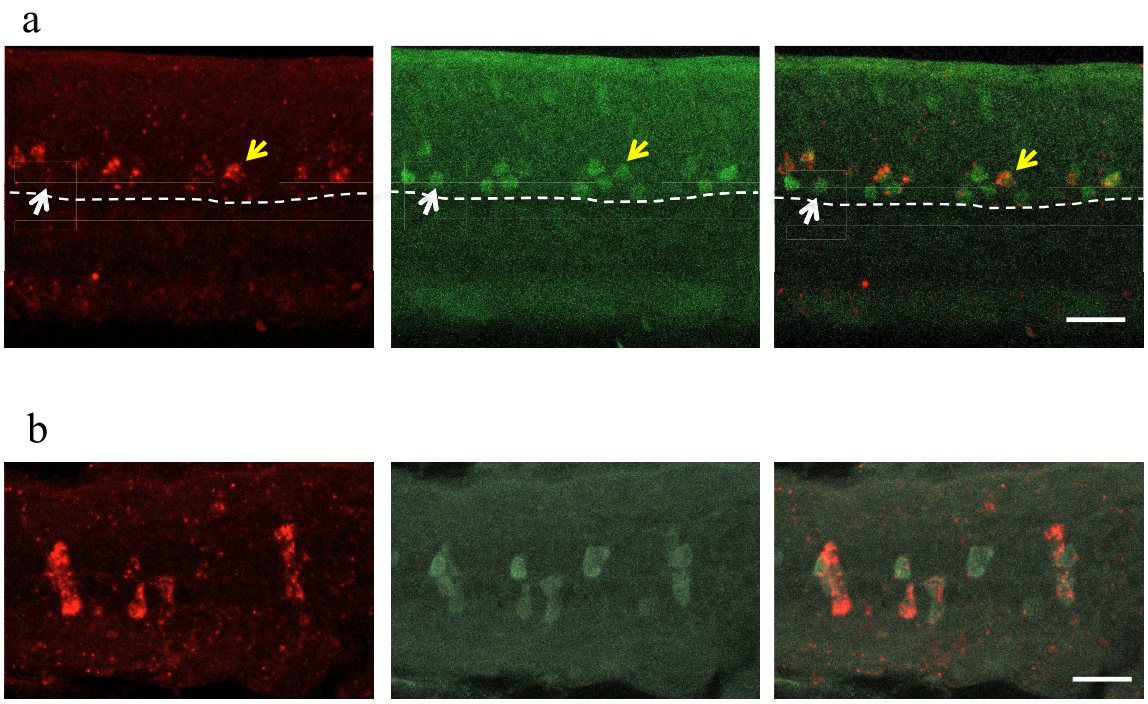

Figure 4-7. *stac1* is expressed in GABAergic KA interneurons. (a) Lateral view of 36hpf embryo co-labled with *stac1* riboprobe (left, red), anti-GABA labeling (middle, green), and combined overlay (right) showing co-expression. Dashed line indicates the floor plate, yellow arrow indicates presumptive KA' interneurons and white arrow indicates presumptive KA" expression. Anterior is left, dorsal is up. (b) a dorsal view of 36hpf embryo co-labeled with *stac1* riboprobe (left, red), anti-GABA (middle, green), and overlay (right) showing co-expression. Anterior is left. Scale bar is 25μm. Each image representative of at least three separate experiments.

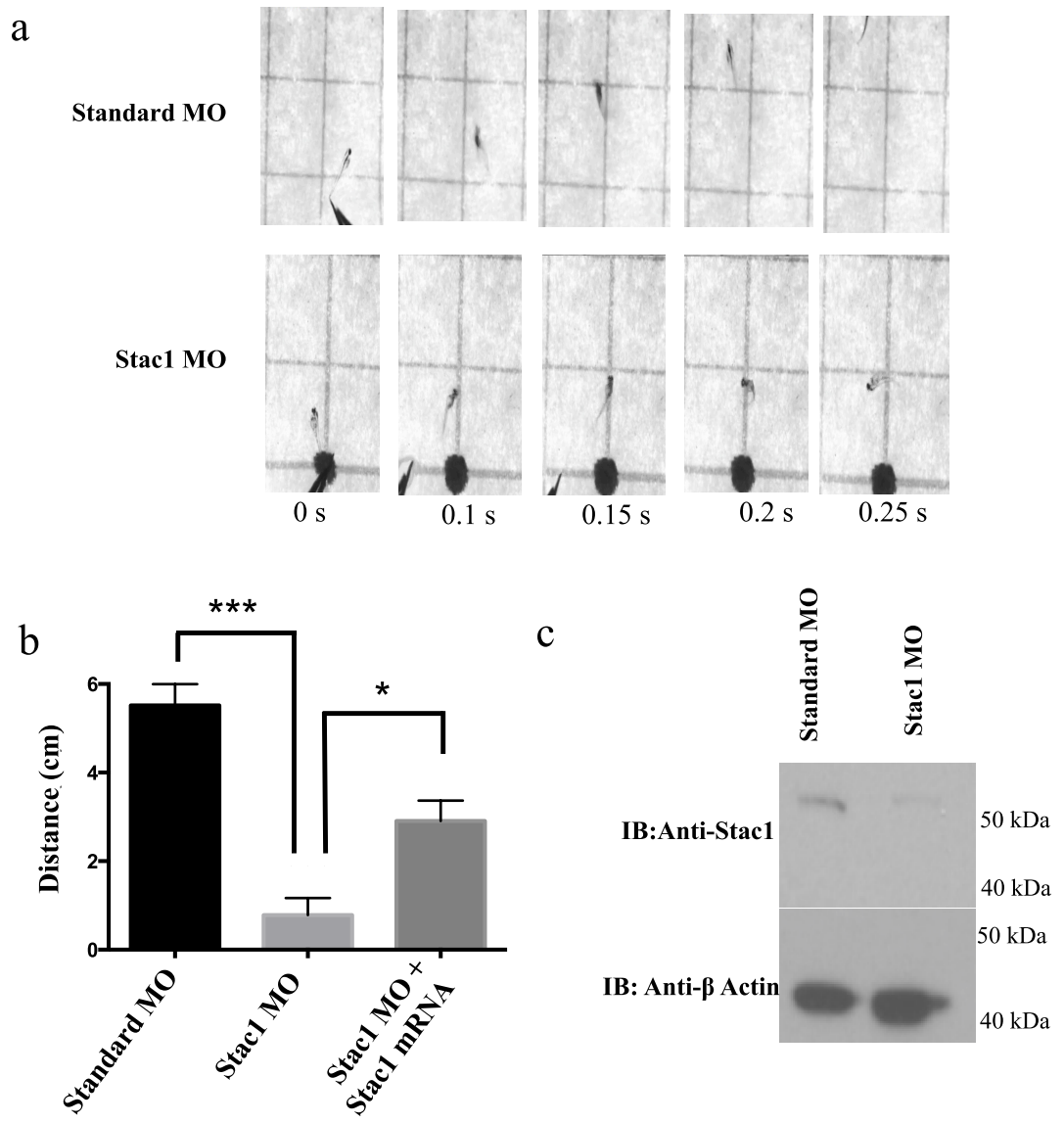

Figure 4-8. Knockdown of Stac1 reduces touch evoked swimming. (a) Representative time-lapse images proceeding from left to right of the touch evoked swimming response of standard MO injected embryos (top row) and Stac1 MO injected embryos (bottom row) at 48hpf. In response to a tail touch (left panels), embryos respond with rhythmic tail beating that propels the embryo away from the stimulus. Stac1 MO embryos have reduced motility levels compared to standard MO injected embryos. Times are indicated on bottom. (b) Quantification of swimming distance of standard MO injected embryos (n = 30) is significantly different from Stac1-MO injected embryos (n = 30) (left and center columns, *** indicates T test $p < 0.0001$). Quantification of swimming of swimming distance of Stac1 MO and Stac1 mRNA co-injected embryos (n = 30) is significantly different than Stac1 MO alone injected embryos (center and right columns, * indicates T test $p < 0.001$). (c) Immunoblots (IB) of whole cell lystate from pooled standard MO (left) and Stac1 MO injected embryos (right) probed with anti-Stac1 (top) and anti-β actin (bottom).

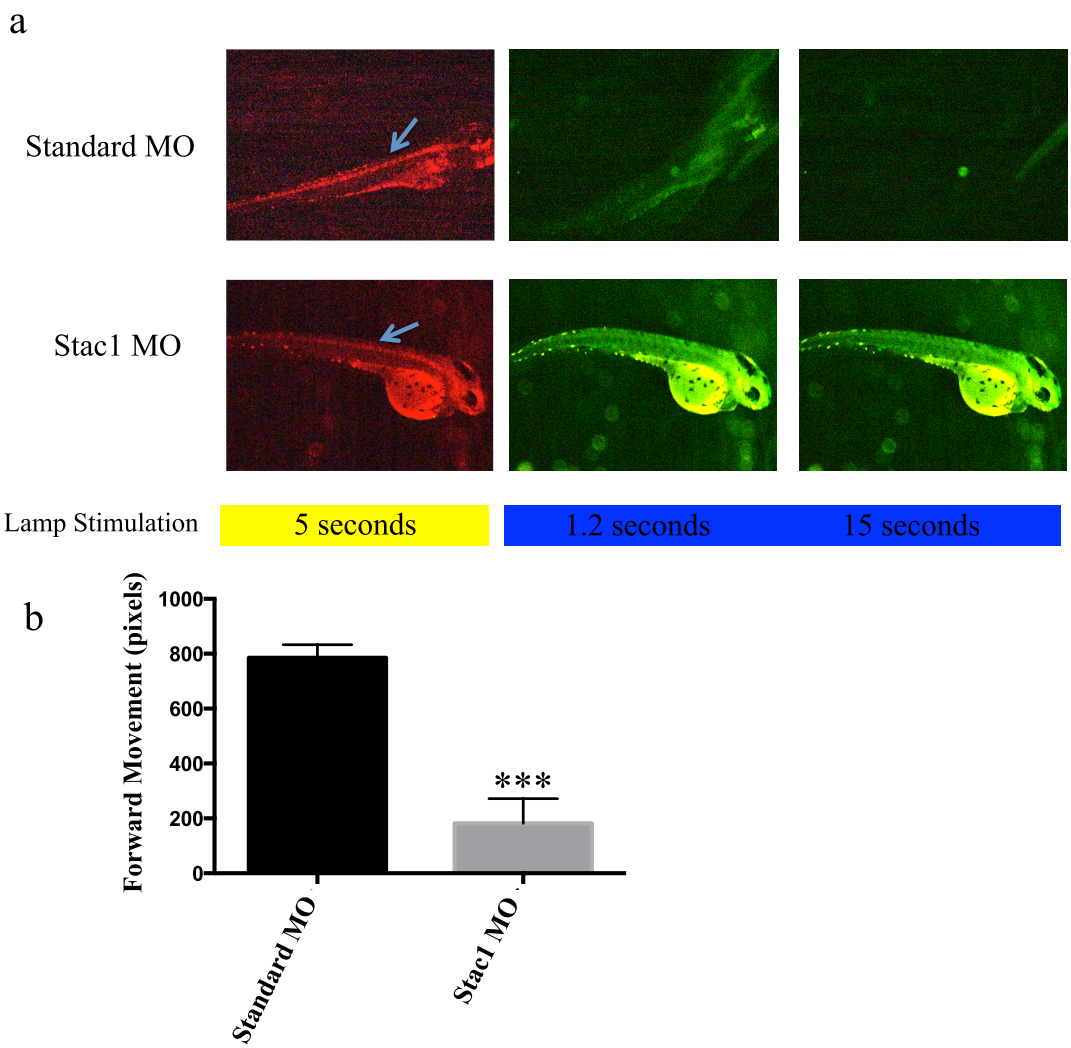

Figure 4-9. Activation of ChR2-mcherry in KA interneurons is capable of driving the CPG in control MO injected embryos, but not Stac1 MO injected embryos. (a) Representative time lapse images of light exposure of standard MO injected (top) and Stac1 MO injected (bottom) 1020t:GAL4, UAS:ChR2-mCherry embryos during exposure to yellow light (left panels), and blue light (center and right panels). Schematic of light color excitation is depicted in colors below, and time in each light light exposure before image is indicated in box. Yellow light excites mCherry expressing KA interneurons and motor neurons in the spinal cord (blue arrows). Blue light activates activates ChR2, activating the neurons in the spinal cord. Standard MO injected embryos respond to blue light with swimming behavior out of frame (top center and right panels). Stac1 MO injected embryos do not swim in response to blue light (bottom center and right panels). Green fluorescence in Stac1 MO injected embryo is due to auto-fluorescence. (b) Quantification of forward movement of tail of blue light activated swimming in 48hpf 1020t:GAL4, UAS:ChR2-mcherry standard MO injected embryos (left, $n = 8$) and Stac1 MO injected embryos (right, $n = 7$, T test $p < 0.001$). Forward movement was limited by distance to edge of viewing areas under the microscope.

CHAPTER V

DISCUSSION AND CONCLUSIONS

The completion of the first draft of the human genome was an enormous technical feat that was greeted with huge fanfare and hyperbolic pronouncements of the dawning of a new age in our understanding of human genetic diseases. Nevertheless, more than a decade later, we are still far from a full understanding of the enormous complexity encoded in our genomes, or how human mutations lead to diseases. It has become clear in the post-genome era that besides the sequence of the human genome, we need an understanding of the cellular functions of the proteins the genome encodes to reach a better comprehension of both human biology and the pathology of human genetic diseases. While the sequence of the human genome did not immediately give us the answers to all of our questions about our DNA, it did provide us with a framework in which similar genes and domains of genes could be compared and new hypotheses of functions could be made. This framework served to strengthen pre-genome project strategies for identifying gene functions such as forward mutagenesis screens and reverse genetics, and has served to accelerate the discoveries of the genetics underlying the complex interactions that occur within a cell.

The studies presented here illustrate how the combination of genomics tools, mutagenesis strategies, and reverse genetics approaches are driving the study of the functions of proteins in our post-genome era, specifically in understanding the functions of two members of the novel gene family, *stac*. Through the use of a zebrafish mutagenesis screen for embryonic motility mutations, we discovered a mutation in the previously novel *stac3* gene that disrupted embryonic swimming behavior. We showed that Stac3 is a skeletal muscle protein that is a member of the EC coupling complex required for normal Ca^{2+} release. Stac3 affects the trafficking, expression and organization of the DHPR to triadic junctions. Furthermore, we find that a mutation in human *STAC3* is the cause of a Native American Myopathy, a human congenital myopathy. The *stac1* gene is a homolog of *stac3* that is expressed in neurons, but has no known function. To explore the function of Stac1 in zebrafish neurons, we first found that *stac1* is expressed specifically in a subset of spinal cord neurons in zebrafish embryos called KA interneurons that are required for the activation of the swimming CPG. Then, using a reverse genetics approach to knockdown expression of Stac1, we found that Stac1 is required for the normal function of KA neurons and touch-induced swimming. With the basics of the functions of Stac1 and Stac3 in place, the next step will be to gain a deeper understanding of the mechanisms of Stac proteins, which will strengthen our knowledge of the cellular biology of skeletal muscle EC coupling and the physiology of neurons.

The future of EC coupling studies and Stac3

Despite the critical importance of the EC coupling complex in muscle contraction, many important details such as the molecular details of protein-protein interactions between DHPR and Ryr that coordinate the gating of Ca^{2+} release, and the trafficking, ordering, and stabilization mechanisms that target the DHPR into tetrads with the RyR1 homotetramers are not well understood (Beam and Bannister, 2010). Much of this stems from major technological limitations, which have hindered the research of EC coupling. Here, I will address several of these limitations as well as possible remedies, and attempt to frame how these solutions may benefit future research into the mechanism of Stac3 in the EC coupling complex.

The difficulty of studying direct protein-protein interactions in the EC coupling complex

Direct interaction between DHPR and RyR1 is thought to mediate EC coupling and is required for Ca^{2+} release from the SR in skeletal muscle (Dulhunty, 2006). However, a mechanistic explanation for how the DHPR and RyR1 couple to activate Ca^{2+} release has not been determined despite decades of dedicated research. One reason for the difficulty researchers have had in unraveling the complicated interactions between the DHPR and RyR1 is due to the weak, transient biochemical interactions that are thought to be instrumental for EC coupling, yet are difficult to assay with classic biochemical techniques. Biochemical assays also often require proteins to be isolated *in vitro,* which may not replicate the complexity of subtle interactions occurring in the macromolecular EC coupling complex.

One way to assay for these subtle biochemical interactions is through the use of Förster resonance energy transfer (FRET) to measure energy transfer between fluorophore-tagged proteins of the EC coupling complex. As energy transfer occurs when two FRET fluorophores are brought into close contact, the FRET ratio can be used as readout of conformational changes that occur between the two fluorophore tagged proteins, which can be indicative of a physical interaction (dos Remedios and Moens, 1995). Furthermore, these interactions can be studied *in vivo* in real time, providing a more representative characterization of physical interactions between proteins. Using FRET techniques, sites of close proximity of the $Ca_v1.1$ and $Ca_v\beta$ with the RyR1 have been found that support previous biochemical interactions between $Ca_v1.1$ and RyR1 (Lu et al., 1994) and $Ca_v\beta1a$ and RyR1 (Papadopoulos et al., 2004; Rebbeck et al., 2011). Additionally, by tagging $Ca_v1.1$ with donor and acceptor fluorophores and comparing FRET ratios of the fusion protein when expressed in *dyspedic* (RyR1 null) myotubes (in which RyR1 is not present in triads) versus *dysgenic* ($Ca_v1.1$ null) myotubes (in which RyR1 is present in triads), regions of the $Ca_v1.1$ that had not been previously implicated as necessary for EC coupling were found to undergo conformational changes in the presence of RyR1 that may be important for EC coupling (Polster et al., 2012). Using FRET to decipher the interactions between Stac3 and $Ca_v1.1$ or Stac3 and $Ca_v\beta$ may provide both the orientations of the two proteins in the EC coupling complex and regions of the proteins where those direct interactions take place.

Another reason for the difficulty in unraveling the protein-protein interactions that are necessary for EC coupling is that post-translational modifications such as protein phosphorylation, may regulate many of these interactions in subtle ways and may mask

important interactions when assayed using classical *in vitro* biochemical techniques to look for direct interactions such as co-immunoprecipitation or yeast 2-hybrid assays. For example phosphorylation of Thr498 in several $Ca_v\beta$ isoforms is required for a direct interaction with CaMKII, which in turn strongly modulates Ca^{2+} release from $Ca_v1.2$ (Grueter et al., 2006; Grueter et al., 2008). Yet the presence of a direct interaction between $Ca_v\beta$ and CaMKII may be missed if assaying for the interaction using *in vitro* biochemical techniques, as the *in vitro* conditions may not replicate the post-translational modifications necessary for the interaction.

The advent of proteomics technologies such as mass spectrometry hold the promise to help unravel complicated EC coupling interactions as well as the post-translational modifications and their influences on the EC coupling complex. Although mass spectrometry will not indicate direct interactions among proteins within a complex, it can provide a quantitative readout of the ratios of components in the complex as well as their phosphorylation states, which can suggest previously unknown post-translational modification dependent interactions between proteins. An illustration of the potential of this technique is a recent report on the immunoprecipitation and mass spectrometry of the Ca_v2 macromolecular complex from the mammalian brain, which allowed a comprehensive and quantitative analysis of the nanoenvironment surrounding the channel, though the phosphorylation states of the proteins involved were not reported (Muller et al., 2010). Similar, but smaller scale mass spectrometry of the pulldown fraction from *muscle actin:*Stac3-GFP transgenic zebrafish muscle lysate was used to determine the molecular complex that surrounds Stac3-GFP (Table 2-1), and the results continue to guide future research. Furthermore, these mass-spectrometry results indicated

that Stac3 contains at least three residues that are found in a phosphorylated state *in vivo* (Table 2-1, data not shown), however if these phosphorylation sites are important in Stac3 function remains unknown. The next step to further dissect the importance of such modifications will be to mutagenize those residues to non-phosphorylated residues, or phospho-mimetic residues, and assay the affect on Stac3 phenotypes.

Mass spectrometry based proteomics could also be useful in understanding Stac3 protein interactions and their involvement in NAM. For example, as the NAM W >S mutation appears to disrupt the binding face of the SH3 domain, it is logical to hypothesize that the mutation disrupts important protein-protein interactions between Stac3 and other proteins. The identity of these binding partners may be determined by separate immunoprecipitations of $Stac3^{wt}$ and $Stac3^{NAM}$ expressed in the *stac3* mutant background, and subsequent comparison of the proteins in the pulldown fractions by mass spectrometry. Proteins that are missing from the pulldown fraction of $Stac3^{NAM}$ expressing myofibers may be important interaction partners of Stac3 that are disrupted by the mutation in the Stac3 NAM SH3 domain. Thus through the use of mass spectrometry, we could identify crucial interactions of Stac3 that are behind the pathology of the NAM disease.

Does Stac3 regulate voltage dependent charge movement of DHPRs and/or Ca^{2+} release?

Critical to a comprehensive understanding of the influence of Stac3 on EC coupling is an electrophysiological analysis of EC coupling in *stac3* mutants, which has not yet been completed. Though the physical components of the EC coupling complex

are present in *stac3* mutant muscle triads, those components do not function correctly, and the exact deficits in the coupling of membrane depolarization to Ca^{2+} release must be teased out experimentally. There are three main ways Stac3 could affect EC coupling which can be assayed by a combination of electrophysiological recordings and Ca^{2+} imaging of *stac3* mutant muscle in comparison to wildtype sibling muscle. First, Stac3 could be required for normal voltage sensing by the DHPR. The ability of the DHPR to sense voltage can be assayed by recording the immobilization resistant intramembrane charge movement of *stac3* mutant myofibers as has been done previously in the study of the *relaxed* zebrafish mutant, where intramembrane charge movement has been found to be almost completely absent (Dayal et al., 2013; Schredelseker et al., 2009; Schredelseker et al., 2005). As intramembrane charge movement is a measure of both functional DHPR expression as well as of charge sensing, and as *stac3* mutants have a ~25% decrease in triadic DHPR expression, the charge movement of DHPRs in *stac3* mutants should be partially reduced (Horstick et al., 2013). However, a more substantial decrease in intramembrane charge movement or a shift in the kinetics of charge movement indicative of improper voltage sensing would indicate that Stac3 is required for normal voltage sensing by the DHPR complex. As charge movement has been shown to be independent of tetrad formation, these results would indicate that Stac3 functions in distinct roles of tetrad formation as well as in supporting proper voltage sensing (Schredelseker et al., 2009).

A second way Stac3 could affect EC coupling is by aiding the communication between the DHPR and the RyR1 in EC coupling. While the voltage sensing capacity of DHPR may function normally, the ability of DHPR to communicate with RyR1 can be

separately disrupted, resulting in decreased Ca^{2+} release (Schredelseker et al., 2009). Proper coupling between the DHPR and RyR1 can be assayed by testing the voltage dependence of Ca^{2+} release with a Ca^{2+} indicator such as Fluo-4 (Schredelseker et al., 2009) or the more recently developed GCaMP6f, which has faster kinetics so may reflect the kinetics of physiological changes in Ca^{2+} more accurately (Chen et al., 2013). Although the release of Ca^{2+} was assayed with GCaMP3 to show that Ca^{2+} release is defective in *stac3* mutant myotubes, GCaMP3 binding of Ca^{2+} exhibits slow kinetics and a careful voltage dependency of Ca^{2+} was not performed. If intramembranous charge movement is normal but the voltage dependency of the kinetics or peak of Ca^{2+} release is disrupted, then Stac3 is required for the coupling the DHPR and RyR1. In fact such separation of charge movement and voltage dependency of Ca^{2+} release was found when expressing cardiac $Ca_v\beta2a$ and ancestral house fly $Ca_v\beta M$ in myotubes of *relaxed* ($Ca_v\beta1$ null) mutants. $Ca_v\beta2a$ and $Ca_v\beta M$ were able to fully restore intramembranous charge movement of *relaxed* embryos, but Ca^{2+} release was defective (Schredelseker et al., 2009). Thus sequences in $Ca_v\beta1a$ that are not conserved in $Ca_v\beta2a$ or $Ca_v\beta M$ are likely required for direct activation of RyR1 by DHPR. Since Stac3 binds $Ca_v\beta1a$ one wonders if these $Ca_v\beta1a$ sequences might serve as the critical points of interaction with Stac3. This could be tested by examining binding between Stac3 and $Ca_v\beta2a$/$Ca_v\beta M$ vs $Ca_v\beta1a$. As the details of the mechanisms for coupling of the DHPR and RyR1 in EC coupling are not well known (Beam and Bannister, 2010), the function of Stac3 in this capacity might lead to new insights in our understanding of mechanism of EC coupling.

A third and final scenario is that Stac3 may play a role in both charge movement and coupling of the DHPR and RyR1, similar to the dual roles that $Ca_v\beta1a$ plays (Dayal

et al., 2013; Schredelseker et al., 2009; Schredelseker et al., 2005). Teasing apart which domains are necessary in different capacities would then be the next goal in studying Stac3. For example, expressing different truncations or mutations of Stac3 in the *stac3* mutant background and assaying the effects on, charge movement and EC coupling might reveal the importance of specific domains in specific capacities of supporting EC coupling. Furthermore, as the Stac1 protein likely contains motifs for triad targeting shared with Stac3, chimera analyses of Stac1 and Stac3 might also be useful.

In parallel to electrophysiological assays of EC coupling in *stac3* mutant muscle, co-immunoprecipitation to further probe which domains are required for interactions with known binding partners $Ca_v\beta1$ or $Ca_v1.1$ L2-3 might help provide rationales as well as support different hypotheses from electrophysiological and Ca^{2+} imaging assays. The $Stac3^{NAM}$ allele makes an appealing starting point for both co-immunoprecipitation studies and electrophysiological characterizations. As $Stac3^{NAM}$ expression in *stac3* mutants appears to give a hypomorphic phenotype (Horstick et al., 2013), it is tempting to speculate that the W284S mutation in the 1st SH3 domain of Stac3 may disrupt one of the activities of Stac3 function while leaving others intact. At the same time, these studies may help reveal insights into the pathology of NAM.

Super resolution microscopy would be useful for examining the mechanism for EC coupling.

While optical imaging of labeled proteins is often a valuable tools in measuring protein expression and localization in cells, the requirement for DHPR and RyR1 proteins to be arranged in patterned arrays that are not visible at diffraction limited resolution

(~250nM) of light makes the study of the expression of the functional EC coupling complex in triads difficult to study. Currently the only way to assay whether DHPRs are patterned into arrays of tetrads is by freeze fracture EM (Block et al., 1988) that is laborious and requires specialized technical expertise. Furthermore, due to the nature of the technique, freeze fracture EM is unable to provide a quantitative readout of RyR1 formations.

A promising, alternative way of assaying the ordered array of DHPR and RyR1 molecules is super-resolution imaging technologies. Recently developed techniques such as photo-activated localization microscopy (PALM) (Betzig et al., 2006), stochastic optical reconstruction microscopy (STORM) (Rust et al., 2006), and stimulated emission depletion microscopy (STED) (Westphal et al., 2008) have been demonstrated to provide resolution down to ~10nM (McKinney et al., 2009). These super resolution techniques take advantage of stochastic fluorescence of fluorescent molecules combined with software that is able to reconstruct the signal of the fluorophores one molecule at a time into a resolved image that surpasses the diffraction limits of light microscopy. Although technically advanced at the level of hardware and software, super resolution techniques mostly rely on existing methods for labeling and/or genetic encoding of fluorescent proteins that are straightforward and well established, making them an ideal replacement for freeze fracture EM. Furthermore, in contrast to freeze fracture EM, super resolution imaging is less invasive, can be used to track proteins in live cells *in vivo* (Eggeling et al., 2013), and can even be used to create 3D reconstructions (Huang et al., 2008).

The use of super resolution techniques is still in its infancy. An unforeseen problem with using these techniques with existing molecular labeling methods is that the

amount of resolution possible becomes limited by the size of the fluorescence labels. For example, an initial attempt to image the arrangements of RyR2 proteins in cardiomyocytes with super-resolution imaging was unable to resolve proteins at the single molecule level at the microscopy level, and instead had to rely on computer modeling and reconstruction to create an image of the orthoganol array of RyR2 receptors (Baddeley et al., 2009). Yet theoretically, as individual RyR proteins are large with each protein in the tetramer containing a radius of around 12 nm (Meng et al., 2007), resolution of individually labeled proteins by super-resolution techniques should be possible using antibody labeling to mark proteins. By using monoclonal antibodies directly conjugated to fluorophores instead of using a fluorophore conjugated secondary antibody one can increase resolution (Baddeley et al., 2009). Direct antibody labeling reduces the variability of secondary antibody labeling as well as reducing the bulk of the labeling proteins, thereby increasing the ability to resolve single proteins. The bulk of the antibody-target protein complex could also be further decreased by using conjugating fluorophore tagged Fab fragments, which would increase the ability to resolve individually labeled molecules.

Despite remaining technical details that need to be sorted out, one of the most exciting advantages of super resolution imaging over EM is the ease at the ability to visualize multiple labels simultaneously in a live undisturbed cell. Freeze fracture EM microscopy has relied on the separate membrane localizations of the DHPR and RyR1, in the T-tubule and the SR respectively, to identify each protein. Therefore, the procedure necessitates separating the two membranes manually before visualizing proteins, a process that is prone to experimental artifacts and makes visualizing the co-alignment of

DHPRs and RyRs together difficult. As the exact alignment of the DHPRs and RyR1s is required for EC coupling, super resolution imaging with anti-DHPR and anti-RyR could be used as a facile, informative diagnostic of the structure of the EC coupling complex, currently unavailable in studies of the EC coupling complex. This technique would immediately be useful in studying the contributions of individual domains of Stac3 to the formation of full tetrads by expressing truncations or mutations of Stac3 such as $Stac3^{NAM}$ in the *stac3* mutant background and assaying the affects on the DHPR and RyR1 arrays in muscle myofibers without using freeze fracture EM. Furthermore, DHPR-RyR interactions have been recently observed in neurons, but the structure and arrangements of the DHPR and RyR proteins in the interactions in neurons are not known (De Crescenzo et al., 2012; De Crescenzo et al., 2006). As neurons are not amenable to freeze fracture electron microscopy, super resolution microscopy may be an ideal way to study such interactions, as well as possible affects of the knockdown of Stac1 on those structures.

Analysis of EC coupling would benefit from heterologous reconstitution of coupling

Reconstitution and manipulation of cardiac EC coupling in heterologous cell culture has led important advancements in our knowledge of the mechanisms that affect cardiac EC coupling (Niggli et al., 2013). However, it has not be possible to successfully reconstitute the skeletal muscle EC coupling heterologously (Suda et al., 1997; Takekura et al., 1995b). As a result, much of skeletal muscle EC coupling research has been conducted through the use of chimera expressions in *dysgenic* ($Ca_v1.1$ null)*, dyspedic* (RyR1 null)*,* or $Ca_v\beta1$ null myotubes. While much has been learned from this research

approach, chimera expression analyses fail to account for the contributions of conserved regions of the chimera that are still able to function with endogenous muscle protein in the expressed cell, masking the contributions of accessory proteins of the EC coupling complex. In order to clearly make arguments of necessity and sufficiency for proteins that contribute to skeletal EC coupling, we must be able to reconstruct the components of the complex and subsequently tease apart each component systematically. Furthermore, reconstitution of the EC coupling complex in heterologous cell culture would also provide a model of skeletal EC coupling that is easier to manipulate than current models, which would make future studies into the mechanisms of EC coupling more accessible for researchers.

Early reports of attempts to reconstitute the skeletal EC coupling complex by co-transfection of each of the DHPR subunits with the RyR1 in CHO cells, found that although the RyR1 retains its ability to form functional arrays, and mammalian DHPRs are found to respond to voltage with L-type current, EC coupling does not occur in the absence of extracellular Ca^{2+} (Suda et al., 1997; Takekura et al., 1995b). It was concluded that skeletal EC coupling requires the DHPR and the RyR1 to be in a close proximity, but the specialized arrangement cannot occur due to the lack of triadic junctions in CHO cells. However, these attempts at reconstitution of the EC coupling complex occurred almost 20 years ago, and in the time since these publications, much has been learned about skeletal EC coupling as well as t-tubule biogenesis (Al-Qusairi and Laporte, 2011). Thus, new attempts at heterologous reconstitution of the EC coupling complex by co-expressing proteins such as Bin1 (Razzaq et al., 2001), Mg29 (Nishi et al., 1999), JPH1

(Komazaki et al., 2002), MTM1 (Al-Qusairi et al., 2009), as well as Stac3 (Horstick et al., 2013), with RyR1 and DHPR is overdue.

Zebrafish model for Native American Myopathy

One domain that appears to be required for Stac3 function is the first SH3 domain that is mutated in NAM. The W > S missense mutation that causes NAM disrupts a surface exposed residue that is highly conserved in SH3 domains and that may be required for the ability of Stac3 to bind an important ligand (Figure 2-18 a,b). Yet as null mutations of Stac3 in zebrafish and mice are embryonic or perinatal lethal, the survival of NAM patients into adulthood suggests that the NAM mutation is a hypomorphic allele of Stac3 that is more functional than mice or zebrafish mutants. Furthermore, rescues with $Stac3^{NAM}$ in the *stac3* mutant background indicate that skeletal muscle expressing $Stac3^{NAM}$ show reduced Ca^{2+} release and reduced rescue of touch evoked swimming in comparison to rescues with $Stac3^{WT}$, yet more skeletal muscle function than in *stac3* mutants (Horstick et al., 2013). Although our initial attempts at modeling the NAM disease in zebrafish revealed a Ca^{2+} release defect associated with $Stac3^{NAM}$, they give an incomplete description of the pathophysiology of the disease, mainly due to the limitations of transient expression of $Stac3^{NAM}$ used in the experiments. Transient expression of DNA in zebrafish embryos is hindered by the inability to control expression levels and results in mosaic expression, making interpretations of relative levels of rescue and subcellular protein localization, difficult to interpret. A cleaner, more informative approach would be to generate a stable transgenic $Stac3^{NAM}$-GFP zebrafish line using established transgenesis techniques (Kawakami, 2007), and crossing the stable

transgene into the *stac3* mutant background to create a zebrafish line only expressing Stac3^{NAM}. Two transgenic lines expressing only Stac3^{wt}-GFP (*stac3^{wt}-GFP; stac3$^{-/-}$*) have already been generated that are phenotypically normal (Horstick et al., 2013), and would make ideal controls for comparison to a *stac3^{NAM}-GFP; stac3$^{-/-}$* zebrafish. Thus, the effect of the NAM mutation on behavior, physiology, and protein trafficking in skeletal muscles could be examined.

The *stac3^{NAM}-GFP; stac3$^{-/-}$* zebrafish would also further establish zebrafish as a model for the NAM disease. The stable and expression of Stac3^{NAM}-GFP in all skeletal muscle fibers rather than in the mosaic pattern seen from transient expression will allow for the determination of the true phenotypic effect on motility of the NAM mutation. Furthermore, the large numbers and fast development of zebrafish larvae make them amenable for use in drug and small molecule screens (Kari et al., 2007; Kokel and Peterson, 2008), which in principle could identify both agonists and inhibitors of Stac3. These could then be tested as candidates for drug development, as well as further revealing the pathology of the disease.

NAM patients are susceptible to malignant hyperthermia (MH) in which patients have a lethal response to anesthesia. MH is characteristic of many mutations in EC coupling but is poorly understood. It would be interesting to see if *stac3^{NAM}-GFP; stac3$^{-/-}$* zebrafish respond to anesthetics with MH. If so these fish could be used to better understand MH and potentially identify agents that might inhibit MH. Thus, transgenic *stac3^{NAM}-GFP; stac3$^{-/-}$* zebrafish might provide valuable insights into the mechanisms of NAM and MH, provide useful small molecules for pharmacological manipulation of EC coupling and be useful for development of drugs for NAM.

The role of Stac1 in Neurons

As the mechanism for Stac3 in muscle has come more into focus, the question of what function Stac1 might be playing in neurons still remains a mystery. One hypothesis is that Stac1 is required for normal Ca^{2+} release from intracellular stores in neurons in a similar way to how Stac3 is required for normal Ca^{2+} release in skeletal muscle. Yet while Ca^{2+} increases in skeletal muscle is primarily used to trigger the contraction machinery, Ca^{2+} increases in neurons is involved in a plethora of specialized processes such as signal integration, action potential propagation, as well as synaptic release (Berridge, 1998). Adding complexity to the issue, increased intracellular Ca^{2+} concentration in neurons can result from an influx of extracellular Ca^{2+} through Ca_vs or by release from intracellular stores such as the ER, and different processes are activated based on the Ca^{2+} concentration within a specific micro-domain of the cell. Although extracellular Ca^{2+} influx through Ca_vs has a well-established role in initiation of synaptic transmission (Tsien et al., 1988), the role of Ca^{2+} release from intracellular stores, mediated by RyR or Inositol 1,4,5-trisphosphate receptors (IP_3R) in the ER, is less well understood (Catterall, 2011). Thus defining a clear role for Stac1 function in neurons may not be as straightforward as the role of Stac3 in supporting EC coupling in skeletal muscle.

The role of intracellular Ca^{2+} release in neurons has been difficult to study, in part because Ca^{2+} can function as a messenger in multiple pathways based on localization and the concentration within specific microdomains. Neurotransmitter release, for example, is triggered by Ca^{2+} release that must be in close proximity of the synaptic vesicles and exocytotic machinery, and some small focal Ca^{2+} transients do not activate

neurotransmitter release presumably because they are slightly too distant to the neurotransmitter release machinery (ZhuGe et al., 2006). Although the influx of extracellular Ca^{2+} influx is clearly important for synaptic transmission, it is possible that contributions of Ca^{2+} from internal stores may also modulate synaptic transmission. In fact Ca^{2+} stores in nerve terminals have been implicated in long-term potentiation (Lauri et al., 2003) and long term depression of synapses (Unni et al., 2004), and Ca^{2+} dysregulation resulting from intracellular Ca^{2+} release has been implicated in a number of diseases such as Alzheimer's disease, schizophrenia, and bipolar disorder (Berridge, 2013).

The mechanisms for intracellular Ca^{2+} release are not well understood. ER has been observed to extend as a continuous network throughout neurons, and has been proposed to act as a neuron-within-a-neuron, storing signals such as Ca^{2+} for release into the cytosol (Berridge, 1998). So far no junctions of the plasmamembrane and ER have been observed that might be similar to triadic junctions seen in skeletal muscle. However, RyR and IP_3R gate the intracellular Ca^{2+} stores, and can be activated by Ca^{2+}- induced-Ca^{2+} release or intracellular messengers such as cyclic ADP, or $InsP_3$. Thus, extracellular Ca^{2+} influx through Ca_vs can be a trigger for further release of Ca^{2+} intracellular stores by diffusion of extracellular Ca^{2+} to RyR1 or IP_3R. However, just as in cardiac muscle, Ca^{2+}-induced-Ca^{2+} release is relatively slow, and release of Ca^{2+} stores in neurons has been observed on faster time scales, indicating other mechanisms may also be involved (Akita and Kuba, 2000; Chavis et al., 1996). One mechanism that occurs independently of Ca^{2+}-induced-Ca^{2+} release is found in cerebellar granule cells. Here activation of the type-1 metatropic glutamate receptor induces an L-type Ca^{2+} current and intracellular Ca^{2+}

release that is blocked by ryanodine and occurs independently of Ca^{2+}-induced-Ca^{2+} release (Chavis et al., 1996). Additionally, RyR1 co-immunoprecipitates with $Ca_v1.2$ and $Ca_v1.3$ from rat brain, indicating Ca_vs may be in complex with RyR *in vivo* (Mouton et al., 2001). However, a mechanistic explanation for how these Ca_v-RyR interactions occur is unknown.

In addition to global release of intracellular Ca^{2+} stores, small flashes of Ca^{2+} transients from intracellular stores, referred to as Ca^{2+} syntillas, have been observed in neurons. Ca^{2+} syntillas occur in the absence of Ca^{2+} influx into the cell and are triggered independently of Ca^{2+} -induced Ca^{2+} release (De Crescenzo et al., 2004). In contrast to Ca^{2+} influx through Ca_vs, Ca^{2+} syntillas increase in frequency but not size during depolarization, and require RyR1 for Ca^{2+} release (De Crescenzo et al., 2004). As RyR is not voltage sensitive, Ca_v was proposed to be a co-activator, similar to the DHPR-RYR interaction in skeletal muscle, and pharmacological as well as subcellular localization data support that conclusion (De Crescenzo et al., 2006). The mechanisms by which a DHPR would activate RyR-gated internal Ca^{2+} stores, and the necessity of syntillas in neuronal function, however, has remained inconclusive and controversial (De Crescenzo et al., 2012; McNally et al., 2009; Ouyang et al., 2005).

Part of the difficulty in studying Ca_v-RyR Ca^{2+} release mechanisms in neurons stems from the overlapping expression profiles and functions of isoforms of Ca_v and RyR proteins. There are three RyR isoforms expressed in neurons, and nine types of Ca_v expressed in neurons (Catterall, 2011) with potentially overlapping, combinatory, and subdivided functions, making dissecting the contributions of individual proteins difficult. For instance, $Ca_v1.2$ may function in gating extracellular Ca^{2+} entry as well as in a direct

interaction activating ER localized RyR1, 2, or 3 but could be compensated for in certain situations by $Ca_v1.3$. This makes identifying the necessities of certain isoforms complicated, and interpreting the phenotypes of knockout animals difficult. Since neuronal Stacs appear to be expressed in mutually exclusive cell types (Legha et al., 2010), getting at how Ca^{2+} released from internal stores may regulate synaptic function may be easier by examining Stacs. Here the fact that Stac1 is exclusively expressed by KA neurons in zebrafish embryos should be most useful.

Conclusion

Overall, our studies on the Stac1 and Stac3 proteins have provided some interesting groundwork for investigation of the novel *stac* gene family. Remarkably, only five years ago, a report on the mapping of NAM restricted the locus to a region of the human genome containing 135 protein-coding genes including Stac3 but although sequencing was performed on several candidate genes to identify the locus of NAM, sequencing of Stac3 was not attempted because there was no reason to suspect that it could be basis for NAM (Stamm et al., 2008b). Our experiments have both identified Stac3 as a critical component of the EC coupling complex that is mutated in NAM and elucidated a function for Stac1 in neurons, making it unlikely Stac genes will be similarly overlooked in the future.

BIBLIOGRAPHY

Abe, T., Kurosaki, C., Yoshida, M., Hayashi, F., Hirota, H., Yokoyama, S., RIKEN Structural Genomics/Proteomics Initiative (2006). Solution structure of RSGI RUH-051, a C1 domain of STAC3 from human cDNA 2DB6.

Adams, B.A., Tanabe, T., Mikami, A., Numa, S., and Beam, K.G. (1990). Intramembrane charge movement restored in dysgenic skeletal muscle by injection of dihydropyridine receptor cDNAs. Nature *346*, 569-572.

Ahern, C.A., Arikkath, J., Vallejo, P., Gurnett, C.A., Powers, P.A., Campbell, K.P., and Coronado, R. (2001a). Intramembrane charge movements and excitation-contraction coupling expressed by two-domain fragments of the Ca2+ channel. Proceedings of the National Academy of Sciences of the United States of America *98*, 6935-6940.

Ahern, C.A., Bhattacharya, D., Mortenson, L., and Coronado, R. (2001b). A component of excitation-contraction coupling triggered in the absence of the T671-L690 and L720-Q765 regions of the II-III loop of the dihydropyridine receptor alpha(1s) pore subunit. Biophysical journal *81*, 3294-3307.

Akita, T., and Kuba, K. (2000). Functional triads consisting of ryanodine receptors, Ca(2+) channels, and Ca(2+)-activated K(+) channels in bullfrog sympathetic neurons. Plastic modulation of action potential. J Gen Physiol *116*, 697-720.

Al-Qusairi, L., and Laporte, J. (2011). T-tubule biogenesis and triad formation in skeletal muscle and implication in human diseases. Skeletal muscle *1*, 26.

Al-Qusairi, L., Weiss, N., Toussaint, A., Berbey, C., Messaddeq, N., Kretz, C., Sanoudou, D., Beggs, A.H., Allard, B., Mandel, J.L.*, et al.* (2009). T-tubule disorganization and defective excitation-contraction coupling in muscle fibers lacking myotubularin lipid phosphatase. Proceedings of the National Academy of Sciences of the United States of America *106*, 18763-18768.

Almagor, L., Chomsky-Hecht, O., Ben-Mocha, A., Hendin-Barak, D., Dascal, N., and Hirsch, J.A. (2012). The role of a voltage-dependent Ca2+ channel intracellular linker: a structure-function analysis. J Neurosci *32*, 7602-7613.

Altier, C., Garcia-Caballero, A., Simms, B., You, H., Chen, L., Walcher, J., Tedford, H.W., Hermosilla, T., and Zamponi, G.W. (2010). The Cavbeta subunit prevents RFP2-

mediated ubiquitination and proteasomal degradation of L-type channels. Nat Neurosci *14*, 173-180.

Altier, C., Garcia-Caballero, A., Simms, B., You, H., Chen, L., Walcher, J., Tedford, H.W., Hermosilla, T., and Zamponi, G.W. (2011). The Cavbeta subunit prevents RFP2-mediated ubiquitination and proteasomal degradation of L-type channels. Nature neuroscience *14*, 173-180.

Amaral, M.D. (2004). CFTR and chaperones: processing and degradation. Journal of molecular neuroscience : MN *23*, 41-48.

Anderson, A.A., Altafaj, X., Zheng, Z., Wang, Z.M., Delbono, O., Ronjat, M., Treves, S., and Zorzato, F. (2006). The junctional SR protein JP-45 affects the functional expression of the voltage-dependent Ca2+ channel Cav1.1. J Cell Sci *119*, 2145-2155.

Arikkath, J., and Campbell, K.P. (2003). Auxiliary subunits: essential components of the voltage-gated calcium channel complex. Current opinion in neurobiology *13*, 298-307.

Armstrong, C.M., and Bezanilla, F. (1973). Currents related to movement of the gating particles of the sodium channels. Nature *242*, 459-461.

Armstrong, C.M., and Bezanilla, F. (1974). Charge movement associated with the opening and closing of the activation gates of the Na channels. The Journal of general physiology *63*, 533-552.

Armstrong, C.M., Bezanilla, F.M., and Horowicz, P. (1972). Twitches in the presence of ethylene glycol bis(-aminoethyl ether)-N,N'-tetracetic acid. Biochimica et biophysica acta *267*, 605-608.

Baddeley, D., Jayasinghe, I.D., Lam, L., Rossberger, S., Cannell, M.B., and Soeller, C. (2009). Optical single-channel resolution imaging of the ryanodine receptor distribution in rat cardiac myocytes. Proceedings of the National Academy of Sciences of the United States of America *106*, 22275-22280.

Bandschapp, O., and Girard, T. (2012). Malignant hyperthermia. Swiss medical weekly *142*, w13652.

Bannister, R.A. (2007). Bridging the myoplasmic gap: recent developments in skeletal muscle excitation-contraction coupling. Journal of muscle research and cell motility *28*, 275-283.

Bannister, R.A., and Beam, K.G. (2005). The alpha1S N-terminus is not essential for bi-directional coupling with RyR1. Biochemical and biophysical research communications *336*, 134-141.

Bannister, R.A., and Beam, K.G. (2009). Ryanodine modification of RyR1 retrogradely affects L-type Ca(2+) channel gating in skeletal muscle. Journal of muscle research and cell motility *30*, 217-223.

Bannister, R.A., Colecraft, H.M., and Beam, K.G. (2008a). Rem inhibits skeletal muscle EC coupling by reducing the number of functional L-type Ca2+ channels. Biophysical journal *94*, 2631-2638.

Bannister, R.A., Grabner, M., and Beam, K.G. (2008b). The alpha(1S) III-IV loop influences 1,4-dihydropyridine receptor gating but is not directly involved in excitation-contraction coupling interactions with the type 1 ryanodine receptor. The Journal of biological chemistry *283*, 23217-23223.

Bannister, R.A., Papadopoulos, S., Haarmann, C.S., and Beam, K.G. (2009). Effects of inserting fluorescent proteins into the alpha1S II-III loop: insights into excitation-contraction coupling. The Journal of general physiology *134*, 35-51.

Beam, K.G., Adams, B.A., Niidome, T., Numa, S., and Tanabe, T. (1992). Function of a truncated dihydropyridine receptor as both voltage sensor and calcium channel. Nature *360*, 169-171.

Beam, K.G., and Bannister, R.A. (2010). Looking for answers to EC coupling's persistent questions. The Journal of general physiology *136*, 7-12.

Beam, K.G., Knudson, C.M., and Powell, J.A. (1986). A lethal mutation in mice eliminates the slow calcium current in skeletal muscle cells. Nature *320*, 168-170.

Beard, N.A., Laver, D.R., and Dulhunty, A.F. (2004). Calsequestrin and the calcium release channel of skeletal and cardiac muscle. Progress in biophysics and molecular biology *85*, 33-69.

Beguin, P., Mahalakshmi, R.N., Nagashima, K., Cher, D.H., Ikeda, H., Yamada, Y., Seino, Y., and Hunziker, W. (2006). Nuclear sequestration of beta-subunits by Rad and Rem is controlled by 14-3-3 and calmodulin and reveals a novel mechanism for Ca2+ channel regulation. Journal of molecular biology *355*, 34-46.

Beguin, P., Mahalakshmi, R.N., Nagashima, K., Cher, D.H., Kuwamura, N., Yamada, Y., Seino, Y., and Hunziker, W. (2005a). Roles of 14-3-3 and calmodulin binding in subcellular localization and function of the small G-protein Rem2. The Biochemical journal *390*, 67-75.

Beguin, P., Mahalakshmi, R.N., Nagashima, K., Cher, D.H., Takahashi, A., Yamada, Y., Seino, Y., and Hunziker, W. (2005b). 14-3-3 and calmodulin control subcellular distribution of Kir/Gem and its regulation of cell shape and calcium channel activity. J Cell Sci *118*, 1923-1934.

Beguin, P., Nagashima, K., Gonoi, T., Shibasaki, T., Takahashi, K., Kashima, Y., Ozaki, N., Geering, K., Iwanaga, T., and Seino, S. (2001). Regulation of Ca2+ channel expression at the cell surface by the small G-protein kir/Gem. Nature *411*, 701-706.

Beguin, P., Ng, Y.J., Krause, C., Mahalakshmi, R.N., Ng, M.Y., and Hunziker, W. (2007). RGK small GTP-binding proteins interact with the nucleotide kinase domain of Ca2+-channel beta-subunits via an uncommon effector binding domain. J Biol Chem *282*, 11509-11520.

Benzer, S. (1967). BEHAVIORAL MUTANTS OF Drosophila ISOLATED BY COUNTERCURRENT DISTRIBUTION. Proc Natl Acad Sci U S A *58*, 1112-1119.

Bernhardt, R.R., Chitnis, A.B., Lindamer, L., and Kuwada, J.Y. (1990). Identification of spinal neurons in the embryonic and larval zebrafish. J Comp Neurol *302*, 603-616.

Bernhardt, R.R., Patel, C.K., Wilson, S.W., and Kuwada, J.Y. (1992). Axonal trajectories and distribution of GABAergic spinal neurons in wildtype and mutant zebrafish lacking floor plate cells. J Comp Neurol *326*, 263-272.

Berridge, M.J. (1998). Neuronal calcium signaling. Neuron *21*, 13-26.

Berridge, M.J. (2013). Dysregulation of neural calcium signaling in Alzheimer disease, bipolar disorder and schizophrenia. Prion *7*, 2-13.

Berrout, J., and Isokawa, M. (2009). Homeostatic and stimulus-induced coupling of the L-type Ca2+ channel to the ryanodine receptor in the hippocampal neuron in slices. Cell calcium *46*, 30-38.

Betzig, E., Patterson, G.H., Sougrat, R., Lindwasser, O.W., Olenych, S., Bonifacino, J.S., Davidson, M.W., Lippincott-Schwartz, J., and Hess, H.F. (2006). Imaging intracellular fluorescent proteins at nanometer resolution. Science *313*, 1642-1645.

Beurg, M., Sukhareva, M., Ahern, C.A., Conklin, M.W., Perez-Reyes, E., Powers, P.A., Gregg, R.G., and Coronado, R. (1999). Differential regulation of skeletal muscle L-type Ca2+ current and excitation-contraction coupling by the dihydropyridine receptor beta subunit. Biophysical journal *76*, 1744-1756.

Beurg, M., Sukhareva, M., Strube, C., Powers, P.A., Gregg, R.G., and Coronado, R. (1997). Recovery of Ca2+ current, charge movements, and Ca2+ transients in myotubes deficient in dihydropyridine receptor beta 1 subunit transfected with beta 1 cDNA. Biophysical journal *73*, 807-818.

Bichet, D., Cornet, V., Geib, S., Carlier, E., Volsen, S., Hoshi, T., Mori, Y., and De Waard, M. (2000). The I-II loop of the Ca2+ channel alpha1 subunit contains an endoplasmic reticulum retention signal antagonized by the beta subunit. Neuron *25*, 177-190.

Block, B.A., Imagawa, T., Campbell, K.P., and Franzini-Armstrong, C. (1988). Structural evidence for direct interaction between the molecular components of the transverse tubule/sarcoplasmic reticulum junction in skeletal muscle. The Journal of cell biology *107*, 2587-2600.

Bower, N.I., de la Serrana, D.G., Cole, N.J., Hollway, G.E., Lee, H.T., Assinder, S., and Johnston, I.A. (2012). Stac3 is required for myotube formation and myogenic differentiation in vertebrate skeletal muscle. J Biol Chem *287*, 43936-43949.

Bozler, E. (1952). Evidence of an ATP-actomyosin complex in relaxed muscle and its response to calcium ions. The American journal of physiology *168*, 760-765.

Brillantes, A.B., Ondrias, K., Scott, A., Kobrinsky, E., Ondriasova, E., Moschella, M.C., Jayaraman, T., Landers, M., Ehrlich, B.E., and Marks, A.R. (1994). Stabilization of calcium release channel (ryanodine receptor) function by FK506-binding protein. Cell *77*, 513-523.

Brown, T.G. (1914). On the nature of the fundamental activity of the nervous centres; together with an analysis of the conditioning of rhythmic activity in progression, and a theory of the evolution of function in the nervous system. The Journal of physiology *48*, 18-46.

Buck, A.H. (1888). Embracing the Entire Range of Scientific and Practical Medicine and Allied Science, . A Reference Handbook of the Medical Sciences *Volume 6*.

Buraei, Z., and Yang, J. (2010). The ss subunit of voltage-gated Ca2+ channels. Physiological reviews *90*, 1461-1506.

Burgess, H.A., Johnson, S.L., and Granato, M. (2009). Unidirectional startle responses and disrupted left-right co-ordination of motor behaviors in robo3 mutant zebrafish. Genes, brain, and behavior *8*, 500-511.

Buss, R.R., and Drapeau, P. (2000). Physiological properties of zebrafish embryonic red and white muscle fibers during early development. J Neurophysiol *84*, 1545-1557.

Cao, G., Platisa, J., Pieribone, V.A., Raccuglia, D., Kunst, M., and Nitabach, M.N. (2013). Genetically targeted optical electrophysiology in intact neural circuits. Cell *154*, 904-913.

Carbonneau, L., Bhattacharya, D., Sheridan, D.C., and Coronado, R. (2005). Multiple loops of the dihydropyridine receptor pore subunit are required for full-scale excitation-contraction coupling in skeletal muscle. Biophysical journal *89*, 243-255.

Carpenter, D., Ringrose, C., Leo, V., Morris, A., Robinson, R.L., Halsall, P.J., Hopkins, P.M., and Shaw, M.A. (2009). The role of CACNA1S in predisposition to malignant hyperthermia. BMC medical genetics *10*, 104.

Catterall, W.A. (2011). Voltage-gated calcium channels. Cold Spring Harbor perspectives in biology *3*, a003947.

Catterall, W.A., Perez-Reyes, E., Snutch, T.P., and Striessnig, J. (2005). International Union of Pharmacology. XLVIII. Nomenclature and structure-function relationships of voltage-gated calcium channels. Pharmacological reviews *57*, 411-425.

Cauvin, C., Loutzenhiser, R., and Van Breemen, C. (1983). Mechanisms of calcium antagonist-induced vasodilation. Annual review of pharmacology and toxicology *23*, 373-396.

Chandler, W.K., Rakowski, R.F., and Schneider, M.F. (1976). Effects of glycerol treatment and maintained depolarization on charge movement in skeletal muscle. The Journal of physiology *254*, 285-316.

Chavis, P., Fagni, L., Lansman, J.B., and Bockaert, J. (1996). Functional coupling between ryanodine receptors and L-type calcium channels in neurons. Nature *382*, 719-722.

Chen, H.L., Yuh, C.H., and Wu, K.K. (2010). Nestin is essential for zebrafish brain and eye development through control of progenitor cell apoptosis. PloS one *5*, e9318.

Chen, T.W., Wardill, T.J., Sun, Y., Pulver, S.R., Renninger, S.L., Baohan, A., Schreiter, E.R., Kerr, R.A., Orger, M.B., Jayaraman, V.*, et al.* (2013). Ultrasensitive fluorescent proteins for imaging neuronal activity. Nature *499*, 295-300.

Chen, Y.H., Li, M.H., Zhang, Y., He, L.L., Yamada, Y., Fitzmaurice, A., Shen, Y., Zhang, H., Tong, L., and Yang, J. (2004). Structural basis of the alpha1-beta subunit interaction of voltage-gated Ca2+ channels. Nature *429*, 675-680.

Cheng, W., Altafaj, X., Ronjat, M., and Coronado, R. (2005). Interaction between the dihydropyridine receptor Ca2+ channel beta-subunit and ryanodine receptor type 1 strengthens excitation-contraction coupling. Proceedings of the National Academy of Sciences of the United States of America *102*, 19225-19230.

Chopra, N., Yang, T., Asghari, P., Moore, E.D., Huke, S., Akin, B., Cattolica, R.A., Perez, C.F., Hlaing, T., Knollmann-Ritschel, B.E.*, et al.* (2009). Ablation of triadin causes loss of cardiac Ca2+ release units, impaired excitation-contraction coupling, and cardiac arrhythmias. Proceedings of the National Academy of Sciences of the United States of America *106*, 7636-7641.

Colon-Gonzalez, F., and Kazanietz, M.G. (2006). C1 domains exposed: from diacylglycerol binding to protein-protein interactions. Biochim Biophys Acta *1761*, 827-837.

Cornet, V., Bichet, D., Sandoz, G., Marty, I., Brocard, J., Bourinet, E., Mori, Y., Villaz, M., and De Waard, M. (2002). Multiple determinants in voltage-dependent P/Q calcium

channels control their retention in the endoplasmic reticulum. The European journal of neuroscience *16*, 883-895.

Couchoux, H., Bichraoui, H., Chouabe, C., Altafaj, X., Bonvallet, R., Allard, B., Ronjat, M., and Berthier, C. (2011). Caveolin-3 is a direct molecular partner of the Cav1.1 subunit of the skeletal muscle L-type calcium channel. The international journal of biochemistry & cell biology *43*, 713-720.

Cowling, B.S., Toussaint, A., Amoasii, L., Koebel, P., Ferry, A., Davignon, L., Nishino, I., Mandel, J.L., and Laporte, J. (2011). Increased expression of wild-type or a centronuclear myopathy mutant of dynamin 2 in skeletal muscle of adult mice leads to structural defects and muscle weakness. The American journal of pathology *178*, 2224-2235.

Cui, W.W., Low, S.E., Hirata, H., Saint-Amant, L., Geisler, R., Hume, R.I., and Kuwada, J.Y. (2005). The zebrafish shocked gene encodes a glycine transporter and is essential for the function of early neural circuits in the CNS. J Neurosci *25*, 6610-6620.

Curtis, B.M., and Catterall, W.A. (1984). Purification of the calcium antagonist receptor of the voltage-sensitive calcium channel from skeletal muscle transverse tubules. Biochemistry *23*, 2113-2118.

Dale, N., Roberts, A., Ottersen, O.P., and Storm-Mathisen, J. (1987). The morphology and distribution of 'Kolmer-Agduhr cells', a class of cerebrospinal-fluid-contacting neurons revealed in the frog embryo spinal cord by GABA immunocytochemistry. Proceedings of the Royal Society of London Series B, Containing papers of a Biological character Royal Society (Great Britain) *232*, 193-203.

Darwin, C. (1859). The origin of species. *Vol. 11, of 51.*

Dayal, A., Bhat, V., Franzini-Armstrong, C., and Grabner, M. (2013). Domain cooperativity in the beta1a subunit is essential for dihydropyridine receptor voltage sensing in skeletal muscle. Proceedings of the National Academy of Sciences of the United States of America *110*, 7488-7493.

Dayal, A., Schredelseker, J., Franzini-Armstrong, C., and Grabner, M. Skeletal muscle excitation-contraction coupling is independent of a conserved heptad repeat motif in the C-terminus of the DHPRbeta(1a) subunit. Cell Calcium *47*, 500-506.

De Brabander, M.J., Van de Veire, R.M., Aerts, F.E., Borgers, M., and Janssen, P.A. (1976). The effects of methyl (5-(2-thienylcarbonyl)-1H-benzimidazol-2-yl) carbamate, (R 17934; NSC 238159), a new synthetic antitumoral drug interfering with microtubules, on mammalian cells cultured in vitro. Cancer research *36*, 905-916.

De Crescenzo, V., Fogarty, K.E., Lefkowitz, J.J., Bellve, K.D., Zvaritch, E., MacLennan, D.H., and Walsh, J.V., Jr. Type 1 ryanodine receptor knock-in mutation causing central core disease of skeletal muscle also displays a neuronal phenotype. Proc Natl Acad Sci U S A *109*, 610-615.

De Crescenzo, V., Fogarty, K.E., Lefkowitz, J.J., Bellve, K.D., Zvaritch, E., MacLennan, D.H., and Walsh, J.V., Jr. (2012). Type 1 ryanodine receptor knock-in mutation causing central core disease of skeletal muscle also displays a neuronal phenotype. Proc Natl Acad Sci U S A *109*, 610-615.

De Crescenzo, V., Fogarty, K.E., Zhuge, R., Tuft, R.A., Lifshitz, L.M., Carmichael, J., Bellve, K.D., Baker, S.P., Zissimopoulos, S., Lai, F.A.*, et al.* (2006). Dihydropyridine receptors and type 1 ryanodine receptors constitute the molecular machinery for voltage-induced Ca2+ release in nerve terminals. J Neurosci *26*, 7565-7574.

De Crescenzo, V., ZhuGe, R., Velazquez-Marrero, C., Lifshitz, L.M., Custer, E., Carmichael, J., Lai, F.A., Tuft, R.A., Fogarty, K.E., Lemos, J.R.*, et al.* (2004). Ca2+ syntillas, miniature Ca2+ release events in terminals of hypothalamic neurons, are increased in frequency by depolarization in the absence of Ca2+ influx. J Neurosci *24*, 1226-1235.

De Jongh, K.S., Merrick, D.K., and Catterall, W.A. (1989). Subunits of purified calcium channels: a 212-kDa form of alpha 1 and partial amino acid sequence of a phosphorylation site of an independent beta subunit. Proceedings of the National Academy of Sciences of the United States of America *86*, 8585-8589.

De Waard, M., Scott, V.E., Pragnell, M., and Campbell, K.P. (1996). Identification of critical amino acids involved in alpha1-beta interaction in voltage-dependent Ca2+ channels. FEBS Lett *380*, 272-276.

De Waard, M., Witcher, D.R., Pragnell, M., Liu, H., and Campbell, K.P. (1995). Properties of the alpha 1-beta anchoring site in voltage-dependent Ca2+ channels. J Biol Chem *270*, 12056-12064.

Delcomyn, F. (1980). Neural basis of rhythmic behavior in animals. Science *210*, 492-498.

Denning, G.M., Anderson, M.P., Amara, J.F., Marshall, J., Smith, A.E., and Welsh, M.J. (1992). Processing of mutant cystic fibrosis transmembrane conductance regulator is temperature-sensitive. Nature *358*, 761-764.

Detrich, H.W., 3rd, Westerfield, M., and Zon, L.I. (1999). Overview of the Zebrafish system. Methods in cell biology *59*, 3-10.

Dolphin, A.C. (2003). Beta subunits of voltage-gated calcium channels. Journal of bioenergetics and biomembranes *35*, 599-620.

Dolphin, A.C. (2012). Calcium channel auxiliary alpha2delta and beta subunits: trafficking and one step beyond. Nature reviews Neuroscience *13*, 542-555.

dos Remedios, C.G., and Moens, P.D. (1995). Fluorescence resonance energy transfer spectroscopy is a reliable "ruler" for measuring structural changes in proteins. Dispelling the problem of the unknown orientation factor. Journal of structural biology *115*, 175-185.

Dowling, J.J., Gibbs, E.M., and Feldman, E.L. (2008). Membrane traffic and muscle: lessons from human disease. Traffic (Copenhagen, Denmark) *9*, 1035-1043.

Dowling, J.J., Vreede, A.P., Low, S.E., Gibbs, E.M., Kuwada, J.Y., Bonnemann, C.G., and Feldman, E.L. (2009). Loss of myotubularin function results in T-tubule disorganization in zebrafish and human myotubular myopathy. PLoS genetics *5*, e1000372.

Drapeau, P., Ali, D.W., Buss, R.R., and Saint-Amant, L. (1999). In vivo recording from identifiable neurons of the locomotor network in the developing zebrafish. J Neurosci Methods *88*, 1-13.

Drapeau, P., Saint-Amant, L., Buss, R.R., Chong, M., McDearmid, J.R., and Brustein, E. (2002). Development of the locomotor network in zebrafish. Prog Neurobiol *68*, 85-111.

Dreosti, E., Odermatt, B., Dorostkar, M.M., and Lagnado, L. (2009). A genetically encoded reporter of synaptic activity in vivo. Nature methods *6*, 883-889.

Driever, W., Solnica-Krezel, L., Schier, A.F., Neuhauss, S.C., Malicki, J., Stemple, D.L., Stainier, D.Y., Zwartkruis, F., Abdelilah, S., Rangini, Z.*, et al.* (1996). A genetic screen for mutations affecting embryogenesis in zebrafish. Development (Cambridge, England) *123*, 37-46.

Dulhunty, A.F. (2006). Excitation-contraction coupling from the 1950s into the new millennium. Clinical and experimental pharmacology & physiology *33*, 763-772.

Dulhunty, A.F., and Gage, P.W. (1973). Electrical properties of toad sartorius muscle fibres in summer and winter. The Journal of physiology *230*, 619-641.

Durieux, A.C., Vignaud, A., Prudhon, B., Viou, M.T., Beuvin, M., Vassilopoulos, S., Fraysse, B., Ferry, A., Laine, J., Romero, N.B.*, et al.* (2010). A centronuclear myopathy-dynamin 2 mutation impairs skeletal muscle structure and function in mice. Human molecular genetics *19*, 4820-4836.

Ebashi, S., Endo, M., and Otsuki, I. (1969). Control of muscle contraction. Quarterly reviews of biophysics *2*, 351-384.

Eggeling, C., Willig, K.I., and Barrantes, F.J. (2013). STED microscopy of living cells--new frontiers in membrane and neurobiology. Journal of neurochemistry *126*, 203-212.

Ellgaard, L., Molinari, M., and Helenius, A. (1999). Setting the standards: quality control in the secretory pathway. Science (New York, NY) *286*, 1882-1888.

Esteve, E., Eltit, J.M., Bannister, R.A., Liu, K., Pessah, I.N., Beam, K.G., Allen, P.D., and Lopez, J.R. (2010). A malignant hyperthermia-inducing mutation in RYR1 (R163C): alterations in Ca2+ entry, release, and retrograde signaling to the DHPR. The Journal of general physiology *135*, 619-628.

Fabiato, A. (1983). Calcium-induced release of calcium from the cardiac sarcoplasmic reticulum. The American journal of physiology *245*, C1-14.

Feng, W., Tu, J., Yang, T., Vernon, P.S., Allen, P.D., Worley, P.F., and Pessah, I.N. (2002). Homer regulates gain of ryanodine receptor type 1 channel complex. The Journal of biological chemistry *277*, 44722-44730.

Finlin, B.S., Crump, S.M., Satin, J., and Andres, D.A. (2003). Regulation of voltage-gated calcium channel activity by the Rem and Rad GTPases. Proc Natl Acad Sci U S A *100*, 14469-14474.

Flanagan-Steet, H., Fox, M.A., Meyer, D., and Sanes, J.R. (2005). Neuromuscular synapses can form in vivo by incorporation of initially aneural postsynaptic specializations. Development *132*, 4471-4481.

Flucher, B.E., Kasielke, N., Gerster, U., Neuhuber, B., and Grabner, M. (2000a). Insertion of the full-length calcium channel alpha(1S) subunit into triads of skeletal muscle in vitro. FEBS Lett *474*, 93-98.

Flucher, B.E., Kasielke, N., and Grabner, M. (2000b). The triad targeting signal of the skeletal muscle calcium channel is localized in the COOH terminus of the alpha(1S) subunit. The Journal of cell biology *151*, 467-478.

Flucher, B.E., Obermair, G.J., Tuluc, P., Schredelseker, J., Kern, G., and Grabner, M. (2005). The role of auxiliary dihydropyridine receptor subunits in muscle. Journal of muscle research and cell motility *26*, 1-6.

Flucher, B.E., Phillips, J.L., and Powell, J.A. (1991). Dihydropyridine receptor alpha subunits in normal and dysgenic muscle in vitro: expression of alpha 1 is required for proper targeting and distribution of alpha 2. The Journal of cell biology *115*, 1345-1356.

Flucher, B.E., Takekura, H., and Franzini-Armstrong, C. (1993). Development of the excitation-contraction coupling apparatus in skeletal muscle: association of

sarcoplasmic reticulum and transverse tubules with myofibrils. Developmental biology *160*, 135-147.

Flucher, B.E., Weiss, R.G., and Grabner, M. (2002). Cooperation of two-domain Ca(2+) channel fragments in triad targeting and restoration of excitation-contraction coupling in skeletal muscle. Proceedings of the National Academy of Sciences of the United States of America *99*, 10167-10172.

Foley, J.E., Maeder, M.L., Pearlberg, J., Joung, J.K., Peterson, R.T., and Yeh, J.R. (2009). Targeted mutagenesis in zebrafish using customized zinc-finger nucleases. Nat Protoc *4*, 1855-1867.

Fosset, M., Jaimovich, E., Delpont, E., and Lazdunski, M. (1983). [3H]nitrendipine receptors in skeletal muscle. The Journal of biological chemistry *258*, 6086-6092.

Frankenhaeuser, B., and Hodgkin, A.L. (1957). The action of calcium on the electrical properties of squid axons. The Journal of physiology *137*, 218-244.

Franzini-Armstrong, C. (1970). STUDIES OF THE TRIAD : I. Structure of the Junction in Frog Twitch Fibers. The Journal of cell biology *47*, 488-499.

Franzini-Armstrong, C. (1991). Simultaneous maturation of transverse tubules and sarcoplasmic reticulum during muscle differentiation in the mouse. Developmental biology *146*, 353-363.

Franzini-Armstrong, C., and Jorgensen, A.O. (1994). Structure and development of E-C coupling units in skeletal muscle. Annual review of physiology *56*, 509-534.

Franzini-Armstrong, C., Protasi, F., and Ramesh, V. (1998). Comparative ultrastructure of Ca2+ release units in skeletal and cardiac muscle. Annals of the New York Academy of Sciences *853*, 20-30.

Freise, D., Held, B., Wissenbach, U., Pfeifer, A., Trost, C., Himmerkus, N., Schweig, U., Freichel, M., Biel, M., Hofmann, F.*, et al.* (2000). Absence of the gamma subunit of the skeletal muscle dihydropyridine receptor increases L-type Ca2+ currents and alters channel inactivation properties. The Journal of biological chemistry *275*, 14476-14481.

Fuller-Bicer, G.A., Varadi, G., Koch, S.E., Ishii, M., Bodi, I., Kadeer, N., Muth, J.N., Mikala, G., Petrashevskaya, N.N., Jordan, M.A.*, et al.* (2009). Targeted disruption of the voltage-dependent calcium channel alpha2/delta-1-subunit. American journal of physiology Heart and circulatory physiology *297*, H117-124.

Gach, M.P., Cherednichenko, G., Haarmann, C., Lopez, J.R., Beam, K.G., Pessah, I.N., Franzini-Armstrong, C., and Allen, P.D. (2008). Alpha2delta1 dihydropyridine receptor subunit is a critical element for excitation-coupled calcium entry but not for formation of tetrads in skeletal myotubes. Biophysical journal *94*, 3023-3034.

Galizzi, J.P., Fosset, M., and Lazdunski, M. (1984). [3H] verapamil binding sites in skeletal muscle transverse tubule membranes. Biochemical and biophysical research communications *118*, 239-245.

Gerhard, D.S., Wagner, L., Feingold, E.A., Shenmen, C.M., Grouse, L.H., Schuler, G., Klein, S.L., Old, S., Rasooly, R., Good, P.*, et al.* (2004). The status, quality, and expansion of the NIH full-length cDNA project: the Mammalian Gene Collection (MGC). Genome research *14*, 2121-2127.

Gerster, U., Neuhuber, B., Groschner, K., Striessnig, J., and Flucher, B.E. (1999). Current modulation and membrane targeting of the calcium channel alpha1C subunit are independent functions of the beta subunit. J Physiol *517 (Pt 2)*, 353-368.

Glass, A.S., and Dahm, R. (2004). The zebrafish as a model organism for eye development. Ophthalmic research *36*, 4-24.

Golling, G., Amsterdam, A., Sun, Z., Antonelli, M., Maldonado, E., Chen, W., Burgess, S., Haldi, M., Artzt, K., Farrington, S.*, et al.* (2002). Insertional mutagenesis in zebrafish rapidly identifies genes essential for early vertebrate development. Nat Genet *31*, 135-140.

Gonzalez-Gutierrez, G., Miranda-Laferte, E., Neely, A., and Hidalgo, P. (2007). The Src homology 3 domain of the beta-subunit of voltage-gated calcium channels promotes endocytosis via dynamin interaction. J Biol Chem *282*, 2156-2162.

Gonzalez-Serratos, H., Valle-Aguilera, R., Lathrop, D.A., and Garcia, M.C. (1982). Slow inward calcium currents have no obvious role in muscle excitation-contraction coupling. Nature *298*, 292-294.

Goulding, M. (2009). Circuits controlling vertebrate locomotion: moving in a new direction. Nat Rev Neurosci *10*, 507-518.

Gout, I., Dhand, R., Hiles, I.D., Fry, M.J., Panayotou, G., Das, P., Truong, O., Totty, N.F., Hsuan, J., Booker, G.W.*, et al.* (1993). The GTPase dynamin binds to and is activated by a subset of SH3 domains. Cell *75*, 25-36.

Grabner, M., Dirksen, R.T., and Beam, K.G. (1998). Tagging with green fluorescent protein reveals a distinct subcellular distribution of L-type and non-L-type Ca2+ channels expressed in dysgenic myotubes. Proceedings of the National Academy of Sciences of the United States of America *95*, 1903-1908.

Grabner, M., Dirksen, R.T., Suda, N., and Beam, K.G. (1999). The II-III loop of the skeletal muscle dihydropyridine receptor is responsible for the Bi-directional coupling with the ryanodine receptor. The Journal of biological chemistry *274*, 21913-21919.

Granato, M., van Eeden, F.J., Schach, U., Trowe, T., Brand, M., Furutani-Seiki, M., Haffter, P., Hammerschmidt, M., Heisenberg, C.P., Jiang, Y.J., *et al.* (1996). Genes controlling and mediating locomotion behavior of the zebrafish embryo and larva. Development *123*, 399-413.

Gregg, R.G., Messing, A., Strube, C., Beurg, M., Moss, R., Behan, M., Sukhareva, M., Haynes, S., Powell, J.A., Coronado, R., *et al.* (1996). Absence of the beta subunit (cchb1) of the skeletal muscle dihydropyridine receptor alters expression of the alpha 1 subunit and eliminates excitation-contraction coupling. Proceedings of the National Academy of Sciences of the United States of America *93*, 13961-13966.

Grueter, C.E., Abiria, S.A., Dzhura, I., Wu, Y., Ham, A.J., Mohler, P.J., Anderson, M.E., and Colbran, R.J. (2006). L-type Ca2+ channel facilitation mediated by phosphorylation of the beta subunit by CaMKII. Molecular cell *23*, 641-650.

Grueter, C.E., Abiria, S.A., Wu, Y., Anderson, M.E., and Colbran, R.J. (2008). Differential regulated interactions of calcium/calmodulin-dependent protein kinase II with isoforms of voltage-gated calcium channel beta subunits. Biochemistry *47*, 1760-1767.

Haffter, P., Granato, M., Brand, M., Mullins, M.C., Hammerschmidt, M., Kane, D.A., Odenthal, J., van Eeden, F.J., Jiang, Y.J., Heisenberg, C.P., *et al.* (1996). The identification of genes with unique and essential functions in the development of the zebrafish, Danio rerio. Development *123*, 1-36.

Halling, D.B., Aracena-Parks, P., and Hamilton, S.L. (2006). Regulation of voltage-gated Ca2+ channels by calmodulin. Science's STKE : signal transduction knowledge environment *2006*, er1.

Halloran, M.C., Sato-Maeda, M., Warren, J.T., Su, F., Lele, Z., Krone, P.H., Kuwada, J.Y., and Shoji, W. (2000). Laser-induced gene expression in specific cells of transgenic zebrafish. Development *127*, 1953-1960.

Hamilton, S.L. (2005). Ryanodine receptors. Cell Calcium *38*, 253-260.

Hanlon, M.R., Berrow, N.S., Dolphin, A.C., and Wallace, B.A. (1999). Modelling of a voltage-dependent Ca2+ channel beta subunit as a basis for understanding its functional properties. FEBS Lett *445*, 366-370.

Hardy, K., Mansfield, L., Mackay, A., Benvenuti, S., Ismail, S., Arora, P., O'Hare, M.J., and Jat, P.S. (2005). Transcriptional networks and cellular senescence in human mammary fibroblasts. Mol Biol Cell *16*, 943-953.

Higashijima, S., Okamoto, H., Ueno, N., Hotta, Y., and Eguchi, G. (1997). High-frequency generation of transgenic zebrafish which reliably express GFP in whole muscles or the whole body by using promoters of zebrafish origin. Developmental biology *192*, 289-299.

Hirata, H., Carta, E., Yamanaka, I., Harvey, R.J., and Kuwada, J.Y. (2009). Defective glycinergic synaptic transmission in zebrafish motility mutants. Frontiers in molecular neuroscience *2*, 26.

Hirata, H., Saint-Amant, L., Downes, G.B., Cui, W.W., Zhou, W., Granato, M., and Kuwada, J.Y. (2005). Zebrafish bandoneon mutants display behavioral defects due to a mutation in the glycine receptor beta-subunit. Proceedings of the National Academy of Sciences of the United States of America *102*, 8345-8350.

Hirata, H., Saint-Amant, L., Waterbury, J., Cui, W., Zhou, W., Li, Q., Goldman, D., Granato, M., and Kuwada, J.Y. (2004). accordion, a zebrafish behavioral mutant, has a muscle relaxation defect due to a mutation in the ATPase Ca2+ pump SERCA1. Development (Cambridge, England) *131*, 5457-5468.

Hirata, H., Watanabe, T., Hatakeyama, J., Sprague, S.M., Saint-Amant, L., Nagashima, A., Cui, W.W., Zhou, W., and Kuwada, J.Y. (2007). Zebrafish relatively relaxed mutants have a ryanodine receptor defect, show slow swimming and provide a model of multi-minicore disease. Development *134*, 2771-2781.

Horstick, E. (2012). Characterization of the Novel Zebrafish Motor Mutant mi34. PhD dissertation.

Horstick, E.J., Linsley, J.W., Dowling, J.J., Hauser, M.A., McDonald, K.K., Ashley-Koch, A., Saint-Amant, L., Satish, A., Cui, W.W., Zhou, W.*, et al.* (2013). Stac3 is a component of the excitation-contraction coupling machinery and mutated in Native American myopathy. Nature communications *4*, 1952.

Houde, D., Arndt, J., Domeier, W., Berkowitz, S., and Engen, J.R. (2009). Characterization of IgG1 conformation and conformational dynamics by hydrogen/deuterium exchange mass spectrometry. Analytical chemistry *81*, 2644-2651.

Howe, K., Clark, M.D., Torroja, C.F., Torrance, J., Berthelot, C., Muffato, M., Collins, J.E., Humphray, S., McLaren, K., Matthews, L.*, et al.* (2013). The zebrafish reference genome sequence and its relationship to the human genome. Nature *496*, 498-503.

Huang, B., Jones, S.A., Brandenburg, B., and Zhuang, X. (2008). Whole-cell 3D STORM reveals interactions between cellular structures with nanometer-scale resolution. Nature methods *5*, 1047-1052.

Hulme, J.T., Ahn, M., Hauschka, S.D., Scheuer, T., and Catterall, W.A. (2002). A novel leucine zipper targets AKAP15 and cyclic AMP-dependent protein kinase to the C terminus of the skeletal muscle Ca2+ channel and modulates its function. The Journal of biological chemistry *277*, 4079-4087.

Hulme, J.T., Konoki, K., Lin, T.W., Gritsenko, M.A., Camp, D.G., 2nd, Bigelow, D.J., and Catterall, W.A. (2005). Sites of proteolytic processing and noncovalent association of

the distal C-terminal domain of CaV1.1 channels in skeletal muscle. Proceedings of the National Academy of Sciences of the United States of America *102*, 5274-5279.

Huxley, A.F., and Taylor, R.E. (1958). Local activation of striated muscle fibres. The Journal of physiology *144*, 426-441.

Hwang, W.Y., Fu, Y., Reyon, D., Maeder, M.L., Tsai, S.Q., Sander, J.D., Peterson, R.T., Yeh, J.R., and Joung, J.K. (2013). Efficient genome editing in zebrafish using a CRISPR-Cas system. Nature biotechnology *31*, 227-229.

Inui, M., Saito, A., and Fleischer, S. (1987). Purification of the ryanodine receptor and identity with feet structures of junctional terminal cisternae of sarcoplasmic reticulum from fast skeletal muscle. The Journal of biological chemistry *262*, 1740-1747.

Jaillon, O., Aury, J.M., Brunet, F., Petit, J.L., Stange-Thomann, N., Mauceli, E., Bouneau, L., Fischer, C., Ozouf-Costaz, C., Bernot, A*., et al.* (2004). Genome duplication in the teleost fish Tetraodon nigroviridis reveals the early vertebrate proto-karyotype. Nature *431*, 946-957.

Jamieson, J.D., and Palade, G.E. (1968). Intracellular transport of secretory proteins in the pancreatic exocrine cell. IV. Metabolic requirements. The Journal of cell biology *39*, 589-603.

Jayaraman, T., Brillantes, A.M., Timerman, A.P., Fleischer, S., Erdjument-Bromage, H., Tempst, P., and Marks, A.R. (1992). FK506 binding protein associated with the calcium release channel (ryanodine receptor). The Journal of biological chemistry *267*, 9474-9477.

Jin, L., Han, Z., Platisa, J., Wooltorton, J.R., Cohen, L.B., and Pieribone, V.A. (2012). Single action potentials and subthreshold electrical events imaged in neurons with a fluorescent protein voltage probe. Neuron *75*, 779-785.

Johnson, J.E., Giorgione, J., and Newton, A.C. (2000). The C1 and C2 domains of protein kinase C are independent membrane targeting modules, with specificity for phosphatidylserine conferred by the C1 domain. Biochemistry *39*, 11360-11369.

Jurynec, M.J., Xia, R., Mackrill, J.J., Gunther, D., Crawford, T., Flanigan, K.M., Abramson, J.J., Howard, M.T., and Grunwald, D.J. (2008). Selenoprotein N is required for ryanodine receptor calcium release channel activity in human and zebrafish muscle. Proceedings of the National Academy of Sciences of the United States of America *105*, 12485-12490.

Kaisto, T., and Metsikko, K. (2003). Distribution of the endoplasmic reticulum and its relationship with the sarcoplasmic reticulum in skeletal myofibers. Experimental cell research *289*, 47-57.

Kane, D.A., and Kimmel, C.B. (1993). The zebrafish midblastula transition. Development (Cambridge, England) *119*, 447-456.

Kaneko, T., Li, L., and Li, S.S. (2008). The SH3 domain--a family of versatile peptide- and protein-recognition module. Front Biosci *13*, 4938-4952.

Kari, G., Rodeck, U., and Dicker, A.P. (2007). Zebrafish: an emerging model system for human disease and drug discovery. Clin Pharmacol Ther *82*, 70-80.

Karin, N.J., and Settle, V.J. (1992). The sarcoplasmic reticulum Ca(2+)-ATPase, SERCA1a, contains endoplasmic reticulum targeting information. Biochemical and biophysical research communications *186*, 219-227.

Karlsson, J., von Hofsten, J., and Olsson, P.E. (2001). Generating transparent zebrafish: a refined method to improve detection of gene expression during embryonic development. Marine biotechnology (New York, NY) *3*, 522-527.

Kawai, J., Suzuki, H., Hara, A., Hirose, K., and Watanabe, S. (1998). Human and mouse chromosomal mapping of Stac, a neuron-specific protein with an SH3 domain. Genomics *47*, 140-142.

Kawakami, K. (2007). Tol2: a versatile gene transfer vector in vertebrates. Genome Biol *8 Suppl 1*, S7.

Kimura, Y., Okamura, Y., and Higashijima, S. (2006). alx, a zebrafish homolog of Chx10, marks ipsilateral descending excitatory interneurons that participate in the regulation of spinal locomotor circuits. J Neurosci *26*, 5684-5697.

Klaus, M.M., Scordilis, S.P., Rapalus, J.M., Briggs, R.T., and Powell, J.A. (1983). Evidence for dysfunction in the regulation of cytosolic Ca2+ in excitation-contraction uncoupled dysgenic muscle. Developmental biology *99*, 152-165.

Knollmann, B.C., Chopra, N., Hlaing, T., Akin, B., Yang, T., Ettensohn, K., Knollmann, B.E., Horton, K.D., Weissman, N.J., Holinstat, I.*, et al.* (2006). Casq2 deletion causes sarcoplasmic reticulum volume increase, premature Ca2+ release, and catecholaminergic polymorphic ventricular tachycardia. The Journal of clinical investigation *116*, 2510-2520.

Kokel, D., and Peterson, R.T. (2008). Chemobehavioural phenomics and behaviour-based psychiatric drug discovery in the zebrafish. Brief Funct Genomic Proteomic *7*, 483-490.

Komazaki, S., Ito, K., Takeshima, H., and Nakamura, H. (2002). Deficiency of triad formation in developing skeletal muscle cells lacking junctophilin type 1. FEBS Lett *524*, 225-229.

Kopito, R.R. (1999). Biosynthesis and degradation of CFTR. Physiological reviews *79*, S167-173.

Kugler, G., Grabner, M., Platzer, J., Striessnig, J., and Flucher, B.E. (2004a). The monoclonal antibody mAB 1A binds to the excitation--contraction coupling domain in the II-III loop of the skeletal muscle calcium channel alpha(1S) subunit. Archives of biochemistry and biophysics *427*, 91-100.

Kugler, G., Weiss, R.G., Flucher, B.E., and Grabner, M. (2004b). Structural requirements of the dihydropyridine receptor alpha1S II-III loop for skeletal-type excitation-contraction coupling. The Journal of biological chemistry *279*, 4721-4728.

Kumari, S., Mg, S., and Mayor, S. (2010). Endocytosis unplugged: multiple ways to enter the cell. Cell research *20*, 256-275.

Lai, F.A., Erickson, H.P., Rousseau, E., Liu, Q.Y., and Meissner, G. (1988). Purification and reconstitution of the calcium release channel from skeletal muscle. Nature *331*, 315-319.

Lauri, S.E., Bortolotto, Z.A., Nistico, R., Bleakman, D., Ornstein, P.L., Lodge, D., Isaac, J.T., and Collingridge, G.L. (2003). A role for Ca2+ stores in kainate receptor-dependent synaptic facilitation and LTP at mossy fiber synapses in the hippocampus. Neuron *39*, 327-341.

Lefkowitz, J.J., Fogarty, K.E., Lifshitz, L.M., Bellve, K.D., Tuft, R.A., ZhuGe, R., Walsh, J.V., Jr., and De Crescenzo, V. (2009). Suppression of Ca2+ syntillas increases spontaneous exocytosis in mouse adrenal chromaffin cells. J Gen Physiol *134*, 267-280.

Legha, W., Gaillard, S., Gascon, E., Malapert, P., Hocine, M., Alonso, S., and Moqrich, A. (2010). stac1 and stac2 genes define discrete and distinct subsets of dorsal root ganglia neurons. Gene Expr Patterns *10*, 368-375.

Lemos, J.R., and Nowycky, M.C. (1989). Two types of calcium channels coexist in peptide-releasing vertebrate nerve terminals. Neuron *2*, 1419-1426.

Leong, P., and MacLennan, D.H. (1998). The cytoplasmic loops between domains II and III and domains III and IV in the skeletal muscle dihydropyridine receptor bind to a contiguous site in the skeletal muscle ryanodine receptor. The Journal of biological chemistry *273*, 29958-29964.

Lim, W.A., Richards, F.M., and Fox, R.O. (1994). Structural determinants of peptide-binding orientation and of sequence specificity in SH3 domains. Nature *372*, 375-379.

Lippincott-Schwartz, J., Donaldson, J.G., Schweizer, A., Berger, E.G., Hauri, H.P., Yuan, L.C., and Klausner, R.D. (1990). Microtubule-dependent retrograde transport of

proteins into the ER in the presence of brefeldin A suggests an ER recycling pathway. Cell *60*, 821-836.

Liu, Q., Chen, B., Yankova, M., Morest, D.K., Maryon, E., Hand, A.R., Nonet, M.L., and Wang, Z.W. (2005). Presynaptic ryanodine receptors are required for normal quantal size at the Caenorhabditis elegans neuromuscular junction. J Neurosci *25*, 6745-6754.

Llano, I., Gonzalez, J., Caputo, C., Lai, F.A., Blayney, L.M., Tan, Y.P., and Marty, A. (2000). Presynaptic calcium stores underlie large-amplitude miniature IPSCs and spontaneous calcium transients. Nat Neurosci *3*, 1256-1265.

Lorenzon, N.M., Haarmann, C.S., Norris, E.E., Papadopoulos, S., and Beam, K.G. (2004). Metabolic biotinylation as a probe of supramolecular structure of the triad junction in skeletal muscle. The Journal of biological chemistry *279*, 44057-44064.

Low, S.E., Amburgey, K., Horstick, E., Linsley, J., Sprague, S.M., Cui, W.W., Zhou, W., Hirata, H., Saint-Amant, L., Hume, R.I.*, et al.* (2011). TRPM7 is required within zebrafish sensory neurons for the activation of touch-evoked escape behaviors. J Neurosci *31*, 11633-11644.

Low, S.E., Ryan, J., Sprague, S.M., Hirata, H., Cui, W.W., Zhou, W., Hume, R.I., Kuwada, J.Y., and Saint-Amant, L. (2010a). touche Is required for touch-evoked generator potentials within vertebrate sensory neurons. J Neurosci *30*, 9359-9367.

Low, S.E., Zhou, W., Choong, I., Saint-Amant, L., Sprague, S.M., Hirata, H., Cui, W.W., Hume, R.I., and Kuwada, J.Y. (2010b). Na(v)1.6a is required for normal activation of motor circuits normally excited by tactile stimulation. Dev Neurobiol *70*, 508-522.

Lu, X., Xu, L., and Meissner, G. (1994). Activation of the skeletal muscle calcium release channel by a cytoplasmic loop of the dihydropyridine receptor. The Journal of biological chemistry *269*, 6511-6516.

Lu, Z., Joseph, D., Bugnard, E., Zaal, K.J., and Ralston, E. (2001). Golgi complex reorganization during muscle differentiation: visualization in living cells and mechanism. Molecular biology of the cell *12*, 795-808.

Mahalakshmi, R.N., Nagashima, K., Ng, M.Y., Inagaki, N., Hunziker, W., and Beguin, P. (2007). Nuclear transport of Kir/Gem requires specific signals and importin alpha5 and is regulated by calmodulin and predicted serine phosphorylations. Traffic (Copenhagen, Denmark) *8*, 1150-1163.

Maltez, J.M., Nunziato, D.A., Kim, J., and Pitt, G.S. (2005). Essential Ca(V)beta modulatory properties are AID-independent. Nat Struct Mol Biol *12*, 372-377.

Marder, E., and Bucher, D. (2001). Central pattern generators and the control of rhythmic movements. Curr Biol *11*, R986-996.

Marks, B., Stowell, M.H., Vallis, Y., Mills, I.G., Gibson, A., Hopkins, C.R., and McMahon, H.T. (2001). GTPase activity of dynamin and resulting conformation change are essential for endocytosis. Nature *410*, 231-235.

Masuda, A., Ushida, K., and Okamoto, T. (2005). New fluorescence correlation spectroscopy enabling direct observation of spatiotemporal dependence of diffusion constants as an evidence of anomalous transport in extracellular matrices. Biophysical journal *88*, 3584-3591.

Mayer, B.J. (2001). SH3 domains: complexity in moderation. J Cell Sci *114*, 1253-1263.

McCudden, C.R., Hains, M.D., Kimple, R.J., Siderovski, D.P., and Willard, F.S. (2005). G-protein signaling: back to the future. Cellular and molecular life sciences : CMLS *62*, 551-577.

McCurley, A.T., and Callard, G.V. (2008). Characterization of housekeeping genes in zebrafish: male-female differences and effects of tissue type, developmental stage and chemical treatment. BMC molecular biology *9*, 102.

McFarland, T.P., Milstein, M.L., and Cala, S.E. (2010). Rough endoplasmic reticulum to junctional sarcoplasmic reticulum trafficking of calsequestrin in adult cardiomyocytes. Journal of molecular and cellular cardiology *49*, 556-564.

McKinney, S.A., Murphy, C.S., Hazelwood, K.L., Davidson, M.W., and Looger, L.L. (2009). A bright and photostable photoconvertible fluorescent protein. Nature methods *6*, 131-133.

McNally, J.M., De Crescenzo, V., Fogarty, K.E., Walsh, J.V., and Lemos, J.R. (2009). Individual calcium syntillas do not trigger spontaneous exocytosis from nerve terminals of the neurohypophysis. J Neurosci *29*, 14120-14126.

Meissner, G. (1986). Ryanodine activation and inhibition of the Ca2+ release channel of sarcoplasmic reticulum. The Journal of biological chemistry *261*, 6300-6306.

Meng, X., Xiao, B., Cai, S., Huang, X., Li, F., Bolstad, J., Trujillo, R., Airey, J., Chen, S.R., Wagenknecht, T.*, et al.* (2007). Three-dimensional localization of serine 2808, a phosphorylation site in cardiac ryanodine receptor. J Biol Chem *282*, 25929-25939.

Miranda-Laferte, E., Gonzalez-Gutierrez, G., Schmidt, S., Zeug, A., Ponimaskin, E.G., Neely, A., and Hidalgo, P. Homodimerization of the Src Homology 3 Domain of the Calcium Channel {beta}-Subunit Drives Dynamin-dependent Endocytosis. J Biol Chem *286*, 22203-22210.

Moghadaszadeh, B., Petit, N., Jaillard, C., Brockington, M., Quijano Roy, S., Merlini, L., Romero, N., Estournet, B., Desguerre, I., Chaigne, D.*, et al.* (2001). Mutations in

SEPN1 cause congenital muscular dystrophy with spinal rigidity and restrictive respiratory syndrome. Nature genetics *29*, 17-18.

Monnier, N., Procaccio, V., Stieglitz, P., and Lunardi, J. (1997). Malignant-hyperthermia susceptibility is associated with a mutation of the alpha 1-subunit of the human dihydropyridine-sensitive L-type voltage-dependent calcium-channel receptor in skeletal muscle. American journal of human genetics *60*, 1316-1325.

Morello, J.P., Petaja-Repo, U.E., Bichet, D.G., and Bouvier, M. (2000). Pharmacological chaperones: a new twist on receptor folding. Trends in pharmacological sciences *21*, 466-469.

Morton, C.J., and Campbell, I.D. (1994). SH3 domains. Molecular 'Velcro'. Curr Biol *4*, 615-617.

Mouton, J., Marty, I., Villaz, M., Feltz, A., and Maulet, Y. (2001). Molecular interaction of dihydropyridine receptors with type-1 ryanodine receptors in rat brain. The Biochemical journal *354*, 597-603.

Movilla, N., and Bustelo, X.R. (1999). Biological and regulatory properties of Vav-3, a new member of the Vav family of oncoproteins. Mol Cell Biol *19*, 7870-7885.

Muller, C.S., Haupt, A., Bildl, W., Schindler, J., Knaus, H.G., Meissner, M., Rammner, B., Striessnig, J., Flockerzi, V., Fakler, B*., et al.* (2010). Quantitative proteomics of the Cav2 channel nano-environments in the mammalian brain. Proceedings of the National Academy of Sciences of the United States of America *107*, 14950-14957.

Murmu, M.S., Stinnakre, J., and Martin, J.R. (2010). Presynaptic Ca2+ stores contribute to odor-induced responses in Drosophila olfactory receptor neurons. The Journal of experimental biology *213*, 4163-4173.

Muto, A., Ohkura, M., Abe, G., Nakai, J., and Kawakami, K. (2013). Real-time visualization of neuronal activity during perception. Curr Biol *23*, 307-311.

Naganawa, Y., and Hirata, H. (2011). Developmental transition of touch response from slow muscle-mediated coilings to fast muscle-mediated burst swimming in zebrafish. Dev Biol *355*, 194-204.

Nakai, J., Dirksen, R.T., Nguyen, H.T., Pessah, I.N., Beam, K.G., and Allen, P.D. (1996). Enhanced dihydropyridine receptor channel activity in the presence of ryanodine receptor. Nature *380*, 72-75.

Nakai, J., Ogura, T., Protasi, F., Franzini-Armstrong, C., Allen, P.D., and Beam, K.G. (1997). Functional nonequality of the cardiac and skeletal ryanodine receptors. Proceedings of the National Academy of Sciences of the United States of America *94*, 1019-1022.

Nakai, J., Tanabe, T., Konno, T., Adams, B., and Beam, K.G. (1998). Localization in the II-III loop of the dihydropyridine receptor of a sequence critical for excitation-contraction coupling. The Journal of biological chemistry *273*, 24983-24986.

Nakano, Y., Fujita, M., Ogino, K., Saint-Amant, L., Kinoshita, T., Oda, Y., and Hirata, H. (2010). Biogenesis of GPI-anchored proteins is essential for surface expression of sodium channels in zebrafish Rohon-Beard neurons to respond to mechanosensory stimulation. Development *137*, 1689-1698.

Nance, J.R., Dowling, J.J., Gibbs, E.M., and Bonnemann, C.G. (2012). Congenital myopathies: an update. Current neurology and neuroscience reports *12*, 165-174.

Nasevicius, A., and Ekker, S.C. (2000). Effective targeted gene 'knockdown' in zebrafish. Nature genetics *26*, 216-220.

Nelson, B.R., Wu, F., Liu, Y., Anderson, D.M., McAnally, J., Lin, W., Cannon, S.C., Bassel-Duby, R., and Olson, E.N. (2013). Skeletal muscle-specific T-tubule protein STAC3 mediates voltage-induced Ca2+ release and contractility. Proceedings of the National Academy of Sciences of the United States of America *110*, 11881-11886.

Nesvizhskii, A.I., Keller, A., Kolker, E., and Aebersold, R. (2003). A statistical model for identifying proteins by tandem mass spectrometry. Analytical chemistry *75*, 4646-4658.

Neuhuber, B., Gerster, U., Doring, F., Glossmann, H., Tanabe, T., and Flucher, B.E. (1998). Association of calcium channel alpha1S and beta1a subunits is required for the targeting of beta1a but not of alpha1S into skeletal muscle triads. Proceedings of the National Academy of Sciences of the United States of America *95*, 5015-5020.

Niggli, E., Ullrich, N.D., Gutierrez, D., Kyrychenko, S., Polakova, E., and Shirokova, N. (2013). Posttranslational modifications of cardiac ryanodine receptors: Ca(2+) signaling and EC-coupling. Biochimica et biophysica acta *1833*, 866-875.

Nishi, M., Komazaki, S., Kurebayashi, N., Ogawa, Y., Noda, T., Iino, M., and Takeshima, H. (1999). Abnormal features in skeletal muscle from mice lacking mitsugumin29. The Journal of cell biology *147*, 1473-1480.

Nixon, S.J., Wegner, J., Ferguson, C., Mery, P.F., Hancock, J.F., Currie, P.D., Key, B., Westerfield, M., and Parton, R.G. (2005). Zebrafish as a model for caveolin-associated muscle disease; caveolin-3 is required for myofibril organization and muscle cell patterning. Human molecular genetics *14*, 1727-1743.

Nusslein-Volhard, C. (2002). Zebrafish- Practical Approach.

Opatowsky, Y., Chen, C.C., Campbell, K.P., and Hirsch, J.A. (2004). Structural analysis of the voltage-dependent calcium channel beta subunit functional core and its complex with the alpha 1 interaction domain. Neuron *42*, 387-399.

Ouyang, K., Zheng, H., Qin, X., Zhang, C., Yang, D., Wang, X., Wu, C., Zhou, Z., and Cheng, H. (2005). Ca2+ sparks and secretion in dorsal root ganglion neurons. Proc Natl Acad Sci U S A *102*, 12259-12264.

Paolini, C., Fessenden, J.D., Pessah, I.N., and Franzini-Armstrong, C. (2004). Evidence for conformational coupling between two calcium channels. Proceedings of the National Academy of Sciences of the United States of America *101*, 12748-12752.

Papadopoulos, S., Leuranguer, V., Bannister, R.A., and Beam, K.G. (2004). Mapping sites of potential proximity between the dihydropyridine receptor and RyR1 in muscle using a cyan fluorescent protein-yellow fluorescent protein tandem as a fluorescence resonance energy transfer probe. The Journal of biological chemistry *279*, 44046-44056.

Paredes, R.M., Etzler, J.C., Watts, L.T., Zheng, W., and Lechleiter, J.D. (2008). Chemical calcium indicators. Methods (San Diego, Calif) *46*, 143-151.

Park, H.C., Shin, J., and Appel, B. (2004). Spatial and temporal regulation of ventral spinal cord precursor specification by Hedgehog signaling. Development *131*, 5959-5969.

Pate, P., Mochca-Morales, J., Wu, Y., Zhang, J.Z., Rodney, G.G., Serysheva, II, Williams, B.Y., Anderson, M.E., and Hamilton, S.L. (2000). Determinants for calmodulin binding on voltage-dependent Ca2+ channels. The Journal of biological chemistry *275*, 39786-39792.

Percival, J.M., and Froehner, S.C. (2007). Golgi complex organization in skeletal muscle: a role for Golgi-mediated glycosylation in muscular dystrophies? Traffic (Copenhagen, Denmark) *8*, 184-194.

Pirone, A., Schredelseker, J., Tuluc, P., Gravino, E., Fortunato, G., Flucher, B.E., Carsana, A., Salvatore, F., and Grabner, M. (2010). Identification and functional characterization of malignant hyperthermia mutation T1354S in the outer pore of the Cavalpha1S-subunit. American journal of physiology Cell physiology *299*, C1345-1354.

Polster, A., Ohrtman, J.D., Beam, K.G., and Papadopoulos, S. (2012). Fluorescence resonance energy transfer (FRET) indicates that association with the type I ryanodine receptor (RyR1) causes reorientation of multiple cytoplasmic domains of the dihydropyridine receptor (DHPR) alpha(1S) subunit. The Journal of biological chemistry *287*, 41560-41568.

Porter, K.R., and Palade, G.E. (1957). Studies on the endoplasmic reticulum. III. Its form and distribution in striated muscle cells. The Journal of biophysical and biochemical cytology *3*, 269-300.

Powell, J.A., Petherbridge, L., and Flucher, B.E. (1996). Formation of triads without the dihydropyridine receptor alpha subunits in cell lines from dysgenic skeletal muscle. The Journal of cell biology *134*, 375-387.

Pragnell, M., De Waard, M., Mori, Y., Tanabe, T., Snutch, T.P., and Campbell, K.P. (1994). Calcium channel beta-subunit binds to a conserved motif in the I-II cytoplasmic linker of the alpha 1-subunit. Nature *368*, 67-70.

Proenza, C., O'Brien, J., Nakai, J., Mukherjee, S., Allen, P.D., and Beam, K.G. (2002). Identification of a region of RyR1 that participates in allosteric coupling with the alpha(1S) (Ca(V)1.1) II-III loop. The Journal of biological chemistry *277*, 6530-6535.

Proenza, C., Wilkens, C., Lorenzon, N.M., and Beam, K.G. (2000). A carboxyl-terminal region important for the expression and targeting of the skeletal muscle dihydropyridine receptor. The Journal of biological chemistry *275*, 23169-23174.

Protasi, F., Franzini-Armstrong, C., and Allen, P.D. (1998). Role of ryanodine receptors in the assembly of calcium release units in skeletal muscle. The Journal of cell biology *140*, 831-842.

Qin, X.R., Suetake, T., Hayashi, F., Yokoyama, S., RIKEN Structural Genomics/Proteomics Initiative (2006). PDB ID: 2DL4. Unpublished data.

Rahkila, P., Alakangas, A., Vaananen, K., and Metsikko, K. (1996). Transport pathway, maturation, and targetting of the vesicular stomatitis virus glycoprotein in skeletal muscle fibers. Journal of cell science *109 (Pt 6)*, 1585-1596.

Rahkila, P., Luukela, V., Vaananen, K., and Metsikko, K. (1998). Differential targeting of vesicular stomatitis virus G protein and influenza virus hemagglutinin appears during myogenesis of L6 muscle cells. The Journal of cell biology *140*, 1101-1111.

Rainier, S., Sher, C., Reish, O., Thomas, D., and Fink, J.K. (2006). De novo occurrence of novel SPG3A/atlastin mutation presenting as cerebral palsy. Archives of neurology *63*, 445-447.

Ralston, E., Lu, Z., and Ploug, T. (1999). The organization of the Golgi complex and microtubules in skeletal muscle is fiber type-dependent. The Journal of neuroscience : the official journal of the Society for Neuroscience *19*, 10694-10705.

Razzaq, A., Robinson, I.M., McMahon, H.T., Skepper, J.N., Su, Y., Zelhof, A.C., Jackson, A.P., Gay, N.J., and O'Kane, C.J. (2001). Amphiphysin is necessary for organization of the excitation-contraction coupling machinery of muscles, but not for synaptic vesicle endocytosis in Drosophila. Genes & development *15*, 2967-2979.

Rebbeck, R.T., Karunasekara, Y., Gallant, E.M., Board, P.G., Beard, N.A., Casarotto, M.G., and Dulhunty, A.F. (2011). The beta(1a) subunit of the skeletal DHPR binds to

skeletal RyR1 and activates the channel via its 35-residue C-terminal tail. Biophysical journal *100*, 922-930.

Rios, E., and Brum, G. (1987). Involvement of dihydropyridine receptors in excitation-contraction coupling in skeletal muscle. Nature *325*, 717-720.

Roberts, A., Soffe, S.R., Wolf, E.S., Yoshida, M., and Zhao, F.Y. (1998). Central circuits controlling locomotion in young frog tadpoles. Annals of the New York Academy of Sciences *860*, 19-34.

Rogalski, A.A., Bergmann, J.E., and Singer, S.J. (1984). Effect of microtubule assembly status on the intracellular processing and surface expression of an integral protein of the plasma membrane. The Journal of cell biology *99*, 1101-1109.

Rossi, D., Barone, V., Giacomello, E., Cusimano, V., and Sorrentino, V. (2008). The sarcoplasmic reticulum: an organized patchwork of specialized domains. Traffic (Copenhagen, Denmark) *9*, 1044-1049.

Rust, M.J., Bates, M., and Zhuang, X. (2006). Sub-diffraction-limit imaging by stochastic optical reconstruction microscopy (STORM). Nature methods *3*, 793-795.

Saint-Amant, L., and Drapeau, P. (1998). Time course of the development of motor behaviors in the zebrafish embryo. J Neurobiol *37*, 622-632.

Saint-Amant, L., and Drapeau, P. (2003). Whole-cell patch-clamp recordings from identified spinal neurons in the zebrafish embryo. Methods Cell Sci *25*, 59-64.

Saint-Amant, L., Sprague, S.M., Hirata, H., Li, Q., Cui, W.W., Zhou, W., Poudou, O., Hume, R.I., and Kuwada, J.Y. (2008). The zebrafish ennui behavioral mutation disrupts acetylcholine receptor localization and motor axon stability. Dev Neurobiol *68*, 45-61.

Saito, A., Hino, S., Murakami, T., Kanemoto, S., Kondo, S., Saitoh, M., Nishimura, R., Yoneda, T., Furuichi, T., Ikegawa, S.*, et al.* (2009). Regulation of endoplasmic reticulum stress response by a BBF2H7-mediated Sec23a pathway is essential for chondrogenesis. Nature cell biology *11*, 1197-1204.

Salas, P.J., Misek, D.E., Vega-Salas, D.E., Gundersen, D., Cereijido, M., and Rodriguez-Boulan, E. (1986). Microtubules and actin filaments are not critically involved in the biogenesis of epithelial cell surface polarity. The Journal of cell biology *102*, 1853-1867.

Sander, J.D., Cade, L., Khayter, C., Reyon, D., Peterson, R.T., Joung, J.K., and Yeh, J.R. (2011). Targeted gene disruption in somatic zebrafish cells using engineered TALENs. Nature biotechnology *29*, 697-698.

Saraste, J., Palade, G.E., and Farquhar, M.G. (1986). Temperature-sensitive steps in the transport of secretory proteins through the Golgi complex in exocrine pancreatic cells. Proceedings of the National Academy of Sciences of the United States of America *83*, 6425-6429.

Satoh, J., Nanri, Y., and Yamamura, T. (2006). Rapid identification of 14-3-3-binding proteins by protein microarray analysis. J Neurosci Methods *152*, 278-288.

Schneider, M.F., and Chandler, W.K. (1973). Voltage dependent charge movement of skeletal muscle: a possible step in excitation-contraction coupling. Nature *242*, 244-246.

Schoonheim, P.J., Arrenberg, A.B., Del Bene, F., and Baier, H. (2010). Optogenetic localization and genetic perturbation of saccade-generating neurons in zebrafish. J Neurosci *30*, 7111-7120.

Schramm, M., Thomas, G., Towart, R., and Franckowiak, G. (1983). Novel dihydropyridines with positive inotropic action through activation of Ca2+ channels. Nature *303*, 535-537.

Schredelseker, J., Dayal, A., Schwerte, T., Franzini-Armstrong, C., and Grabner, M. (2009). Proper restoration of excitation-contraction coupling in the dihydropyridine receptor beta1-null zebrafish relaxed is an exclusive function of the beta1a subunit. The Journal of biological chemistry *284*, 1242-1251.

Schredelseker, J., Di Biase, V., Obermair, G.J., Felder, E.T., Flucher, B.E., Franzini-Armstrong, C., and Grabner, M. (2005). The beta 1a subunit is essential for the assembly of dihydropyridine-receptor arrays in skeletal muscle. Proceedings of the National Academy of Sciences of the United States of America *102*, 17219-17224.

Schredelseker, J., Shrivastav, M., Dayal, A., and Grabner, M. (2010). Non-Ca2+-conducting Ca2+ channels in fish skeletal muscle excitation-contraction coupling. Proceedings of the National Academy of Sciences of the United States of America *107*, 5658-5663.

Scott, E.K., Mason, L., Arrenberg, A.B., Ziv, L., Gosse, N.J., Xiao, T., Chi, N.C., Asakawa, K., Kawakami, K., and Baier, H. (2007). Targeting neural circuitry in zebrafish using GAL4 enhancer trapping. Nat Methods *4*, 323-326.

Sencer, S., Papineni, R.V., Halling, D.B., Pate, P., Krol, J., Zhang, J.Z., and Hamilton, S.L. (2001). Coupling of RYR1 and L-type calcium channels via calmodulin binding domains. The Journal of biological chemistry *276*, 38237-38241.

Serysheva, II, Ludtke, S.J., Baker, M.R., Chiu, W., and Hamilton, S.L. (2002). Structure of the voltage-gated L-type Ca2+ channel by electron cryomicroscopy. Proceedings of the National Academy of Sciences of the United States of America *99*, 10370-10375.

Sewry, C.A., Jimenez-Mallebrera, C., and Muntoni, F. (2008). Congenital myopathies. Current opinion in neurology *21*, 569-575.

Shimoda, N., Knapik, E.W., Ziniti, J., Sim, C., Yamada, E., Kaplan, S., Jackson, D., de Sauvage, F., Jacob, H., and Fishman, M.C. (1999). Zebrafish genetic map with 2000 microsatellite markers. Genomics *58*, 219-232.

Slavik, K.J., Wang, J.P., Aghdasi, B., Zhang, J.Z., Mandel, F., Malouf, N., and Hamilton, S.L. (1997). A carboxy-terminal peptide of the alpha 1-subunit of the dihydropyridine receptor inhibits Ca(2+)-release channels. The American journal of physiology *272*, C1475-1481.

Sorrentino, V., and Volpe, P. (1993). Ryanodine receptors: how many, where and why? Trends Pharmacol Sci *14*, 98-103.

Stamm, D.S., Aylsworth, A.S., Stajich, J.M., Kahler, S.G., Thorne, L.B., Speer, M.C., and Powell, C.M. (2008a). Native American myopathy: congenital myopathy with cleft palate, skeletal anomalies, and susceptibility to malignant hyperthermia. American journal of medical genetics Part A *146A*, 1832-1841.

Stamm, D.S., Powell, C.M., Stajich, J.M., Zismann, V.L., Stephan, D.A., Chesnut, B., Aylsworth, A.S., Kahler, S.G., Deak, K.L., Gilbert, J.R.*, et al.* (2008b). Novel congenital myopathy locus identified in Native American Indians at 12q13.13-14.1. Neurology *71*, 1764-1769.

Strausberg, R.L., Feingold, E.A., Grouse, L.H., Derge, J.G., Klausner, R.D., Collins, F.S., Wagner, L., Shenmen, C.M., Schuler, G.D., Altschul, S.F.*, et al.* (2002). Generation and initial analysis of more than 15,000 full-length human and mouse cDNA sequences. Proc Natl Acad Sci U S A *99*, 16899-16903.

Strube, C., Beurg, M., Sukhareva, M., Ahern, C.A., Powell, J.A., Powers, P.A., Gregg, R.G., and Coronado, R. (1998). Molecular origin of the L-type Ca2+ current of skeletal muscle myotubes selectively deficient in dihydropyridine receptor beta1a subunit. Biophysical journal *75*, 207-217.

Suda, N., Franzius, D., Fleig, A., Nishimura, S., Bodding, M., Hoth, M., Takeshima, H., and Penner, R. (1997). Ca2+-induced Ca2+ release in Chinese hamster ovary (CHO) cells co-expressing dihydropyridine and ryanodine receptors. The Journal of general physiology *109*, 619-631.

Suzuki, H., Kawai, J., Taga, C., Yaoi, T., Hara, A., Hirose, K., Hayashizaki, Y., and Watanabe, S. (1996). Stac, a novel neuron-specific protein with cysteine-rich and SH3 domains. Biochem Biophys Res Commun *229*, 902-909.

Sweitzer, S.M., and Hinshaw, J.E. (1998). Dynamin undergoes a GTP-dependent conformational change causing vesiculation. Cell *93*, 1021-1029.

Takekura, H., Nishi, M., Noda, T., Takeshima, H., and Franzini-Armstrong, C. (1995a). Abnormal junctions between surface membrane and sarcoplasmic reticulum in skeletal muscle with a mutation targeted to the ryanodine receptor. Proceedings of the National Academy of Sciences of the United States of America *92*, 3381-3385.

Takekura, H., Paolini, C., Franzini-Armstrong, C., Kugler, G., Grabner, M., and Flucher, B.E. (2004). Differential contribution of skeletal and cardiac II-III loop sequences to the assembly of dihydropyridine-receptor arrays in skeletal muscle. Molecular biology of the cell *15*, 5408-5419.

Takekura, H., Takeshima, H., Nishimura, S., Takahashi, M., Tanabe, T., Flockerzi, V., Hofmann, F., and Franzini-Armstrong, C. (1995b). Co-expression in CHO cells of two muscle proteins involved in excitation-contraction coupling. Journal of muscle research and cell motility *16*, 465-480.

Takeshima, H., Iino, M., Takekura, H., Nishi, M., Kuno, J., Minowa, O., Takano, H., and Noda, T. (1994). Excitation-contraction uncoupling and muscular degeneration in mice lacking functional skeletal muscle ryanodine-receptor gene. Nature *369*, 556-559.

Takeshima, H., Nishimura, S., Matsumoto, T., Ishida, H., Kangawa, K., Minamino, N., Matsuo, H., Ueda, M., Hanaoka, M., Hirose, T.*, et al.* (1989). Primary structure and expression from complementary DNA of skeletal muscle ryanodine receptor. Nature *339*, 439-445.

Tanabe, T., Beam, K.G., Adams, B.A., Niidome, T., and Numa, S. (1990). Regions of the skeletal muscle dihydropyridine receptor critical for excitation-contraction coupling. Nature *346*, 567-569.

Tanabe, T., Beam, K.G., Powell, J.A., and Numa, S. (1988). Restoration of excitation-contraction coupling and slow calcium current in dysgenic muscle by dihydropyridine receptor complementary DNA. Nature *336*, 134-139.

Tanabe, T., Takeshima, H., Mikami, A., Flockerzi, V., Takahashi, H., Kangawa, K., Kojima, M., Matsuo, H., Hirose, T., and Numa, S. (1987). Primary structure of the receptor for calcium channel blockers from skeletal muscle. Nature *328*, 313-318.

Tang, W., Sencer, S., and Hamilton, S.L. (2002). Calmodulin modulation of proteins involved in excitation-contraction coupling. Frontiers in bioscience : a journal and virtual library *7*, d1583-1589.

Tartakoff, A.M., and Vassalli, P. (1977). Plasma cell immunoglobulin secretion: arrest is accompanied by alterations of the golgi complex. The Journal of experimental medicine *146*, 1332-1345.

Tassin, A.M., Paintrand, M., Berger, E.G., and Bornens, M. (1985). The Golgi apparatus remains associated with microtubule organizing centers during myogenesis. The Journal of cell biology *101*, 630-638.

Tian, L., Hires, S.A., Mao, T., Huber, D., Chiappe, M.E., Chalasani, S.H., Petreanu, L., Akerboom, J., McKinney, S.A., Schreiter, E.R.*, et al.* (2009). Imaging neural activity in worms, flies and mice with improved GCaMP calcium indicators. Nature methods *6*, 875-881.

Tsien, R.W., Lipscombe, D., Madison, D.V., Bley, K.R., and Fox, A.P. (1988). Multiple types of neuronal calcium channels and their selective modulation. Trends in neurosciences *11*, 431-438.

Unni, V.K., Zakharenko, S.S., Zablow, L., DeCostanzo, A.J., and Siegelbaum, S.A. (2004). Calcium release from presynaptic ryanodine-sensitive stores is required for long-term depression at hippocampal CA3-CA3 pyramidal neuron synapses. J Neurosci *24*, 9612-9622.

Van Petegem, F., Clark, K.A., Chatelain, F.C., and Minor, D.L., Jr. (2004). Structure of a complex between a voltage-gated calcium channel beta-subunit and an alpha-subunit domain. Nature *429*, 671-675.

Vilella, A.J., Severin, J., Ureta-Vidal, A., Heng, L., Durbin, R., and Birney, E. (2009). EnsemblCompara GeneTrees: Complete, duplication-aware phylogenetic trees in vertebrates. Genome research *19*, 327-335.

Volgraf, M., Gorostiza, P., Numano, R., Kramer, R.H., Isacoff, E.Y., and Trauner, D. (2006). Allosteric control of an ionotropic glutamate receptor with an optical switch. Nature chemical biology *2*, 47-52.

Volpe, P., Villa, A., Podini, P., Martini, A., Nori, A., Panzeri, M.C., and Meldolesi, J. (1992). The endoplasmic reticulum-sarcoplasmic reticulum connection: distribution of endoplasmic reticulum markers in the sarcoplasmic reticulum of skeletal muscle fibers. Proceedings of the National Academy of Sciences of the United States of America *89*, 6142-6146.

Walker, C., and Streisinger, G. (1983). Induction of Mutations by gamma-Rays in Pregonial Germ Cells of Zebrafish Embryos. Genetics *103*, 125-136.

Warnock, D.E., Hinshaw, J.E., and Schmid, S.L. (1996). Dynamin self-assembly stimulates its GTPase activity. J Biol Chem *271*, 22310-22314.

Weiss, N., Legrand, C., Pouvreau, S., Bichraoui, H., Allard, B., Zamponi, G.W., De Waard, M., and Jacquemond, V. (2010). In vivo expression of G-protein beta1gamma2 dimer in adult mouse skeletal muscle alters L-type calcium current and excitation-contraction coupling. J Physiol *588*, 2945-2960.

Westerfield, M., McMurray, J.V., and Eisen, J.S. (1986). Identified motoneurons and their innervation of axial muscles in the zebrafish. J Neurosci *6*, 2267-2277.

Westphal, V., Rizzoli, S.O., Lauterbach, M.A., Kamin, D., Jahn, R., and Hell, S.W. (2008). Video-rate far-field optical nanoscopy dissects synaptic vesicle movement. Science *320*, 246-249.

Wilkens, C.M., and Beam, K.G. (2003). Insertion of alpha1S II-III loop and C terminal sequences into alpha1H fails to restore excitation-contraction coupling in dysgenic myotubes. Journal of muscle research and cell motility *24*, 99-109.

Wood, S.J., and Slater, C.R. (2001). Safety factor at the neuromuscular junction. Prog Neurobiol *64*, 393-429.

Wyart, C. (2012). Personal Communication.

Wyart, C., Del Bene, F., Warp, E., Scott, E.K., Trauner, D., Baier, H., and Isacoff, E.Y. (2009). Optogenetic dissection of a behavioural module in the vertebrate spinal cord. Nature *461*, 407-410.

Yang, L., Rastegar, S., and Strahle, U. (2010a). Regulatory interactions specifying Kolmer-Agduhr interneurons. Development *137*, 2713-2722.

Yang, T., Suhail, Y., Dalton, S., Kernan, T., and Colecraft, H.M. (2007). Genetically encoded molecules for inducibly inactivating CaV channels. Nature chemical biology *3*, 795-804.

Yang, T., Ta, T.A., Pessah, I.N., and Allen, P.D. (2003). Functional defects in six ryanodine receptor isoform-1 (RyR1) mutations associated with malignant hyperthermia and their impact on skeletal excitation-contraction coupling. The Journal of biological chemistry *278*, 25722-25730.

Yang, T., Xu, X., Kernan, T., Wu, V., and Colecraft, H.M. (2010b). Rem, a member of the RGK GTPases, inhibits recombinant CaV1.2 channels using multiple mechanisms that require distinct conformations of the GTPase. J Physiol *588*, 1665-1681.

Yasuda, T., Delbono, O., Wang, Z.M., Messi, M.L., Girard, T., Urwyler, A., Treves, S., and Zorzato, F. (2013). JP-45/JSRP1 variants affect skeletal muscle excitation-contraction coupling by decreasing the sensitivity of the dihydropyridine receptor. Human mutation *34*, 184-190.

Yizhar, O., Fenno, L.E., Davidson, T.J., Mogri, M., and Deisseroth, K. (2011). Optogenetics in neural systems. Neuron *71*, 9-34.

Zaal, K.J., Reid, E., Mousavi, K., Zhang, T., Mehta, A., Bugnard, E., Sartorelli, V., and Ralston, E. (2011). Who needs microtubules? Myogenic reorganization of MTOC,

Golgi complex and ER exit sites persists despite lack of normal microtubule tracks. PloS one *6*, e29057.

Zafra-Ruano, A., and Luque, I. (2012). Interfacial water molecules in SH3 interactions: Getting the full picture on polyproline recognition by protein-protein interaction domains. FEBS Lett *586*, 2619-2630.

Zhang, G., Kazanietz, M.G., Blumberg, P.M., and Hurley, J.H. (1995). Crystal structure of the cys2 activator-binding domain of protein kinase C delta in complex with phorbol ester. Cell *81*, 917-924.

Zhang, J.F., Ellinor, P.T., Aldrich, R.W., and Tsien, R.W. (1994). Molecular determinants of voltage-dependent inactivation in calcium channels. Nature *372*, 97-100.

Zhang, M., Chang, H., Zhang, Y., Yu, J., Wu, L., Ji, W., Chen, J., Liu, B., Lu, J., Liu, Y., *et al.* (2012). Rational design of true monomeric and bright photoactivatable fluorescent proteins. Nature methods *9*, 727-729.

Zhou, M., Horita, D.A., Waugh, D.S., Byrd, R.A., and Morrison, D.K. (2002). Solution structure and functional analysis of the cysteine-rich C1 domain of kinase suppressor of Ras (KSR). J Mol Biol *315*, 435-446.

Zhou, W., Horstick, E.J., Hirata, H., and Kuwada, J.Y. (2008). Identification and expression of voltage-gated calcium channel beta subunits in Zebrafish. Dev Dyn *237*, 3842-3852.

Zhou, W., Saint-Amant, L., Hirata, H., Cui, W.W., Sprague, S.M., and Kuwada, J.Y. (2006). Non-sense mutations in the dihydropyridine receptor beta1 gene, CACNB1, paralyze zebrafish relaxed mutants. Cell Calcium *39*, 227-236.

ZhuGe, R., DeCrescenzo, V., Sorrentino, V., Lai, F.A., Tuft, R.A., Lifshitz, L.M., Lemos, J.R., Smith, C., Fogarty, K.E., and Walsh, J.V., Jr. (2006). Syntillas release Ca2+ at a site different from the microdomain where exocytosis occurs in mouse chromaffin cells. Biophys J *90*, 2027-2037.